The dynamic interplay of mechanisms governing infiltration into structured and layered soil columns

---

A thesis
submitted in partial fulfilment
of the requirements for the Degree of
Doctor of Philosophy

at

Lincoln University

by

Sam Carrick

Lincoln University

2009

Declaration: Prior Publication of Parts of this Thesis

Parts of this thesis have been (i) presented at conferences and were included in the conference proceedings, or (ii) published in a non-referred journal.

(i) Conference presentations and proceedings

Carrick, S.; Almond, P.; Buchan, G (2008) The reality versus conventional wisdom of measuring infiltration in structured and layered field soils. Geophysical Research Abstracts, Vol. 10. European Geosciences Union conference, Vienna, April 2008 (Oral presentation)
(includes parts of chapters 6 and 7)

Carrick, S.; Almond, P.; Buchan, G; Smith, N. (2008) In-situ characterisation of soil hydraulic attributes for the individual layers of a multilayered soil column. Geophysical Research Abstracts, Vol. 10. European Geosciences Union conference, Vienna, April 2008 (Poster presentation)
(includes parts of chapter 7)

(ii) Articles published in non-referred journals

Carrick, S. (2007) Preferential flow through soils. Soil Horizons. Issue 16, September 2007, pp 8. Manaaki Whenua / Landcare Research.
(includes parts of chapter 5)

Carrick, S.; Smith, N.; Buchan, G (2008) Measurement of preferential flowpaths in a layered soil column: 1. Improving the tension infiltrometer for measuring infiltration, drainage, and solute leaching. WISPAS, issue 99, pp 5 – 6. HortResearch, Palmerston North.
(includes parts of chapter 3)

Carrick, S.; Buchan, G.; Almond, P (2009) Could hydrophobicity influence soil infiltration rate – even around field capacity or wetter? WISPAS, issue 102, pp 5 - 7. Plant and Food Research, Palmerston North.
(includes parts of chapter 3 and 6)

Abstract of a thesis submitted in partial fulfilment of the
requirements for the Degree of Doctor of Philosophy

THE DYNAMIC INTERPLAY OF MECHANISMS GOVERNING INFILTRATION INTO STRUCTURED AND LAYERED SOIL COLUMNS

by Sam Carrick

Worldwide there is considerable concern over the effects of human activities on the quantity and quality of freshwater. Measurement of infiltration behaviour will be important for improving freshwater management. This study identifies that New Zealand has a sporadic history of measuring soil water movement attributes on a limited number of soil types, although the current practical demand should be large for management of irrigation, dairy farm effluent disposal, as well as municipal / domestic waste- and storm-water disposal.

Previous research has demonstrated that infiltration behaviour is governed by the interplay between numerous mechanisms including hydrophobicity and preferential flow, the latter being an important mechanism of contaminant leaching for many NZ soils. Future characterisation will need to recognise the dynamic nature of these interactions, and be able to reliably characterise the key infiltration mechanisms. Since macropores are responsible for preferential flow, it is critical that infiltration studies use a representative sample of the macropore network. The aim of this project was to study the mechanisms governing the infiltration behaviour of a layered soil in large (50 x 70 cm) monolith lysimeters, where the connectivity of the macropore network remains undisturbed.

Four lysimeters of the Gorge silt loam were collected, a structured soil with four distinct layers. On each lysimeter there were four separate infiltration experiments, with water applied under suctions of 0, 0.5, 1, and 1.5 kPa by a custom-built tension infiltrometer. Each lysimeter was instrumented with 30 tensiometers, located in arrays at the layer boundaries. There was also a field experiment using ponded dye infiltration to visually define preferential flowpaths.

Analysis of dye patterns, temporal variability in soil matric potential (Ψ_m), and solute breakthrough curves all show that preferential flow is an important infiltration mechanism. Preferential flowpaths were activated when Ψ_m was above -1.5 kPa. During saturated

infiltration, at least 97% of drainage was through the 'mobile' pore volume of the lysimeter (θ_m), estimated among the lysimeters at 5.4 – 8.7 % of the lysimeter volume.

Early-time infiltration behaviour did not show the classical square-root of time behaviour, indicating sorptivity was not the governing mechanism. This was consistent across the four lysimeters, and during infiltration under different surface imposed suctions. The most likely mechanism restricting sorptivity is weak hydrophobicity, which appears to restrict infiltration for the first 5 – 10 mm of infiltration. Overall, the Gorge soil's early-time infiltration behaviour is governed by the dynamic interaction between sorptivity, hydrophobicity, the network of air-filled pores, preferential flow and air encapsulation.

Long-time infiltration behaviour was intimately linked to the temporal dynamics of Ψ_m, which was in turn controlled by preferential flow and soil layer interactions. Preferential flowpaths created strong inter-layer connectivity by allowing an irregular wetting front to reach lower layers within 2 – 15 mm of infiltration. Thereafter, layer interactions dominate infiltration for long-time periods, as Ψ_m in soil layers with different $K(\Psi_m)$ relationships self-adjusts to try to maintain a constant Darcy velocity. An important finding was that Ψ_m rarely attained the value set by the tension infiltrometer during unsaturated infiltration. The results show that 'true' steady-state infiltration is unlikely to occur in layered soils. A quasi-steady state was identified once the whole column had fully wet and layer interactions had settled to where Ψ_m changes occurred in unison through each soil layer. Quasi-steady state was difficult to identify from just the cumulative infiltration curve, but more robustly identified as when infiltration matched drainage, and Ψ_m measurements showed each layer had a stable hydraulic gradient.

I conclude that the *in-situ* hydraulic conductivity, $K(\Psi_m)$, of individual soil layers can be accurately and meaningfully determined from lysimeter-scale infiltration experiments. My results show that $K(\Psi_m)$ is different for each soil layer, and that differences are consistent among the four lysimeters. Under saturated flow the subsoil had the lowest conductivity, and was the restricting layer. Most interestingly this pattern reversed during unsaturated flow. As Ψ_m decreased below -0.5 to -1 kPa, the subsoil was markedly more conductive, and the topsoil layers became the restricting layers. All four soil layers demonstrate a sharp decline in $K(\Psi_m)$ as Ψ_m decreases, with a break in slope at ~ -1 kPa indicating the dual-permeability nature of all layers.

Keywords: Infiltration, layered soil, preferential flow, sorptivity, hydraulic conductivity, hydrophobicity, dual-permeability, mobile water content, lysimeter, tension infiltrometer

Acknowledgements

This thesis is dedicated to my beautiful wife, Denise, and our two children, Rose and Tom. Denise has shown endless love, support, understanding and confidence in me throughout this long process. Both Rose and Tom were born during this time, and their constant growth and joy in life has continually refreshed my energy. I am blessed to have such a wonderful family.

I would like to express sincere thanks to my supervisory team, Dr. Peter Almond and Dr. Graeme Buchan, for their excellent supervision. They have shown constant encouragement, patience, and guidance as both the project and my personal circumstances evolved. I am most grateful for the friendship that has developed, and may it last for many years to come. I also wish to thank my associate supervisor, Dr. Carol Smith, whose door was always open for support and advice during the early stages of the project.

I would also like to acknowledge the financial support of AGMARDT for my PhD scholarship. I see it as a privilege to have held this award from an organisation that has such high prestige in New Zealand's agricultural community. I am also grateful for the operational funding from Landcare Research and the Centre for Soil and Environmental Quality, Lincoln University. In particular I would like to thank Dr. Allan Hewitt and Prof. Keith Cameron who have both shown great generosity and confidence in my ability.

I owe special thanks to the technical support of Neil Smith, whose skills and wisdom ensured the success of this project. Under Neil's tutelage I have grown from virtual illiteracy to being skilled in the measurement of soil hydraulic attributes. I am proud of the experimental setup that we built on a shoestring budget, and admire the commitment that Neil showed to my project, which was beyond the requirements of his job. I would also like to acknowledge Leanne and Joy for laboratory analysis; Trevor and Nigel for help with the experimental setup; Prof. A. McKinnon and Dr. K. Unsworth for help with the image analysis; Roger and Vicki for the good times when tutoring the soils laboratory classes; as well as Matthew and Carole for the laughs we had in sharing our respective office and laboratory.

Finally, thanks also go out to all the staff and students of Soil and Physical Sciences Group. Many of you have offered advice, help and friendship over the last few years. I have truly felt at home and have really enjoyed my time amongst you. You only have to meet the people to see why the ongoing success of the group is no surprise.

Table of Contents

List of Tables

List of Figures

List of Plates

List of Equations

Notations

Abbreviations

	Definition	Units
A	Infiltration model parameter related to the soil's hydraulic conductivity (Equation 6-1)	
AFP	Air-filled porosity at field capacity, which is the void space at Ψ_m between 0 to -10 kPa	%
AWC	Available water storage capacity, which is the pore volume between Ψ_m of -10 to -1500 kPa	%
b	Parameter in Equation 6-4	
BMP	Best management practice	
$CaCl_2$	Calcium chloride	
$CaS0_4$	Calcium sulphate	
C:N	Carbon nitrogen ratio	
D	Dispersion coefficient	$cm^2\ d^{-1}$
$D(\theta_v)$	Soil water diffusivity function	$mm^2\ hr^{-1}$
DSE	Dairy shed effluent	
HSL	Hue, saturation, and lightness of a photographic image	
I	Cumulative infiltration	mm
I_c	Antecedent water storage capacity available for infiltration	mm
i_t	Infiltration rate	$mm\ hr^{-1}$
i.d.	Internal diameter	
K	Hydraulic conductivity	$mm\ hr^{-1}$
*K**	Hydraulic conductivity at the 'break-point' separating the macro- and mesopore regions of the $K(\Psi_m)$ relationship	$mm\ hr^{-1}$
K_{cs}	Saturated hydraulic conductivity of glass bead contact material	$mm\ hr^{-1}$
K_i	Hydraulic conductivity at the antecedent matric potential	$mm\ hr^{-1}$
K_0	Hydraulic conductivity at the matric potential set by the tension infiltrometer	$mm\ hr^{-1}$
K_{sat}	Saturated hydraulic conductivity	$mm\ hr^{-1}$
$K(\Psi_m)$	Hydraulic conductivity at the soil matric potential	$mm\ hr^{-1}$
$K_e(\Psi_m)$	Profile effective conductivity of the whole soil column	$mm\ hr^{-1}$
$K(\theta_v)$	Hydraulic conductivity at a volumetric soil water content	$mm\ hr^{-1}$
KBr	Potassium bromide	
KPI	Key performance indicator	
L	Transport length	cm
L1 … L6	Lysimeter 1, lysimeter 2, lysimeter 3, or lysimeter 6	
LTAR	Long-term soil acceptance rate for domestic effluent disposal	
MIM	Mobile-immobile model of solute transport	

MSE	Mean square error	
NES	National Environmental Standard	
NSD	National Soils Database	
o.d.	Outer diameter	
PET	Potential evapo-transpiration	mm
PV	Average water-filled pore volume of the soil column	
R	Retardation factor	
R^2	Regression coefficient	
REV	Representative elementary volume	
RI	Repellency Index	
RMA	Resource Management Act 1991	
S	Soil sorptivity	mm $hr^{-1/2}$
S_e	Sorptivity of ethanol	mm $hr^{-1/2}$
S_w	Sorptivity of water	mm $hr^{-1/2}$
s.e.	Standard error of the mean	
SWAMP	Soil Water Assessment and Measurement Programme	
t	Time	hr
t_0	Time when actual infiltration into the soil commences	hr
t_c	Infiltration time dominated by sorptivity	hr
t_{grav}	Time during infiltration at which the effect of gravity on flow equals that of capillarity	hr
Tp	Temperature	^oC
T_z	Tensiometer	
$\sqrt{t}$, $t^{1/2}$	Square root of time	$hr^{1/2}$
v	Pore water velocity	cm d^{-1}
V_c	Core volume	cm^3
V_i	Indent volume	cm^3
$W_{1..3}$	Weight of soil	g
W_s	Weight of sand	g
WCR	Water content reflectometer	
Z_0	Nominal soil surface	
Z_L	Depth of a lower soil layer boundary below the nominal soil surface	mm
Z_U	Depth of a upper soil layer boundary below the nominal soil surface	mm

Greek Symbols

	Definition	Units
Ψ_i	Antecedent matric potential prior to infiltration	kPa
Ψ_L	Mean Ψ_m at the lower boundary of a soil layer	mm
Ψ_m	Soil matric potential	kPa
Ψ_m^*	Soil matric potential at the 'break-point' separating the macro- and mesopore regions of the $K(\Psi_m)$ relationship	kPa
Ψ_0	Matric potential measured at the nominal soil surface	kPa
Ψ_{TI}	Suction applied by the tension infiltrometer	kPa
Ψ_U	Mean Ψ_m at the upper boundary of a soil layer	mm
θ_i	Antecedent volumetric water content	%
θ_{im}	Immobile water content	%
θ_m	Mobile water content	%
θ_g	Gravimetric water content	%
θ_v	Volumetric water content	%
$\theta_v(\Psi_m)$	Soil water characteristic	
ε_a	Air-filled porosity	%
ε_{anf}	'Non-fillable' air-filled porosity	%
ε_t	Total porosity	%
Φ	Flux potential	$mm^2\ hr^{-1}$
λ_m	Characteristic mean pore size	mm
ρ_b	Soil bulk density	$g\ cm^{-3}$
$\rho_{b(s)}$	Bulk density of sand	$g\ cm^{-3}$
ρ_p	Soil particle density	$g\ cm^{-3}$
ρ_w	Density of water	$g\ cm^{-3}$
ω	Mass transfer parameter	
α	Mass transfer coefficient	d^{-1}
α_1	Slope of the macropore region of the $K(\Psi_m)$ relationship	
α_2	Slope of the mesopore region of the $K(\Psi_m)$ relationship	
α^*	Sorptive number	mm^{-1}

Terms

The following terms are defined as follows for this thesis, because they may have multiple or ambiguous definitions in the research literature.

Antecedent infiltration capacity

The depth (mm) of infiltrating water required to wet the 0 – 5 cm layer from Ψ_i to the 'target' Ψ_m, set by the suction of the tension infiltrometer.

Macropores

The pore network corresponding to Ψ_m between 0 and -1.5 kPa.

Mesopores

The pore network corresponding to Ψ_m between -1.5 and -10 kPa.

Micropores

The pore network corresponding to Ψ_m less than -10 kPa.

Preferential flow

The non-equilibrium movement of water and solutes through the soil, with flow concentrated in certain regions of the pore network (i.e. mainly macropores), whilst other regions of the soil matrix are effectively by-passed.

Suction

Suction is used to describe the water status imposed by the tension infiltrometer at the surface boundary, or the suction applied to the lower boundary of the soil column. These external applied suctions are always expressed as positive values.

Chapter 1
General Introduction

1.1 Background to the study

Worldwide there is considerable concern over the effects of human activities on the quantity and quality of freshwater. The OECD Environmental Outlook to 2030 identifies water scarcity, groundwater quality, as well as agricultural water use and pollution as critical issues over the coming decades (OECD, 2008). In the United States about 13% of farmland streams and 20% of groundwater wells have nitrate concentrations that exceed the federal drinking water standard. Chemical contamination (e.g. pesticides) exceeds benchmarks for aquatic life in 57% of farmland streams and 83% of urban streams (The Heinz Centre, 2008). Even in lightly populated New Zealand the freshwater resources show considerable contamination, where 56% of monitored lakes have high to very high nutrient levels, with 13% classified as having nutrient-saturated hypertrophic status. Bacterial contamination means that 20% of monitored groundwater wells are unsafe to drink, whilst 39% show elevated nitrogen levels (Ministry for the Environment, 2007).

There is no doubt that measurement of infiltration behaviour is critical for addressing these issues. Infiltration characteristics of the soil surface determine whether irrigation or rainwater move to surface water as runoff, infiltrate into soil storage, or move through the soil as drainage to groundwater. Likewise, infiltration is a key process determining the degree to which contaminants interact with the filtering and buffering capability of soil. It is arguable that efficient use of water for agricultural crops and effective protection of freshwater from contamination could be greatly enhanced by a better understanding of soil infiltration dynamics.

Unfortunately, traditional soil resource evaluation has generally not measured soil hydraulic attributes, resulting in a lack of good quality data, which some argue hinders progress on some key issues of sustainable land management (McKenzie et al., 2000; Webb, 2003; 2000). In New Zealand the history of measuring soil water movement attributes has been sporadic. In the 1970's the Soil Bureau had a programme to characterise the unsaturated conductivity at field capacity (i.e. matric potential, Ψ_m, = -10 kPa) for the topsoil and subsoil of 22 soil series, representing six major soil groups

(Gradwell, 1974; Gradwell, 1979). This was followed in the 1980's by the Soil Water Assessment and Measurement Programme (SWAMP) (Watt et al., 1982), which measured the saturated and unsaturated hydraulic conductivity (Ψ_m = -0.4 kPa) of 43 taxonomic and agriculturally significant soils.

There have also been other reasonably extensive regional programmes, for example:

- In the 1960's – 70's there was a series of investigations to study both the irrigation suitability, as well as effects of irrigation on soils in a number of areas of Central and North Otago. This work focussed on soil physical properties to 30 – 60 cm depth, including measurements of ponded surface infiltration for soils of the Arrow, Ida and upper Clutha valleys (Rickard and Cossens, 1966; 1968).

- Gradwell and Rijkse (1988) assessed the irrigation suitability of eight soils in the Gisborne Plains, and measured the unsaturated conductivity at Ψ_m of -5, -10, and -20 kPa for individual soil layers to a depth of 60 – 76 cm.

- Webb et al. (2003; 2000) studied spatial variability of saturated and unsaturated hydraulic conductivity (Ψ_m = -0.4 kPa) of eight Canterbury soils, measuring the topsoil and one or two subsoil horizons.

A number of other special purpose surveys have characterised infiltration attributes of the topsoil only. The temporal change in the ponded surface infiltration rate following application of dairy shed effluent was studied by Greenwood (1999) for eight Southland soils. Taylor et al. (2008) compared the effects of landuse (forestry versus pasture) on the ponded surface infiltration rate of four Waikato soils, whilst Drewry et al. (2000) compared the effect of sheep or dairy grazing on topsoil (0 – 25 cm depth) saturated hydraulic conductivity for a number of Southland soils. A number of studies have also looked at the effects of treading on both saturated and unsaturated hydraulic conductivity to 25 cm soil depth (Greenwood and McNamara, 1992; Singleton et al., 2000).

Collectively these research programmes appear to have built up a reasonably large knowledge base. However, the National Soils Database (NSD) has water movement attributes for only the 43 pedons from the SWAMP programme, yet approximately 2000 soil series have been recognised. Even if the datasets from the other projects were collated the total characterised soil series would still be < 100. A few key soil types have

been intensively studied (i.e. Horotui, Manawatu, Templeton, and Lismore soils) which has lead to a comprehensive understanding of their hydraulic behaviour. However, there is presently no ongoing measurement programme to fill the wider knowledge gap, despite the NSD being recognised as a nationally significant database by central government.

Research continues to demonstrate that infiltration behaviour is truly dynamic, and governed by the interplay between numerous mechanisms such as hydrophobicity and preferential flow, as well as the strong influence of land management practices. Clearly future characterisation will need to recognise this dynamic nature, and be able to reliably measure the key infiltration mechanisms. In particular, evidence is building that preferential flow is an important mechanism of contaminant leaching for many New Zealand soils (McLeod et al., 2008). Conditions leading to preferential flow, and the processes by which it occurs, should be seen as critical avenues for future research.

In a review of the literature, Jarvis (2007) identified that preferential flowpaths are consistently activated in areas of soil wetted to matric potentials above -1 kPa. Reliable characterisation of preferential flow therefore requires measurement of infiltration and water movement attributes over at least this range of matric potentials. New Zealand studies have typically focussed on just two matric potentials, 0 and -0.4 kPa, often using small cores (e.g. 10 cm diameter x 4 cm deep). Serious doubt has been raised about the suitability of small cores for measuring water-movement attributes, due to their potential to provide an unrealistic representation of the abundance and connectivity of macropores. Since macropores are responsible for preferential flow, it follows that measurements must use a representative sample of the macropore network.

Large monolith lysimeters provide both a potentially representative volume and intact layering, ensuring vertical continuity in the pore network. Lysimeters have become a standard sampling volume in New Zealand, particularly for research into contaminant leaching, with 50 cm diameter by 70 cm depth commonly used. One exciting option is to extend the scope of lysimeter research to characterisation of infiltration and water movement attributes. Durner et al. (2008) recently simulated water movement in layered monoliths and explored the potential for using lysimeter experiments to calculate the *in-situ* hydraulic attributes of each soil layer. This project applies this approach to a real soil, as well as studying how mechanisms such as preferential flow influence the infiltration behaviour.

1.2 Aims and objectives of the study

The main aims of this project were as follows:

- To study the mechanisms governing the infiltration behaviour of an undisturbed layered soil, particularly preferential flow.
- To characterise the *in-situ* hydraulic conductivity of individual soil layers.

To achieve these goals, the main objectives of this study were as follows:

1. To obtain experimental results enabling comparison of different methods of characterising the preferential flow behaviour.
2. To determine the key mechanisms that govern early-time infiltration behaviour, and their potential effect on deriving hydraulic attributes from early-time data.
3. To determine the key mechanisms governing long-time infiltration behaviour, and to test if the *in-situ* hydraulic conductivity of individual soil layers can be reliably determined.

The following secondary objectives establish the practical relevance of this study:

4. To review the practical demand in New Zealand for measurement of soil infiltration attributes
5. To review what mechanisms could influence the reliability of these measurements.
6. To design and construct a tension infiltrometer – lysimeter system that minimises measurement errors.

1.3 Layout of the thesis

This thesis comprises eight chapters including this general introduction and the conclusions chapters. Chapter 2 is the literature review, and specifically addresses objectives 4 and 5. Chapter 3 describes the experimental methods, and addresses objective 6. Chapter 4 provides a background overview, for the soil studied, of the environmental, chemical and physical attributes that could influence the infiltration behaviour observed in the following chapters. Chapters 5, 6, and 7 focus on each of the objectives 1 to 3, respectively.

Chapter 2
Literature Review

2.1 Introduction

The previous chapter raised the question of whether measurement of soil infiltration and water movement attributes is relevant to sustainable land management in New Zealand. This key question is addressed in the first section of this review. The following sections look at technical aspects of soil hydraulic characterisation, including the applicability of tension infiltrometers, and what mechanisms influence variability, and hence the accuracy, of these measurements.

2.2 What is the practical demand for attributes derivable from infiltration studies?

The primary legislation governing sustainable land management in New Zealand is the Resource Management Act 1991 (RMA). The RMA defines sustainable management in terms of sustaining the potential of natural and physical resources to meet the reasonably foreseeable needs of future generations; safeguarding the life-supporting capacity of water, soil and ecosystems; and avoiding, remedying or mitigating any adverse effects of activities on the environment. Local government is primarily responsible for implementation of the RMA, with an Environment Court as an independent arbitrator. This is supposed to be under the guidance of central government, although it has been criticised for providing little statutory guidance in the form of national standards and policy statements to local authorities regarding implementation of the RMA and environmental monitoring (OECD, 2007).

Local government has made good progress in managing *point* sources of pollution, but *diffuse* pollution of freshwater from land activities remains a significant challenge (Ministry for the Environment, 2007; OECD, 2007). Central government is slowly responding and has agreed to a strategy to improve freshwater management, protect our freshwater resources into the future, and acknowledge the fundamental importance of water to all New Zealanders. As a result, the Ministry for the Environment is currently developing a series of national environmental standards (NES) to improve the

management of freshwater. An NES is a legally enforceable regulation, under section 43 of the RMA, with the NES for sources of human drinking water now in force (Ministry for the Environment, 2007). Other freshwater related NES's being developed are for on-site waste water disposal, measurement of water takes, and ecological flows and water levels (Ministry for the Environment, 2008).

At the implementation level, the new NES's provide greater clarity over the expected environmental standards, and identify where work needs to be done. Inevitably this will result in tighter regulation and monitoring, which in turn require more detailed measurement to test whether or not standards are being met by a certain land activity. The following sections review the major issues where soil infiltration studies are relevant, some of the research that has been done, and highlight the potential for future research.

Irrigation

Irrigation is the major user of freshwater resources in New Zealand, accounting for 80% of all allocated water (Statistics New Zealand, 2007). Irrigation development has been rapid, roughly doubling in area every 12 years since the late 1970s (Irrigation New Zealand, 2007). In 2007 about four percent of farmland was irrigated (Statistics New Zealand, 2007), mostly for pastoral land uses, with Irrigation New Zealand (2009) predicting that the irrigated area could double to reach one million hectares by 2020. Spray irrigation accounts for 74% of the irrigated area, with 18% irrigated by flood irrigation, and 7% by micro systems (Statistics New Zealand, 2007). In general irrigation has been highly successful, with the irrigated areas producing about three times as much as an equivalent area farmed under dryland systems (Irrigation New Zealand, 2007). However, increasing pressure has been placed on improving the efficiency of irrigation systems in order to maintain and improve economic and environmental performance.

In particular, flood irrigation (also called border dyke irrigation) has been linked to adverse effects on surface and groundwater quality (Carey et al., 2004; Close et al., 2008; McDowell and Rowley, 2008; Monaghan et al., 2009; Nash and Barlow, 2008). Monaghan et al. (2009) monitored linkages between land management activities and stream water quality of a 5230 ha catchment in north Otago, New Zealand. They concluded that flood irrigation of 1900 ha was a major pollution source, due to excess irrigation generating surface runoff and entrainment of nitrogen, phosphorus, and faecal bacteria. The research also highlighted the importance of the infiltration characteristics of

different soil types; for example the mean runoff was 52% of the applied volume on the poorly drained Temuka soils. This dropped to 25% on the free draining Eyre and Paparua soils, although the total water loss is generally higher on free draining soils due to soil drainage (Nash and Barlow, 2008), with some studies measuring significant contaminant leaching (Close et al., 2008; Jiang et al., 2008; Toor et al., 2004).

Theoretically, water use efficiency is much higher under spray irrigation because the lower application rates reduce runoff and drainage (Di et al., 1998; Nash and Barlow, 2008). On free draining soils significant reductions in contaminant leaching have been measured when switching from flood to spray irrigation (Jiang et al., 2008; Toor et al., 2004). Close et al. (2008) note that groundwater studies have found very low microbial contamination under dairy farms using spray irrigation (centre pivots) compared to the high levels in their flood irrigated study area. However, Nash and Barlow (2008) highlight that spray irrigation efficiency can vary markedly according to different irrigator types and operator practice. Non-uniform spray patterns and even minor surface undulations can easily lead to localised ponding, even if the paddock-averaged application rate appears to be quite low. Spray irrigation can also be applied over a much wider range of slopes, but unless the application rate can be adjusted to different areas the varying infiltration rates can lead to generation of surface runoff and subsoil lateral flow.

In response to concerns over the economic and environmental efficiency of current systems, an irrigation code of practice has been developed to provide guidance on acceptable irrigation design (Irrigation New Zealand, 2007). The code of practice identifies key performance indicators (KPI's) that are necessary to obtain a quantifiable measure of the system efficiency. Matching the irrigation system to the soil infiltration rate and water holding capacity are identified as necessary to assess the water use efficiency KPI, whilst drainage and runoff losses are important for the system efficiency KPI. The code of practice recommends either making on-site measurements (no methods specified), or using previously measured values specific to the soil type, or using general values based on the soil texture. It is highlighted that the infiltration rate is temporally variable, according to the antecedent wetness and the duration of the irrigation event. Guidelines on the maximum application rates are provided according to soil texture, with values adjusted depending on the land slope and duration of the irrigation event. For

example, the maximum recommended application rate for a silt loam is 15 – 20 mm hr^{-1} for a 10 minute irrigation, decreasing to 5 – 10 mm hr^{-1} for a 60 minute irrigation.

Dairy farm effluent disposal

Dairy products are New Zealand's largest export earner (Statistics New Zealand, 2007), with considerable expansion in the intensity and area farmed over the last 15 years. Between 1994 and 2002 the dairy farming area increased by 12% and the average stocking rate by 19% (Ritchie et al., 2006b). This expansion and intensification has caused degradation of surface and groundwater quality (Close et al., 2008; Flemmer and Flemmer, 2008; Monaghan et al., 2008b; Monaghan et al., 2007b). The dairy industry has recognised the importance of this issue and prepared the Dairy Industry Strategy for Sustainable Environmental Management (DairyNZ, 2006). The strategy identifies reducing nitrogen and phosphate loss to water, and microbial contamination of surface water as priorities for the next 10 years.

The disposal of dairy shed effluent (DSE) is a major sustainable management issue. Between 1997 and 2000, 960 million cubic metres of DSE was produced (Flemmer and Flemmer, 2008). In response, the dairy industry has produced a comprehensive guide to the management of DSE (Ritchie et al., 2006a). Considerable focus is given to land treatment of DSE because it has become the preferred treatment option of Regional Councils (Houlbrooke et al., 2004). Ritchie et al. (2006a) set out a number of best management practices (BMP's) which are encouraged by regional councils. A key BMP is to avoid both surface ponding and DSE infiltrating below the topsoil (200 mm soil depth). Ideally DSE is only applied once the topsoil has dried to 50% of its water holding capacity, with a maximum application depth of 25 mm. Guidelines on the maximum application rates are provided according to soil texture, ranging from 32 mm hr^{-1} for sand and pumice soils, down to 10 mm hr^{-1} for silt loam and clay soils. An optimum BMP of 10 mm hr^{-1} or less is generally recommended by Regional Councils, with application rates >20 – 30 mm hr^{-1} considered risky.

There is considerable ongoing research on the effectiveness of land treatment of DSE, with a comprehensive review of the literature by Houlbrooke et al. (2004). This research indicates that there is still much progress to be made. Management of DSE applications on poorly drained soils, and soils that exhibit preferential flow behaviour is proving to be a major challenge, as is managing losses of total P and pathogens (Collins et al., 2007;

Houlbrooke et al., 2004; Houlbrooke et al., 2008; Monaghan et al., 2007b). Monaghan et al. (2008b) argue that there are a range of technologies that can deliver substantial improvements, but it is important that they are matched to the physical resources. Collins et al. (2007) specify soil type as a key factor in the transfer of faecal microbes to water, whilst Hawke and Summers (2006) raise concern that the majority of studies have been on only a few 'keystone' soil types. Increased knowledge of soil infiltration dynamics would be of high practical value to successful BMP implementation, particularly the interlinkage between infiltration and water storage attributes, and the activation of preferential flowpaths. The use of general 'rule of thumb' values, such as saturated infiltration rates based on soil texture, may no longer be appropriate.

Municipal and domestic sewage disposal

Municipal and domestic sewage disposal is an important issue for sustainable management in New Zealand, where approximately 1.5 billion litres of municipal and domestic wastewater are discharged every day. Most wastewater is treated by public wastewater treatment plants, although there are about 270,000 domestic on-site systems in New Zealand, disposing of wastewater for 15 – 20% of the population. In total, about 30 – 35% of wastewater is disposed of to land (Ministry for the Environment., 2007).

Concern about the performance of on-site disposal systems has prompted the National Environmental Standard for On-site Waste Water Systems to be proposed (Ministry for the Environment, 2008). The Ministry for the Environment estimates that the failure rates of onsite systems range from 15 – 50 %, which equates to between 40,000 and 130,000 systems nationally. Of particular concern is aging septic tanks, which represent the majority of domestic systems. Septic tanks are a 'primary' treatment system, with the majority of the wastewater treatment occurring in the soil of the disposal field. The primary reason for failure is that the hydraulic load does not match the drainage properties of the soil in the disposal field (Leonard and Gilpin, 2006; Ministry for the Environment, 2008). Run-off to surface water can occur if the hydraulic conductivity of the disposal field soil is exceeded, or rapid transfer to groundwater can occur if the hydraulic conductivity of the disposal field is too great.

All on-site systems require a land treatment disposal field, following the design criteria of Australia/New Zealand Standard 1547: 2000 (AS/NZS, 2000). The design options for the disposal field depend on the soil category determined by the soil texture. Measurement of

saturated hydraulic conductivity is recognised as a useful tool to confirm the soil category, but a morphology based soil description is seen as generally adequate. The soil category is matched to the best estimate of effluent infiltration capacity known as the long-term acceptance rate (LTAR). LTAR is always less than the saturated hydraulic conductivity, due to the effects of 'clogging mechanisms'.

Importantly, it is recognised that there is a limited LTAR database, which is extrapolated to other soils based on properties such as texture, structure, and permeability (AS/NZS, 2000). Improved knowledge of soil infiltration and water movement attributes would greatly benefit the LTAR database. This was demonstrated in a four year study of wastewater application to four different soil types (Barton et al., 2005; Sparling et al., 2006). Leaching losses varied significantly between soil types, and were not necessarily related to soil texture. The Pumice and Allophanic soils had the lowest losses, which were attributed to a porous soil structure promoting matrix flow, whereas the Gley soil had significantly larger losses attributed to strong preferential flow and a low-porosity matrix. There was also evidence that wastewater application sometimes resulted in a temporal change in soil hydraulic attributes, which has also been observed in other research (Cook et al., 1994b; Menneer et al., 2001; Vogeler, 2009). Although not mandatory in terms of regulations, the New Zealand Guidelines for Utilisation of Sewage Effluent on Land also clearly identifies the value of site-specific measurement of soil chemical and physical attributes, including infiltration rates, hydraulic conductivity and water-holding capacity (Whitehouse et al., 2000).

Municipal stormwater disposal

Disposal of urban stormwater to land has become an integral component of urban development in New Zealand (Christchurch City Council, 2008; NZWERF, 2004; Selwyn District Council, 2009). An example is the integrated catchment management plan for Lincoln township where 4 – 5% of the urban catchment is allocated to stormwater treatment (Selwyn District Council, 2008). Stormwater systems aim to act as both a storage mechanism to control the rate of discharge, and also as a contaminant filtering and buffering mechanism to remove contaminated particulate matter, reduce dissolved contaminant concentrations, and reduce the bioavailability of residual dissolved contaminants (Christchurch City Council, 2003). Stormwater contaminants may include

suspended solids, hydrocarbons, nutrients (e.g. nitrogen and phosphorus), heavy metals, micro-organisms and various chemicals.

Ground soakage facilities include soakage chambers, vegetated swales, rain gardens, infiltration basins, wetlands and riparian plantings. The specific design is strongly influenced by the likely contaminant level, soil type, and groundwater characteristics. Approval of any ground soakage area requires measurement of any soil limitations to absorb the discharge. This includes measurement of the site infiltration and water holding capacity, assessment of the soil's ability to treat contaminants in the discharge, as well as the potential effects of contaminant accumulation in the soil (Canterbury Regional Council, 2002). A critical function of these facilities is to have the capacity to absorb the 'first flush' stormwater (15 – 20 mm) which typically has the highest contaminant levels.

The soil infiltration rate (i_t) is the only soil attribute that has specific guidelines. Guidelines use steady-state ponded i_t derived from either a double-ring infiltrometer or subsoil percolation from a soakage pit (Christchurch City Council, 2003). Environment Canterbury argues that soakage pits give more accurate results than double ring infiltrometers, which tend to overestimate i_t by ~40%. In Canterbury, the maximum i_t of ground soakage areas is set at 50 mm hr^{-1}, with a minimum of 1 mm hr^{-1}, although the preferred minimum is 20 mm hr^{-1}. (Canterbury Regional Council, 2009; Christchurch City Council, 2003). In Auckland the minimum i_t is 3 mm hr^{-1}, or 30 mm hr^{-1} for areas of fractured basalt and associated highly permeable soils (NZWERF, 2004).

Despite the increasing use of ground soakage there appears to be little published research on its effectiveness under New Zealand conditions. Stormwater management guides provide only generalised treatment efficiencies, ranging from 10 – 80% depending on the type of soakage facility and pollutant (Christchurch City Council, 2003; NZWERF, 2004; Selwyn District Council, 2008). There has been some site-specific research, but this appears to be mostly confined to the Auckland region. Measurement of grassed swale infiltration characteristics found that they had poor physical condition for both plant growth and stormwater treatment (McLaren et al., 2005; Simcock et al., 2005). Infiltration followed preferential flowpaths, with compacted and low permeability layers at shallow depth leading to waterlogging and lateral flow. Research has also found the type of soil material affects the treatment efficiency of raingardens, where a layered soil (at least 1 m deep) is constructed to absorb and filter stormwater. Trowsdale and Simcock

(2008) found that a raingarden constructed using soil overburden from a limestone quarry was able to remove the majority of contaminants. Simcock et al. (2006) found that Allophanic soil material maintained a higher infiltration rate and treatment efficiency than the Ultic soil material typical of the Auckland area.

Research into soil contaminant management

Over the last 20 years New Zealand has seen considerable research investment into soil contaminant levels, transfer mechanisms, and potential mitigation techniques. There are a number of thorough reviews of the research into contaminant transfer from land activities. Cameron et al. (1997) provide an overall review of waste streams in New Zealand and the effects of land application of wastes on plant production, soil quality, and the environment. Contaminant transfer from pastoral agriculture has had substantial research, particularly with regard to nitrogen, phosphorus, and pathogen losses from dairy farming (Collins et al., 2007; Gillingham and Thorrold, 2000; Monaghan, 2008; Monaghan et al., 2008b; Monaghan et al., 2007). Considerable research has also been carried out on the fate and behaviour of pesticides (see Sarmah et al. (2004) for a review).

A recurring theme in contaminant transport research is the important influence of soil type (Collins et al., 2007; Monaghan, 2008). For example, in Canterbury much greater nitrogen leaching has been measured from stony Lismore soils compared to the deep stone-free Templeton soil (Di and Cameron, 2002a; Silva et al., 1999). A soil's winter-time drainage characteristics has been identified as critical for nitrogen leaching, particularly in cool-temperate regions where there is little winter-time plant growth (Monaghan, 2008). Two key soil mechanisms that are regularly identified are runoff and preferential flow, particularly in the studies of phosphorus, pathogen, and pesticides (Collins et al., 2007; Monaghan et al., 2007; Sarmah et al., 2004). These two mechanisms are directly driven by a particular soil's infiltration and water movement dynamics. For example, heavy textured and poorly drained soils are often more susceptible to runoff, as well as preferential flow where artificial drainage networks have been installed (Monaghan et al., 2007b; Wilcock et al., 2006). McLeod et al. (2008) found that although Allophanic and Pumice soils have a high infiltration capacity and conductivity (low runoff potential) they also have a high microbe retention capacity (low preferential flow potential). This was attributed to the high storage porosity of the fine structure, which has strong connectivity to infiltrating water due the extensive inter-aggregate pore network.

Environmental modelling

Environmental modelling is increasingly becoming an important tool for sustainable land management. Models that have implicit soil water movement algorithms tend to be applied at the pedon scale, usually to simulate specific experiments. The GLEAMS, LEACHM, HYDRUS, and SPASMO models are commonly used in New Zealand to simulate leaching of contaminants such as pesticides (Close et al., 2003; Sarmah et al., 2005; Sarmah et al., 2006); nitrate (Lilburne and Webb, 2002; Lilburne et al., 2003; Webb et al., 2001); faecal coliforms (Jiang et al., 2008; Pang et al., 2008); and heavy metals (Clothier et al., 2006). There are also examples of using these models to simulate contaminant transport at larger scales. HYDRUS has been used at the paddock scale to simulate pesticide transport (Pang et al., 2000) and the movement of a contaminant plume from septic tanks (Pang et al., 2006). The SPASMO model has also been used to simulate potential contaminant transfer from land application of municipal wastewater (Green, 2007) and future nitrate leaching from a disused sheep feedlot (Rosen et al., 2004).

Models used at farm to national scales tend not to use soil water movement functions *per se*, but use more general mass balances (Di et al., 2005; Elliot et al., 2008; Parfitt et al., 2008; Saggar et al., 2007). For example, the widely used OVERSEER model predicts phosphorus and nitrogen losses at the farm scale by using soil parameters such as soil type, depth, organic matter, texture, and drainage class to model drainage / runoff generated from the mean annual rainfall surplus (rainfall in excess of evapo-transpiration) (McDowell et al., 2005; Power et al., 2002; Thomas et al., 2005). The mass balance approach is justified on the grounds that large scale simulations are coarser in their predictive accuracy, with factors such as land-use pattern and climate variables tending to swamp the effect of profile-scale water movement processes. A criticism of water movement models is that they have a complex array of parameters, for which data are typically not available.

Future development of environmental models is likely to be within an integrated modelling platform, where models operating at different scales are nested. An example of this approach is the CLUES decision support system which integrates a number of models such as SPASMO and OVERSEER to predict the effects of land-use change at the catchment to national scale (Elliot et al., 2008). Within this type of framework soil water movement models such as SPASMO have a number of potential functions, such as

predicting contaminant transfer from specific high load sites (e.g. municipal stormwater disposal). These models will also continue to have an important role in exploring the interactions of various mechanisms driving experimental results, which will provide understanding that can be fed into models operating at coarser scales. As such, further research into infiltration and water movement dynamics can only enhance the predictive capabilities of models operating at all scales, particularly when there is characterisation of new soil types. An example of this knowledge transfer is the inclusion of hydrophobicity in the OVERSEER model. OVERSEER has also been used to demonstrate how better accuracy in estimates of nitrogen leaching could greatly improve estimates of national N_2O emissions (Clough et al., 2007; Thomas et al., 2005).

2.3 The demand for infiltration attributes: some key research gaps

It is clear from this review that the need for infiltration studies exists, driven by legislative requirements and industry best management practices. The review has highlighted the following research gaps:

1. A wider range of soil types needs to be characterised. Historically, research has been largely centred on a few key soil types (i.e. Te Kowhai, Horotui, Manawatu, Tokomaru, Templeton, and Lismore soils).

2. Preferential flow is a key transport process that needs to be an integral component of soil hydraulic characterisation.

3. Soil texture class is the most commonly used basis for predicting hydraulic attributes. The reliability of this approach should be determined, particularly because pedotransfer modelling results often show poor predictions when solely using texture.

4. Measurements should not just be confined to steady-state saturated infiltration, but also encompass near-saturated infiltration. Spray irrigation is widespread and should result in unsaturated infiltration. Land treatment of the 'first flush' stormwater will at least in part include unsaturated infiltration, and be influenced by soil attributes such as sorptivity, hydrophobicity, and preferential flow.

This study specifically addresses research gaps 2 and 4.

2.4 The use of tension infiltrometers in infiltration studies

Tension infiltrometers are the standard apparatus for measuring unsaturated infiltration (Cook, 2008; McKenzie and Cresswell, 2002b; Reynolds, 2008). A thorough review of the benefits and limitations of different infiltration measurement methods is provided by Clothier (2001), and methods to measure unsaturated conductivity are reviewed by Dirksen (2001). For field measurement of saturated infiltration, the use of ponded infiltration from a ring is still recommended (McKenzie and Cresswell, 2002b), primarily because of the low cost, ease of use, low skill requirement, and ease of data analysis (Clothier, 2001). It is for these reasons that ponded ring infiltration is generally how the land management industry quantifies soil infiltration behaviour (refer to previous section). However, a number of studies have shown that measuring just the saturated infiltration is not sufficient to understand a soil's infiltration behaviour, particularly because unsaturated infiltration is the norm in most soils (Jarvis, 2007). Also the abundance and connectivity of the macropore network can vary greatly, meaning near-saturated infiltration behaviour may not easily be predicted from just saturated infiltration measurements (Bagarello et al., 2000; White et al., 1992).

Clothier (2001) argues that tension infiltrometers have the highest overall utility, primarily because of the information content in the measurements. The value arises from quantifying infiltration behaviour under a range of surface imposed suctions, usually between 0 to 2 kPa. The cumulative infiltration curve is typically used to derive information about the transmission properties of a soil, in particular the hydraulic conductivity at matric potentials set by the suction of the infiltrometer (Lin and McInnes, 1995; McKenzie et al., 2001; Messing and Jarvis, 1993; Thony et al., 1991). The hydraulic conductivity function, $K(\Psi_m)$, can then be constructed from infiltration experiments at a range of suctions. Together with the soil water characteristic, $\theta_v(\Psi_m)$, the $K(\Psi_m)$ or the soil water diffusivity function, $D(\theta_v)$, are vital to understanding a soil's hydraulic behaviour, and are necessary for solving Richards' equation, which is the basis for many environmental models (Clothier and Scotter, 2002).

There has also been substantial research on the theory used to derive hydraulic attributes from infiltrometer data, particularly on deriving $K(\Psi_m)$ from three dimensional infiltration, with a number of thorough reviews in the literature (Angulo-Jaramillo et al.,

2000; Clothier and Scotter, 2002; Clothier, 2001; Logsdon and Jaynes, 1993; McKenzie et al., 2002d). The method of Reynolds and Elrick (1991) is recommended as the most robust by McKenzie et al. (2002d) and Reynolds (2008), where $K(\Psi_m)$ is derived from a sequence of steady-state measurements made at decreasing suctions at a single location. Derivation of $K(\Psi_m)$ is straight forward for one dimensional infiltration, such as in soil cores, where under steady-state flow $K(\Psi_m)$ is derived using Darcy's law. For laboratory measurements on soil cores the standard method is to apply the same suction as the infiltrometer to the core base, and then $K(\Psi_m)$ is simply equal to the steady-state infiltration rate (Cook, 2008; McKenzie et al., 2002e).

Another hydraulic parameter often characterised by tension infiltrometers is soil sorptivity (Clothier and White, 1981; Minasny and McBratney, 2000). Sorptivity describes the rate at which soil capillary forces (i.e. matric potential, Ψ_m) draw water into the soil during the initial stages of infiltration. Sorptivity has been shown to be particularly important for estimating the time to ponding, and thus the initiation of macropore flow and then surface runoff (Clothier et al., 1981; Kumke and Mullins, 1997). Methods to derive sorptivity from infiltration data are reviewed by Minasny and McBratney (2000). Effort has also been focussed on developing methods to use sorptivity measurements to derive other hydraulic attributes such as $K(\Psi_m)$, with a review of methods by Angulo-Jaramillo (2000) and Vandervaere et al. (2000). This research is driven by recognition that steady-state can often take a long time to attain and therefore may not be practically achievable, as well as that early-time infiltration contains considerable valuable information on other attributes (Angulo-Jaramillo et al., 2000).

Tension infiltrometer data have also been used to derive information about a number of other attributes, such as the mobile water content (θ_m) and the mass exchange coefficient (α), which determine the pattern of solute transport in soils with macropore networks (AnguloJaramillo et al., 1997; Casey et al., 1997; Casey et al., 1998; Clothier et al., 1995; Langner et al., 1999). Infiltration data are also used to characterise soil structural parameters, such as the characteristic mean pore size (λ_m), which can be used to quantify changes in soil structure resulting from perturbations such as rainstorms (White and Perroux, 1989), or soil tillage (AnguloJaramillo et al., 1997; Bodner et al., 2008; Reynolds et al., 1995; White et al., 1992).

The value of tension infiltrometers was demonstrated in the classic study of Clothier and White (1981), who showed that controlling the surface suction in order to exclude large macropores resulted in a sorptivity less than half that of saturated infiltration, when macropores were active. A review of preferential flow by Jarvis (2007) identifies that experimental evidence consistently shows preferential flow becoming increasingly important when Ψ_m wets to above -1 kPa. Tension infiltrometers allow researchers to isolate the macropore network which is responsible for preferential flow, and thereby study factors and processes which influence contaminant transport.

2.5 What mechanisms may influence the reliability of infiltration measurements?

Despite the widespread use of tension infiltrometers to study unsaturated infiltration behaviour, there are also a number of research articles that highlight the potential for uncertainty. Most of the sources of uncertainty are generic and could confound results regardless of the infiltration method (White et al., 1992). Examples of generic uncertainties are the effects of sample volume, hydrophobicity, and pore network instability, whilst instrument artefacts such as the effect of contact material are more specific to tension infiltrometers.

Despite hydraulic conductivity being one of the most variable soil attributes (Dirksen, 2001; Hillel, 1998; McKenzie and Cresswell, 2002b; Warrick and Nielsen, 1980), few studies include consideration of the magnitude and sources of uncertainty (Dirksen, 2001). This large variability means that a large number of samples are required to estimate the spatial mean with an acceptable level of confidence. This in turn equates to a high measurement cost, which is why there have been few surveys of soil infiltration and water transmission attributes.

The above factors not only contribute to the spatial variability, they also affect the quality of hydraulic attributes that are interpreted from the measurements. This is because interpretation of hydraulic behaviour is typically based on Richards' equation, which assumes that unique and definable $K(\Psi_m)$ and $\theta_v(\Psi_m)$ functions exist (Clothier and Scotter, 2002; Hopmans et al., 2002; White et al., 1992). For this assumption to be valid, any effects of mechanisms such as temperature, entrapped air, water repellency, and non-uniform wetting due to preferential flow would have to be negligible. Further, the soil

pore network is also assumed to be temporally stable, so dynamic mechanisms such as swelling, biological activity, and cultivation should have negligible effect (Clothier and Scotter, 2002; Hopmans et al., 2002).

It has been suggested that a substantial proportion of the variability that has been measured for hydraulic conductivity may be due to uncertainty arising from the measurement technique, such as inappropriate sample volumes (McKenzie and Cresswell, 2002b). This following section reviews potential sources of uncertainty in tension infiltrometer measurements.

2.5.1 Instrument error

Tension infiltrometer errors

Tension infiltrometers are generally constructed and operated according to the criteria of Perroux and White (1988). They specified criteria designed to avoid errors introduced by the conductivity of the infiltrometer membrane, and the size of the air-entry pipe from the bubble tower to the disk. Criteria were also provided for the sorptivity and conductivity of the contact material (discussed in the following section), as well as the design of the bubble tower used to set the suction imposed by the infiltrometer.

Since this original design, there have been a number of proposed modifications. Some have been minor, such as the design of Ankeny et al. (1988) where the bubble tower has multiple air-entry tubes at pre-set depths corresponding to suctions of interest, with a particular suction simply selected by opening and shutting of inlet valves on each tube. Close et al. (1998) argue that tension infiltrometer measurements are sensitive to small variations in experimental procedures. They emphasise great care should be taken to seal the edges of the infiltration membrane to the disk to prevent air leaks when under suction. They further recommend that pre-soaking the disk before experiments also improves the membrane's ability to hold the applied suction. It is also recommended that the tension infiltrometer should be pre-tested for air leaks, as well as to calibrate the correct water level in the bubble tower to achieve the desired surface-imposed suction (Ankeny, 1992; McKenzie et al., 2002d; Reynolds, 2008).

A number of authors emphasise the importance of having the capability to use different sized water reservoirs, as suggested by Perroux and White (1988). This capability means the reservoir diameter can be matched to the expected flow rate, with a small diameter

used for increased accuracy of measuring slow infiltration rates (Ankeny et al., 1988; Walker et al., 2006). Pressure transducers are also being increasingly used to automatically measure the changes in reservoir water height as infiltration proceeds. Casey and Derby (2002) show that the best method is to use a differential pressure transducer, which has a very high precision in measuring the water height (standard deviation = 0.05 mm), and virtually eliminates problems in measuring water height caused by bubbling. A number of other advantages have been identified, such as increasing the measurement speed and resolution, particularly during early-time and under high infiltration rates. Likewise, automatic measurement is particularly useful under slow infiltration, allowing longer experiment duration (e.g. overnight), as well as improving the capability for simultaneous operation of multiple infiltrometers, and improving the ease of data management for analysis (Ankeny, 1992; Ankeny et al., 1988; Casey and Derby, 2002; Johnson et al., 2005; White et al., 1992). However, there are some reservations over the reliability of automated systems, mostly over the sensitivity of pressure transducers under field conditions (Ankeny, 1992; McKenzie and Cresswell, 2002b).

It has also become common to use a two piece infiltrometer, where the water reservoir is mounted separate to the disk, and connected by a flexible supply tube (Casey and Derby, 2002; Walker et al., 2006). The primary reason for this is to minimise compaction of the soil surface by the weight of infiltrometer, as well as minimising disruption to the infiltrometer contact caused through small movements of the reservoir by the wind or the operator (McKenzie et al., 2002d). However, Walker et al. (2006) have shown that the size of water supply pipe can affect the infiltrometer suction. Under high flow rates (>200 cm^3 min^{-1}) the frictional resistance of the standard 12.7 mm diameter supply tube caused the infiltrometer suction to increase by up to 0.15 kPa. An alternative approach has been proposed where a single-piece infiltrometer is used with a supporting tripod that clamps around the reservoir. The tripod acts to hold the infiltrometer steady, as well as supporting the infiltrometer weight (Ankeny, 1992; Prieksat et al., 1992).

Temperature-induced pressure fluctuations within the air-space of the water reservoir and bubble tower are another source of error (Castiglione et al., 2005b; Castiglione et al., 2005). Pressure fluctuations are caused by air-pockets being confined and not completely free to expand or contract in response to temperature variations. This effect only becomes

strong under slow infiltration where the bubble rate is low (Castiglione et al., 2005b). On field soils the infiltration rate is usually sufficiently fast that the high bubble rate and decreasing reservoir water level tend to mitigate any temperature-induced pressure fluctuations. These experiments also tend to be of short-duration which often reduces the scale of temperature fluctuations (Castiglione et al., 2005b).

Poor soil surface contact

Good contact between the infiltrometer base and the soil is essential when using tension infiltrometers (Perroux and White, 1988). To ensure good contact a smooth layer of contact material must be placed on the soil surface (Clothier, 2001; McKenzie et al., 2000; Minasny and McBratney, 2000; Reynolds, 2006; Reynolds, 2008; Reynolds and Zebchuk, 1996). Despite its importance, most researchers have paid little attention to the potential effect of the contact material on their results (Reynolds and Zebchuk, 1996).

It is well recognised that the initial wetting of the contact material can limit the use of early-time infiltration data. This is because the high sorptivity of the contact material can mask the response of the soil and make it difficult to identify when infiltration into the soil begins. To overcome this problem a number of methods have been developed to identify the initial period of contact material wetting in the cumulative infiltration data (Cook, 2008; Minasny and McBratney, 2000; Reynolds, 2008). Minasny and McBratney (2000) have also found that, even after accounting for the effect of the initial contact material wetting, early-time infiltration was always faster when contact material was used, and attributed this to better contact with the soil surface. In other experiments using the same material as the present study, no difference was found in the saturated long-time i_t between the tension infiltrometer and ponded infiltration (Bagarello et al., 2000), whereas during unsaturated infiltration long-time i_t was 30% greater (Bagarello et al., 2001). In contrast, Everts and Kanwar (1993) found that the use of a medium sand contact material significantly reduced the saturated i_t, compared to ponded infiltration. However, Bagarello et al. (2000) repeated their experiment and found no effect on the saturated i_t when using two different contact materials.

Additional research has also shown that the suction applied by the tension infiltrometer is 'offset' by the contact material, resulting in a lower suction applied at the soil surface (Reynolds and Zebchuk, 1996). This loss of suction was found to vary according to flow rate and the contact material thickness. Reynolds (2006) shows that this discrepancy can

affect the accuracy of derived hydraulic attributes, particularly in the macropore range where small changes in soil matric potential can result in large changes in conductivity.

Close et al. (1998) used an iodide dye to visually map the infiltration pattern from a tension infiltrometer through the contact sand and into the soil. For repeat experiments under the same unsaturated suction (0.3 kPa) i_t was positively correlated with the dyed area. The pattern of flowpaths in the soil also generally followed the wetting pattern of the contact material. Unfortunately, the physical and hydraulic attributes of the silica sand contact material were not specified. Experience at Lincoln University has shown that it is difficult to achieve reliable contact using fine to medium silica sand (Neil Smith, pers. comm.). Also the experiments of Close et al. (1998) used dry soil columns (4.6% moisture by weight), which raises the possibility that hydrophobicity may have been present.

To address these issues it has been suggested that greater attention be paid to both the type and preparation of contact material (Bagarello et al., 2001; Reynolds and Zebchuk, 1996). In the original design specifications for the tension infiltrometer, Perroux and White (1988) specified that the contact material should be of minimal thickness (3 – 5 mm), have a sorptivity and conductivity that is higher than the soil's, and that these attributes should change minimally as the suction applied by the infiltrometer increases. Reynolds and Zebchuk (1996) identified a glass bead material which met these criteria, with additional benefits of chemical inertness, reusability, and low variability in hydraulic attributes. A modified form of Darcy's law was proposed to allow calculation of the offset in surface suction caused by the contact material. It has also been recommended that a membrane be placed between the contact material and the soil surface to prevent the contact material infilling macropores (Bagarello et al., 2001; Reynolds, 2008; Reynolds and Zebchuk, 1996). Close et al. (1998) also developed a preparation technique to improve the contact uniformity between the infiltrometer and the contact material.

The use of tensiometers with tension infiltrometers

It is clear that there are a number of areas in the design and operation of tension infiltrometers where the suction applied by the infiltrometer may be compromised. This supports the argument by Dirksen (2001) that measurements of $K(\Psi_m)$ should not rely on the externally applied hydraulic gradient, but that the hydraulic gradient *within the soil* should be directly measured with tensiometers. Unfortunately, this is not the standard

practice with tension infiltrometers, as almost all published research implicitly assumes that the infiltrometer suction sets the Ψ_m of the soil. In two of the few experiments that have measured Ψ_m under a tension infiltrometer, both Wang et al. (1998b) and Silva et al. (1999) observed that Ψ_m did not match the applied surface suction. In these studies, Ψ_m was 1 to 7 kPa more negative than the applied infiltrometer suction. Importantly, the study of Wang et al. (1998b) shows that this discrepancy can occur at shallow depth (2.5 and 5 cm depth), whilst in the leaching study of Silva et al. (1999) Ψ_m was consistently more negative at all depths of a 70 cm deep lysimeter, and over long-time periods of 2 to 10 weeks.

However, tensiometers require careful calibration and installation to minimise errors, particularly where there is a small hydraulic gradient or small flux (Dirksen, 2001; Fluhler et al., 1976; Mohrath et al., 1997; Schwarzel et al., 2006; Tamari et al., 1993). Tensiometer error largely arises from the accuracy in the pressure calibration and in defining the depth of installation. It is important to note that most of these studies use an evaporation method to determine $K(\Psi_m)$, where the flux is small and there are small depth increments (2 – 10 mm) between tensiometers. Both of these increase the sensitivity to tensiometer errors. Dirksen (2001) also recommends increasing the number of tensiometers at a particular depth, in order to reduce relative error.

2.5.2 Identification of steady-state flow

Interpretation of tension infiltrometer data relies on the shape of the cumulative infiltration curve. The most common model used to represent infiltration behaviour is that of Philip (1957), which predicts that at early-time sorptivity should dominate and cumulative infiltration (I) should be linear with the square root of time, whilst at long-time, gravity should dominate and I will be linear with time, and reflect the soil hydraulic conductivity.

In general, steady-state analysis is the preferred method to interpret $K(\Psi_m)$ as it is seen to be more accurate, but steady-state can take a long time to reach, making measurements more costly (Dirksen, 2001; White et al., 1992). The time to reach steady-state can vary greatly among soils. White et al. (1992) generalise that steady-state flow usually takes under six hours for field measurements with a 200 mm diameter disk, but may be much longer for heavy textured soils. Thony et al. (1991) found that the early-time phase lasted

for 5 hours for a heavy clay soil, but only 8 seconds for a loam. Cook and Broeren (1994) observed that for the same soil type the time to reach steady-state varied greatly between 1 and 69 hours, depending on the disk radii and the suction applied. In a review of infiltration studies, White and Sully (1987) calculated that steady-state took between 1 and 34 hours, with a geometric mean of ~ 2 hours. They proposed that under saturated infiltration, steady-state is achieved in the order of 1 – 10 hours.

Recognising steady-state requires subjective judgement and patience (Clothier, 2001; Wang et al., 1998b; White et al., 1992). Vandervaere et al. (2000) argues that it is often questionable to assume that a real steady-state has been reached at the end of an experiment. In theory, steady-state flow is achieved when the cumulative infiltration curve becomes linear. As a guide, McKenzie et al. (2002d) recommend the linear slope should be constant for a minimum of five consecutive measurements. The standard laboratory method for cores or columns is to identify when drainage matches infiltration (Cook, 2008; Dirksen, 1999). If the flux at both ends of the column is equal, then it is assumed that the hydraulic gradient must also be constant. Dirksen (2001) recommends that the most robust method to determine steady state is to measure directly the hydraulic gradient, where a time-constant water flux and hydraulic gradient equates to steady state conditions. Where previous knowledge of the likely magnitudes of hydraulic attributes are available, then the expected time to steady state can be estimated using the following equation (White and Sully, 1987),

$$t_{grav} = \left(\frac{S(\Psi_0, \Psi_i)}{K_0 - K_i} \right)^2 \qquad \text{Equation 2-1}$$

where S is the soil sorptivity (a function of the supply water potential Ψ_0 and the antecedent soil matric potential Ψ_i); K_0 is the conductivity at the supply water potential and K_i is the conductivity at the antecedent soil matric potential. Philip (1969) defines t_{grav} as the time at which the effect of gravity on flow equals that of capillarity.

Where it takes prohibitively long to reach steady-state, it has been suggested that it may be best to focus on early-time data from which much useful information can be extracted (Cook and Broeren, 1994; White et al., 1992). However, in practice, the early-time phase is often short and difficult to identify, particularly when obscured by the initial infiltration into the contact material (Clothier, 2001).

2.5.3 Sample volume

Sample volume is an important source of variability for measurements of hydraulic conductivity at Ψ_m between -10 to 0 kPa (i.e. field capacity to saturation), where the majority of water transmission occurs through macropores (Iwata et al., 1995; McKenzie and Cresswell, 2002c; Miyazaki, 2006). Determination of an appropriate sample volume is often based on the concept of a representative elementary volume (REV), which is defined by Bear (1972) as the smallest volume that contains a representation of the variation in all element forms and proportions present in a system.

The REV will be dependent on both the nature of the process under investigation, and the scale at which the process is being studied (Iwata et al., 1995; Miyazaki, 2006; van Es, 2002). For example, an REV for studying water movement is likely to be much larger for saturated macropore flow, than unsaturated flow through mesopores at field capacity. The REV for saturated infiltration into a soil with macropores has been proposed as at least 0.5 metres length, increasing to > 5 metres at the paddock scale (Miyazaki, 2006). Lauren et al. (1988) estimated a representative area of 0.5 m^2 for their structured clay soil, whilst McKenzie et al. (2002b) recommend laboratory measurements should use cores 22 cm diameter and 20 cm deep. As a general indication it has been proposed that a REV should contain at least 20 structural units (McKenzie and Cresswell, 2002c; van Es, 2002).

Effect on hydraulic conductivity measurement

Research has generally focussed on the effect of sample volume on a horizon's saturated hydraulic conductivity (K_{sat}). Whilst variability consistently decreases as sample height and area increase, the mean may increase or decrease, depending on the spatial distribution of macropores. The classic study is by Anderson and Bouma (1973), who used dye to show that the vertical continuity of macropores was artificially enhanced in the shorter cores. They concluded that as sample height increased, the vertical continuity in macropores decreased and their effect on water flow became less significant and K_{sat} decreased.

Similar results were obtained by Lauren et al. (1988), who measured the effect of sample area on the K_{sat} of a clayey textured horizon *in situ* at 37 locations using five different sized columns, with successively smaller columns constructed within the previous column. Iversen et al. (2001) concluded that the REV was different among types of soil.

Three horizons from each of two structured clay loam soils and two structureless sandy soils were compared. The structured soils had more variable K_{sat} values, with different core sizes leading to statistically different K_{sat} in four of the six horizons, as well as the profile average of the three combined horizons. For the unstructured soils there was no significant difference between the profile average K_{sat} values, although a sample volume effect was observed for three of the six horizons. Fuentes and Flury (2005) is the only study that includes the effect of sample volume on unsaturated hydraulic conductivity. Hydraulic conductivity varied considerably with core length, and showed a strong volume effect when Ψ_m was wetter than -1.2 kPa. However, the usefulness of the study is limited because only a single, small 9 cm diameter core was used.

Effect on solute transport

Despite the large amount of research published on solute transport, there appears to be little research on the effect of sample volume on the measurement of solute transport processes such as preferential flow. The effect of sample volume on water and solute transport was researched by Parker and Albrecht (1987) for the A and B horizons of a clayey textured soil. For both horizons it was observed that the mean K_{sat} and solute dispersivity increased as sample volume increased. The breakthrough curves of solute concentration in drainage water were similar for the small and medium cores, whereas the breakthrough curve of the large cores was markedly different for both soil horizons. However, the reliability of the research may be limited as the core sizes are still small compared to the potential REV, as indicated by other research on clayey textured soils (Davis et al., 1999; Lauren et al., 1988).

Effect on spatial variability

The effect of using three different sample volumes to measure the spatial variability in K_{sat} along a transect for a sandy loam soil was studied by Mallants et al. (1997). It was observed that as the sample volume increased the mean and variability of K_{sat} values decreased, and it was concluded that the changes in variability were most likely a reflection of the degree to which the soil macro-pore network was represented. Haws et al. (2004) observed a similar pattern of decreasing spatial variability as the sample area increased when measuring the saturated surface infiltration of one soil type at the hillslope scale, as well as at the landscape scale, which combined three different soil types. At both scales an infiltration area of 20 x 20 cm could not reveal the spatial

structure because local scale heterogeneities dominated, whereas the spatial structure became clearer using sample areas of 60 x 60 and 100 x 100 cm. In contrast to Mallants et al. (1997), the mean values increased as the sample area increased.

Relevance for modelling

Despite the sensitivity of water and solute transport models to the accuracy and precision of soil hydraulic parameters (Walker et al., 2000; Zavattaro and Grignani, 2001), little research has focussed on validating models using parameters derived at different sample volume scales. The sensitivity of a catchment water yield model to laboratory measured K_{sat} using different-sized cores from a clayey textured soil was researched by Davis et al. (1999). Model outputs produced good predictions using data from the large cores (22.3 x 30 cm core), but were extremely poor when using the small cores (6.3 x 7.3 cm), which had measured K_{sat} values one to three orders of magnitude lower. It was concluded that the small cores were not of sufficient size to incorporate macropores, and therefore represented properties of matrix flow. Significant changes in the macropore network were observed to occur with depth, and indicated that the REV would not necessarily be the same for all layers of a soil.

Sample volumes used in New Zealand research

In the national SWAMP study the surface soil K_{sat} was measured *in-situ* using ponded infiltration from dual rings of different sizes (10 to 50 cm diameter), whilst the K_{sat} and unsaturated hydraulic conductivity of subsoil horizons was measured using small cores (98 mm diameter by 65 mm high) (Joe and Watt, 1984; Watt and Vincent, 1991; Watt et al., 1992). A number of other studies have also used similar-sized small cores to measure saturated and unsaturated hydraulic conductivity (Drewry and Paton, 2000b; Drewry et al., 2000; Greenwood, 1999; Greenwood and McNamara, 1992; Singleton et al., 2000; Webb, 2003; Webb et al., 2000). Slightly smaller cores have been used to measured unsaturated conductivity near field capacity (Gradwell, 1974; Gradwell, 1979; Gradwell and Rijkse, 1988). The *in-situ* field measurements of ponded surface infiltration rate have tended to use dual rings of similar size to the SWAMP study (Greenwood, 1999; Taylor et al., 2008), whilst Cook and Broeren (1994) measured *in-situ* unsaturated surface infiltration from 5 and 10 cm diameter tension infiltrometers.

Although there has been no direct study in NZ on sample volume effects on infiltration measurements, the research reviewed in this section indicates that small core size used in

the SWAMP study is not likely to contain an REV for many soils, particularly for measuring hydraulic conductivity in the macropore range (i.e. at or near saturation).

2.5.4 Soil heterogeneity

Hydrophobicity

Hydrophobicity is a widespread phenomenon in field soils. A detailed bibliography of worldwide research is given by Dekker et al. (2005). It is generally attributed to organic coatings on soil particles causing a non-zero contact angle between soil and water. Severe repellency occurs when the contact angle is larger than 90^{o}, whereas 'sub-critical' hydrophobicity occurs when the contact angle is between $0 – 90^{o}$. Sub-critical hydrophobicity is often difficult to observe because wetting does occur, albeit at a retarded rate, although it is recognised as the most widespread form of hydrophobicity (Wallis et al., 1991). It has also been claimed that most soils will exhibit some degree of sub-critical hydrophobicity (Hallett et al., 2001), particularly in uncultivated soils (Doerr et al., 2006; Jarvis et al., 2008).

Sub-critical hydrophobicity is increasingly recognised as a mechanism that can inhibit early-time infiltration rates and patterns (Jarvis et al., 2008). Tillman et al. (1989) observed that sub-critical hydrophobicity lowered the potential topsoil sorptivity by an order of magnitude, even though there was no visual evidence of hydrophobicity. Wallis (1991) showed that 14 New Zealand soils from three different regions, with a wide range of textures, all exhibited varying degrees of hydrophobicity at field moisture conditions. Even for soils with weak apparent hydrophobicity it was demonstrated that early-time infiltration could potentially be reduced by approximately one order of magnitude, under a five minute, high intensity rainfall of 5 year return interval. Clothier et al. (2000; 1996) observed that the influence of sub-critical hydrophobicity persisted for about 100 minutes. Concern was raised that many tension-infiltrometer experiments are of similar short duration, meaning the presence of sub-critical hydrophobicity could easily be missed, and lead to under-estimates of attributes such as hydraulic conductivity.

Hydrophobicity has also been identified as an important mechanism that generates preferential flow. Research has observed this phenomenon in sand, loam, heavy clay, and peat soils, but the majority of work has been in the Netherlands and has focussed on the generation of preferential 'finger' flow in hydrophobic sandy soils (Dekker et al., 2005;

Jarvis et al., 2008). Although both hydrophobicity and preferential flow have been observed to have widespread occurrence in NZ soils, only Clothier et al. (2000) studied the interrelationship. It was concluded that hydrophobicity did generate preferential flow, which over long-time infiltration weakened as hydrophobicity broke down.

Air encapsulation and entrapment

Infiltration is effectively a two-phase flow system, where infiltrating water also displaces pore air (Faybishenko, 1999; Hillel, 1998). Generally it is thought that this displacement occurs readily, and therefore infiltration only needs to be studied purely in terms of the water phase dynamics. However, studies have shown that the air phase can have a large influence on infiltration, either as entrapped air ahead of the wetting front, or as encapsulated air bubbles in the transmission zone (Constantz et al., 1988; Faybishenko, 1999; Wang et al., 1997).

Air encapsulation is thought to occur because the pore velocity varies across different parts of the pore network, meaning some pore spaces fill before others (Constantz et al., 1988). During saturated infiltration into different soils it has been shown that encapsulated air reduced the potential infiltration rate by 0.5 to 2 orders of magnitude (Constantz et al., 1988; Faybishenko, 1999). Air encapsulation is thought to be greatest in soils with a large distribution in pore water velocities (e.g. strongly aggregated soils), although the key factor is not the volume of encapsulated air, but its impact on the connectivity of the infiltrating pore network. For example, Constantz et al. (1988) measured during saturated infiltration that encapsulated air was three times greater in a sand compared to a loam soil, yet the effect on the infiltration rate was the same. The effects of air encapsulation may also vary during an infiltration event, with Faybishenko (1999) showing that approximately half of the encapsulated air can be considered mobile and moves together as bubbles with the infiltrating water, and half is immobile and can only be slowly removed by dissolution into water. Fayer and Hillel (1986) consider that it would take at least several days of infiltration before diffusion into water of the immobile air starts to become important.

Air entrapment occurs where a high water table (within 2 metres of the surface) or slowly permeable subsoil restricts the displacement of soil air, and has been observed under flood irrigation or intense sprinkler irrigation (Fayer and Hillel, 1986; Grismer et al., 1994; Hammecker et al., 2003; Latifi et al., 1994; Navarro et al., 2008). Wang et al.

(1998) identify that entrapped air can often cause a surging infiltration rate (i_t), where i_t initially slows as entrapped air restricts wetting front penetration. Entrapped air will then continue to compress until the air pressure is sufficient that it escapes to the surface, which causes a sharp drop in air pressure ahead of the wetting front, allowing it to advance more rapidly and i_t to increase.

It is important to note that research seems to have focussed on the effect on saturated infiltration, even though unsaturated infiltration is more typical in field soils. In terms of New Zealand research there appears to be no research on the effects of air encapsulation / entrapment. Air encapsulation / entrapment could also be an important mechanism during unsaturated infiltration. For example, during near-saturated infiltration air encapsulation may block a macropore and slow infiltration markedly. Conversely encapsulation in mesopores may result in localised wetting such that macropore flow is activated.

Preferential flow

The most commonly encountered limitation for deriving soil hydraulic attributes from infiltration data is the requirement that the soil be uniform and homogeneous (White et al., 1992). This assumption sees infiltration progressing as a uniform piston-like wetting front moving downwards sequentially through one soil layer and then the next (Smettem and Smith, 2002). Typically this assumption is thought to be true when infiltration is confined to the soil matrix, where variations in pore water velocities are not great, and capillarity is able to even out local heterogeneities. However, once the flux exceeds the saturated conductivity of the matrix, water can enter macropores, often greatly increasing the range of conducting pore water velocities, resulting in preferential flow and non-uniformity in the wetting pattern (Clothier, 2001). A number of other mechanisms can also generate preferential flow, such as hydrophobicity, air encapsulation, and textural layering.

A common characteristic is that preferential flowpaths can cause the wetting front to initially by-pass large areas of the soil matrix, resulting in a complex array of wetting fronts progressing both vertically and laterally. Another outcome of activating preferential flowpaths is that they can considerably shorten the time for the wetting front to reach lower soil layers. Overall this can affect measurements as the infiltration rate may not follow the simple two-phase pattern predicted by the Philip model, but rather

reflect a complex interaction where flow through different parts of the pore network is dominated by either capillary or gravity forces.

The occurrence and mechanisms of preferential flow behaviour have been widely studied in the literature, with a number of thorough reviews (Beven and Germann, 1982; Bouma, 1981; Clothier et al., 2008; Hendrickx and Flury, 2001; Jarvis, 2007; Miyazaki, 2006). A key finding of Jarvis (2007) is that experimental evidence consistently shows that preferential flow becomes increasingly important as Ψ_m wets to above -1 kPa. This is the operational range of tension infiltrometers, and is one of the prime reasons why their use has become so popular. Despite this, many tension infiltrometer applications assume that infiltration occurs uniformly, even though research indicates that preferential flow behaviour is common in many soils. Interestingly, it is also apparent from these reviews that there has not been much research on the effect of preferential flow behaviour on tension infiltrometer measurements, and the subsequent derivation of hydraulic attributes, even though non-uniformity is often attributed as the cause of negative $K(\Psi_m)$ values when using steady-state analysis (White et al., 1992).

In the first section of this review it was shown that preferential flow has been identified as an important mechanism in the transport of a number of contaminants through New Zealand soils. An initial national survey indicates that the potential for preferential flow is likely to be widespread in New Zealand soils (McLeod et al., 2008; McLeod et al., 2003), although this has been limited to only 10 soil types under constant flux irrigation of 5 mm hr^{-1} (McLeod et al., 2004; McLeod et al., 2003; McLeod et al., 2001; Pang et al., 2008). However, the frequency and mechanisms behind the initiation of preferential flow are not well understood, except perhaps for a few intensively studied soils such as the Manawatu fine sandy loam.

Soil layering

A common assumption of infiltration measurements is that there will be sufficient time for steady-state infiltration to develop before interference from the wetting of lower layers, which may have distinctly different $K(\Psi_m)$ relationships (McKenzie and Cresswell, 2002b). This assumption is the major weakness of *in-situ* tension infiltrometry according to Dirksen (2001). Soil layering can also violate the assumptions that the measurement volume is homogeneous with a uniform antecedent water content (Vandervaere et al., 2000). A number of studies have also demonstrated that soil layering can be a key

phenomenon in instigating preferential flow, particularly fingering, when a layer of fine texture overlies a coarse textured layer (Hill and Parlange, 1972; Miyazaki, 2006).

The expected behaviour of infiltration into layered soils is thoroughly reviewed by Iwata (1995). In essence, if soil layers have contrasting $K(\Psi_m)$ curves, then the infiltration behaviour should be driven by layer interactions as each soil layer attempts to match Darcy velocities, by adjusting Ψ_m and thus the layer conductivity. For example, if $K_{\text{layerA}} > K_{\text{layerB}}$, then excess water will accumulate at the base of layer A, causing Ψ_{layerB} to increase until the Darcy velocity is in equilibrium (i.e. layer B gets *wetter*). Conversely, if $K_{\text{layerA}} < K_{\text{layerB}}$ then the water supply from layer A is limiting, causing Ψ_{layerB} to decrease until the Darcy velocity is in equilibrium (i.e. with layer B *drier* than layer A). In practice the response from an individual layer is not instantaneous, and it is likely that feedback loops occur. For example, if $K_{\text{layerA}} < K_{\text{layerB}}$ then Ψ_{layerB} will decrease (i.e. drain), but if the response is slow then at least the lower part of layer A will also drain because K_{layerB} is higher, which may further reduce K_{layerA} and causing Ψ_{layerB} to decrease further.

This behaviour was observed by Silva et al. (1999) who measured Ψ_m at 3 depths in a lysimeter during saturated and unsaturated (0.5 kPa surface suction) leaching experiments, over respective 2 and 10 week time periods. At all depths Ψ_m was consistently 1 to 4 kPa more negative than the applied surface suction. This was attributed to self-adjustment in a vertically layered soil profile, where Ψ_m kept adjusting toward an equilibrium profile, with a local conductivity and hydraulic gradient in each layer that maintained a constant Darcy velocity through the profile.

There have been both experimental and theoretical studies on infiltration into layered soils (Chu and Marino, 2005; Smith, 1990; Yang et al., 2006), but Iwata (1995) notes that overall, experimental data are insufficient. Most studies have been on the effects of surface crusts (Smith, 1990), fingering, or water storage dynamics in fine over coarse textured soils. Smettem and Smith (2002) have also identified that there has been no detailed investigation of the effect of soil layering on surface-measured hydraulic attributes derived from infiltration studies. This is important, because in practice soil layering occurs near the soil surface (Vandervaere et al., 2000; White et al., 1992).

The potential problems of soil layer interference is a strong justification for concentrating on measuring early-time infiltration, where the smaller sample volume is more likely to

comply with the necessary assumptions of homogeneity and uniform water content (Clothier and Scotter, 2002). Alternatively, Lin and McInnes (1998) measured $K(\Psi_m)$ of a clayey subsoil during a single tension infiltrometer experiment by incrementally reducing the suctions from 1.2 to 0 kPa, with only short equilibration times of 10 to 30 minutes. They argue that because the soil was pre-wet that quasi-steady infiltration could be reached in a few minutes, which is as good an estimate of steady infiltration rate that can be expected under most field conditions, and avoids problems with interference from a lower layer. Using dye analysis they showed that, when the experiment was limited to unsaturated infiltration, the wetting front penetrated 0.2 m depth, but when it included saturated infiltration the front reached 0.4 to 0.5 m. The dye also showed that for all the experiments infiltration was highly non-uniform and confined to preferential flowpaths, which raises questions about the assumption of steady-state flow. The New Zealand National Soils Database also shows that it is not uncommon for layering to occur within 0.2 m depth, which brings into question the universal validity of this approach.

Hysteresis

It is generally recognised that $K(\Psi_m)$ is hysteretic, usually to the extent that $\theta_v(\Psi_m)$ is hysteretic (Dirksen, 2001). This is important because different methods of determining water movement attributes use different approaches, such as measuring $K(\Psi_m)$ during wetting or draining, as well as during downward or upward flow. The likelihood of hysteresis means that great care should be taken in combining data from different methods to widen the range over which $K(\Psi_m)$ is characterised (McKenzie et al., 2001). Care also needs to be taken in appropriate application of the data, such as only using data measured during downward wetting to model infiltration behaviour.

The value of tension infiltrometers is that they allow us to study the near-saturated *wetting* behaviour of a soil. However, McKenzie et al. (2002b) argue that while most field experiments measure the wetting curve of $K(\Psi_m)$, most laboratory experiments measure the desorption curve. Close et al. (1998) also identify that soil is often prewet or even saturated prior to taking negative head readings. This approach is the basis of the method proposed by Ankeny (1991) and McKenzie et al. (2002e), where steady-state saturated flow is established, then a sequence of steady-state measurements are made as the suction is progressively increased. However, White et al. (1992) note that whilst this approach allows rapid measurement, it may be affected by drainage-induced hysteresis.

McKenzie et al. (2001) measured significant hysteresis in nine different soils when $K(\Psi_m)$ was measured by tension infiltrometer in steps of decreasing suction (i.e. wetting) or increasing suction (i.e. draining). Logsdon et al. (1993b) observed that hysteresis was more evident at 0.3 kPa suction where differences of 120 – 160% in $K(\Psi_m)$ were measured, compared to only 20% difference in values at 1.5 kPa suction. Bargarello et al. (2005) observed the same pattern, consistent with the claim by McKenzie et al. (2002b) that hysteresis is only significant at matric potentials very close to saturation.

To overcome the problems of hysteretic behaviour, Dirksen (2001) suggests determining $K(\theta_v)$, which typically exhibits negligible hysteresis (Dirksen, 2001; McKenzie and Cresswell, 2002b). However, this involves measurement of θ_v *in-situ*, and assumes that θ_v is uniform with depth. The other problem is the sensitivity of the water content measurement devices where accuracies of ± 1 – 3% are typical. This sensor accuracy may become quite restrictive in characterising $K(\theta_v)$ of the macropore network, where a only a small increase in θ_v can result in a large increase in conductivity.

Pore network instability

A fundamental assumption when interpreting soil hydraulic attributes from infiltration data is that the pore network is rigid and stable with time. As previously noted, stability is particularly important for application of Richards' equation, which assumes that unique and definable $K(\Psi_m)$ and $\theta_v(\Psi_m)$ functions exist. However, a number of studies have shown that this is a tenuous assumption. Temporal dynamics in $K(\Psi_m)$ have been shown to be particularly strong in soils with shrink / swell characteristics, such as vertic soils with swelling clays or soils high in organic matter (Bagarello et al., 2006; Dikinya et al., 2008; McKenzie and Cresswell, 2002b). Excessive exchangeable sodium which can arise from irrigation and groundwater management practices, can cause structural collapse and decline in $K(\Psi_m)$. Although there have been many studies on soils with these attributes, characterising their hydraulic behaviour remains a substantial challenge (Bagarello et al., 2006; McKenzie and Cresswell, 2002b; Smiles, 2002).

Changes in $K(\Psi_m)$ due to climatic variation, ranging over time scales from a few hours following a rainfall event to seasonal changes have been observed (Bodner et al., 2008; Messing and Jarvis, 1993; White and Perroux, 1989). Temporal dynamics in $K(\Psi_m)$ have also been associated with land management activities such as: crop type (Bodner et al., 2008); effluent disposal (Greenwood, 1999); and tillage (Angulo-Jaramillo et al., 2000;

Moret and Arrue, 2007; Reynolds et al., 1995; Sauer et al., 1990). Of particular interest is that the strongest temporal dynamics often appear to be in the largest macropores, and therefore affect infiltration measurements at suctions less than ~0.5 kPa (AnguloJaramillo et al., 1997; Moret and Arrue, 2007; White et al., 1992). This indicates that preferential flow behaviour will be strongly affected by temporal dynamics in $K(\Psi_m)$.

Clearly, great care needs to be taken to standardise a number of antecedent conditions if results between infiltration experiments are to be comparable. A clear relationship between steady-state infiltration and the antecedent moisture content is often observed for clay soils (Lin et al., 1998; Reynolds and Zebchuk, 1996b), although Bargarello et al. (2000) also observed a similar pattern for a sandy loam soil. Bargarello et al. (2000) also concluded that different site preparation procedures had a significant influence on the experimental results. Under a surface suction of 1.2 kPa the conductivity values were always higher when the surface layer of soil (10 mm depth) was removed. In contrast, Schwarzel and Punzel (2007) attributed surface sealing as the mechanism behind the lower infiltration rates measured by a tension infiltrometer, when compared to measurements by a hood infiltrometer. They suggested that disturbance during surface preparation and establishment of the contact layer resulted in smearing and clogging of the surface pores.

Biological activity

Temporal variability in infiltration measurements may also be due to soil fauna, micro organisms, and plant root growth. Earthworms are well recognised as causing variability, particularly when measuring the macropore network in small cores (McKenzie and Cresswell, 2002b). Micro organism activity has also been shown to cause temporal declines in measurements of $K(\Psi_m)$ over several days (Ragusa et al., 1994; Seki et al., 1998; Yarwood et al., 2006). There are also other studies that have attributed temporal variations to microbial activity, though without direct evidence. McKenzie et al. (2001) observed temporal variation in $K(\Psi_m)$ of cores sampled from sub-humid climates (500 – 600 mm annual rainfall), and attributed this to rapid microbial growth caused by the unusually wet conditions maintained in the cores during the experiments. Faybishenko (1999) proposed that micro-organisms can increase infiltration rate by consuming encapsulated air, whilst also decreasing the infiltration rate by biofilm accumulation clogging the pore network. Other authors have suggested that root growth in macropores

can have a large influence on seasonal dynamics of $K(\Psi_m)$ in cropping soils (Bodner et al., 2008; McKenzie and Cresswell, 2002b).

Thymol has been recommended as an inhibitor of biological activity (McKenzie et al., 2002d; Skaggs et al., 2002a). Debate exists about the need for biological inhibitors, particularly if the purpose is to assess field soil dynamics. However, they are applicable if measurements create conditions that may not occur in the field, such as wetting the soil to near-saturation for prolonged periods which may artificially enhance microbial activity. It is under these sustained wet conditions that pronounced effects of microbial activity have been observed (McKenzie et al., 2001; Ragusa et al., 1994; Seki et al., 1998). Generally, biological inhibitors are recommended if the purpose is to study the physical processes of water flow (McKenzie and Cresswell, 2002b; McKenzie et al., 2001)

Temperature fluctuations

As previously noted, temperature fluctuations can affect the air pressure within tension infiltrometers, and consequently the suction applied at the soil surface. Temperature fluctuations also affect the viscosity of both the resident soil water as well as the infiltrating water from the infiltrometer (White et al., 1992). McKenzie et al. (2002b) argue that temperature effects on infiltration measurements are rarely considered, even though they are potentially a large source of error. They observe that in Australia seasonal temperatures can vary by 20^{o}C during fieldwork, which may affect inter-study comparisons. Similar fluctuations could be expected in New Zealand, especially in the South Island. This may be important for not just comparing field results, but comparing field with laboratory data, where measurements are typically under controlled conditions at ~20^{o}C. The use of 20^{o}C as the standard reference is also questionable, when in New Zealand infiltration typically occurs at much lower temperatures. For example, the mean annual soil temperature for the soil used in this study is 10 ^{o}C.

The experimental research is limited, and mostly shows the effect of temperature on laboratory measurements of $K(\Psi_m)$ (Constantz, 1982; Constantz and Murphy, 1991; Stoffregen et al., 1999). Recent research has also shown that temperature can have a significant effect on the infiltration rate of large scale infiltration basins (Braga et al., 2007; Emerson and Traver, 2008; Lin et al., 2003). It is generally assumed that the temperature dependence of $K(\Psi_m)$ is primarily driven by the effect of temperature on viscosity, where water's viscosity changes by ~2% per degree Celsius, resulting in $K(\Psi_m)$

doubling if temperature increases by 30^{o}C (Lin et al., 2003; Stoffregen et al., 1999). However, Stoffregen et al. (1999) argue that research findings are contradictory, which may be a reflection of different experimental methods, and failure to control the effects of other variables. The consensus of these studies is that the effect of temperature tends to be greater than that predicted by changes in viscosity, suggesting that the temperature sensitivity of other factors such as electrolyte effects, surface tension, and air entrapment may be important (Constantz, 1982; Lin et al., 2003; McKenzie and Cresswell, 2002b; Stoffregen et al., 1999).

2.5.5 The reliability of infiltration measurements - research gaps

The first section of this review established that there is a practical demand in NZ for infiltration studies, driven by legislative requirements and industry best management practices. In the second half of this review it has been shown that tension infiltrometers have the potential to meet this demand. Tension infiltrometers have been widely used to characterise many of the hydraulic attributes of interest, with considerable research also into the methods and theory necessary to obtain reliable laboratory and field measurements.

However, it is also clear from the second half of this review that there are a number of mechanisms that can introduce error into infiltration measurements, which are likely to be a source of the spatial variability previously observed. If there is to be a future revival of infiltration studies on NZ soils, then these studies need to be backed up by knowledge and management of measurement uncertainties.

This thesis aims to improve the management of possible measurement uncertainties by researching the following knowledge gaps:

1. There is little experimental research on using large lysimeters for measuring infiltration and water movement attributes. Lysimeters may mitigate sample volume problems associated with the traditional small core measurements. Previous research has shown that large errors can arise from using small sample volumes to measure $K(\Psi_m)$. This is often attributed to the connectivity of the macropore network being artificially enhanced. I explore the potential for determining the $K(\Psi_m)$ of individual layers *in-situ*, where the connectivity is undisturbed (chapter 7).

2. Preferential flow has been identified as an important mechanism governing near-saturated infiltration behaviour. Research also shows that it is a widespread phenomenon in NZ soils. However, the mechanisms behind preferential flow initiation, and its persistence during infiltration, are not well understood. Chapter 5 presents results from three different methods of characterising preferential flow, and examines how each method complements our understanding of the mechanism.

3. There are few experimental datasets quantifying the internal behaviour of layered soils during infiltration.

4. Only a few studies have quantified the errors in $K(\Psi_m)$ measurements. In this study there is a rigorous attempt to identify and limit sources of temporal and spatial uncertainty. There is also an attempt to quantify the instrument error in chapter 3, and in chapter 7 errors are fully propagated through to the derived $K(\Psi_m)$ values.

5. This review identifies that there is no clear 'best practice' for determining when steady-state has been established. Chapter 7 explores how different approaches to determine steady-state affect the $K(\Psi_m)$ relationship.

6. There is limited research on the combined effects of preferential flow, soil layering, and hydrophobicity on infiltration measurements, and their influences on measured hydraulic attributes. Chapter 6 studies the influence of these mechanisms on early-time infiltration, and Chapter 7 identifies the main mechanisms governing long-time infiltration measurements.

With regard to the thesis objectives: research gap 2 relates to objective 1; research gap 6 relates to objective 2; research gaps 1, 3, 4, 5, and 6 relate to objective 3; and research gap 4 relates to objectives 3 and 6.

Chapter 3
Methods

3.1 Field sampling

Field sampling was carried out during October 2005. This involved the collection of lysimeters, description of soil profiles, and a dye infiltration study.

3.1.1 Location of sampling sites

The sampling location, ~6.5 km north of Methven at grid reference 2400205E 5736438N on the Canterbury Plains, was selected as being representative of the Gorge soil series. The sampling site was chosen to suit the farmer (David Barlass), in the centre of a paddock that was about to be ploughed for sowing of new pasture. The site had been under permanent pasture for at least 20 years and used for semi-intensive sheep and cattle grazing (David Barlass, *personal comm*.). Plate 3-1 shows the location of each lysimeter, and the three sites used for the dye study and description of morphological attributes. Only the four lysimeters that were used in the infiltration experiments are marked. The locations of the dye and profile description sites were chosen to be at the centre and each end of the sampling trench.

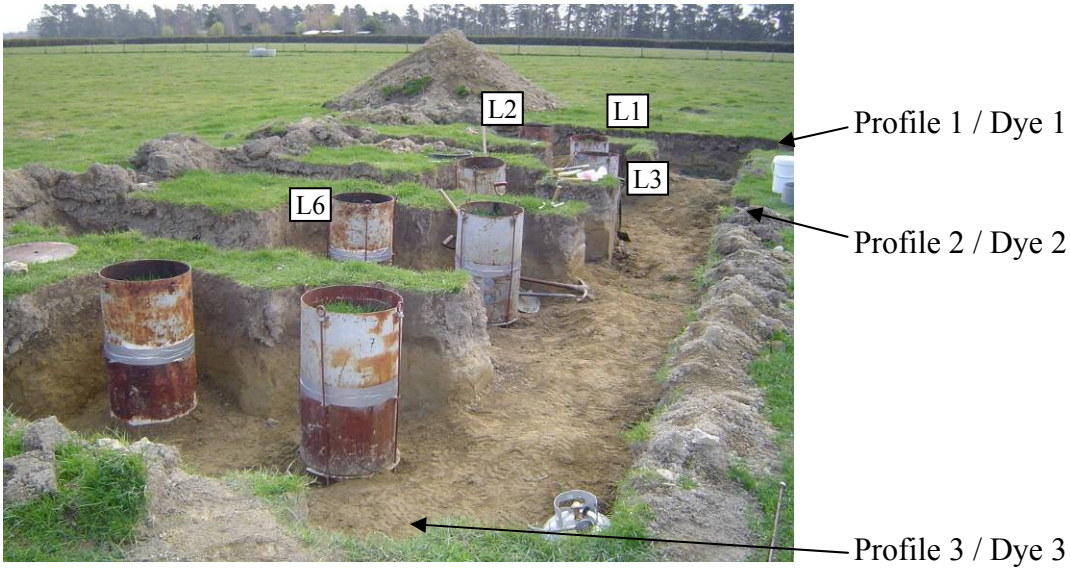

Plate 3-1 Location of the lysimeters, as well as the three sites used for the dye study and description of morphological attributes.

3.1.2 Description of soil morphological attributes

Soil morphology was described at three locations, following the method of Milne et al. (1995). At each location a 1 m^2 vertical face was excavated 0.3 m back from the trench wall. Soil description focussed on identifying the functionally different soil horizons based on differences in soil colour, structure size, shape, and density, and root distribution. Moisture content was also measured *in-situ* using the Campbell Scientific CS620 Hydrosense, with 20 cm sensor rods attached. Accuracy of the CS620 is ± 3% volumetric water content. Permeability class was also estimated following the method of Griffiths et al. (1999), from *in-situ* measurements of packing density and aggregate coatings, as well as laboratory assessment of aggregate size distribution.

Aggregate-size distribution

Aggregate size distribution was assessed following the method of Griffiths et al. (1999). At each location a large soil block was carved out at three soil depths (5 – 25 cm, 30 – 50 cm, 60 – 80 cm). Approximately 16 kg was collected from the topsoil, and 18 – 20 kg from the subsoil. The soil blocks were then kept moist by placing in large plastic bags, whilst transporting them back to the soil physics laboratory at Lincoln University. The total weight of each block was recorded, before each block was dropped from a height of 0.5 m to separate the individual aggregates. The mass of soil from each block was then passed through a range of sieves with 2, 4, 10, 20, 50, and 100 mm openings. The weight of soil aggregates retained on each sieve was then recorded.

Aggregate stability

Aggregate stability was measured on samples collected during a reconnaissance survey of the sampling site. A small soil pit was excavated, and samples removed from the topsoil (10 – 15 cm depth) and the subsoil (40 – 50 cm depth). Aggregate stability was assessed on field-moist 2 – 4 mm aggregates, using the wet-sieve stability test, based on the method of Nimmo and Perkins (2002). Ten replicate sub samples (100 g) were placed in the 2 mm sieves of the wet-sieve apparatus, which was then run for 15 minutes. The soil retained on the sieve was then collected and oven dried at 105^{o}C. Aggregate stability is expressed as the mean of the 10 replicate sub samples using the equation:

$$\text{Aggregate stability (\%)} = \frac{W_2}{W_1} \times 100 \qquad \text{Equation 3-1}$$

where W_1 is the total soil weight (oven dried equivalent) added to the wet-sieve apparatus, and W_2 is the oven dry weight of soil retained on the wet sieves.

Aggregate stability was also assessed using the dispersion and slaking test. This involved taking field moist aggregates (collected during the reconnaissance survey) and submersing them in water-filled petri dishes for 24 hours. The petri dishes were then photographed to visually show the degree of dispersion or slaking that occurred.

3.1.3 Ponded infiltration of dye tracer

The infiltration of a dye tracer was studied at 3 sites, located ~1 m behind the sites of the described profiles (Plate 3-1). At each site a lysimeter casing (50 cm diameter) was pushed ~1 cm into the soil surface, with moist soil mounded around the outside of the casing to aid the edge seal (Plate 3-2). A total of 50 mm depth of dye solution was applied manually in increments to maintain a constant 10 mm ponding depth. The dye used was Brilliant Blue FCF (C.I. 4290) at the concentration of 5 g litre^{-1}. Brilliant Blue dye was selected because it has been successfully used in a number of previous studies, and at the applied concentration should pose low environmental toxicity (Flury and Fluhler, 1994).

After 16 – 20 hrs each dye site was excavated to create a vertical face through the centre of the infiltration ring, approximately 90 cm wide and high. The face was framed with a reference ruler marked in 5 cm increments. Each site was then photographed using a four megapixel digital camera under similar sunny daylight conditions, between 11 am and 1 pm on 3 consecutive days. Horizontal sections (50 cm wide by 90 cm long) were then excavated and photographed at soil depths of 2, 20, 40, and 60 cm from the soil surface.

Plate 3-2 Use of the lysimeter casing (50 cm diameter) to apply 50 mm depth of Brilliant Blue FCF dye solution as ponded infiltration.

Image analysis of dye pattern

Image analysis of the dye pattern was carried out for each horizontal section. For consistency the portion of each image corresponding to the 20 x 20 cm square under the centre of the infiltration ring was selected for analysis. In this zone where infiltration was essentially one dimensional and there was minimal geometric distortion in the image. The photographs were analysed by the Robolab software (developed at TUFT University, College of Engineering, Medford, MA USA[http://www.ceeo.tufts.edu]) using a program written by Professor A. McKinnon and Dr. K. Unsworth, of the Applied Computing Department, Lincoln University.

To overcome any potential exposure differences in the photographs the program converts the photo into a HSL (Hue, Saturation, Lightness) image, where the value of the hue essentially represents the colour of the image independent of its brightness. The program analysed the dye density of each pixel, based on classifying whether the hue was in one of three threshold ranges: no dye, pale dye, or dense dye. The threshold values were established by selecting a small segment (i.e. ~4 cm^2) which contained discrete areas of each density, then manually adjusting the threshold values for the hue to visually distinguish the different dye densities. The threshold values were then tested against other small segments to ensure consistent classification. Each 20 x 20 cm square was then analysed using the same threshold values, with the dye density presented as the percentage of pixels that were classified as no dye, pale dye, or dense dye.

3.1.4 Sampling of lysimeters

Following the profile descriptions and dye study, eight intact soil monolith lysimeters (50 cm diameter x 70 cm depth) were collected from the locations shown in Plate 3-1. To reduce costs, each lysimeter casing comprised two recycled 50 cm deep casings stacked together (refer to Plate 3-3). The main steps are shown in Plate 3-3, with each step as follows:

A. An excavator was used to dig a 1 m deep trench network that left four 1.5 m wide undisturbed soil blocks. Two lysimeters were then excavated from each block, located ~50 cm in from the edge to avoid any fractured zones along the margins of the trench.

B. The lysimeters were collected by manually carving a cylindrical pedestal slightly larger in diameter than the lysimeter casing. Once 5 – 10 cm of the pedestal was excavated (photo B1) the lysimeter casing was pushed downwards (photo B2). The step was repeated until the lysimeter was 75 cm deep (photo B3). The 70 – 75 cm depth increment was later removed and replaced with drainage material (refer section 3.2, below).

C. To minimise disturbance of the column the lysimeter case had a 5 cm deep internal cutting ring, which was the only part of the lysimeter in contact with the soil as the casing was pushed downwards. The cutting ring left a 5 mm annular gap between the soil column and the rest of the casing, which was then filled with heated and liquefied petroleum jelly (photo C1). This was done in two stages, with the lower casing annulus filled first before the upper casing was slid over the column and subsequently sealed.

D. The lysimeters were then left overnight for the petroleum jelly to solidify. Once the petroleum jelly cooled and solidified all gaps between the column and the casing were filled (photo C2), preventing any edge-flow down the lysimeter wall during the infiltration experiments (Cameron et al., 1992). A cutting plate was used to detach the column from the underlying soil. A purpose-built frame was mounted around the base of the lysimeter, which acted to guide the circular cutting plate as a hydraulic ram pushed the plate under the lysimeter. The cutting plate was then bolted to the lysimeter casing using four lifting rods (photo D).

E. The lysimeters were then lifted from the trench by a front end loader, using a chain hoist that attached to the top of the lifting rods. Four lysimeters at a time were loaded onto a specially designed, air suspended trailer, and transported back to Lincoln University (photo E).

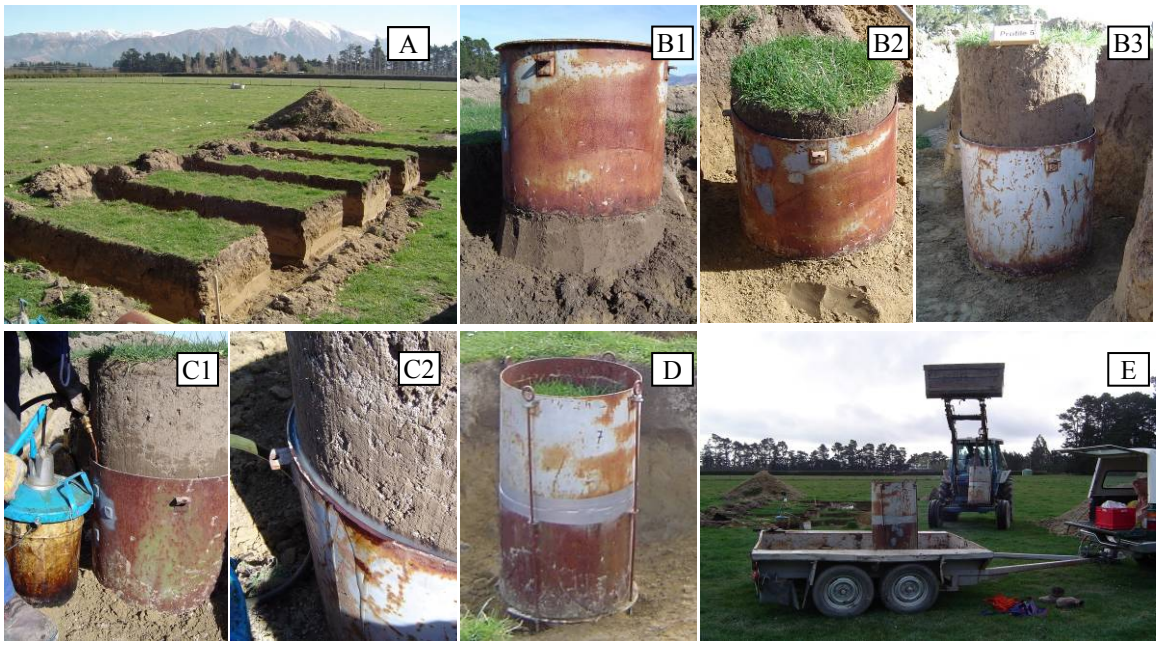

Plate 3-3 The major steps in the collection of the monolith lysimeters. The details of each step are outlined in the preceding text.

3.2 Lysimeter preparation and pre-experiment storage

After transportation back to the Lincoln University lysimeter laboratory the drainage base was installed for each lysimeter (Plate 3-4), using the following steps.

A. The top of the lysimeter was packed with air cushions, and a top plate temporarily fitted and held in place by the lifting rods. A specially made iron collar was attached, which allowed the lysimeter to be lifted and inverted using a tractor (photo A).

B. The cutting plate was then removed and the lowest 5 cm of the soil column was excavated (photo B).

C. Any smeared soil with blocked pores was then removed by applying a 1 cm thick layer of plaster of paris (photo C). Once hardened the plaster of paris was then broken and removed, which in turn tends to roughen and 'peel' the underlying soil surface.

D. The base of the lysimeter was then filled with a gravel (67%) and sand (33%) mixture, which acts as the drainage layer (photo D). A new steel base plate was then bolted back onto the base of the lysimeter. To enable drainage the base plate has seven equally spaced channels radiating out from the central 12 mm diameter

drainage hole. Lysimeters were then re-inverted and the top plate removed. The base plate and centre join between the two casings where then sealed with a layer of silicone sealant to prevent any water leakage during the infiltration experiments. The water characteristic of the drainage layer was measured (refer section 3.10). During the experiments the Ψ_m of this layer was between -3.5 to 0 kPa, which corresponds to θ_v of 14 – 25%. Most of this moisture content is interpreted as drainage pores, as the water content at -10 kPa (i.e. field capacity) was ~4%.

Plate 3-4 Steps in the installation of the lysimeter drainage base, with each step described in the preceding text.

After installation of the drainage base the lysimeters were stored outside for between 6 – 18 months, before the infiltration experiments began. The lysimeters were maintained by regularly trimming of the pasture, and applying irrigation to supplement rainfall and keep the column moisture content near field capacity.

3.3 Lysimeter setup and sensor instrumentation

About two weeks before infiltration experiments began the relevant lysimeter was moved by a front end loader into the experiment shed. The purpose of the shed was to partly control the effect of temperature on the experiments, particularly to buffer against rapid temperature fluctuations, as well as to protect instruments. The lysimeter was placed on a 1 metre high stand and secured to shelving (Plate 3-5), upon which the infiltrometer water reservoir was mounted. This setup allowed up to three lysimeters to be installed, although in practice only two were installed at once.

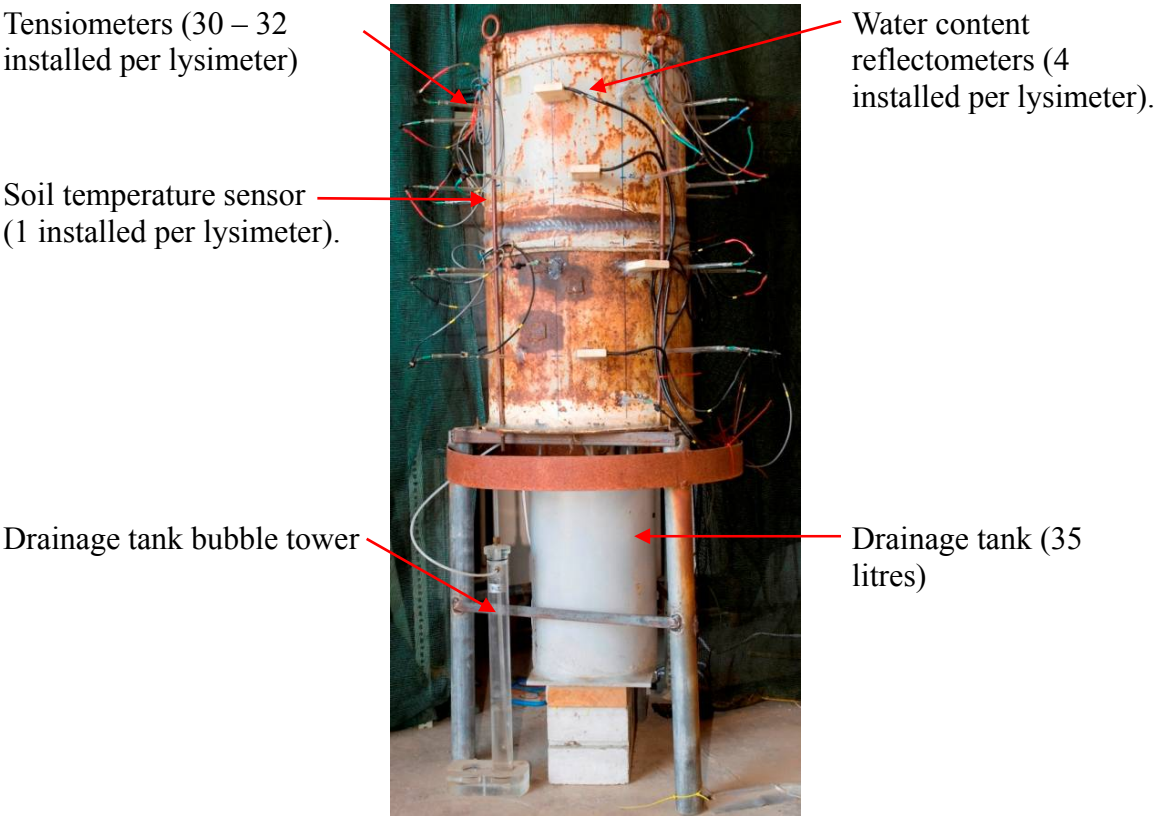

Plate 3-5 Experimental setup for Lysimeter 1.

Sensor layout for each lysimeter

Once installed the drainage tank was connected and the lysimeter instrumented with tensiometers, water content reflectometers (WCR), and a soil temperature sensor. Plate 3-5 illustrates the instrumentation used for lysimeters 1 and 3. A slightly different pattern of tensiometer placement was used for lysimeters 2 and 6. Sensor numbers and layout for each lysimeter are given in Table 3-1. Instrument placement was measured as a depth from the nominal soil surface, which was defined for each lysimeter following the method described in section 3.4 below.

Table 3-1 shows the 'operational' number of tensiometers at each depth for individual experiments, where sometimes a tensiometer had failed due to air bubbles inside the ceramic cup or condensation forming in the pressure transducer. Tensiometer failure was easily identified in the data as when readings became clearly erratic and showed no relationship to the behaviour of other sensors at that depth. Although not shown in Table 3-1, lysimeter 2 had a further 4 tensiometers at each of the 10, 30, and 50 cm depths. The data from these additional depths were not used in the results chapters, because it was observed that the major changes in tensiometer behaviour coincided with soil layer

boundaries, so it was decided to just use the 2, 20, 40 and 60 cm depth increments to allow a more consistent and clear comparison between lysimeters.

Lysimeter infiltration experiment		Depth increment					
		Surface	2 cm	20 cm	40 cm	60 cm	70 cm
L1	0 kPa	1 Tz	7 Tz; 1 WCR	7 Tz; 1 WCR	7 Tz; 1 WCR	7 Tz; 1 WCR	1 Tz
	0.5 kPa	1 Tz	7 Tz; 1 WCR	7 Tz; 1 WCR	7 Tz; 1 WCR	7 Tz; 1 WCR	1 Tz
	1 kPa	1 Tz	6 Tz; 1 WCR	6 Tz; 1 WCR	7 Tz; 1 WCR	6 Tz; 1 WCR	1 Tz
	1.5 kPa	1 Tz	6 Tz; 1 WCR	7 Tz; 1 WCR	7 Tz; 1 WCR	7 Tz; 1 WCR	1 Tz
L2	0 kPa	1 Tz	4 Tz; 1 WCR	4 Tz; 1 WCR	4 Tz; 1 WCR	4 Tz; 1 WCR	1 Tz
	0.5 kPa	1 Tz	4 Tz; 1 WCR	3 Tz; 1 WCR	4 Tz; 1 WCR	3 Tz; 1 WCR	1 Tz
	1 kPa	1 Tz	4 Tz; 1 WCR	3 Tz; 1 WCR	3 Tz; 1 WCR	3 Tz; 1 WCR	1 Tz
	1.5 kPa	1 Tz	4 Tz; 1 WCR	3 Tz; 1 WCR	3 Tz; 1 WCR	3 Tz; 1 WCR	1 Tz
L3	0 kPa	1 Tz	7 Tz; 1 WCR	7 Tz; 1 WCR	7 Tz; 1 WCR	7 Tz; 1 WCR	1 Tz
	0.5 kPa	1 Tz	7 Tz; 1 WCR	7 Tz; 1 WCR	7 Tz; 1 WCR	7 Tz; 1 WCR	1 Tz
	1 kPa	1 Tz	7 Tz; 1 WCR	7 Tz; 1 WCR	7 Tz; 1 WCR	7 Tz; 1 WCR	1 Tz
	1.5 kPa	1 Tz	7 Tz; 1 WCR	7 Tz; 1 WCR	7 Tz; 1 WCR	7 Tz; 1 WCR	1 Tz
L6	0 kPa	1 Tz	1 WCR	8 Tz; 1 WCR	10 Tz; 1 WCR	11 Tz; 1 WCR	
	0.5 kPa	1 Tz		8 Tz	10 Tz	13 Tz	
	1 kPa	1 Tz		8 Tz	10 Tz	13 Tz	
	1.5 kPa	1 Tz		8 Tz	10 Tz	13 Tz	

Table 3-1 The number of 'operational' sensors at each depth increment for each lysimeter, during infiltration experiments under surface imposed suctions of 0, 0.5, 1, and 1.5 kPa. The table shows the number of tensiometers (Tz), and water content reflectometers (WCR).

At each depth increment the replicate tensiometers were installed at regular intervals around the lysimeter circumference, with the number of intervals varying depending on the number of sensors. For example, in Plate 3-5 Lysimeter 1 has an array of seven tensiometers installed at 45^{o} intervals, with the WCR installed in the spare interval. To minimise any potential 'shadow' effect from tensiometers above, the 20 and 60 cm depth increments were rotated 22^{o} so that the tensiometers were located mid-interval of the above and below tensiometer arrays. As shown in Plate 3-5 the WCR's were also rotated 22^{o} at each depth increment. The soil temperature sensor was always located at 20 cm depth.

The following sections describe the detailed methods of construction, calibration, and installation for each type of sensor.

3.3.1 Tensiometers

The tensiometers were custom made, with the key features shown in Plate 3-6. A thorough review of tensiometer theory, construction and operation is provided by Young and Sisson (2002). All tensiometers were installed horizontally, with a 9 mm wood auger used to bore a cavity 100 mm into the soil column. This meant the actual sensing volume of the tensiometer cup was located at 70 – 100 mm from the edge of the soil column. To ensure the tensiometer was horizontal, a small level was attached to the drill. In practice some deviation from horizontal did occur, with the standard error in the tensiometer depth locations at a particular depth increment estimated as ± 5 mm. Waterproof silicone sealant was used to seal the hole where the tensiometer body passed through the lysimeter casing.

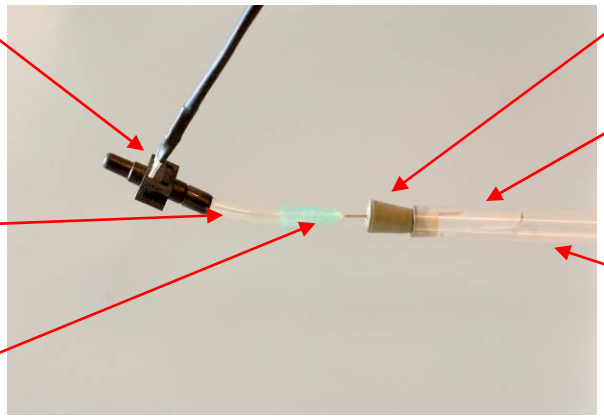

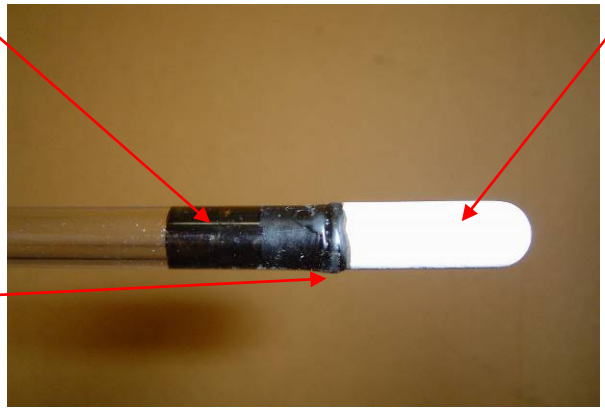

Plate 3-6 Key design features of the tensiometers. Top photo shows the transducer end of tensiometer, whilst bottom photo shows the cup end which was installed 100 mm into the soil column.

Once installed, the tensiometers were filled with de-aired water and initially flushed daily to remove any air-bubbles. Because the soil columns were at or near field capacity the tensiometers usually became stable after a couple of days. The continual monitoring with pressure transducers meant the presence of any new air bubbles was easily identified in

the data because the reading became clearly erratic, and showed no relationship to the behaviour of other sensors at that depth.

Tensiometer water pressures were measured with differential pressure transducers, which measured the difference between atmospheric and tensiometer pressure, the latter assumed to be in equilibrium with the soil matric potential at the location of the ceramic cup. The pressure transducers were calibrated following the method of Young and Sisson (2002). Tensiometers were calibrated as an array connected to a hanging water column held under various suctions (Plate 3-7). A datalogger was used to record the voltage output of each transducer as the water column suction was increased in 100 mm (1 kPa) increments from 0 to 1000 mm (0 – 10 kPa) suction. The recorded voltage was an average of 10 measurements at 5 second intervals. Linear regression was used to establish the relationship between transducer voltage and water column suction (R^2 >0.99999). From the calibration experiments the average transducer error in measuring suction was ±0.004 kPa (0.4 mm), with only a small variability observed in this error (0.0004 kPa s.e.). The uncertainty in reading the water column scale was ±0.5 mm, resulting in a total calibration error of ±0.01 kPa.

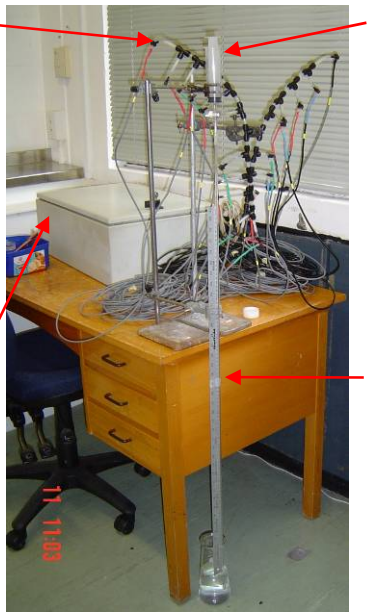

Plate 3-7 Laboratory set-up used to calibrate the change in output voltage of each pressure transducer as the suction of a hanging water column is increased.

Pressure transducers are also known to be sensitive to temperature, although the transducer model used did have an in-built thermistor for automatic compensation. However, Young and Sisson (2002) recommend separate temperature calibration if

accurate readings are required. Despite the automatic compensation the pressure transducers used in this study were still found to be temperature sensitive, which varied between transducers. To reduce this sensitivity a separate temperature calibration was required. The pressure transducers were placed in an incubator with the output voltage measured as the temperature was changed in increments of 5^{o}C, from 5 to 30 ^{o}C. Linear regression was used to establish the relationship between transducer voltage and temperature (R^2 >0.9).

In the datalogger programme the temperature calibration equation was used to correct in real-time the transducer output voltage, before the suction calibration equation was applied to convert the voltage to soil matric potential (i.e. pressure in kPa). The errors of both calibration equations are additive, with an average combined error of ±0.007 kPa, with only a small variability observed in this error (0.001 kPa s.e.). Together with the potential error of the scale reading in the suction calibration (0.005 kPa) and the potential error from non-horizontal tensiometer installation (0.05 kPa) the overall average error for the tensiometers is estimated as ±0.06 kPa.

Another potential source of significant error is the effect of temperature on the gas pressure of the measurement air-pocket (Butters and Cardon, 1998; Warrick et al., 1998). Figure 3-1 shows the strongest observed tensiometer response to air temperature fluctuations that was observed during the experiments of this study. As shown in Figure 3-1 the tensiometer measurements fluctuate by a maximum of 0.2 – 0.4 kPa during the strongest temperature spikes. This is consistent with other research, with Butters and Cardon (1998) observing minimal temperature sensitivity in tensiometers with a small volume air-pocket (4.8 x 10^3 mm^3) and high cup conductance. In this study high-flow cups were used and the air-pocket was typically kept to 3 – 7 x 10^2 mm^3. Warrick et al. (1998) also found that the hydraulic conductivity of the soil surrounding the cup has a significant influence, which is consistent with this study where temperature sensitivity only became apparent under slow unsaturated infiltration. For example, the temperature effect shown in Figure 3-1 becomes apparent when the soil layers are dry enough that hydraulic conductivity is between 0.01 – 0.45 mm hr^{-1}.

In this study it is also important that the tensiometers show a fast response to changes in soil matric potential, particularly to detect preferential flow during the early stages of infiltration. Figure 3-2 demonstrates the rapid *in-situ* response of tensiometers in

lysimeter 1 to a sharp infiltration 'flush' caused by the removal of the tension infiltrometer. The seven tensiometers at 2 cm depth all respond within 1 to 3 minutes, which is similar to the water content reflectometer which should show immediate response to the wetting front. The overall tensiometer response is ~ 1 minute slower, which may indicate a slight delay in the tensiometer response or could reflect the influence of non-uniform penetration of the wetting front due to preferential flowpaths.

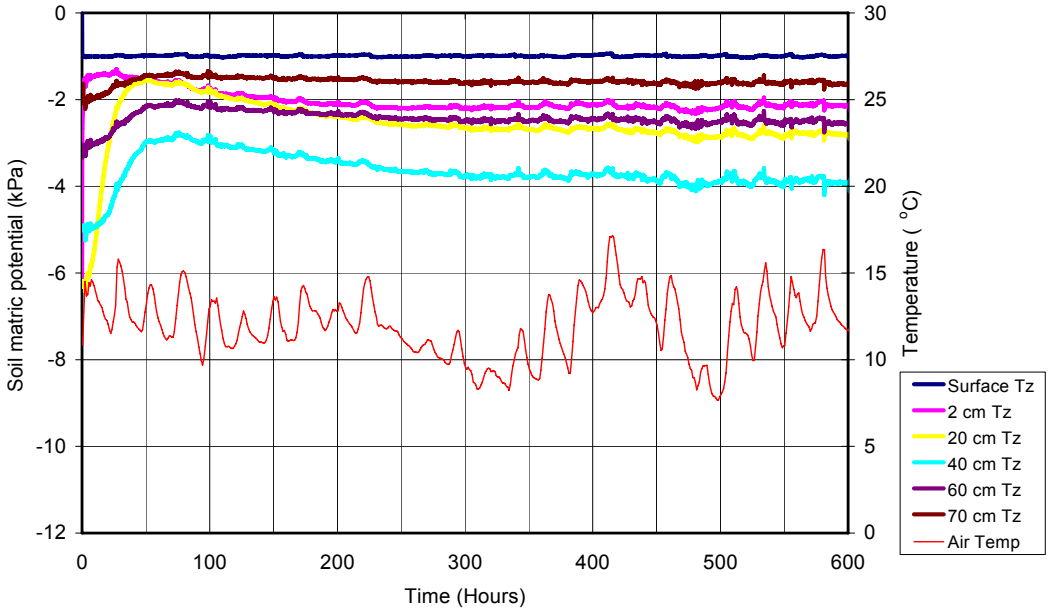

Figure 3-1 The effect of air temperature fluctuations on the spatial average tensiometer (Tz) measurements of soil matric potential at different depths of lysimeter 1, during infiltration under 1 kPa surface suction.

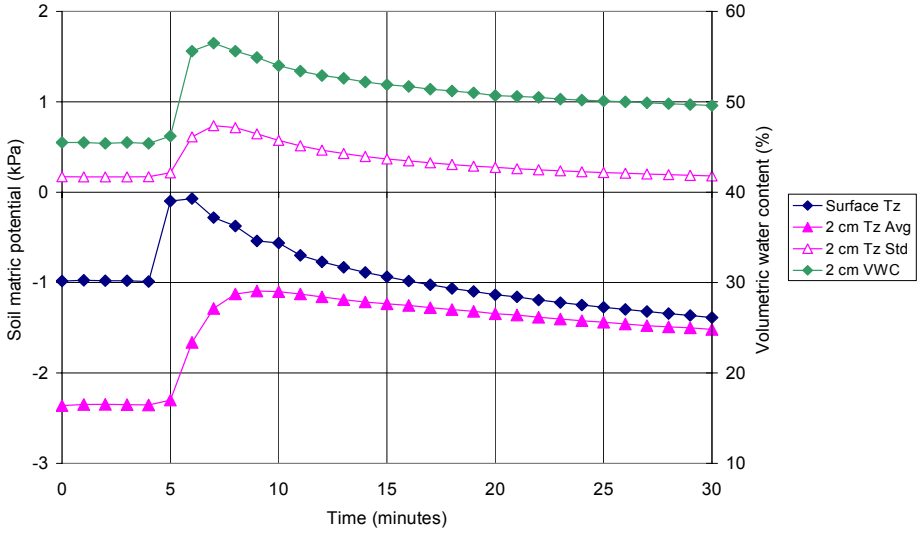

Figure 3-2 The response of tensiometers (Tz) and the water content reflectometer (VWC) at 2 cm depth to a short infiltration 'flush' caused by the removal of the tension infiltrometer. The infiltration flush is shown by the surface tensiometer showing a sharp loss of suction at 5 minutes.

3.3.2 Water content reflectometers

The dynamics of volumetric water content (θ_v) was measured using CS616 Water Content Reflectometers (WCR) (Campbell Scientific Inc., Utah, USA). For lysimeter 6, θ_v was only measured under saturated infiltration (0 kPa experiment), because the WCR's were not available for the other experiments. The WCR's were installed horizontally with the aid of a small level.

The CS616 measures the travel times of a train of square waves along two 30 cm long stainless steel rods which are inserted in parallel into the soil column. The travel time depends on the dielectric constant of the soil surrounding the rods, which in turn depends on the soil water content (Campbell Scientific, 2006). A calibration equation is used to convert the period measurement to θ_v . The manufacturer recommends that their standard quadratic calibration equation should provide accurate estimates of θ_v in soils with bulk electrical conductivity less than 0.5 dS m^{-1}, bulk density less than 1.55 g cm^{-3}, and clay content less than 30% (Campbell Scientific, 2006). Because the soil used in this study meets these requirements it was deemed satisfactory to use the manufacturer's calibration equation, which should provide an estimate of θ_v with a maximum error of ±3% (Campbell Scientific, 2006). The precision of the measurement is better than 0.1%, meaning the WCR should be highly accurate when determining changes in water content.

Temperature sensitivity

The manufacturer also states that the CS616 is sensitive to soil temperature fluctuations, and provides a separate temperature calibration equation, which was used in this study. Despite using the temperature calibration the results of some medium- to long-time unsaturated infiltration experiments suggested that a temperature dependence of θ_v remained, such as L2 at 1 and 1.5 kPa suction where infiltration rate (i_t) and matric potential (Ψ_m) both increase then decrease, while θ_v kept increasing.

The apparent temperature dependence of θ_v was most obvious in infiltration experiments that continued for longer than 20 – 30 hrs, when θ_v often exhibited a cyclic rise and fall pattern, which occurred simultaneously at all depths. Over time periods of >100 hrs there were small amplitude diurnal cycles as well as the larger amplitude multi-day cycles, where θ_v changed by up to 4% over a period of days (Figure 3-3). In Figure 3-3 θ_v increases then decreases over the 200 – 400 hr period, whilst Ψ_m is either steady (2cm

depth) or decreasing (40 cm depth). Over the same time period both the infiltration and drainage rates show a slow steady decrease, which is consistent with the expected response from the observed Ψ_m pattern.

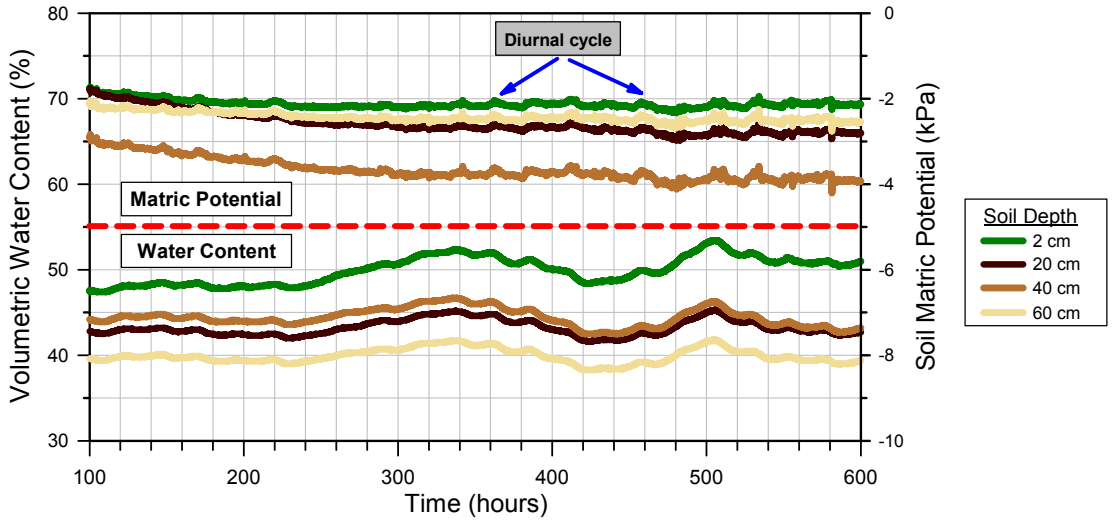

Figure 3-3 Comparison of the pattern in volumetric water content and matric potential during long-time infiltration into Lysimeter 1, with infiltration under 1 kPa surface suction.

The long-time cycle in θ_v appears to consistently mirror similar cycles in soil temperature (refer Appendix 1), and is therefore interpreted as temperature dependent error. The previous version of the WCR (model CS615) has been shown to be sensitive to temperature fluctuations, which are not adequately compensated by the manufacturer's temperature calibration (Stenger et al., 2005; Western and Seyfried, 2005). Western and Seyfried (2005) conclude that the new CS616 model used in this study is also likely to show marked temperature sensitivity. This is primarily due to using a low measurement frequency at which the soils dielectric is strongly affected by the temperature sensitivity of the soils electrical conductivity.

Figure 3-4 shows that the CS616 used in this study does have strong temperature sensitivity, and that the manufacturer's temperature calibration does not adequately compensate for this sensitivity. Figure 3-4 also shows that the temperature sensitivity changes with water content. The temperature sensitivity in Figure 3-4 is ~3 – 4 % per 5^{o}C shift in temperature, which roughly equates to the cyclic fluctuations observed in during the medium to long-time infiltration experiments.

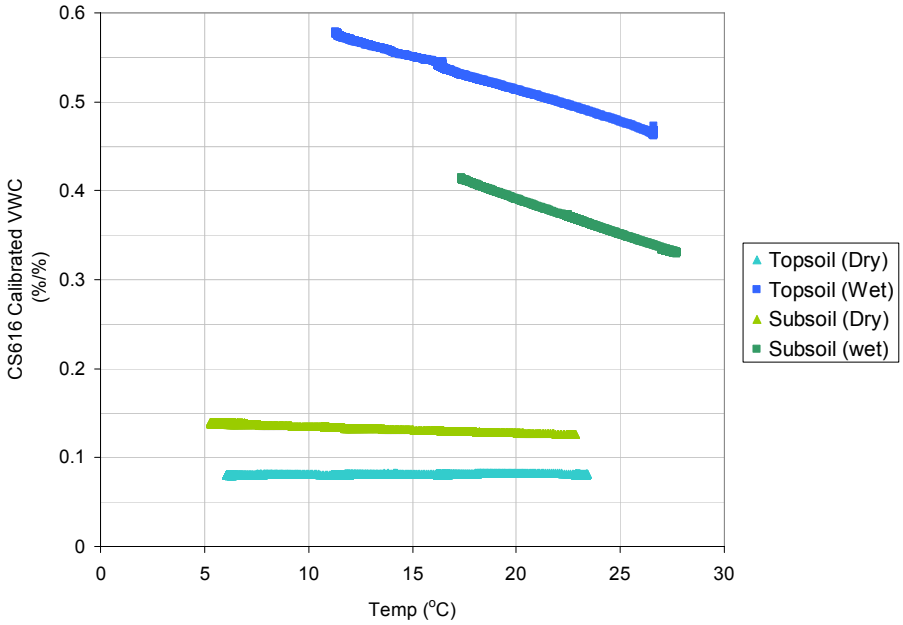

Figure 3-4 Effect of temperature on the WCR measurement of soil water content, when measured in chambers of repacked soil held at a stable water content. The WCR used the standard manufacturers' temperature calibration.

Use of water content reflectometer data

Retrospective correction of the WCR temperature sensitivity would require extensive recalibration (Western and Seyfried, 2005) and was deemed to be unnecessary for this project. The WCR data is used in chapter 6 to estimate the air-filled porosity (ε_a) and the antecedent infiltration capacity (I_c), although it is only used to support the primary estimates of I_c based on the small core measurements of the $\theta_v(\Psi_m)$ relationship.

Interpretation of air-filled porosity

The WCR data were also used to estimate the change in ε_a during early-time infiltration, but the data should be valid because only a small soil temperature variation occurred over the time-period of interest. During saturated infiltration the temperature variation was less than 0.5°C (Appendix 1). The unsaturated experiments were over a longer time-frame, but the maximum variation was ~2.5°C, which would introduce a maximum error of 2% to the WCR measurement. The ε_a was calculated as the difference between total porosity (ε_t) and water-filled porosity (θ_v) measured by the *in-situ* WCR using the equation,

$$\varepsilon_a = \varepsilon_t - \theta_v \qquad \text{Equation 3-2}$$

with ε_t determined from 3 small cores sampled from the same soil depth as the WCR (refer section 3.10, Equation 3-7).

3.3.3 Temperature sensors

The temperature sensors were custom made using a thermistor (Model LM35CZ, National Semiconductor) coated in resin and waterproofing membrane. The sensors were 65 mm long by 9 mm in diameter. One sensor measured air temperature, and another was installed horizontally at 20 cm depth in each lysimeter, with a 9 mm wood auger used to bore a cavity 100 mm into the soil column. The cavity behind the sensor was backfilled with some of the excavated soil. Each temperature sensor was calibrated in a water bath, by recording its voltage output as the bath temperature was changed in 10^{o}C increments, over the range 0 – 40^{o}C. Linear regression was used to establish the relationship between output voltage and temperature (R^2 >0.9999). From the calibration experiments the average error in measuring temperature was ±0.3^{o}C, with only a small variability observed in this error (±0.02 ^{o}C).

3.3.4 Drainage tank

The drainage tank volume was 35 litres, equivalent to 0.5 pore volume of the lysimeter. This meant that the tank did not have to be emptied during infiltration experiments, except during the tracer leaching experiments. During the unsaturated infiltration experiments the same suction as the infiltrometer was applied to the drainage tank, which in turn applied this suction to the base of the soil columns. The drainage tank suction was maintained using a vacuum pump to pull air out of the tank, which in turn pulled new air into the tank under suction via a bubble tower. The vacuum pump was a modified aquarium air pump, adapted from the method of Magesan et al. (1995).

The height of water in the drainage tank was automatically measured using a Dry Gas Bubble Unit (Model ISD DBU-01, Scott Technical Instruments Ltd, Hamilton, NZ) which monitors water depth by bubbling gas through a tube at the base of the tank and monitoring the gas pressure changes at the point of bubbling with a pressure transducer (0 – 1 PSI, Model GS2, Scott Technical Instruments Ltd, Hamilton, NZ). Each drainage tank was individually calibrated by filling and then incrementally draining it. For each drainage increment the weight of water and transducer output were recorded, with linear regression used to establish the relationship between the two values (R^2 >0.99999).

It was also necessary to account for the suction applied in the drainage tank headspace, which varied between experiments as well as during long-time experiments where the

bubble tower water tended to evaporate, and needed periodic topping up. The variations in the headspace suction were important because they affected the bubbling pressure of the water level sensor. This was overcome by installing an additional differential pressure sensor to measure the pressure in the tank headspace. The headspace transducer was calibrated to establish the relationship between headspace suction and output voltage (R^2 >0.99999). The datalogger then used this relationship to calculate a suction offset, which in turn was used to correct the water level transducer measurement. From these calibration experiments, the average transducer error in measuring cumulative drainage was ±0.2 mm, with only a small variability observed in this error (±0.01 mm s.e.).

3.3.5 Datalogger programme

A CR1000 datalogger (Campbell Scientific Inc., Utah, USA) was used to monitor all the sensor measurements. The datalogger's sensor capacity was increased to 77 sensors by connecting two multiplexers (Model AM16/32, Campbell Scientific Inc., Utah, USA). A laptop computer was connected to the datalogger to monitor sensor behaviour in real-time or otherwise download data from the logger. The enhanced datalogger sensor capacity enabled two lysimeters to be installed simultaneously. The datalogger programme was designed to allow each lysimeter to be operated independently, so that experimental changes on one did not affect the sensors monitoring the other lysimeter.

The datalogger recorded the sensor measurements every minute. For infiltration over periods longer than one day, the rate of change in WCR and tensiometer measurements was slow, and it was considered more accurate to output data as the mean and standard deviation over a 10 minute period. The datalogger was also programmed to output data for individual sensors, as well as the spatial average and standard deviation for the array of tensiometers at each depth. Cumulative infiltration and drainage were also recorded as 10 minute means, although every millimetre of cumulative infiltration (and corresponding drainage) was also recorded with a one minute resolution. Soil and air temperature were recorded as hourly means.

3.4 Design of the tension infiltrometer system

The tension infiltrometer system was custom built following the criteria of Perroux and White (1988). The key design features of each infiltrometer component are described in the following sections.

Water reservoir

The water reservoir was designed to be mounted separately to the infiltrometer disk, with the key features shown in Plate 3-8. The reservoir was mounted on shelving behind each lysimeter, at a height where the air-inlet pipe from the bubble tower was ~ 1 – 2 cm above the nominal soil surface. This provided an offset that reduced the infiltrometer suction, but was overcome by increasing the water level in the bubble tower, based on the actual soil surface suction measured by the *in-situ* tensiometer (refer to the contact material section below). This offset also allowed the bubble tower to still operate and control the surface suction during saturated infiltration experiments, where the surface suction was maintained at or slightly above 0 kPa.

A 16 mm internal diameter (i.d.) clear flexible pipe was used to supply water from the reservoir to the infiltrometer disk, together with 13.5 mm i.d. pipe fittings. Based on the research of Walker et al. (2006) the flow resistance of the supply pipe should not influence the infiltrometer suction unless the infiltration rate exceeded 95 – 127 mm hr^{-1}, which was not exceeded during the infiltration experiments of this study.

The reservoir volume was 70 litres, equivalent to 1 pore volume of the lysimeter. Hence the reservoir did not have to be refilled during infiltration experiments, except during the tracer leaching experiments. The height of water in the reservoir was automatically measured using a differential pressure transducer (0 – 1 psi, Micro Switch 26PCAFA6D), which measured the pressure difference between the reservoir base and the air-filled headspace at the top of the reservoir. Casey and Derby (2002) show that use of a differential transducer virtually eliminates variability in the tank pressure caused by air bubbles from the air-inlet pipe.

Each pressure transducer was individually calibrated by filling the reservoir and then incrementally draining it. For each increment the weight of water and transducer output were recorded, with linear regression used to establish the relationship between the two values (R^2 >0.99999). Each transducer was also temperature calibrated (refer section 3.3.1). The datalogger was then used to calculate infiltration using the temperature-corrected relationship between transducer output voltage and water level height in the reservoir. From the calibration experiments the average transducer error in measuring infiltration was ±0.3 mm, with only a small variability observed in this error (0.03 mm s.e.).

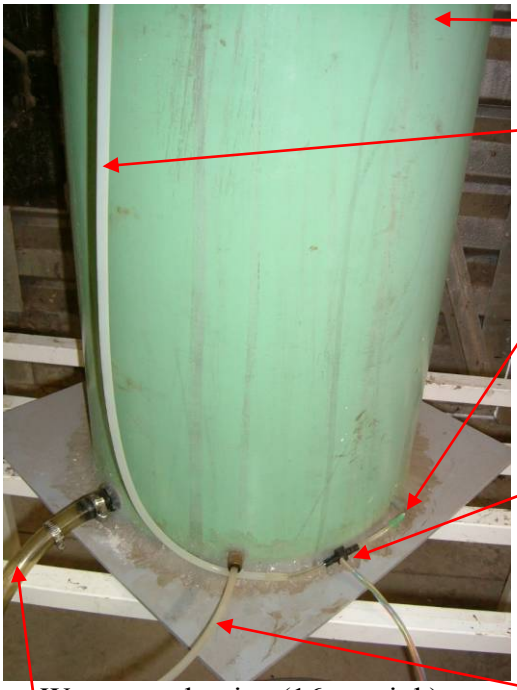

Plate 3-8 Key design features of the water reservoir.

Tension infiltrometer disk

The tension infiltrometer is shown in Plate 3-9 and is similar to that used by Silva et al. (2000). The infiltrometer disk was 480 mm in diameter, and constructed from clear 38 mm thick acrylic. Water was supplied from a centre pipe to a 460 mm diameter by 4 mm deep chamber that had been cut by lathe into the base of the disk. A perforated stainless steel plate was mounted at the base of the water chamber, to provide a level and firm base for the infiltrometer membrane.

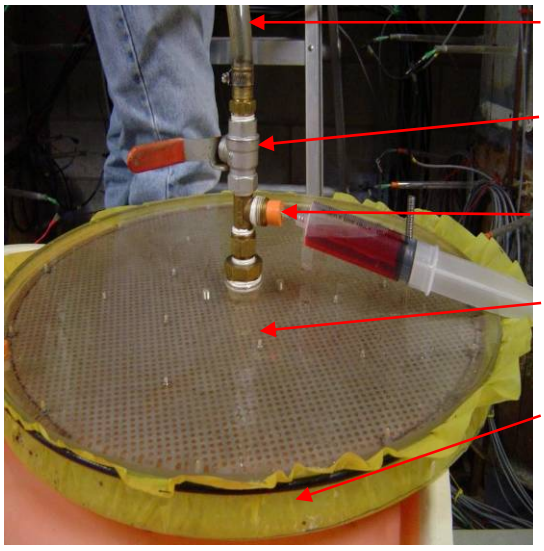

Plate 3-9 Key design features of the tension infiltrometer disk.

Bubble tower

A bubble tower was used to set the water suction within the tension infiltrometer. Usually the height of water in the bubble tower sets the suction, however the bubble tower was connected to the base of the water reservoir which, as discussed earlier, was mounted slightly above the soil surface. Together with the effect of the contact material this provided an offset that reduced the infiltrometer suction. This was overcome by increasing the water level in the bubble tower, based on the actual soil surface suction measured by the *in-situ* tensiometer (refer to the following section).

Another potential problem is maintaining constant suction when infiltration is either slow or over long-time periods, where loss of suction can occur from problems such as small air leaks in the infiltrometer system, or condensation in air pipes. To overcome this issue a vacuum pump was connected to the top of the water supply tank to ensure that the bubble tower was constantly bubbling. The vacuum pump was a modified aquarium air pump, adapted from the method of Magesan et al. (1995). The advantage of the vacuum pump is that it enables a constant suction to be established in the tension infiltrometer prior to installation on the soil surface. This minimises the chance of a flush of water during installation which may cause lower infiltrometer suction than that desired, activating parts of the pore network intended to be excluded from infiltration. Another advantage is that the constant pumping of air mitigates any temperature induced pressure fluctuations within the air-space of the water reservoir and bubble tower, as identified by Castiglione et al. (2005b; 2005).

Contact material

The contact material used was a fine glass bead material (Spheriglass, no. 2227, Potters Industries Ltd.), following the recommendation of Reynolds and Zebchuk (1996) and Reynolds (2006; 2008). The physical and hydraulic attributes of the glass beads are described by Reynolds and Zebchuk (1996) and Bagarello et al. (2001). Reynolds and Zebchuk (1996) identified that the resistance of the contact material can result in a lower suction at the soil surface (Ψ_0) than the suction applied by the infiltrometer (Ψ_{TI}). To overcome this, a rapid response tensiometer was installed at the base of the contact material layer (photo A, Plate 3-10), and centred at the nominal soil surface, $Z_{0,}$ (defined in the following section). This method worked by simply adjusting the height of water in the bubble tower until Ψ_0 measured by the tensiometer was at the desired level.

The contact material has an air entry value of ~6 kPa suction, so is effectively saturated over the infiltrometer's operational range. This enabled the tensiometer tip to simply be a piece of the infiltrometer membrane, resulting in rapid response to changes in Ψ_0. The tensiometer body was constructed from opaque semi-rigid nylon tubing (4 mm i.d.), sealed at the external end with a rubber septum. Tensiometer pressure was monitored with a pressure transducer connected to the datalogger. Because Ψ_0 was measured continuously any changes in Ψ_0 were known, e.g. due to evaporation of water in the bubble tower causing a gradual loss of suction over long-time experiments. The tensiometer allowed Ψ_0 to be continuously measured with an accuracy of ±0.1 kPa, taking into account errors from calibration and installation of the tensiometer (refer section 3.3.1), and uncertainty in the definition of the nominal soil surface (defined in the following section).

To prevent infilling and blockage of soil pores a nylon retaining membrane with a pore size of 90 μm was placed on the soil surface prior to installing the contact material. Following Bagarello et al. (2001) the retaining membrane was soaked overnight prior to installation. Excess water was shaken off before the retaining membrane was gently pressed onto the soil surface to ensure good contact. Immediately prior to initiation of an experiment the retaining membrane was installed (photo B, Plate 3-10), followed by a 10 mm deep layer of contact material (photo C, Plate 3-10). The contact material was then smoothed and levelled to ensure an even contact surface, as well as a uniform infiltrometer suction (McKenzie et al., 2002). A 5 mm groove was always made at the outer edge (by the lysimeter casing wall), to allow soil air to escape and to enable space for the contact material to deform during infiltrometer installation (Close et al., 1998).

Plate 3-10 Installation of the contact material on the soil surface, with each step described in the preceding text. The tensiometer that measured the surface suction applied by the infiltrometer is shown by the arrow in Plate A.

Definition of the nominal soil surface

Defining the nominal soil surface, $Z_{0,}$ is critical for the accurate use of tension infiltrometers (McKenzie et al., 2002; Reynolds, 2008). This is because of the known offset that the contact material thickness has on the infiltrometer suction, as well as any additional offset to the suction imposed by the height of the air-inlet from the bubble tower relative to Z_0. As previously discussed, this study overcomes these offsets by direct measurement of Ψ_0 at Z_0. However, there is still some error in Ψ_0, propagated from uncertainty in Z_0 due to undulations in the soil surface. For each lysimeter Z_0 was defined as the average depth of the soil surface from the rim of the lysimeter casing. The soil surface depth was measured at 40 locations, with each point measured at 5 cm increments along transects across the diameter of the lysimeter, where each transect was equi-spaced at 0, 45, 90 and 135^o. As a result the standard error in Z_0 was ± 3 – 5 mm across the four lysimeters.

Prior to the measurements for defining the nominal soil surface, all vegetation was carefully removed using scissors. Mostly the soil surface was relatively level and was left undisturbed, although any large undulations (> ~2cm high) were removed by using a knife to carefully pick the surface. This did not cause any obvious smearing or pore blockage because of the strong aggregation, which meant the surface picking generally dislodged intact aggregates.

3.5 Infiltration experiments using the tension infiltrometer

For each lysimeter there were four separate infiltration experiments, with the tension infiltrometer supplying water under surface-imposed suctions of 0, 0.5, 1 and 1.5 kPa. Generally there was also at least one other 'unpublished' experiment for each lysimeter, due to failed experiments where the infiltrometer lost suction. The experiments always went in the order of 1, 0.5, 1.5 and then 0 kPa. This was because it was assumed that the unsaturated experiments were less likely to cause disruption to the pore network, compared to the saturated experiment. The saturated experiment was also immediately followed by prolonged tracer leaching experiments, where the column was saturated under high flow rates until 1.5 – 1.9 pore volumes of drainage had been measured. The alternating sequence of infiltration suctions would not have induced hysteresis because

each was carried out as a separate experiment, with a drainage period in between to establish similar antecedent conditions.

The steps required in preparing and initiating each infiltration experiment are described in the following sections.

Antecedent soil moisture status

Between experiments the lysimeter was drained for 7 – 10 days to achieve similar antecedent conditions, as indicated by measurements of soil matric potential (Ψ_m). During this period the tensiometers were monitored to check that the readings were stable, and if necessary were flushed with de-aired water to remove any air-bubbles. The antecedent measurements of the tensiometers, WCR's, and temperature sensors were always recorded during the pre-experiment period.

Preparation of infiltration solution

The infiltrometer water reservoir was filled with an infiltration solution of tap water (equivalent to untreated irrigation water), 0.005 M $CaS0_4$, and saturated with thymol (0.5 g $litre^{-1}$). The $CaS0_4$ was added to promote aggregate stability and the thymol to inhibit biological activity (McKenzie and Cresswell, 2002b; Skaggs et al., 2002a). The thymol was observed to also inhibit earthworm activity, with a number of dead earthworms always found around at the soil surface at the end of the first infiltration experiment. The infiltration solution was always prepared several days prior to the experiment, to allow any air bubbles arising from the reservoir filling to come out of solution.

Drainage tank preparation

The drainage tank was always emptied between experiments, although during the unsaturated experiments ~ 1 – 2 litres of water was left in the base of the tank to ensure submergence of the end of the bubble tube from the water level sensor. Usually the drainage tank was already under suction during the pre-experiment period, to aid the drain down of the soil to the required antecedent soil moisture. Before the start of each experiment the water level in the bubble tower was adjusted so that the suction was the same as that applied by the infiltrometer (i.e. 0, 0.5, 1, or 1.5 kPa suction).

Infiltrometer preparation

One to two days prior to the start of the experiment the tension infiltrometer disk was immersed in a large water bath to pre-soak the infiltrometer membrane. Any air bubbles

were also carefully removed from the disk headspace while the disk was immersed. When the experiment was ready to start, the infiltrometer disk was removed from the water bath, placed in a shallow water tray on a shelf adjacent to the top of the lysimeter, and the water supply pipe from the supply reservoir attached. With the disk shut-off valve closed the bubble tower vacuum pump was activated, to bring the supply reservoir to the experimental suction.

Instigation of infiltration

When the infiltration experiment was ready to start, the retaining cloth and the contact material were installed. The glass beads were levelled and the surface tensiometer was activated by filling the tensiometer with de-aired water, and installing the pressure transducer. As quickly as possible after installation of the contact material the laptop was used to activate the infiltration and drainage tank sensors, immediately followed by installation of the tension infiltrometer. The infiltrometer was always installed under suction to prevent any infiltration 'flushes'. This was achieved by opening the disk shut off valve just before installation onto the contact material. Because the supply reservoir was already under suction, opening the shut-off valve meant the disk went to suction immediately.

In the first few experiments it was found to be difficult to achieve good contact between the infiltrometer and the contact material, with a few failed experiments where air leaks developed through the infiltrometer membrane. This was overcome by a technique adapted from Close et al. (1998). To ensure good contact the infiltrometer was placed on the contact material and held firmly downwards, whilst being gently rotated back and forth until the infiltrometer had sucked onto the beads. When good contact had been established across the infiltrometer base, the suction prevented the infiltrometer from being easily rotated. It was also found that better contact was established if the contact material was pre-moistened. This also meant that it was easier to fill and activate the surface tensiometer. Pre-moistened contact material also reduced the effects of 'artificial' sorptivity that is generated from the wetting of dry contact material (discussed further in chapter 6).

3.6 Tracer leaching experiments

To distinguish preferential flowpaths, the leaching pattern of an anion tracer pulse was measured during the saturated infiltration experiments (i.e. 0 kPa surface suction). The tracer leaching pattern was also measured during a single unsaturated infiltration experiment with L6, where infiltration was under a surface suction of 1.5 kPa.

A new technique was developed for the tracer application, with a rubber septum in the water supply pipe used to inject a concentrated tracer pulse into the tension infiltrometer (Figure 3-5). This avoids the problems identified by Silva et al. (1999) in studying preferential infiltration, where removal of the infiltrometer to directly apply the tracer onto the soil surface was thought to result in a mixture of preferential and temporary bypass flow, with some of the tracer moving into the soil matrix by the time the infiltrometer was re-installed. This direct injection technique allows controlled-suction solute leaching experiments, with the tracer applied without disturbance of the conducting pore network, thus ensuring that the tracer solution leaches through those pores active in the *infiltration* process. This is illustrated in Figure 3-5, where under 1.5 kPa surface suction the infiltration rate is not uniform across the lysimeter surface, with one side of the lysimeter having a more actively conducting pore network, resulting in preferential infiltration of the tracer.

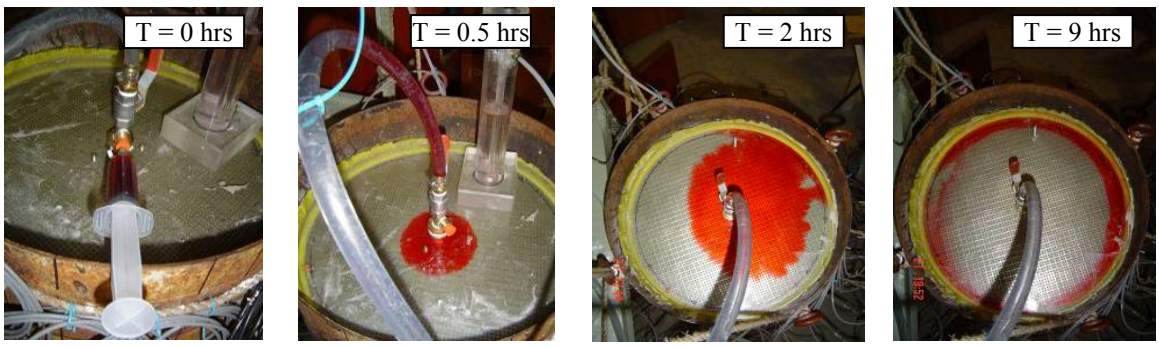

Figure 3-5 Injection of $CaCl_2$ tracer into the tension infiltrometer, set at 1.5 kPa surface suction, during steady state infiltration into L6. Added dye shows the spreading of the injected tracer pulse.

Two anion tracers were used, 0.05M $CaCl_2$ and 0.0025M KBr, because two tracer experiments were conducted on the same lysimeter. This avoided the risk of residual tracer contaminating the second tracer experiment. For consistency the same tracer was used to study the same experimental conditions. The KBr tracer was used across all four lysimeters to study preferential flow arising from a steady-state application under

saturated infiltration. The $CaCl_2$ tracer was used on L1 and L3 to study early-time saturated infiltration, and on L6 to study steady-state unsaturated infiltration. In order to accurately know the actual amount of tracer injected, the weight of each injected pulse was recorded. This allowed the exact anion concentration in each pulse to be calculated. For example, the KBr tracer applied a bromide concentration of between 298 – 314 mg $litre^{-1}$ across the four lysimeters. For the steady-state applications ~188 ml of tracer solution was injected, equivalent to 1 mm depth of infiltration. In order to study preferential flowpaths during the high infiltration rates of early-time infiltration, a smaller volume (~ 40 ml) of higher concentration $CaCl_2$ tracer was injected.

The early-time tracer application occurred as the infiltrometer was installed onto the contact material, whereas the steady-state applications occurred after 80 – 100 mm of cumulative infiltration, and the tensiometers indicated relatively uniform matric potential at each soil depth. An air bubble was injected into the water supply pipe prior to the pulse injection, to isolate the tracer pulse from the infiltrating water, and minimise dilution of the pulse before it moved into the infiltrometer headspace. As shown in Figure 3-5, red food colouring was also added to the tracer solution, so the movement of the tracer pulse within the infiltrometer could be observed.

The pattern of tracer movement through the soil column was monitored by measuring the anion tracer concentration in the drainage water. Drainage samples were collected at increments of 0.02 – 0.05 pore volumes (PV) until approximately 1 PV, increasing to 0.1 PV increments until the experiment was completed at 1.5 – 1.9 PV of drainage. Here PV was assessed as the average *water-filled* pore volume of the soil column during the experiment. The unsaturated tracer experiment was finished after 1.25 PV of drainage because of the long time the experiment took, and the tracer concentration in the leachate appeared to have returned to background levels. Leachate samples were then stored in a freezer until analysis, when the tracer anion concentration was measured by an Ion Exchange Chromatograph (Dionex DX-120) by the Analytical Services Laboratory at Lincoln University.

3.7 Lysimeter dissection

Following completion of the infiltration and leaching experiments the lysimeters were dissected to collect cores and bulk samples for measurement of soil physical and chemical

properties at different depths. To do this the drainage base plate was removed, and new base plate fitted that had a smaller diameter than the lysimeter casing. The lysimeter was then lifted onto a custom built frame (photo A, Plate 3-11). Two winches, attached on either side of the lysimeter, were used to evenly slide the lysimeter casing down in 10 cm increments. A knife was then used to remove the petroleum jelly layer and expose the soil column.

Each column was dissected to collect the following samples:

A. Three large cores (22 diameter x 22 cm deep) for hydraulic conductivity measurements of the individual soil layers. The first core was from 0 – 20 cm (Layers S and A), then 21 – 41 cm (Layer AB), and 42 – 62 cm (Layer B).

B. Three replicate small cores (10 cm diameter by 5 cm deep) were sampled at each of 10 depths to measure the soil water characteristic, $\theta_v(\Psi_m)$, and bulk density. Single bulk samples (~200 grams) were also collected from the same depths for measurement of the $\theta_v(\Psi_m)$ at -100 and -1500 kPa.

C. Single bulk samples (~200 grams) were collected in 5 cm depth increments for measurement of soil chemical properties.

Plate 3-11 The apparatus used to dissect each lysimeter (Photo A), and the sampling pattern followed to collect the large and small cores (Photo B).

The dissection followed a set pattern, as shown in photo B of Plate 3-11. At each depth increment the large core was sampled from a location slightly offset from the centre, and

the small cores in the space between the large core and at least 2 cm from the column side. The bulk samples were collected from the area between the small cores. Because the same locations were used at each depth increment, the cores measured characteristics of the soil pore network in vertical sections down the soil column. There was always a 1 – 2 cm gap between each depth increment of the small cores, due to lost soil from slicing off the upper core and then preparing the surface for the next core. Among the four lysimeters the depth increments of the small core sampling tended to be similar (as shown in Chapter 4 results).

To extract the cores a knife was used to carve a small column slightly larger than the core casing (photo B, Plate 3-11). The lower edge of each core had a sharpened cutting edge, so that excess soil was carved away when the core was carefully pushed down the column. The small cores were then sliced off using a knife, and a wire garrotte used to slice off the large cores. To aid sampling, the inside of the small core rings was smeared with petroleum jelly, whereas the large cores had a cutting ring which left an annular gap which was then filled with liquefied petroleum jelly, in the same manner as the lysimeters (refer section 3.1.4).

After sampling, all samples were placed in plastic bags to prevent evaporation. The small cores and bulk samples were stored in a cool store at 4^{o}C until they were required, whilst the large cores were moved straight to the physics laboratory for preparation.

3.8 Hydraulic conductivity measurement using large cores from individual horizons

The key features of the experimental setup to measure hydraulic conductivity of the large cores is shown in Plate 3-1. The method is only briefly described here because the data were not required for the thesis, except for the saturated infiltration experiment on the topsoil core from L3. Essentially the design features, construction, calibration, and operation of the tension infiltrometer system and tensiometers were the same as those used at the lysimeter scale, and described in detail in earlier sections. The only difference was that the water tanks and infiltrometer were smaller. The measurement errors were similar to those calculated for the lysimeter experiments.

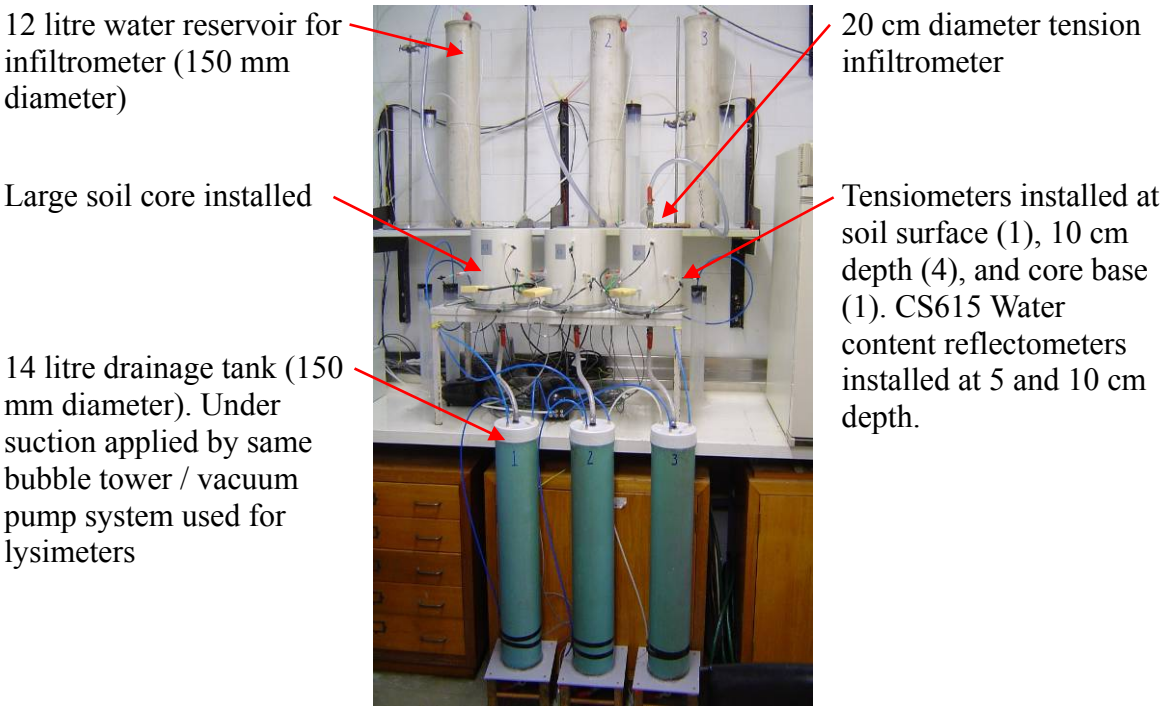

Plate 3-12 The experimental setup used to measure hydraulic conductivity of the large cores.

The whole system was also controlled by a datalogger, but with a scaled-down programme to suit the number of sensors. Because of the shorter experiment duration and fewer sensors the datalogger was programmed to measure every 10 seconds. However, outside of early-time saturated infiltration it was more appropriate to output data as 1 minute averages.

The experiments were conducted at a similar antecedent matric potential to that measured for that particular soil depth in the corresponding lysimeter. The core preparation was similar to the lysimeters, except for the cores from the AB and B layers. Although the core bases were peeled with plaster of paris prior to the installation of the drainage layer, this method was not used at the surface of these cores. This is because the peeling tended to remove entire aggregates, creating large undulations which may have made it difficult to establish uniform infiltrometer contact, and to accurately measure the surface suction. Instead, the infiltration surface was carefully prepared using a sharp knife to remove any smearing, which was checked using a magnifying glass.

3.9 Measurement of hydrophobicity

The degree of hydrophobicity was assessed following the intrinsic sorptivity method described by Tillman et al. (1989) and Wallis et al. (1991). This approach compares the

sorptivity of water versus ethanol, where 95% ethanol is used as a reference liquid that is not affected by hydrophobic compounds during infiltration. The experimental setup used to measure hydrophobicity is shown in Plate 3-13. Infiltration of water and ethanol was measured during separate experiments for each core, where a 10 cm diameter infiltrometer supplied the infiltrating solution under a surface suction of 0.4 kPa. Drainage from the base of the core was also under the same suction. Cumulative infiltration was manually recorded from the burette supply reservoir. Readings were taken every 10 seconds during the first minute, increasing to 30 second intervals up to 10 minutes, and then every minute until a clear steady-state was reached. Accuracy of the burette readings was ±~0.01 mm infiltration.

Plate 3-13 Key features of the experimental setup used to measure hydrophobicity of small cores (10 cm diameter by 5 cm depth).

3.10 Measurement of the soil water characteristic, bulk density, total porosity and particle size distribution

Soil water characteristic (-0.5 to -10 kPa)

The soil water characteristic, $\theta_v(\Psi_m)$, was measured in detail from -0.5 to -10 kPa, which was the range of Ψ_m during the lysimeter experiments. Measurements were made on the small cores (10 cm diameter by 5 cm deep) collected during lysimeter dissection, as described in section 3.7. For each core $\theta_v(\Psi_m)$ was measured at -0.5, -1, -1.5, -2, -3, -4, -5, -7, and -10 kPa following the method of Cresswell (2002). The $\theta_v(\Psi_m)$ at saturation (0 kPa) was not directly measured but estimated from total porosity (Equation 3-7).

For each lysimeter three replicate cores were sampled at 10 depths. Cores were prepared by using a sharp knife to trim the soil flush with the core. The sharp knife was used to remove any smearing, and checked with a magnifying glass. Earlier attempts used both plaster of paris and cellulose acetate to peel the core surface, but both tended to cause substantial disturbance as entire aggregates were removed. This disturbance was considered too great, both for estimation of sample volume and ensuring a good soil contact with the tension table.

Prior to measurement all cores were saturated in a water bath by slowly raising the water level from the base over 2 days. Cores were then left saturated for 2 to 4 days, before being transferred to a tension table, with 9 cores on each table. Each tension table was attached to a hanging siphon, which applied a suction determined by the height of the siphon outlet below a reference level. The reference level in this study was set at the centre of the soil cores sitting on the tension table. This was chosen to minimise vertical variation in the core Ψ_m, resulting in an accuracy of ± 0.25 kPa.

The hanging siphon was used to drain the cores to a series of Ψ_m, with a cover used to prevent evaporation from the tension table. The cores were judged to have equilibrated at each Ψ_m when no water drained from the siphon outlet for at least 24 hrs. Equilibration took a minimum of 2 days, increasing to 5 days at -10 kPa. Once the cores had equilibrated they were removed and individual weights recorded. Cores were then replaced on the suction table, with a hand sprayer used to apply a thin sheen of water to the suction table to aid the hydraulic contact between the core and the tension table. The siphon was then lowered to the next suction, and the cores left to drain down to equilibrium.

For each core, $\theta_v(\Psi_m)$ was determined at each Ψ_m using the equation,

$$\theta_v(\Psi_m) = \frac{(W_3 - W_2 - W_1)}{W_1} \times \frac{\rho_b}{\rho_w} \qquad \text{Equation 3-3}$$

where W_1 is the weight of the oven dry soil sample (g), W_2 the weight of the sampling cylinder (g), W_3 the weight of the soil sample and sample cylinder at the given Ψ_m (g), ρ_b the dry bulk density of the soil sample (g / cm^3), and ρ_w is the density of water (1.0 g / cm^3).

Soil water characteristic (-100 and -1500 kPa)

For each lysimeter $\theta_v(\Psi_m)$ at -100 and -1500 kPa was also measured for the same 10 depth increments that the small cores were sampled from. Measurements were completed by the Landcare Research Environmental Chemistry Laboratory, using pressure plate apparatus and following a method similar to that described by Cresswell (2002). One repacked sample from each depth was measured, using soil sampled during lysimeter dissection, as described in section 3.7. Results were supplied on a gravimetric basis, and then converted to θ_v using the equation,

$$\theta_v = \theta_g \, \rho_b / \rho_w$$

Equation 3-4

where θ_g is the gravimetric water content (%w/w), ρ_b the average dry bulk density at that depth (g / cm^3), and ρ_w is the density of water (1.0 g / cm^3).

Bulk density and total porosity

Bulk density was measured using the small cores (10 cm diameter by 5 cm deep) collected for measurement of the soil water characteristic (0 to -10 kPa), following the measurement of $\theta_v(\Psi_m)$ at -10 kPa. First the volume of any indents was determined using quartz sand (1 – 2 mm diameter) carefully levelled to the soil surface. Indent volume was determined using the equation,

$$V_i = W_s \rho_{b(s)}$$

Equation 3-5

where V_i is the indent volume (cm^3), W_s is the weight of the sand used to fill the indents (g), and $\rho_{b(s)}$ the bulk density of the sand (g / cm^3). After careful removal of the sand, the soil was then removed from each core into a drying tin, and placed in an oven at 105^{o}C until constant weight was reached (48 – 72 hours). The soil dry bulk density, ρ_b (g / cm^3), was then calculated using the equation,

$$\rho_b = W_1 / (V_c - V_i)$$

Equation 3-6

where W_1 is the weight of the oven dry soil sample (g), V_c is the core volume (cm^3), and V_i is the indent volume (cm^3).

Total porosity (ε_t) can then be calculated using the equation,

$$\varepsilon_t = 1 - \frac{\rho_b}{\rho_p}$$ Equation 3-7

where ρ_p is the particle density of the soil sample, with 2.65 g / cm^3 used in this study.

Particle size distribution

Particle size distribution was measured for 5 cm depth increments of each lysimeter, using soil sampled during lysimeter dissection, as described in section 3.7. Measurements were completed by the Landcare Research Environmental Chemistry Laboratory, using the standard pipette method (Claydon, 1989).

Particle size distribution was also determined for the sandy gravel that was used as the 5 cm thick drainage layer at the base of the lysimeters. At the end of the lysimeter dissection approximately 2 kg of the drainage layer was collected from lysimeter 2. The gravel (>2.0 mm) and sand (<2.0 mm) fractions were then separated by wet sieving through a 2.0 mm sieve. Both samples were then dried and weighed, and a subsample of the sand fraction collected for particle size analysis by the pipette method.

3.11 Measurement of total carbon, total nitrogen, cation-exchange capacity, and P-retention

Measurement of chemical properties was carried out using subsamples taken from the bulked sample collected from each 5 cm depth increment during lysimeter dissection, as described in section 3.7. Samples were prepared by air-drying for 48 hours, and then sieved through a 2 mm sieve.

Total carbon and nitrogen

Total carbon and nitrogen were measured for all four lysimeters, for every 5 cm depth increment. A subsample of ~0.5 g was taken from each bulked increment sample, and analysed using an Elementar Vario-Max CN analyser by the Analytical Services Laboratory at Lincoln University.

Cation exchange capacity and exchangeable cations

Cation exchange capacity was measured for lysimeter 6, for every 10 cm depth increment. This sample was a 50:50 mix from the two relevant 5 cm depth increment samples. The samples were prepared following the method of Blakemore et al. (1987) and

analysed using a Varian 720-ES Inductively Coupled Plasma Optical Emission Spectrometer, at the Analytical Services Laboratory at Lincoln University,.

P-retention

P-retention was measured for lysimeter 6, for every 10 cm depth increment. The samples were prepared and analysed following the method of Blakemore et al. (1987), by the Landcare Research Environmental Chemistry Laboratory, Palmerston North.

Chapter 4
Physical attributes of the soil columns

4.1 Introduction

In order to understand infiltration behaviour it is important to first understand the physical make-up of the soil. The objective of this chapter is to describe and compare the physical attributes of the soil columns. The environmental context of the soil's location is also described, particularly the rainfall pattern. This knowledge provides a framework to understand the infiltration experiments that are presented in the following chapters. Conversely, the infiltration experiments then provide a basis for judging the relative importance of different physical attributes to the infiltration and movement of water through this soil.

The methods used for measuring the attributes described here are given in chapter 3.

4.2 Climate, parent material, vegetation, and relief

The soil is mapped as the Gorge series (ECAN, 2009; Kear et al., 1967), occupying approximately 4900 hectares (ECAN, 2009), between Methven and the foothills of the Southern Alps. The soil is formed in loess over alluvial gravels, with both materials derived from the Rakaia River to the immediate north. The parent material of the loess and gravels is predominantly hard sandstone (greywacke) eroded from the Southern Alps. The loess is typically 0.45 to ~1 m deep (ECAN, 2009). Most of the area mapped as Gorge series is gently sloping (2 – 7^{o}); with smooth relief, and between 340 to 500 m altitude. Vegetation is predominantly permanent pasture.

Two climate stations are located to the east of the sampling site, with a rainfall only station at Methven (~6.5 km away), and a full climate station at the Highbank Power station (~7.5 km away) (NIWA, 2009). The Highbank station closed in 2001, whilst Methven remains open. The long-term mean annual temperature recorded at Highbank is 10.8^{o}C (1970 to 2001), with a mean annual rainfall of 933 mm. Methven recorded a very similar long-term mean annual rainfall of 924 mm from 1970 to 2008. The rainfall at the sampling site is likely to be higher, as there is a relatively steep rainfall gradient towards the Alps. Figure 4-1 shows the long-term average monthly rainfall, potential evapo-

transpiration (PET), and soil water deficit. Rainfall is reasonably uniform throughout the year, but the PET has a strong seasonal cycle. As a result there is three to five months of the year with no soil water deficit, indicating that there will be a reasonable 'drainage season'.

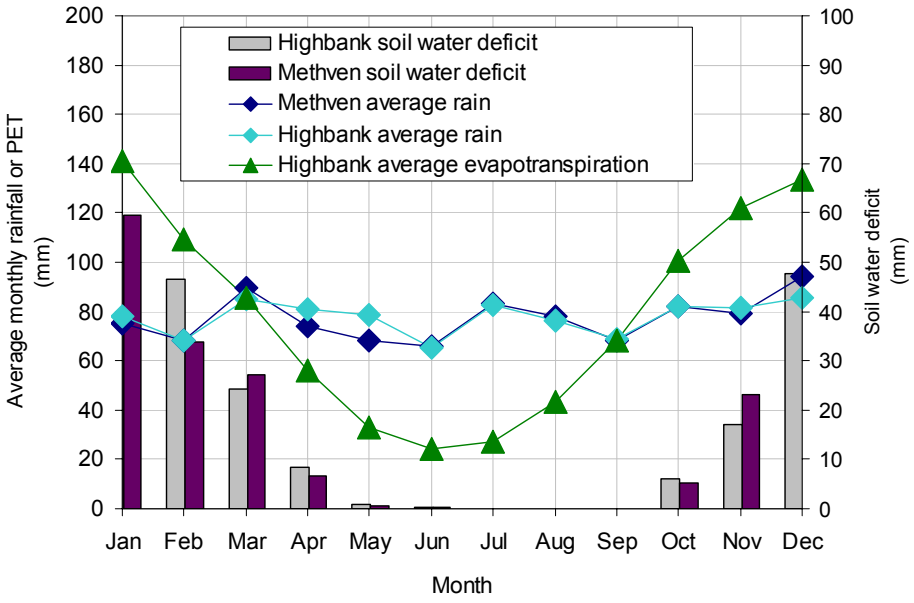

Figure 4-1 Long-term average monthly rainfall, potential evapo-transpiration (PET), and soil water deficit recorded at the Methven (1970 to 2008) and Highbank (1970 to 2001) climate stations (NIWA, 2009). Soil water deficit is estimated by assuming 150 mm soil water storage.

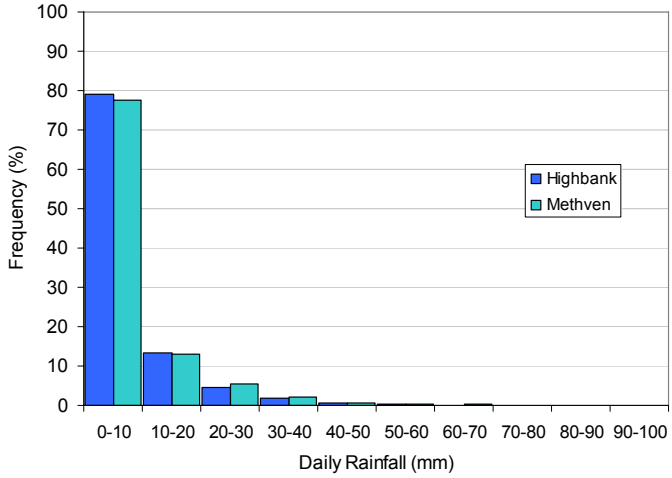

Figure 4-2 Frequency of daily rainfall amounts recorded at the Methven (1970 to 2008) and Highbank (1970 to 2001) climate stations (NIWA, 2009).

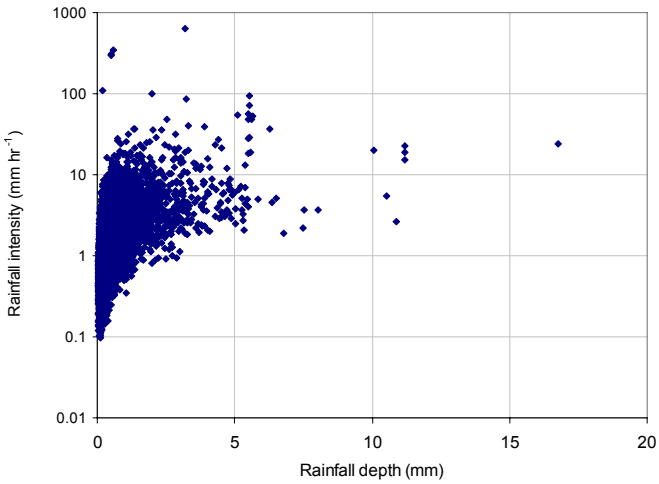

Figure 4-3 The relationship between rainfall depth and intensity for each individual rain event recorded at Highbank climate station from 1986 to 1993 (NIWA, 2009).

The rainfall was typically in small amounts, with less than 10 mm rain on ~78% of rain days (Figure 4-2). Daily rainfalls of 10 – 30 mm are common, occurring on 18% of rain days, hence rainfalls of > 30 mm day^{-1} are rare. Individual rain events are typically less than 5 mm depth, with an intensity of less than 10 mm hr^{-1} (Figure 4-3). Rain events with an intensity of > 10 mm hr^{-1} have a 1.6% frequency. Most rain events are small and light, with only 0.2% of rain events having a depth > 5 mm and an intensity of > 10 mm hr^{-1}. The predicted frequency – magnitude relationship (Figure 4-4) confirms that intense rainfall is a relatively rare phenomenon. The predicted two year return interval of one hour and 24 hour rainfalls are 12 mm and 66 mm, respectively (Thompson, 2002).

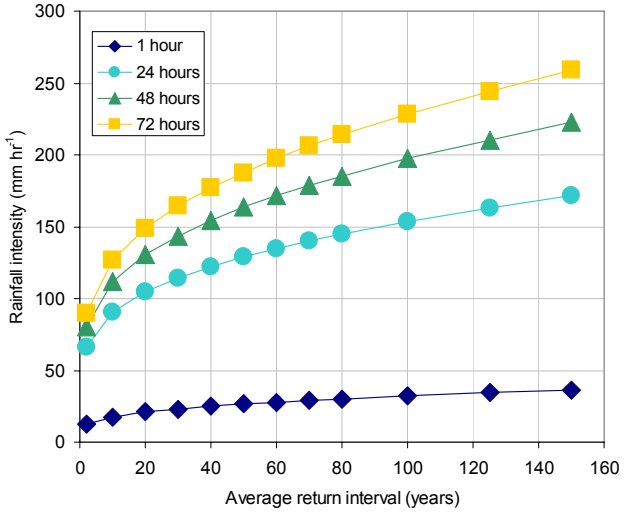

Figure 4-4 The predicted return interval of high intensity rainfalls for the Methven area, over time periods of 1 hour to 3 days (Thompson, 2002).

4.3 Soil classification

The Gorge series is a Typic Firm Brown; stoneless; silty; moderately permeable soil according to the New Zealand Soil Classification (Clayden and Webb, 1994; Hewitt, 1998). This is an unusual taxon for the Canterbury Plains, where soils formed in deep loess are typically found in a drier climate and have a fragipan (ECAN, 2009; Kear et al., 1967). The Gorge series is similar to the Brown soils that have formed in deep loess on the Southland Plains under similar rainfall, where 40 000 hectares are mapped as the Waikiwi and Edendale series (Topoclimate, 2009).

4.4 Soil morphology

The soil morphology was described at three sites where the lysimeters were extracted, and is very similar between the sites (Plate 4-1). A generalised soil description is presented in Table 4-1, with full descriptions from each site presented in Appendix 2. Three distinct layers (horizons) exist: The topsoil to 20 – 25 cm depth and subsoil below 40 – 45 cm are easily identifiable, with an intergrade zone in-between. These layers coincide very closely with the 20 cm increments that are used for defining soil layers in the lysimeter experiments. The uniform yellow-brown colour of the subsoils and the lack of low or high chroma mottles imply the soil is well drained, with rare or absent periods of saturation and anaerobic conditions (Webb et al., 1995). Soil structure is strongly developed in the topsoil, but was not as easy to describe in the subsoil. Nearby road cuttings that had dried showed a distinctive primary structure of large prisms, which although still apparent in the described profiles, was much more subtle. Secondary structural units (polyhedral and smaller prisms) were easier to identify, but they had the tendency to progressively subdivide into smaller and smaller aggregates, which caused concern regarding what was the ‘real’ structure. The subsoil structure became weaker with depth, with a new soil layer recognised below 80 cm where the subsoil was verging on apedal.

Overall the three profiles were very similar, showing a relatively high degree of spatial uniformity in the soil morphology. This was also evident throughout the lysimeter trench, and during the post-experiment dissection of the lysimeters.

Profile 1 Profile 2 Profile 3

Plate 4-1 Soil profiles at each of the three sites where soil morphology was described. The colour difference in Profile 1 is an artefact of the photograph, with similar soil colours described in the field.

Field		Lysimeter		
Horizon	Depth (cm)	Layer	Depth (cm)	Description
Ap	0 – 25	S A	0 – 2 2 – 20	Dark greyish brown (2.5Y 4/2) silt loam; weak soil strength; moderate to high penetration resistance; very high particle packing; strongly developed abundant very fine to fine polyhedral peds; abundant roots between and within peds; indistinct occluded boundary.
AB	25 – 40	AB	20 – 40	Dark greyish brown (2.5Y 4/2) and light yellowish brown (2.5Y 6/4) silt loam; weak soil strength; very high penetration resistance; extremely high particle packing; strongly developed abundant fine polyhedral and many medium to coarse prismatic peds; many reducing to common roots with depth, between and within peds; indistinct occluded boundary.
Bw1	40 – 82	B	40 – 60 (60 – 70 layer present, but no sensors)	Light yellowish brown (2.5Y 6/4) silt loam; slightly firm soil strength; extremely high penetration resistance and particle packing; weakly developed very coarse to extremely coarse prismatic structure, breaking to moderately developed fine to coarse polyhedral and prismatic peds; common reducing to few roots between peds; distinct irregular boundary
Bw2	82 – 110	-		Light yellowish brown (2.5Y 6/4) silt loam; slightly firm soil strength; very high penetration resistance; extremely high particle packing; massive apedal; few roots in macropores; indistinct wavy boundary.
2C	110	Drainage base	70 - 75	On gravels

Table 4-1 A generalised description of the key morphology features, summarised from three profile descriptions (Appendix 2). The field-described horizons are correlated with the equivalent soil layer that was defined for the lysimeter experiments.

4.5 Soil chemistry

The basic chemical attributes are given in Table 4-2. Soil P-retention increases with depth, but is classified as moderate throughout the profile. Cation exchange capacity and base saturation are moderate in the topsoil, and then decrease to low in the intergrade and subsoil layers (Blakemore et al., 1987). Base saturation and calcium levels were expected to be higher, due to the infiltrating solution (0.005M $CaS0_4$) used during the experiments.

Depth	Cation exchange properties cmol(+)/kg					BS	P-ret
(cm)	Ca	Mg	K	Na	CEC	(%)	(%)
0 – 10	8.93	0.37	0.25	0.33	16.84	59	28
10 – 20	5.01	0.22	0.21	0.25	12.66	45	32
20 – 30	4.10	0.21	0.14	0.26	11.94	39	36
30 – 40	3.34	0.17	0.10	0.27	8.95	43	37
40 – 50	2.73	0.11	0.06	0.26	9.14	35	41
50 – 60	2.49	0.12	0.09	0.27	9.13	32	44
60 - 70	2.53	0.13	0.07	0.27	6.94	43	46

Table 4-2 Key chemical attributes.

4.6 Aggregate size distribution

Laboratory sieving of soil aggregates indicated that the soil is strongly aggregated in both the topsoil and subsoil (Figure 4-5). The whole profile is dominated by fine aggregates (< 10 mm diameter), which comprise 83% of the topsoil and 61 – 57% of the two subsoil samples. The similarity of the two subsoil layer samples indicates that there is no significant deterioration of structure with depth in the subsoil.

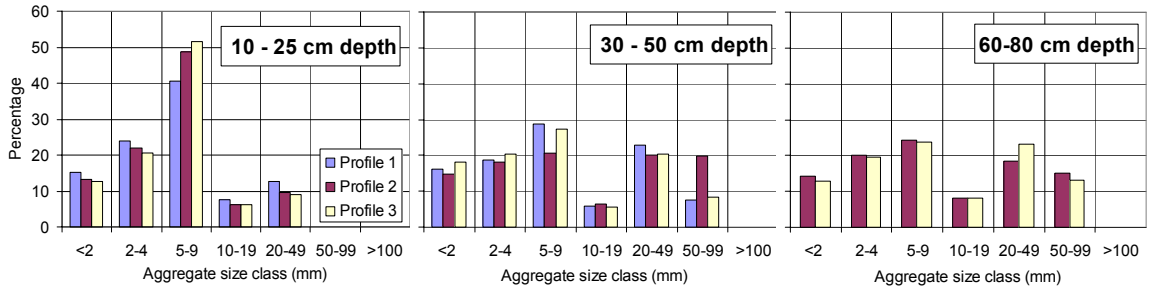

Figure 4-5 Aggregate size distribution at three depths of the soil profiles, as determined by dry-sieving of large samples (16 – 20 kg) collected from the field site.

4.7 Aggregate stability

Aggregate stability was assessed on samples collected from a reconnaissance survey of the sampling site. A wet-sieving stability test indicated 82% stability for the topsoil, and 85% stability for the subsoil. A dispersion test on the same samples also indicated good stability, with minimal dispersion or slaking observed over 24 hours of immersion (Plate 4-2). Leachate collected after at least 400 mm saturated infiltration was consistently clear during all of the infiltration experiments (Plate 4-2), further indicating that the structure was stable during these experimental conditions.

Plate 4-2 Aggregate stability as indicated by immersion for 24 hours, and by the leachate clarity during the saturated infiltration experiments.

4.8 Field estimation of hydraulic conductivity

According to the pedotransfer functions of Griffiths et al. (1999) the soil morphology indicated that the saturated hydraulic conductivity of the topsoil is moderate (18 – 71 mm hr^{-1}), decreasing to very low to low (1 – 17 mm hr^{-1}) in the subsoil. The unsaturated conductivity at a surface suction of 0.4 kPa is estimated as very low (1 – 3.5 mm hr^{-1}) for the topsoil, decreasing to extremely low (< 1 mm hr^{-1}) for the subsoil (Griffiths et al., 1999). A concern with the reliability of these estimates is that the soil was drier than recommended by Griffiths et al. (1999), who note that particle packing measurements are particularly sensitive to moisture content. Consequently, the particle packing for these profiles may be over-estimates, particularly for the topsoil where very high packing does seem excessive for the strongly developed fine structure.

4.9 Soil particle size distribution

Particle size is highly uniform both among the lysimeters, as well as with depth for each lysimeter (Figure 4-6). Across all depths and all lysimeters the mean clay fraction is 26% (0.4% s.e.), with 65 % silt (0.4% s.e.), and 9 % sand (0.2% s.e.).

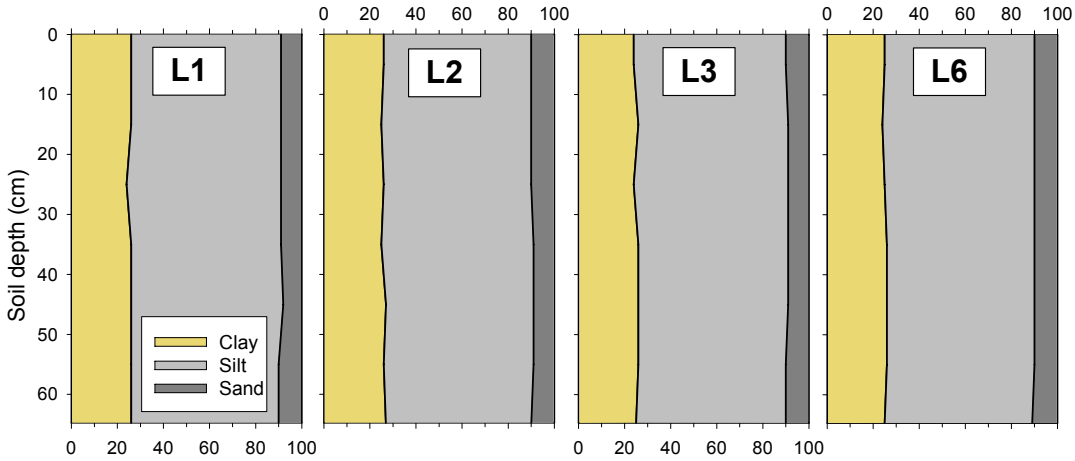

Figure 4-6 Particle size distribution of the four lysimeters, measured in 5 cm depth increments.

4.10 Soil carbon and nitrogen

Carbon and nitrogen show a steady decline with depth for all lysimeters (Figure 4-7). The C:N ratio is stable to 30 cm depth, before increasing at varying rates among lysimeters. The levels of carbon and nitrogen would classify as low to 30 cm depth, declining to very low below 40 cm depth (Blakemore et al., 1987). Of most interest to this study is the total carbon, which is very similar between the lysimeters. Most variation is shown between 25 – 40 cm depth, reflecting an intergrade zone between the topsoil and subsoil. This is shown in Plate 4-1, where over this depth interval there are distinct areas of high-carbon topsoil, and low-carbon subsoil. The other interesting feature is the distinct difference in carbon levels between the 0 – 5 cm depth and the rest of the topsoil (5 – 20 cm depth).

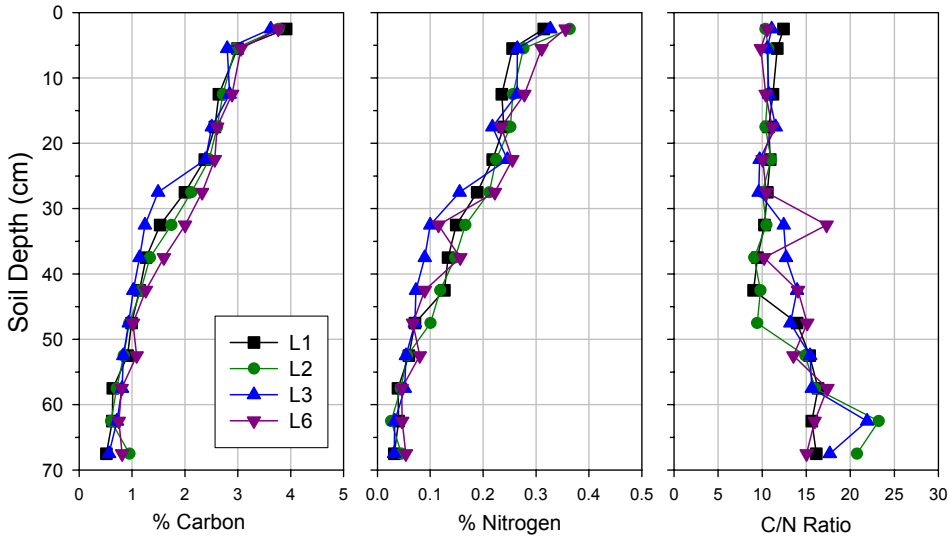

Figure 4-7 Comparison of the total carbon, nitrogen, and C:N ratio of the four lysimeters, measured in 5 cm increments. Data points are shown at the centre of each increment, but are representative of the whole 5 cm increment.

4.11 Bulk density and solid / void relationships

Bulk density consistently increases with depth for all lysimeters (Figure 4-8). Among lysimeters the bulk density at any particular depth is similar, although it becomes more variable in the subsoil. Below 40 cm depth the bulk density increases more sharply with each depth increment, showing that the low organic matter subsoil is now the dominant soil material. The most distinctive feature of Figure 4-8 is the bulk density of the 0 – 5 cm layer, which is clearly much lower than the rest of the topsoil. The 0 – 5 cm layer classifies as moderate bulk density, compared to moderately high for all other depths (McQueen, 1993). Figure 4-8 also shows the pattern of total porosity, with key features that mirror the bulk density pattern. Total porosity classifies as moderate to 40 cm depth, before decreasing to moderate – low, then low below 60 cm (McQueen, 1993).

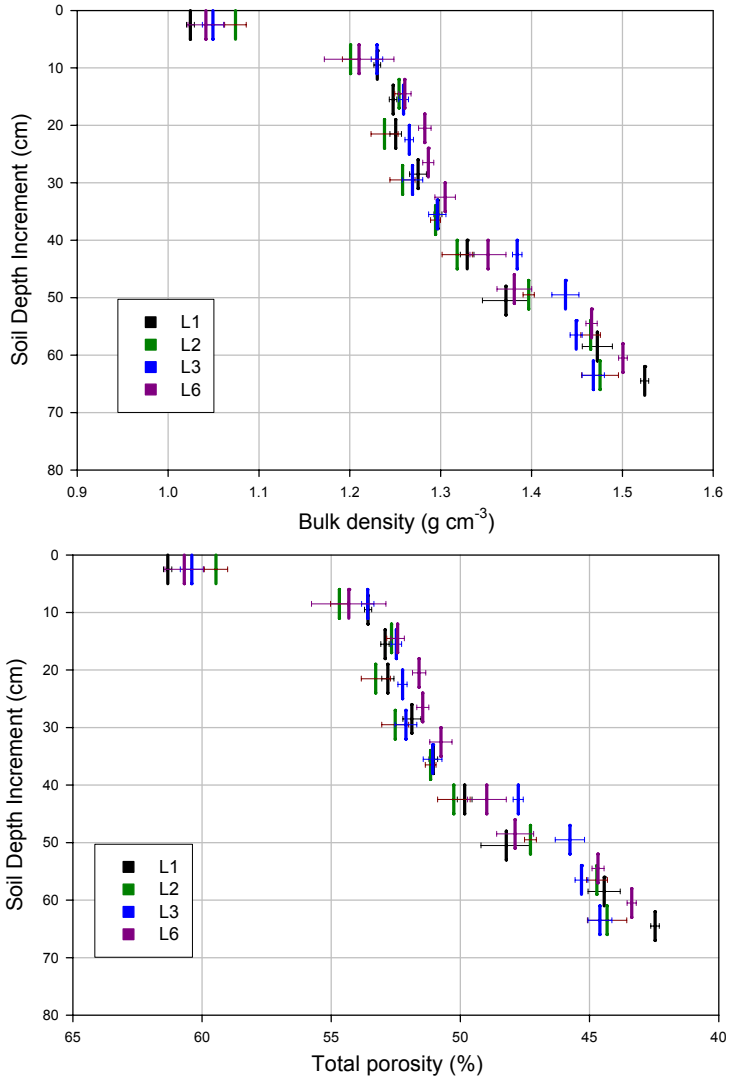

Figure 4-8 Comparison of bulk density and total porosity with depth for each lysimeter, measured in 5 cm increments. Data points are shown as vertical bars to indicate the individual 5 cm depth increment, with horizontal bars showing the standard error of the three replicates of each increment.

The decrease in total porosity with depth appears to be mostly due to a loss in the 'drainage' pores, which drain between 0 to -10 kPa (Figure 4-9). The water held at -10 kPa is a key hydraulic attribute, and is often described as the field capacity or the upper drainable limit. The void space between 0 to -10 kPa is the air-filled porosity at field capacity (AFP) (McKenzie, 2004; McKenzie, 2008; Webb et al., 1995). On average, drainage pores decline by 10.4% down the profile, from about 16% at 0 – 5 cm depth to 6% at 60 cm depth. The average loss in storage pores down the profile is 5.6%. The residual pore network volume varies less than 3 % through the profile. The profile-averaged volume of storage pores ranges from 20 – 27% among the lysimeters. This equates to 140 – 190 mm of plant available water to 70 cm depth. Greater than 150 mm is considered a high water storage capacity (Webb et al., 1995).

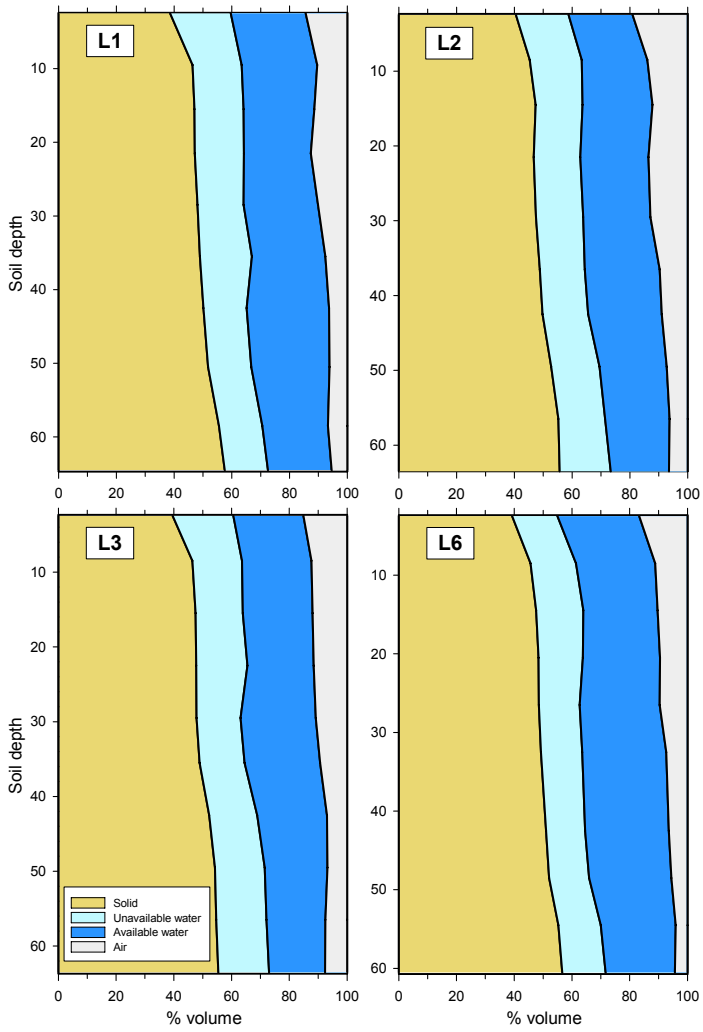

Figure 4-9 The solid / void relationship of the four lysimeters, measured in 5 cm increments. The pore volume between 0 to -10 kPa is classed as drainage / air pores, with storage pores between -10 to -1500 kPa holding the plant-available water. Residual water held below -1500 kPa is classed unavailable.

4.12 Soil water characteristic (-0.5 to -10 kPa)

Detailed results of the soil water characteristic, $\theta_v(\Psi_m)$ for the drainage pore network are shown in Figure 4-10. $\theta_v(\Psi_m)$ declines as matric potential decreases most sharply in layers S & A. The decline in $\theta_v(\Psi_m)$ is greatest between -0.5 to -3 kPa for layers S & A, and between -2 to -5 kPa for the lower layers. Within layers S, A, and B the $\theta_v(\Psi_m)$ consistently declines with each depth increment. Such a pattern is not clear for Layer AB, possibly reflecting its inter-grade nature.

The changes in the $\theta_v(\Psi_m)$ pattern relate well to the morphologically defined soil layers. This is particularly evident in the $\theta_v(\Psi_m)$ between -0.5 to -2 kPa, where there is a sharp decrease in layers S & A, but not apparent in the AB and B layers. This trend highlights a

major decrease in macropore abundance between the topsoil and subsoil. Of interest is that at 19 – 25 cm depth the $\theta_v(\Psi_m)$ pattern is more similar to layer A, indicating that 25 cm depth is possibly a more appropriate boundary for layer A. The 0 – 5 cm depth also has clearly different $\theta_v(\Psi_m)$, again highlighting this depth as a distinct soil layer.

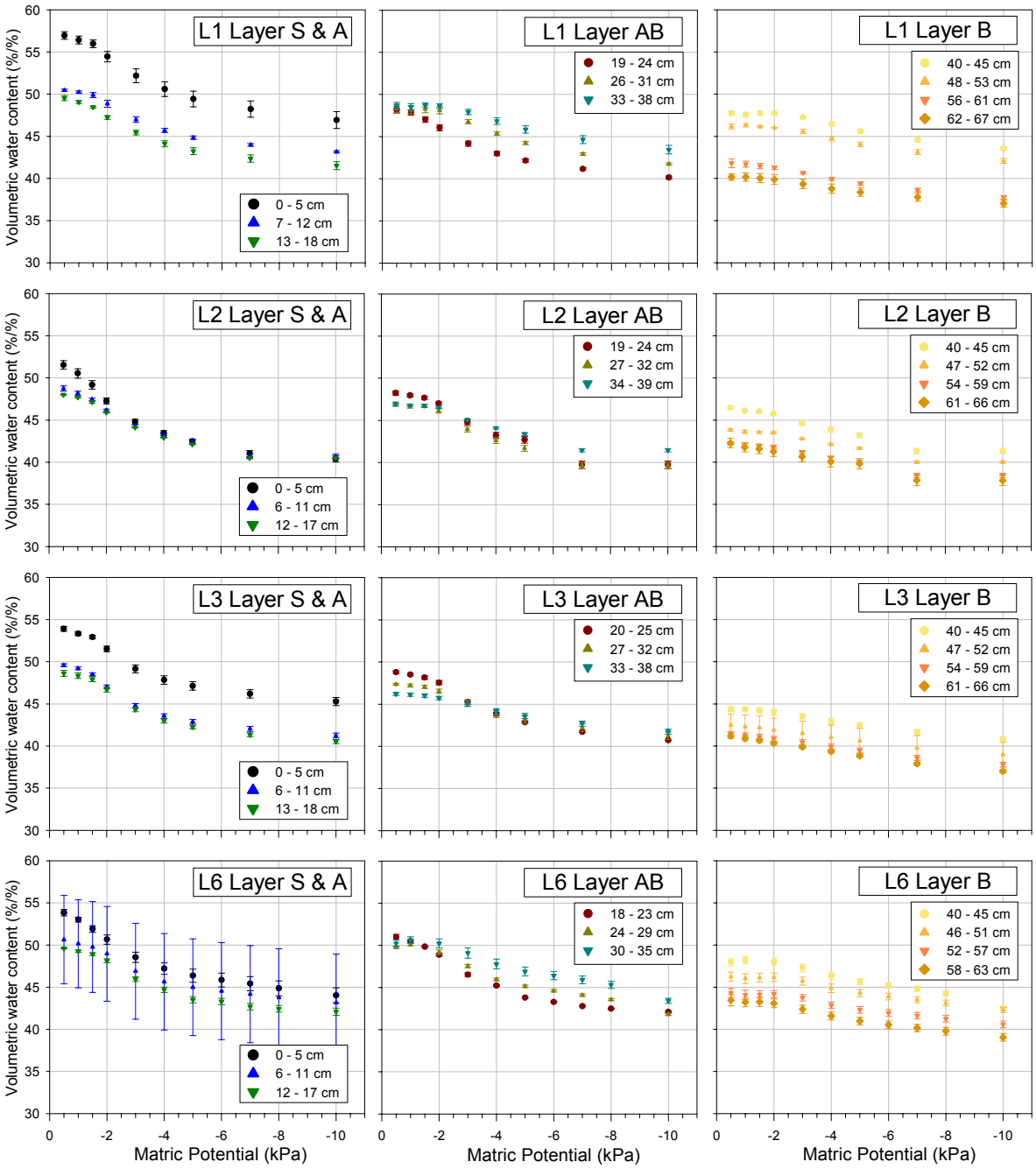

Figure 4-10 The soil water characteristic for the individual layers of each lysimeter over the range of matric potentials between -0.5 to -10kPa. The soil water characteristic was measured for the same 5 cm depth increments as Figure 4-8. Vertical error bars show the standard error of three replicates at each increment. The large error bars for L6 6 -11 cm are thought to be due to measurement error.

4.13 Discussion

Climate station records highlight the importance for land management and environmental protection of understanding infiltration and conductivity behaviour for the Gorge soil, because these records show that there is a regular soil-water 'drainage season'. The flat topography and low slope mean that any surface ponding of surplus water is not likely to generate runoff. Climate records also show that rainfalls are typically of low intensity and amount, further reducing the risk of runoff. Soil colour indicates that periods of saturation are minimal and of short duration. This is further evidence of good drainage and thereby supports the contention that the water surplus moves as drainage rather than runoff.

Soil morphology shows distinct soil layers, where a topsoil, worm-mixed, and subsoil are easily identifiable. Whilst the exact boundary between layers is difficult to define, the layers do approximately correlate with the 20 cm increments that are used for the lysimeter experiments. The measured physical attributes also correlate with the defined soil layers, particularly the pattern in bulk density, soil carbon, and $\theta_v(\Psi_m)$. It is clear from the physical attributes that the 0 – 5 cm depth should be defined as a separate soil layer, even though this was not at first apparent in the soil morphology.

The measurements show a consistent decline in soil porosity with depth, which appears to be mostly due to a reduction in the pore network responsible for drainage. Measurement of $\theta_v(\Psi_m)$ over the drainage-pore range highlights distinct differences between the soil layers, particularly in relative abundance of pores over a particular Ψ_m range. Below 25 cm soil depth the $\theta_v(\Psi_m)$ measurements for each lysimeter detected little or no decline in porosity over the range of -0.5 to -2 kPa. This range is of particular importance for water infiltration and drainage because it includes the macropore network often associated with preferential flow (Jarvis, 2007), and is the pore network of most interest in this study.

Whilst these results appear to highlight a sharp reduction in macropore abundance below the topsoil layer, it may also partly reflect sampling error. This error could arise if macropores occur in spatially distinct regions such as between large aggregates, and the volume and number of cores was too small to 'capture' these regions. It is also possible that the subsoil pore network has an air-entry value such that it resists the applied suction until a critical suction is reached, at which drainage commences. This would be at odds with the morphology which shows good drainage, and also the rapid drainage behaviour

that was observed during the lysimeter experiments. Therefore, if a critical air-entry value is present, it is possibly an artefact of the measurement method.

Sampling error may also arise if the artificially wet conditions during measurement induced atypical wetting of the soil. It was observed that it was difficult to obtain stable weights at these low suctions, with a number of cores appearing to even slightly gain weight as the suction increased from -0.5 to -2 kPa (refer to layer B $\theta_v(\Psi_m)$ pattern, Figure 4-10). The prolonged artificially wet conditions could induce swelling of clays and removal of entrapped air, which would draw water up from the suction plate, and offset water that may have drained at the applied suction. These conditions would not arise in the field situation because of the natural good drainage of the soil.

Another key feature is the remarkable uniformity in soil texture. The measurements show no variability in texture among lysimeters and soil layers. This is important because texture is often used to explain differences in infiltration and drainage behaviour. Texture is also a key parameter in most models that are used to predict soil hydraulic attributes. The uniform texture of this soil indicates that there should be minimal variation in the infiltration and conductivity attributes both among the lysimeters, and between the individual soil layers. This soil does show a consistency between the $\theta_v(\Psi_m)$ pattern, and changes in bulk density and carbon. These results indicate that the reduction in the drainage pore network with soil depth is strongly related to decreasing levels of soil carbon, which is reflected in aggregates increasing in both density and size. The relationship with carbon is not purely causative. There is a correlation between carbon and drainage pores because both in turn are related to biological activity.

Overall the soil morphology and physical attributes indicate that this soil shows high physical fertility. Soil water storage and aeration are seen as key indicators of physical fertility (Webb et al., 1995). The physical measurements show that the soil has high water storage capacity (AWC), and the volume of drainage pores indicate that at field capacity there is adequate air-filled porosity (AFP). This is reflected in the soil colour which indicates good drainage and minimal periods of anaerobic conditions. McKenzie et al. (2004) rate a soil's physical fertility on the relationship between AFP and AWC. The profile-averaged AFP (10%) and AWC (22%) of the Gorge soil would rate as good physical fertility. Physical fertility declines with depth, with good to very good in Layer S decreasing to moderate in the subsoil.

Chapter 5
Comparison of three methods to characterise preferential flow in a layered soil column during infiltration

5.1 Introduction

Research on New Zealand soils indicates that the potential for preferential flow is the norm, rather than the exception (McLeod et al., 2003). Research has also identified that preferential flow is a key hydrological pathway for the leaching of a number of contaminants that pose significant risks to the sustainability of NZ agriculture, including: nitrate (Di and Cameron, 2002b); phosphate (Toor et al., 2005); heavy metals (McLaren et al., 2004); pathogens (Jiang et al., 2005; Jiang et al., 2008; Pang et al., 2008); and dairy-shed effluent (Houlbrooke et al., 2004; Jiang et al., 2008).

Whilst the evidence is building about the potential for preferential flow behaviour in NZ soils, there is limited research on the mechanisms that generate preferential flow, and therefore the likely frequency of occurrence. Internationally there has been considerable published research, with comprehensive reviews by Beven and Germann (1982), Clothier et al. (2008), Hendrickx and Flury (2001), and Jarvis (2007). An important issue identified is that there are numerous preferential flow experiments where the results may be artefacts of unnatural boundary and initial conditions (Clothier et al., 2008; Jarvis, 2007). Jarvis (2007) reviewed 115 published experiments, identifying that ~20% used ponded infiltration or saturated flow, and another ~20% used controlled irrigation fluxes of 10 – 100 mm hr^{-1}. Most of these studies did not state the equivalent rainfall return period, but based on the amount and intensity of water application, Jarvis (2007) interpreted that in most cases the likely return period was years rather than months. It was concluded that relying on extreme flux experiments risks developing a biased understanding of preferential flow behaviour, particularly the frequency of its occurrence and significance over long time frames.

This research project was established to characterise the influence of preferential flowpaths on infiltration behaviour at or near saturation. Importantly, the research was

initiated prior to publication of the reviews by Jarvis (2007) and Clothier et al (2008), who recognised the potential for experimental conditions to create biased impressions of preferential flow behaviour. It is within this context that this chapter provides results from experiments designed to address the question: Does using three different methods provide a consistent understanding of preferential flow behaviour?

The three methods that were used are as follows:

Dye tracer. Brilliant blue dye was used to characterise preferential flowpaths from unconfined ponded infiltration at three field sites. Dye tracers are a common method to visually characterise the presence of preferential flow behaviour in field soils (Flury and Wai, 2003), but typically use high fluxes. The classic study of Flury et al. (1994) irrigated 40 mm over 8 hours, but irrigation was applied as pulses with an intensity of 96 mm hr^{-1}; Weiler and Fluhler (2004) irrigated 75 mm at two sites, using rates of 12 and 60 mm hr^{-1}; Alaoui and Goetz (2008) irrigated 110 mm at 47.5 mm hr^{-1}; and under ponded infiltration Nobles et al. (2004) applied 550 mm; whilst Kim et al. (2004) applied 150 mm.

Tensiometer arrays. The infiltration behaviours of four large lysimeters were studied under controlled surface suctions. At four depths within each lysimeter an array of tensiometers measured the variability in matric potential (Ψ_m), and thus the degree of preferential flow under different infiltration conditions. This is an expanded version of a classic preferential flow study by Bootlink and Bouma (1991), who used arrays of seven tensiometers at three depths to study variability in Ψ_m during infiltration into a 20 x 20 cm soil core. Although there is less published research comparing tensiometer arrays with dye infiltration, there are recent publications where arrays of tensiometers have been used to study temporal and spatial dynamics of preferential flow under natural field conditions (Bradley et al., 2007; Woehling et al., 2008; Zhan et al., 2007).

Drainage Breakthrough Curves. Using the large lysimeters, anion tracers were injected into the infiltrating water, and the pattern of leachate concentration versus cumulative drainage was measured. This is a 'standard' method of studying solute transport (Skaggs et al., 2002a), and has been used in a number of preferential flow studies on New Zealand soils (Jiang et al., 2005; McLeod et al., 2004; McLeod et al., 2003; Silva et al., 2000; Toor et al., 2005).

5.2 Methods

The methods relevant to each of the above experiments are described in chapter 3.

5.3 Results

5.3.1 Ponded infiltration dye study

The results of using brilliant blue dye to characterise preferential flowpaths are presented in Plate 5-2, where photographs of the dye pattern in both vertical and horizontal sections are compared for three locations. These sections show clear preferential flowpaths, particularly at depths below ~30cm, and indicate that the infiltration pattern is strongly associated with soil horizons. Dye infiltration follows a relatively uniform distribution in the A horizon (0 – 20 cm depth), before being channelled into distinct preferential flowpaths in the AB horizon, which then persist deep into the B horizon (>40 cm depth). Overall the dye pattern shows strong similarity between the three sites, indicating spatial consistency in the preferential flow network, and suggests that this is an important hydraulic feature of this soil. At all sites there is uniform dye coverage of the A horizon, and highly localised dye concentration in the subsoil with strong vertical and horizontal interconnectivity of flowpaths. In this soil the subsoil flowpaths that persist to the greatest depth follow interpedal regions between large primary structural units (Plate 5-1), which appear to be prisms of 15 – 50 cm width.

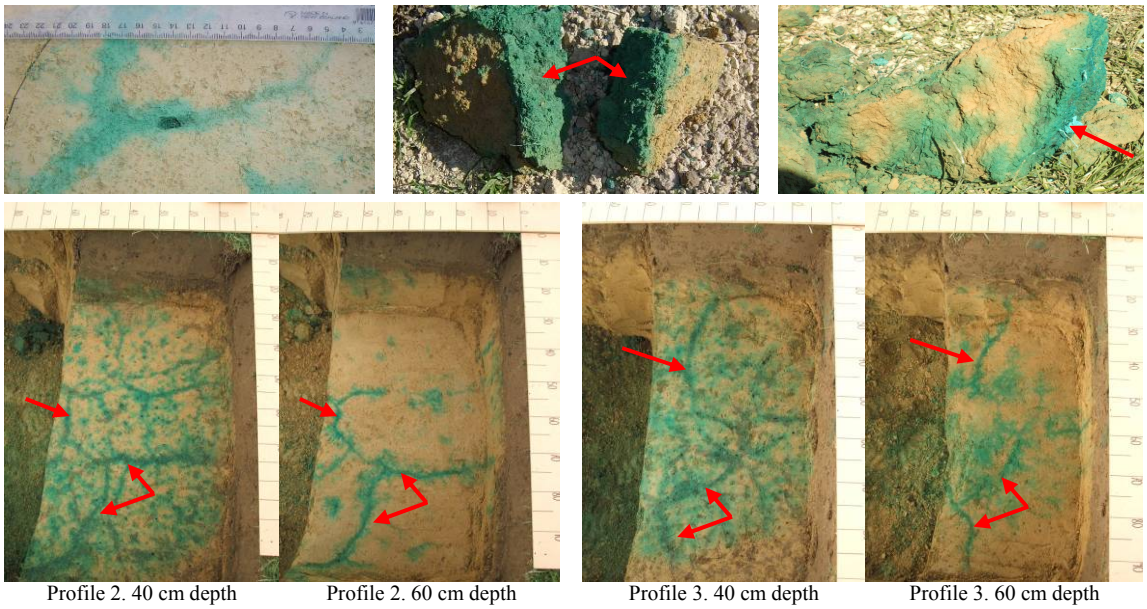

Profile 2. 40 cm depth | Profile 2. 60 cm depth | Profile 3. 40 cm depth | Profile 3. 60 cm depth

Plate 5-1 Photographs of the relationship between dye pattern and soil structure. Major B horizon flowpaths follow interpedal regions between the primary structural units, as highlighted by arrows.

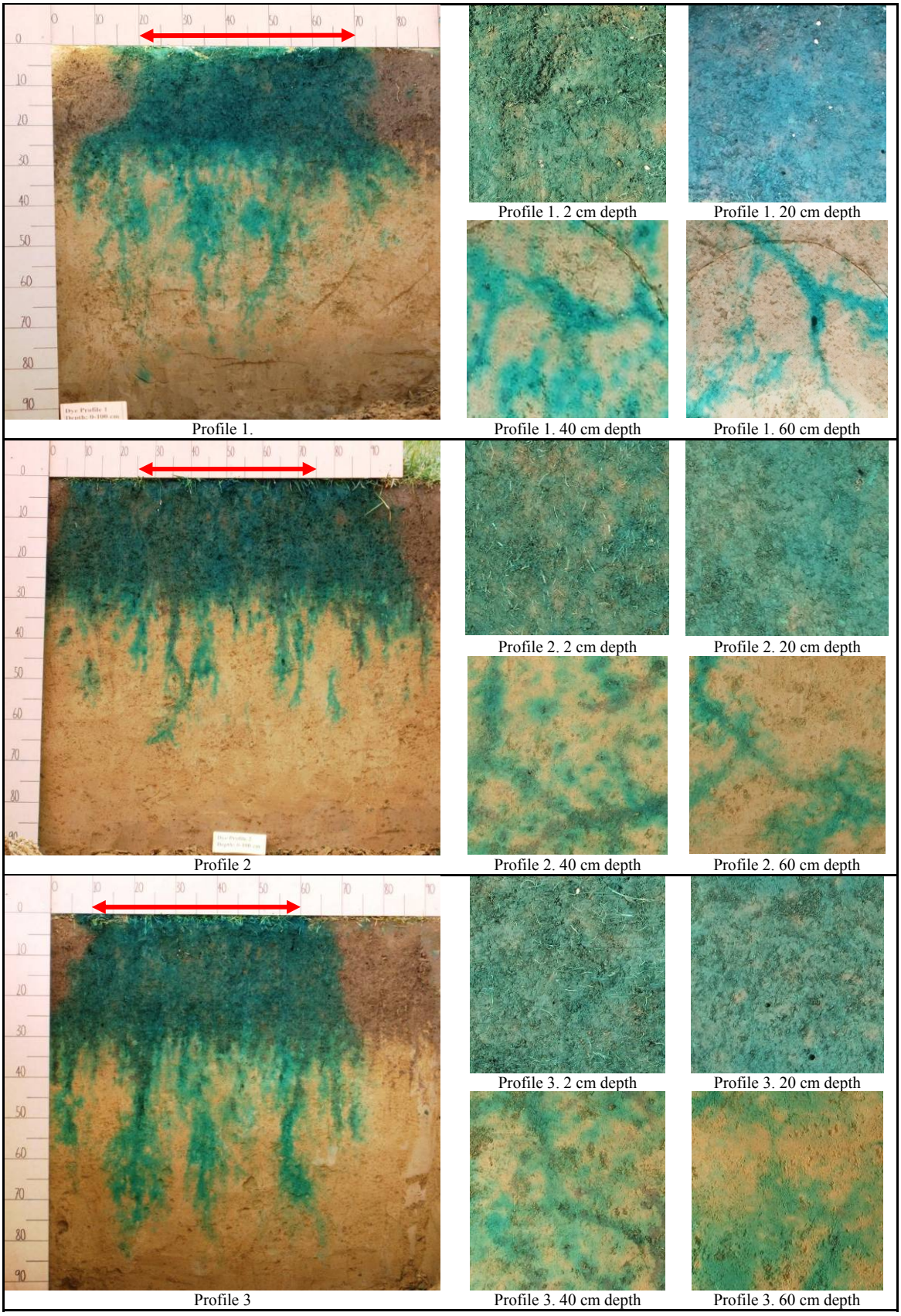

Plate 5-2 Preferential flow patterns following ponded infiltration of 50 mm Brilliant Blue dye from a 50 cm diameter ring. Location of infiltration ring is shown in red, with vertical sections located across the ring centre, and representative 20 x 20 cm horizontal slices at 2, 20, 40, and 60 cm depth.

Although strong preferential flow via interpedal pores is characteristic of soils with structured subsoils (Flury et al., 1994; Nobles et al., 2004), the aggregate size distribution (Figure 4-5, chapter 4) indicated subsoil aggregates were < 10 cm wide, which does not match the dye pattern. It appears that these aggregates are a secondary structure of the large primary units, and that the substructure has greater aggregate packing, creating a less conductive and connected interpedal pore network compared to the primary structural units. In the upper subsoil the dye does appear to penetrate into the pore network of the substructure, but only the primary flowpaths persist below 50 cm depth. The dye pattern shows that the primary flowpaths are often 1 – 2 cm wide, highlighting that preferential flow is not necessarily confined to discrete macropores, but also to regions of well connected macropore sequences (Seyfried and Rao, 1987). The primary flowpath regions are also characterised by clusters of plant roots and earthworm burrows, which would further enhance their conductivity.

5.3.2 Soil matric potential measurements during saturated and unsaturated infiltration

Infiltration experiments were conducted on the four lysimeters using the tension infiltrometer to supply infiltrating water under surface-imposed suctions of 0, 0.5, 1 and 1.5 kPa. The results show that as the surface suction is increased, the infiltration rate (i_t) typically reduced by about two orders of magnitude between saturated infiltration (0 kPa) and infiltration under the largest suction of 1.5 kPa (Figure 6-1, chapter 6).

During the infiltration experiments arrays of tensiometers were used to measure the soil matric potential (Ψ_m) at set depths within each lysimeter (defined in Table 3-1, chapter 3). The spatial average and standard deviation of Ψ_m at depths of 2, 20, 40, and 60 cm are shown in Figure 5-1, which shows the changes in Ψ_m as infiltration time progresses. Note that to enable comparison of all the infiltration experiments, that time is represented on a logarithmic scale.

This section only discusses the pattern in the standard deviation of Ψ_m, which shows the spatial variability in the downward movement of the wetting front, and thus infers the degree of preferential flow. The dynamics of the mean Ψ_m at each depth is discussed in chapter 7.

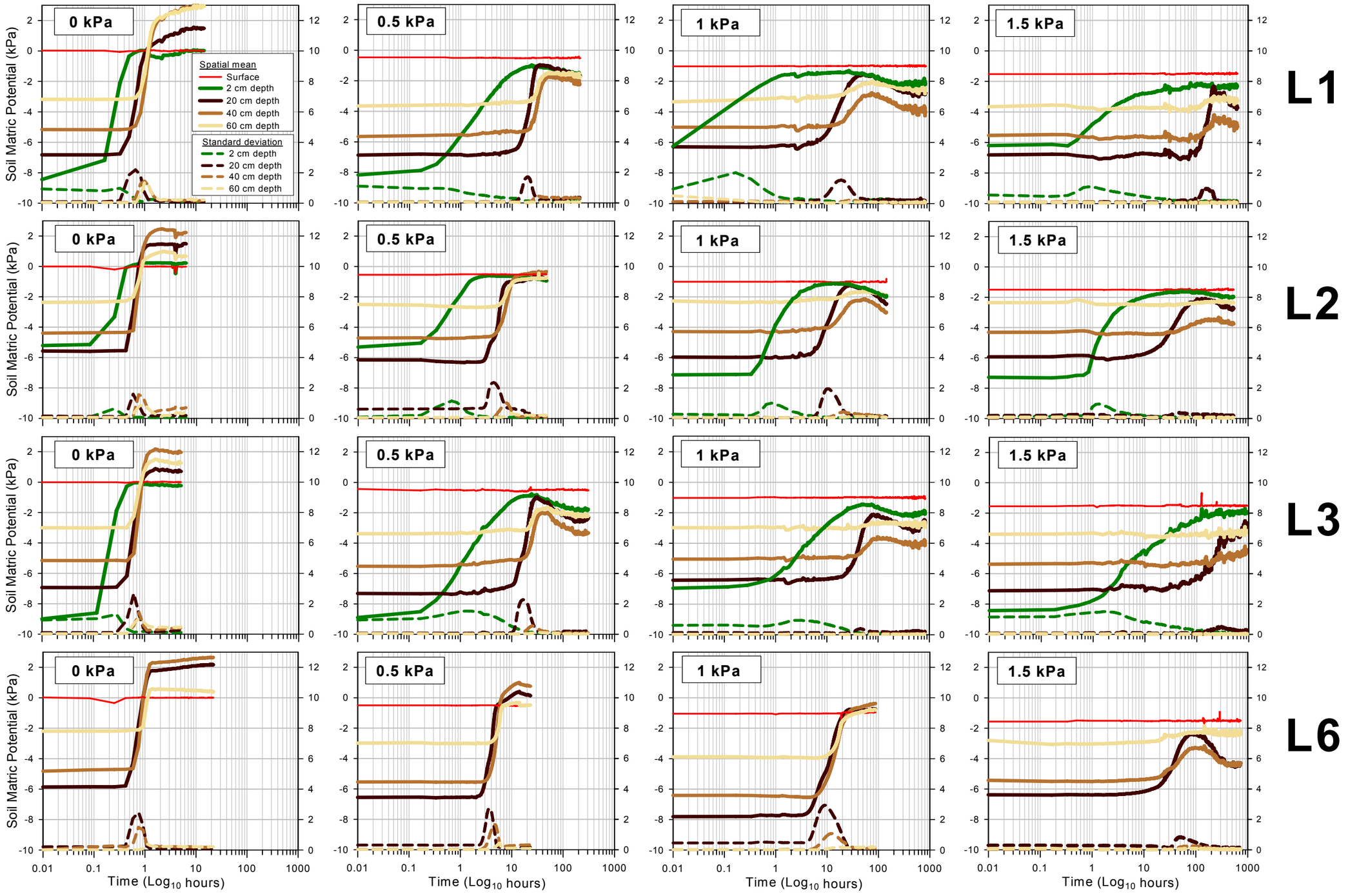

Figure 5-1 Comparison of the dynamics of soil matric potential between lysimeters during infiltration, where infiltration occurs under controlled surface suctions of 0, 0.5, 1 and 1.5 kPa. Solid lines represent the spatial average of Ψ_m at the set soil depths, with the scale on the left Y-axis. Dashed lines represent the spatial standard deviation of Ψ_m at the set soil depths, with the scale on the right Y-axis.

Figure 5-1 clearly shows that the pattern of change in Ψ_m is strongly dynamic. For each lysimeter the pattern changes when infiltration occurs under a different surface suction. Also, for infiltration under the same suction the pattern of Ψ_m varies among the four lysimeters, for example when infiltration occurs under 0.5 kPa surface suction.

The spatial variability in Ψ_m, represented by the standard deviation curves, shows that preferential flow occurs during saturated and unsaturated infiltration, although at the highest surface suction of 1.5 kPa it is not strongly expressed. These measurements are consistent with the review of Jarvis (2007), which concluded that experimental evidence consistently shows that preferential flow becomes increasingly important as Ψ_m wets to above -1 kPa. Jarvis (2007) argues that wetting only needs to occur in small localised areas such as at the soil surface or at layer boundaries to activate preferential flowpaths. This occurred in experiments in this study, where the tension infiltrometer wetted the surface boundary to a defined Ψ_m.

Preferential flow also appears to be greatest in the topsoil, with the standard deviation in Ψ_m at 20 cm depth (base of the topsoil) often peaking at 1.5 to 3 kPa, whereas the standard deviation at 60 cm depth (base of the subsoil) peaks at 0.4 – 1.3 kPa under saturated infiltration, and is much lower under unsaturated infiltration at <0.5 kPa. These observations appear to indicate a general pattern of preferential flow increasing as the wetting front moves down the topsoil, and then decreasing in the lower two horizons. Importantly, during unsaturated infiltration the tensiometers at 60 cm depth detect no or minimal evidence of preferential flow. This is interpreted as reflecting that the channelizing macropores remain empty and the matrix pore network of the B horizon is able to cope with the water flux during unsaturated infiltration, which during the initial wetting of the column is at least one order of magnitude lower than during saturated infiltration. The apparent uniform wetting of the B horizon indicates the unsaturated pore network has sufficient continuity and conductivity to redistribute the uneven wetting front that is generated by the topsoil. This concept is discussed further in Chapter 7.

Interestingly, the spatial standard deviation curves indicate that the peak preferential flow behaviour at 20 cm depth is not necessarily greatest under saturated infiltration, with L2 and L6 both showing the largest variability in Ψ_m under surface suctions of 0.5 and 1 kPa. Preferential flow behaviour also persists for longer periods of time during unsaturated infiltration, lasting for between 3 – 20 hrs compared to ~0.7 – 1 hrs during saturated

infiltration. However, in terms of cumulative infiltration, preferential flow appears to persist longer under saturated infiltration. At 20 cm depth the non-uniform wetting front arrived within 3 – 7 mm cumulative infiltration under both saturated and unsaturated infiltration, with the exception of L3 which took 16 mm during saturated infiltration. Preferential flow then persisted for another 14 – 23 mm of saturated infiltration, compared to 4 – 14 mm during the 0.5 and 1 kPa unsaturated infiltration experiments, with the exception of L6 1kPa which persisted for 20 mm cumulative infiltration (discussed further in section 7.4.1, chapter 7).

Once the soil column has wet up, the variability in Ψ_m becomes minimal, indicating a spatial uniformity at each depth within the column. Even when the soil internally switches from wetting to drainage behaviour (e.g. L2 1 kPa), the change occurs uniformly at each depth. This pattern appears to highlight that preferential flow is strongest during the initial transient wetting of the column, and then lessens under steady-state infiltration.

5.3.3 Leachate tracer concentration

To distinguish between preferential movement of the *infiltrating* water, and displacement of the existing *resident* water, an anion tracer pulse was injected into the tension infiltrometer during some of the experiments presented in section 5.3.2. The pattern of tracer concentration was then measured in the drainage water. The tracer experiments were originally confined to the steady-state phase of *saturated* infiltration, when it was assumed that preferential flow would be most strongly expressed. This is also a common approach used in other preferential flow studies (Jiang et al., 2005; McLeod et al., 2003; Silva et al., 2000). However, measurements of Ψ_m indicated that preferential flow may actually be greatest during the initial transient stages of infiltration, so for L1 and L3 an additional tracer application was applied at the start of the saturated infiltration experiment.

The pattern of tracer movement during *unsaturated* infiltration was also studied for L6, where the tracer was applied during the steady-state phase of infiltration under 1.5 kPa surface suction. Under this surface suction it was assumed that preferential flow would be negligible, based on the review of preferential flow experiments by Jarvis (2007). This experiment took three months to complete, and was not replicated on other lysimeters

because of time-constraints, as well as the practical difficulties of maintaining infiltration under controlled suction for such long-time periods.

The results are presented in Figure 5-2 where the normalised tracer concentration (leachate concentration / pulse concentration) is plotted against the pore volumes (PV) of drainage. Here PV is assessed as the average water-filled pore volume of the soil column during the experiment. If no preferential flow occurred, a tracer application would not be measured in leachate until about 1 PV of drainage, because all the resident soil water would have to be displaced, before the arrival of the tracer as a discrete pulse (Hillel, 1998; Skaggs et al., 2002a).

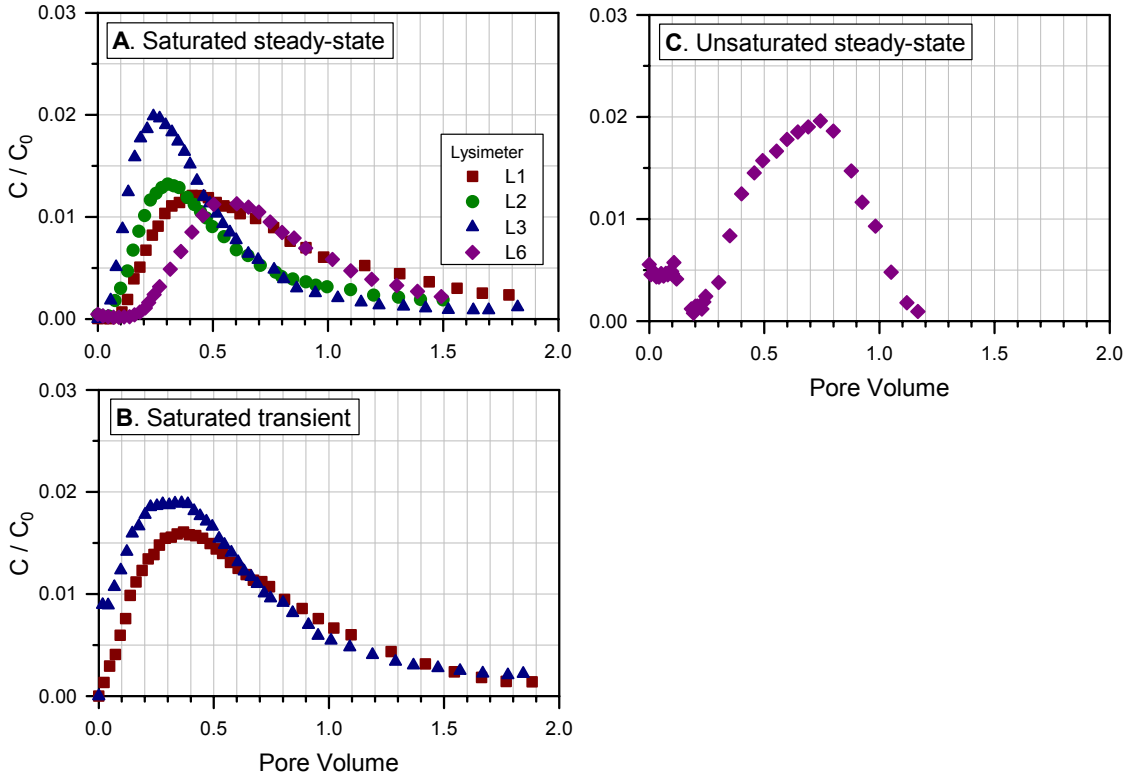

Figure 5-2 Breakthrough curves of relative tracer concentration, measured in pore volume increments of lysimeter drainage, for tracer leached under different flow conditions: A. Bromide tracer applied under saturated conditions, once the infiltration rate had reached steady-state (after 80 – 100 mm cumulative infiltration); B. Chloride tracer applied at the initiation of saturated infiltration (i.e. 0 mm cumulative infiltration); C. Chloride tracer applied under unsaturated flow conditions (infiltration at 1.5 kPa surface suction, lysimeter 6), once the infiltration rate had reached steady-state (41 mm cumulative infiltration).

Under saturated conditions all lysimeters show distinct preferential flow, during both the transient and steady-state phases of infiltration. When the tracer was applied at the start of infiltration it appeared within 0.02 PV of drainage, in contrast to the steady-state application where the tracer was detected within 0.2 PV for all lysimeters. The peak concentration arrived between 0.2 – 0.6 PV, with a similar pattern between the transient and steady-state saturated experiments, except for the L3 steady-state application where the breakthrough curve appears more compressed with a sharp peak.

The saturated steady-state leaching pattern appears to be a function of i_t, where a faster i_t results in greater preferential flow. In these experiments the saturated i_t was in the order L3 > L2 > L1 > L6. The same order was followed for the tracer leaching, where both the initial arrival and peak concentration were detected earliest for L3, and slowest for L6.

Preferential flow also appears to occur under unsaturated conditions, with 1.5 kPa surface imposed suction, and Ψ_m within the soil column between -2.5 to -5 kPa during the experiment (Appendix 4). The leaching pattern is similar to that measured under saturated infiltration for the same lysimeter, except that both the initial and peak concentrations arrived 0.1 – 0.2 PV later under unsaturated flow. However, after the peak concentration the unsaturated breakthrough curve drops off sharply and lacks the long 'tail' characteristic of the saturated breakthrough curve.

Distinct preferential leaching of the same bromide tracer was also observed by Mcleod et al. (2003) on a similar soil type to this experiment. Mcleod et al. (2003) used a constant flux irrigation of 5 mm hr^{-1}, which was below the estimated saturated conductivity and therefore likely to have induced unsaturated leaching. Interestingly, the breakthrough curve was very similar to the saturated L6 experiment of this study (which had an i_t of 5 – 6 mm hr^{-1}), with the tracer arrival and peak concentration at similar PV's of drainage.

5.4 Discussion

The results of the three different experimental methods clearly show that preferential flow is a ubiquitous feature of this soils infiltration behaviour. The following sections discuss how the three methods provide a similar or different understanding of the preferential flow pattern.

5.4.1 Ponded infiltration dye study

Although dye patterns have been used primarily to illustrate the presence of preferential flow under certain infiltration conditions (Flury et al., 1994), there have been a number of attempts to use dye patterns to elucidate understanding of the underlying flow mechanisms. Weiler and Fluher (2004) developed a classification scheme based on the width of the dye flowpaths, where a dominance of flowpaths <2 cm wide indicates flow primarily in macropores, and low interaction with the surrounding soil matrix, whilst a dominance of flowpaths >20 cm wide indicates predominantly matrix flow.

Applying this scheme to the vertical dye patterns in Plate 5-2 suggests that homogenous matrix flow occurs in the A horizon, changing in the subsoil to macropore flow showing mixed interaction with the matrix. The interaction zones vary between 2 – 10 cm, which is interpreted as indicating that the matrix permeability may be spatially heterogenous, or that the flow velocity in preferential flowpaths (macropores) is spatially heterogenous (Weiler and Fluhler, 2004). Uniform topsoil dye distribution appears to be typical of most soils studied using dye infiltration, although this often applies only for the surface layer (0 – 10 cm deep) (Flury et al., 1994; Kim et al., 2004; Öhrström et al., 2002; Weiler and Fluhler, 2004). These previous studies also identify that most soils have the potential for subsoil preferential flow, although the apparent spatial consistency among the three sites of this studies may not be the norm.

The differences in dye coverage at each soil depth are summarised in Figure 5-3, where image analysis has been applied to the horizontal sections in Plate 5-2 to estimate the percentage of soil stained by dye, as well as regions with pale compared to dense dye concentration (as distinguished in Appendix 3). Dye concentration has been previously identified as important for interpretation of preferential flowpaths, where regions of low concentration may not actually represent preferential flowpaths, but lateral mass

exchange between preferential flowpaths and the soil matrix (Alaoui and Goetz, 2008; Forrer et al., 2000; Weiler and Naef, 2003).

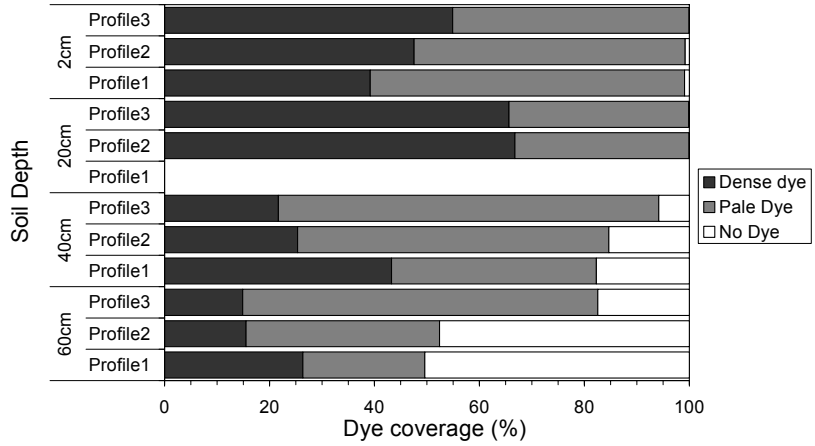

Figure 5-3 Interpretation of the relative density of dye coverage at four depths in each profile, based on the horizontal sections presented in Plate 5-2. Image analysis was not performed on the 20 cm depth of Profile 1 because the photo is over-exposed, although Plate 5-2 shows that the relative dye density is similar to the other profiles.

Figure 5-3 shows that although dye coverage was essentially 100% in the A horizon (0 – 20 cm depth), there are distinct regions of dense and pale dye concentration, with 40 – 65% of the horizon having dense dye concentration. This highlights that the initial interpretation of uniform matrix flow may not be correct, and that preferential flow may be a significant mechanism throughout the whole profile. Preferential flow is obvious in the subsoil, with distinct areas of unstained soil increasing with depth. However, the abundance of densely stained areas is clearly higher in the A horizon, suggesting that preferential flow may actually be greater in this layer. The locations of preferential flowpaths are not easily distinguished for the A horizon, with no apparent primary structural units, or areas with an increased density of roots and biopores. However, Seyfried and Rao's (1987) concept that preferential flow occurs through macropore regions appears to be applicable to both the A and B horizons.

The areas of pale dye are also relatively abundant at all depths, further indicating that lateral mass exchange between preferential flowpaths and the matrix is an important hydraulic feature of this soil. The proportion of dense vs pale dye in the A horizon is similar between the three profiles, but shows greater variability among the three profiles in the subsoil. This supports Weiler and Fluher's (2004) interpretation that spatial heterogeneity exists in the matrix permeability of the interaction zone surrounding the subsoil macropore regions.

5.4.2 Soil matric potential measurements

The preferential flow behaviour observed via the tensiometers generally correlates with the behaviour deduced from the dye infiltration, but a comparison is only relevant to infiltration behaviour under saturated conditions. In particular the tensiometer data support the results of the image analysis of dye concentration, which indicates that preferential flow is a dominant feature of infiltration into the A horizon. Both these methods show that the initial visual impression seen in the dye pattern was misleading, and that the classification by Weiler and Fluhler (2004) of uniform matrix flow through the A horizon was incorrect in this case.

The observed dye pattern probably reflects the second of a two-stage infiltration behaviour observed via the tensiometers. At early-time infiltration the initial wetting follows preferential flowpaths. This is then followed by a second stage when there is reduction of lateral gradients in the matric potential, which results in dye migrating into the matrix. I interpret dye migration as resulting from a number of processes: 1. further vertical infiltration via smaller macro- and meso-pores; 2. lateral infiltration from preferential flowpaths; 3. 'perching' of infiltration water on the B horizon, which has a lower saturated conductivity (refer chapter 7). Perching at the base of the A horizon will slow the flow rate of preferential flowpaths and increase lateral infiltration, as well as 'backfill' the A horizon as water builds up at the base. Evidence of perching can be seen when comparing the dye density at 2 and 20 cm depth in Figure 5-3, where there is a distinct increase in the proportion of dense dye at 20 cm depth. This build up of dense dye at the base of the A horizon is also seen in the vertical sections of Plate 5-2.

However, the tensiometer response at 2 cm depth in Figure 5-1 is not consistent with this interpretation of the A horizon infiltration behaviour. Under all infiltration conditions the 2 cm tensiometers appear to show relatively uniform wetting at the surface, compared to the distinct preferential flow behaviour at 20 cm depth. The 2 cm tensiometers do show an antecedent spatial variability (not present in deeper layers), which appears to persist until this depth is wet up, indicating a degree of preferential flow. The dye density analysis in Figure 5-3 also indicates that preferential flowpaths are present at 2 cm depth. The weak expression of preferential flow response of the 2 cm tensiometers possibly reflects that the surface pore network has greater spatial access to freely available infiltration water that is across the whole soil surface, resulting in a relatively uniform

distribution of matric potential. The pore network at deeper depths within the A horizon does not have such easy access, relying initially on the availability of infiltration water in limited areas associated with preferential flowpaths. Pore size analysis (Figure 4-10, chapter 4) also indicates that the 0 – 5 cm depth has a distinctly greater porosity (particularly macropores) than the rest of the A horizon. The high macroporosity and low variability in tensiometer response indicates a relatively intensive and well connected macropore network, which the 2.5 cm long x 1 cm diameter tensiometer cups appear to invariably intercept. It is for these reasons that it may be justified to recognise the approximately 0 – 5 cm depth as a distinctly different soil layer from the underlying A horizon, particularly when preferential flowpaths are activated. This concept is discussed further in chapter 7.

At first glance the tensiometer response in the B horizon under saturated infiltration appears to indicate that preferential flow was not as strongly expressed as that observed during the dye study. In Figure 5-1 the standard deviation in Ψ_m at 40 and 60 cm depth indicates that preferential flow is consistently weaker than in the A horizon. However, I interpret this as an artefact of the antecedent matric potential (Ψ_i), which is higher (wetter) in the B horizon, particularly at 60 cm depth where Ψ_i is -2 to -3 kPa. The moister B horizon places a greater limit on the possible variation in Ψ_m, compared to the drier A horizon, and therefore may mask the observation of preferential flow in Ψ_m measurements of the B horizon. To overcome these differences in Ψ_i between soil layers and lysimeters, the standard deviation of the tensiometer measurements was normalised by expressing the standard deviation relative to Ψ_i (Figure 5-4).

The pattern of change in the normalised standard deviation shows that significant preferential flow did occur in the B horizon during saturated infiltration. The only exception is at the 60 cm depth for L6, where preferential flow is only weakly expressed. This is interpreted as meaning that L6 may not contain the inter-ped pore network between the primary structural units, which formed the preferential flowpaths identified by the dye infiltration pattern. Although preferential flowpaths clearly exist at the top of the B horizon (40 cm depth), it appears that they do not persist strongly at 60 cm depth. From the dye study the horizontal spacing of the primary flowpaths was estimated at 15 to 50 cm. Thus it is possible that the lysimeter-scale sample volume may be too small to consistently encompass the subsoil macropore flowpaths. This may explain why, in

Figure 5-1, L6 has distinctly different infiltration behaviour to the other lysimeters at infiltration suctions < 1 kPa, where infiltration will occur through the macropore regions. It is possible that the lower saturated infiltration rate of L6 reflects the saturated matrix conductivity, rather than the conductivity of the primary preferential flowpath regions.

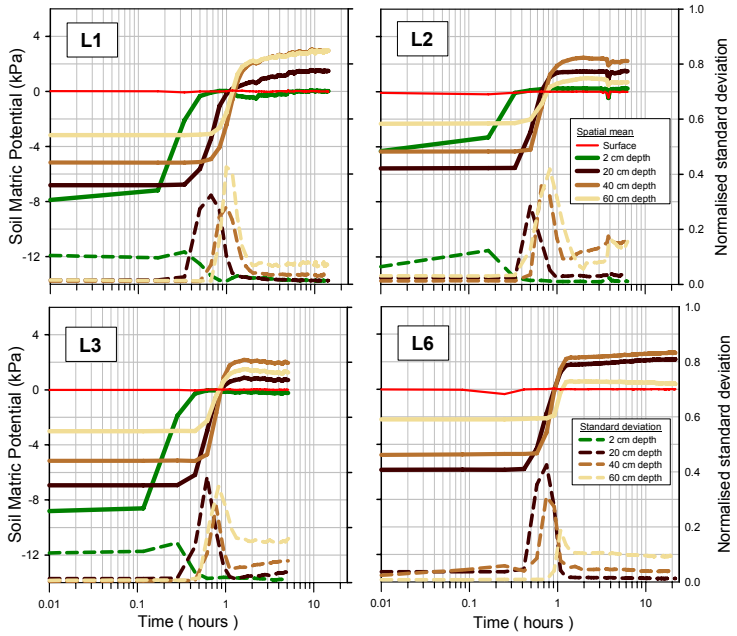

Figure 5-4 Comparison for four lysimeters of changes in soil matric potential during saturated infiltration. Solid lines represent the spatial averages in Ψ_m at set soil depths, with the scale on the left Y-axis. Dashed lines represent the normalised spatial standard deviation in Ψ_m (standard deviation divided by the antecedent matric potential), with the scale on the right Y-axis.

5.4.3 Leachate tracer concentration

These results appear to provide a greater depth in understanding the preferential flow behaviour than that revealed by the variability of Ψ_m alone. The Ψ_m measurements show that preferential flow occurs during the early transient stage of infiltration, when high variability in Ψ_m reflects non-uniform movement of the wetting front. This is supported by rapid tracer leaching in the saturated transient experiment. However, the tracer also showed preferential leaching during steady-state conditions, even when there was minimal variation in Ψ_m. Clearly, uniformity of Ψ_m is no guarantee of minimal preferential flow, as it was earlier interpreted (section 5.3.2). This result shows that preferential flowpaths continue to operate under steady-state infiltration, and appear to dominate long-term infiltration.

The idea that preferential flowpaths can have persistent influence on long-time infiltration is supported by the observation that the degree of steady-state preferential flow is a function of the infiltration rate (i_t), where a faster i_t results in greater preferential flow. The relationship between i_t and preferential flow is also reflected in the cumulative mass tracer recovery (Table 5-1). Cumulative mass recovery by 0.5 PV drainage increased in the same order as steady-state i_t, where L3 > L2 > L1 > L6. However, by 1.5 PV drainage the relationship with i_t is not as clear, demonstrating how the distinct differences in the initial preferential leaching pattern tend to disappear over long-times, resulting in a similar mass recovery.

		Cumulative mass tracer recovery in PV of drainage (%)		
Infiltration conditions	**Lysimeter**	**0.5 PV**	**1 PV**	**1.5 PV**
A. Steady-state saturated	L1	22	44	60
	L2	28	44	51
	L3	39	53	57
	L6	14	46	53
B. Transient saturated	L1	37	67	80
	L3	48	77	87
C. Steady-state unsaturated	L6	21	66	68 (1.24 PV)

Table 5-1 Comparison of cumulative mass tracer recovery from four lysimeters under different flow conditions: A. Bromide tracer applied under saturated conditions, once the infiltration rate had reached steady-state (after 80 – 100 mm cumulative infiltration); B. Chloride tracer applied at the initiation of saturated infiltration (i.e. 0 mm cumulative infiltration); C. Chloride tracer applied under unsaturated flow conditions (infiltration at 1.5 kPa surface suction), once the infiltration rate had reached steady-state (after 41 mm cumulative infiltration).

The mass recovery by 1.5 PV drainage is also not as high as expected, considering the early tracer breakthrough: 40 – 50% of the tracer was not recovered, similar to that observed by McLeod et al. (2003) on a similar soil type, where mass recovery was 55 – 60% by 1 PV. This pattern of mass recovery is interpreted as highlighting duality in the behaviour of preferential flow, where activation of macropores results not just in preferential transport of solutes from the soil surface, but also significant bypass of solutes within the soil matrix. In this sense macropore flow may have a negative consequence if it results in preferential leaching of a contaminant initially located on the soil surface, or a positive consequence if the contaminant is located within the soil matrix, and thus 'protected' from water moving through macropores. The term preferential flow

is typically used to encompass both macropore flow and matrix bypass because of the interlinkage of both processes, although here each process is distinguished separately because of the distinct influence that can be shown for each process on the leaching pattern.

In Figure 5-2 the breakthrough curves under saturated infiltration have a distinctive asymmetric shape, similar to that described during saturated infiltration by Seyfried and Rao (1987), where the early tracer breakthrough was attributed to macropore flow, and the long 'tail' attributed to matrix bypass. In the saturated experiments of this study the tracer infiltration is thought to follow a distribution skewed towards the macropores, resulting in initial preferential leaching. After tracer infiltration the macropores will continue to dominate, but instead the 'background' infiltrometer solution will be preferentially infiltrated, bypassing tracer that has infiltrated into the pore network of the soil matrix. This behaviour supports the claim by Bergstrom et al. (2001) that preferential flow can act to both enhance and reduce contaminant leaching, depending on the initial contaminant location and the degree of interaction between the macropore and matrix pore networks.

Asymmetric breakthrough curves for preferential leaching of bromide tracer were also typical in the study of McLeod et al. (2003) on a similar soil type, where the long tail of the breakthrough curve was attributed to a wide range in the size of conducting pores, giving a greater chance of diffusion into fine pores of the matrix, and hence resulting in matrix bypass flow. The interlinkage of macropore flow and matrix bypass has also been observed during lysimeter studies on other New Zealand soil taxa, which have been shown to demonstrate preferential flow. The soil types, classified according to Hewitt (1998); include: Immature Pallic (Jiang et al., 2005; Pang et al., 2008; Silva et al., 2000); Fragic Pallic (McLeod et al., 2003); Orthic Brown (Pang et al., 2008); Granular (McLeod et al., 2004); as well as Recent and Gley soils (McLeod et al., 2001).

This phenomenon is also demonstrated when comparing the transient and steady-state leaching patterns of L3. In the transient experiment, when the tracer was applied at the start of saturated infiltration, mass recovery was 9% higher at 0.5 PV, and was 30% greater by 1.5 PV of drainage. It appears that macropore flow was greater for the transient application, where more of the tracer was involved in filling of the largest macropores, and thus available to be leached. In contrast, during steady-state infiltration the macropore

network was already water-filled, resulting in a lower i_t, and more tracer infiltration / diffusion into smaller pores, causing more matrix bypass and lower total tracer recovery. This interpretation also correlates with the understanding gained from the dye and Ψ_m measurements, which indicate that preferential flow is greatest during early-time infiltration.

Comparison of mass recovery is difficult for the unsaturated experiment because of the high background chloride in the tap water used for the infiltrating solution. The tracer breakthrough curve was calculated after the leachate tracer concentration had been corrected for the background chloride, using the average of 62 samples from tap water, and from lysimeter leachate where no chloride tracer was applied. Even at the maximum background chloride concentration there is a distinct appearance of the tracer pulse in the leachate (refer to Appendix 5), and the pattern of the tracer breakthrough curve is considered valid. However, the higher than expected tracer concentrations at the start of the experiment (between 0 – 0.15 PV) are suspected to be an artefact of the background chloride concentration, rather than rapid preferential transport of the applied tracer. A tentative interpretation indicates that most of the recoverable mass arrives by 1 PV, but a large portion of the applied tracer (~30 %) may not be recoverable. The missing tail on the breakthrough curve indicates that the 'lost' tracer has infiltrated into the matrix, but in contrast to saturated flow the matrix tracer is more immobile and not able to move back into conducting pores.

Partitioning the pore network into mobile and immobile regions

The most important interpretation of the unsaturated leaching experiment is that the conducting pore network of the unsaturated experiment is likely to have contributed little or none of the tracer leached during saturated conditions. When macropores were excluded during the unsaturated experiment the average drainage rate of L6 was ~0.14 mm hr^{-1}, which would account for only 2.4% of drainage during the saturated experiment. The tracer first arrived in drainage after ~16 days (assuming that chloride levels prior to ~0.2 PV are an artefact of background chloride), whereas under saturated conditions L6 leached 1.5 PV of drainage in ~ 3.6 days.

This suggests that the saturated leaching behaviour of the soil can be described by a dual porosity or dual permeability model, where the pore network can be divided into distinct mobile (θ_m) and immobile regions (θ_{im}). These models assume that almost all water flow

is confined to θ_m, while θ_{im} may act as a source or a sink for solutes in θ_m through mass transfer by molecular diffusion or convection through exchange of water between regions (Simunek and van Genuchten, 2008). Increasingly, dual porosity or permeability models have been used to inversely model measured solute breakthrough curves, to estimate transport parameters such as θ_m. The success of inverse modelling can be improved by independent measurements of as many parameters as possible, with θ_m often identified as a parameter that can be physically measured (Skaggs et al., 2002b).

One approach is to estimate θ_m from the soil water characteristic, although difficulties arise in determining an appropriate physical basis to delineate the θ_m and θ_{im} regions (Skaggs et al., 2002b). A number of authors have identified a sharp increase in hydraulic conductivity and preferential flow when Ψ_m is wetter than -1 kPa, with a decrease in θ_m as Ψ_m wets to saturation, due to activation of large macropores which dominate infiltration (Casey et al., 1998; Ersahin et al., 2002; Langner et al., 1999).

In this study, delineation of θ_m could be based on the distinct difference between infiltration under 1.5 kPa suction and saturated infiltration, where the macropore regions activated under saturated infiltration accounted for approximately 97% of the drainage. In this sense θ_m may be estimated as the volume of pores between saturation and Ψ_m of -5 kPa, which equates to a θ_m estimate among the lysimeters of 5.6 – 8.7%. The lower limit of Ψ_m is based on the unsaturated leaching experiment of L6, where Ψ_m varied between -2.5 and -5 kPa (Appendix 4), as well as similar values and pattern in Ψ_m that were observed for the other lysimeters during the same infiltration conditions (Figure 5-1). The validity of extrapolating the θ_m definition to all the lysimeters is also supported by the lysimeters having a similar i_t of 0.1 – 0.3 mm hr^{-1} under 1.5 kPa surface suction, which then increased by two orders of magnitude during saturated infiltration. The increase in i_t is actually smallest for L6 (~1.4 orders of magnitude), which indicates that the dominance of θ_m is likely to be greater in the other lysimeters during saturated leaching.

A test of the validity of this method is to use the estimate of θ_m as a fixed parameter to inversely model the measured breakthrough curves. The results are presented in Figure 5-5, where the inverse function of the STANMOD programme (Simunek et al., 1999) was used to predict the measured steady-state breakthrough curves under saturated infiltration, using the mobile-immobile model (MIM) of van Genuchten and Wierenga (1976). For an inert, nonreactive solute the MIM may be written as

$$\theta_m \frac{\partial C_m}{\partial t} + \theta_{im} \frac{\partial C_{im}}{\partial t} = \theta_m D \frac{\partial^2 C_m}{\partial z^2} - v\,\theta_m \frac{\partial C_m}{\partial z}$$ Equation 5-1

where θ_m and θ_{im} are the mobile and immobile water contents (L^3/L^3); C_m and C_{im} the solute concentration in the mobile and immobile domains (ML^{-3}); t is time (T); D is the diffusion-dispersion coefficient ($L^2\,T^{-1}$); z is the distance from the inflow boundary in the direction of flow (L); and v is the pore water velocity (LT^{-1}). Exchange between the two domains is described by

$$\theta_{im} \frac{\partial C_{im}}{\partial t} = \alpha(C_m - C_{im})$$ Equation 5-2

where (α) is a first-order mass exchange coefficient (T^{-1}).

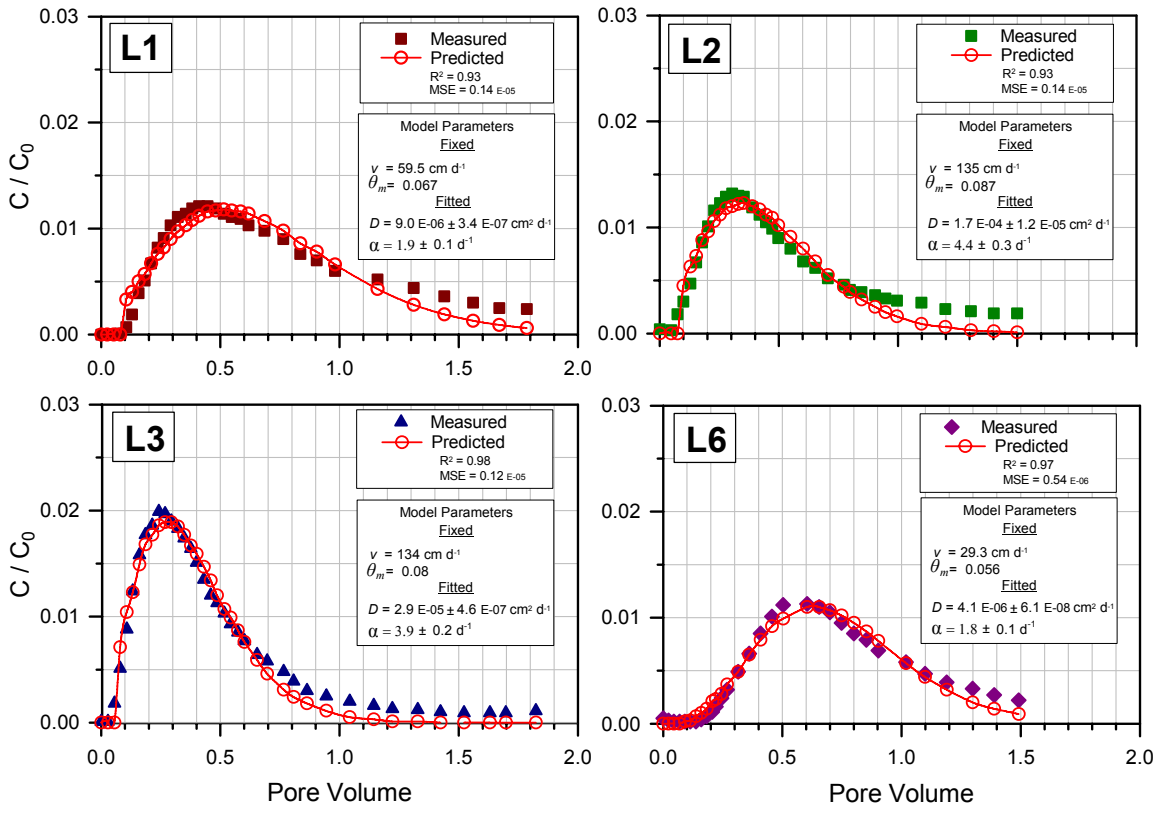

Figure 5-5 Comparison of measured and predicted breakthrough curves of bromide tracer under saturated leaching. Pore water velocity (v) and mobile water content (θ_m) were used as fixed model parameters, whereas the diffusion-dispersion coefficient (D), and mass transfer coefficient (α) were all inversely fitted to the measured breakthrough curve. Parameters were fitted by least-squares optimization, with the goodness of fit shown by the regression coefficient (R^2), mean square error (MSE), and 95% confidence intervals for parameters.

The results indicate that the θ_m estimates of 5.6 – 8.7 % are potentially valid, with a strong relationship ($R^2 > 0.93$) between the measured and predicted breakthrough curves, as well as low mean square error (MSE) and small confidence intervals for the fitted parameters. Although the estimates of θ_m appear to be quite small in relation to published values, a number of those studies measured unsaturated infiltration, where θ_m tends to increase as macropores are excluded (Alletto et al., 2006; Casey et al., 1997; Casey et al., 1998; Clothier et al., 1995; Vogeler et al., 1998). Other studies have estimated θ_m for cases where the soil is likely to have a significantly larger macroporosity, such as measurements for the surface layer (0 – 2 cm) of the topsoil (Casey et al., 1997; Casey et al., 1998), or where repacked columns have been used (Griffioen et al., 1998). When θ_m is normalised against the column water content (θ_m/θ_v), the θ_m/θ_v is very similar in this study to other published data, measured using undisturbed soil columns. In this study θ_m/θ_v ranged between 0.11 – 0.18, compared to an estimate of <0.1 by Jarvis et al. (2008), and 0.2 – 0.3 by Langner et al. (1999). Ross and Smettem (2000) used a θ_m/θ_v of 0.125 to model the drainage response observed by Smettem et al. (1994; 1991).

Pang et al. (2008), used the bromide breakthrough curve of McLeod et al. (2003) and inversely modelled the MIM parameters to yield a θ_m/θ_v value of 0.88. This is much larger than the θ_m/θ_v values of 0.11 – 0.18 estimated for the present study, despite the similarity in soil types used. The discrepancy may result from differences in experimental design. McLeod et al. (2003) used constant flux irrigation of 5 mm hr^{-1}, which was below the saturated conductivity measured in previous research at the same site, and therefore likely to have induced unsaturated leaching compared to the saturated leaching of this study. As previously stated, θ_m tends to increase as the largest macropores are excluded. Also, the lysimeters used were shorter than this study (47 cm compared to 70 cm), so did not include the lower subsoil, which shows distinctive preferential flow paths in the dye analysis of this study (Plate 5-2). An estimated θ_m/θ_v value of 0.88 also appears to be too high in relation to hydraulic attributes that had been previously measured at the same site. This estimate of θ_m/θ_v would mean that water held at a Ψ_m of -1500 kPa (i.e. wilting point) would have to contribute to the tracer transport, using the $\theta_v(\Psi_m)$ data of soil profile SB09215 (Landcare Research, 2008). Yet, at the same site, Gradwell (1979) measured the hydraulic conductivity of the subsoil at a Ψ_m of -10 kPa (i.e. field capacity) to be 1 – 2

x 10^{-4} mm hr^{-1}. These measurements indicate that the pore network below a Ψ_m of -10 kPa should have contributed very little of the drainage in the experiments of McLeod et al. (2003). In this sense it is physically realistic to limit θ_m to the volume of pores between saturation and Ψ_m of -10 kPa, which would result in a θ_m/θ_v value of 0.16, using the $\theta_v(\Psi_m)$ data of soil profile SB09215 (Landcare Research, 2008), and is within the range of θ_m/θ_v estimated in this study.

Overall, the MIM parameters shown in Figure 5-5 follow the pattern that as the estimate of θ_m increases among the lysimeters, it is accompanied by an increase in pore water velocity (*v)* and the dispersion coefficient (*D*). This pattern reflects the fact that θ_m encompasses the macropore region, and therefore an increase in θ_m is due to an increase in large macropores, with a corresponding increase in *v*. The increase in θ_m also increases the range of pore water velocities that contribute to solute transport, and is reflected as an increase in *D*.

The understanding developed from the dye and tensiometer studies indicates that lateral mass transfer between the θ_m and θ_{im} regions is an important hydraulic feature of this soil, and in the MIM model this is characterised by the mass exchange coefficient (α). Griffioen et al. (1998) reviewed a number of studies, and found α varied between 0.002 to 240 d^{-1}, although most studies were for repacked columns. For undisturbed field soils α has been observed to be an important parameter influencing preferential flow, with the largest values under saturated infiltration. Most estimates of α have been for the topsoil and range from 0.2 to 184.6 d^{-1} under saturated infiltration (Casey et al., 1998; Langner et al., 1999; Seyfried and Rao, 1987), whilst for unsaturated infiltration under suctions of 0.03 to 1 kPa, α has been estimated at 0.02 to 1.9 d^{-1} (Alletto et al., 2006; Casey et al., 1997; Casey et al., 1998; Clothier et al., 1995; Jarvis et al., 2008; Tillman et al., 1991). Estimates of α for subsoil horizons is not as common, with values of 0.02 – 0.05 d^{-1} for a silty clay subsoil under unsaturated infiltration at 0.1 kPa suction (Alletto et al., 2006), and 9.6 – 176 d^{-1} for a tropical clay loam under saturated infiltration (Seyfried and Rao, 1987).

In this study α is estimated at 1.8 to 4.4 d^{-1}, but is an effective average of the whole soil column, which is a much larger volume with multiple horizons, than the other studies of undisturbed field soils. The variability in α in this study is much lower than reported in the studies described above, e.g. Casey et al. (1998) measured α to range between 1.9 –

113 d^{-1} under saturated infiltration. A clear positive relationship was also observed between α and v, consistent with literature reviews of other studies (Casey et al., 1997; Griffioen et al., 1998). Importantly, the estimates of α relative to v for this study fall within the pattern identified in these reviews. This positive relationship contradicts the assumption that α represents a first-order process (diffusion), and indicates that convection is also an important process governing the interaction between θ_m and θ_{im} (Casey et al., 1998; Griffioen et al., 1998; Jarvis et al., 2007b). In this sense it is probably more physically realistic to conceptualise the soil as a dual-permeability system, where water flow does occur in at least some portion of θ_{im}, albeit at a much lower flux than water flow in θ_m.

The only fitted parameter which is unusual is the dispersion coefficient (D). The estimated values are very low, compared to published values of D estimated from the MIM model (Clothier et al., 1998; Langner et al., 1999; Seyfried and Rao, 1987; Tillman et al., 1991). In the MIM model, D is effectively determined by the behaviour of the θ_m region, which means that the small predicted D values partly reflect the small θ_m estimate, compared to the other studies. The low D values indicate that within the θ_m region that hydrodynamic dispersion has a small effect on the pattern of solute transport, in comparison to convection (Ersahin et al., 2002). This is possible if the pore network that the solute infiltrates into is characterised by a narrow range of pore velocities, which may happen if θ_m is small, and the bulk of the applied pulse infiltrates into a few large macropores. Clothier et al. (1998) also identify that it is difficult when using inverse modelling to separate the mechanisms of diffusion (parameter α) and dispersion (parameter D), even if unique values for these parameters were to truly exist. This problem may partly explain the unusual values for D that were estimated from the inverse modelling of this study.

Although the small estimated values of D are unusual and warrant further investigation, it is important to note that in the MIM model the influence of D on the predicted breakthrough curve is small (van Genuchten and Wierenga, 1976). In the MACRO dual permeability model the solute transport in the macropore domain is assumed to be dominated by convection, and dispersion is not explicitly accounted for (Jarvis et al., 2007b). Tillman et al. (1991) also observed that dispersivity was less significant than the

relationship between θ_m and θ_{im}, when developing a dual-porosity model to predict bromide infiltration in a field soil.

Perhaps the most important interpretation is that for successful inverse modelling of hydraulic parameters, it is critical to have independent measurements of key hydraulic attributes. This is because of the problem of non-uniqueness that can arise when a number of parameters are simultaneously estimated (Skaggs et al., 2002b). Non-uniqueness arises where different combinations of parameter values can give similar model predictions. The problem of non-uniqueness is illustrated by the discrepancy in estimates of θ_m for this soil type between this study and that of Pang et al. (2008). In my study the measured $K(\Psi_m)$ has been used as a physically-based reference to estimate θ_m, which subsequently constrains estimates of other model parameters. However, the unusually low estimate of D from this approach could also be interpreted as reflecting non-uniqueness, and again highlights the importance of independent measurements to assessing the validity of model predictions. Casey et al (1999) recommend a suitable method is use a tension infiltrometer to apply a sequence of tracers, after which sections of the infiltration surface are sampled at different times to determine θ_m and α (Jaynes et al., 1995). The limitation of this approach is that involves destructive sampling, which may restrict application on lysimeters, which are often collected with the aim of having multiple experiments using the same soil column.

5.5 Summary

The analysis of dye patterns, variability in Ψ_m measurements, and solute breakthrough curves all show that preferential flow is an important infiltration mechanism of this soil type. Overall, the three methods give a similar understanding of preferential flow behaviour, and in combination greatly enhance the interpretation of any one method. This is shown in the dye analysis where the first impression was of homogeneous matrix flow through the A horizon, yet the Ψ_m measurements revealed strong preferential flow. The dye photos were re-interpreted using image analysis of dye density which identified distinct areas of dense dye, indicative of preferential flow paths. Likewise the Ψ_m measurements show that during the steady-state stage of infiltration there is low spatial variation in Ψ_m, which was initially interpreted as indicating minimal preferential flow. However, the solute breakthrough curves show that whilst Ψ_m may have equilibrated there is still distinct preferential flow, although the solute leaching does support the Ψ_m measurements which show that preferential flow is greater during early-time infiltration than at steady-state.

An important observation is that both the dye and solute leaching patterns show a strong interaction between preferential flowpaths and the surrounding matrix. It appears that lateral infiltration from preferential flowpaths is an important mechanism in this soil, where activation of preferential flowpaths results not just in rapid leaching but significant transfer of infiltrating water / solutes into the surrounding matrix at all depths within the soil. Importantly, the results demonstrate a duality in the behaviour of the macropore network, where activation of preferential flow may also result in bypass flow of existing matrix solutes as well as new solute that the soil matrix has 'sequestered' from the preferential flowpaths through lateral infiltration.

The solute leaching and Ψ_m measurements were used to estimate the pore volume of preferential flowpaths, where it was demonstrated that during saturated infiltration approximately 97% of the drainage was through the 'mobile' pore network (θ_m), estimated as between saturation and Ψ_m of -5 kPa. This approach resulted in a θ_m estimate among the lysimeters of 5.4 – 8.7 % of the lysimeter volume, which resulted in good predictions when used as a fixed parameter to inversely model the solute breakthrough curves. This small value of θ_m is further supported by the dye pattern, where the preferential flowpaths that persisted to the greatest depth were associated with interpedal

regions between the primary structural units of the B horizon, identified as large prisms ~15 to 50 cm width.

It is important to recognise that in this study the understanding of preferential flow behaviour was largely elucidated from saturated infiltration conditions, where the infiltration rate was between 5 – 25 mm hr^{-1} for long periods. Jarvis (2007) identifies that using high flux experiments runs the risk of a biased impression of the frequency and behaviour of preferential flow. This is a valid point, as in chapter 4 it was shown that the majority of field infiltration events for this soil are not likely to have such intensity or duration. However, the Ψ_m measurements and unsaturated leaching experiment show that preferential flow also occurs during unsaturated infiltration under small fluxes.

I conclude that the saturated infiltration experiments in this study are valuable, in that they demonstrate the potential behaviour of preferential flow in this soil, and provide a good basis to further develop the knowledge and understanding of infiltration behaviour under field conditions. Further research would also have to recognise that preferential flow behaviour is dependent on the complex interactions between factors such as the rainstorm or irrigation intensity and duration, the soil's infiltration properties (e.g. antecedent wetness, hydrophobicity, sorptivity and conductivity relationships, and soil layering), as well as the dynamics of vegetation and management (Clothier et al., 2008; Jarvis, 2007).

Chapter 6
Is sorptivity the main mechanism governing early-time infiltration of a structured and layered soil column?

6.1 Introduction

All standard infiltration models share the common feature that the infiltration rate (i_t) is higher when water first enters the soil and then decreases with time (Jury and Horton, 2004). The most common model used to represent infiltration behaviour is an analytical solution to Richards equation, derived by Philip (1957) for infiltration into a infinitely deep homogeneous soil at a uniform antecedent water content that has the infiltration surface held at a constant higher water content. The solution of Philip (1957) is typically in the form of a two-parameter equation:

$$I = S\sqrt{t} + At \qquad \text{Equation 6-1}$$

where I is cumulative infiltration, S the soil sorptivity (a function of the supply water potential Ψ_{TI} and the antecedent soil matric potential Ψ_i), t is time, and A is a parameter related to the soil's hydraulic conductivity. Generally it is accepted that at early times the first term of Equation 6-1 is dominant, where the air-filled portion of the pore network exerts sufficient capillary forces (i.e. matric potential, Ψ_m) to cause rapid infiltration of water from the soil surface.

There are numerous examples in the literature where infiltration behaviour can be explained by the Philip equation, with a number of researchers using tension infiltrometers to study the S relationship at near-saturated infiltration conditions (AnguloJaramillo et al., 1997; Clothier and Smettem, 1990; Sauer et al., 1990; Thony et al., 1991). Accurate measurement of S for the surface layer is critical for understanding the dynamics of soil water in response to rainfall or irrigation, and measurement of the $S(\Psi_{TI}, \Psi_i)$ relationship is of particular interest because it is the norm in many agricultural soils for the rate of rainfall or irrigation to be less than the saturated soil infiltration rate (Jarvis, 2007). The short time required to measure S is also seen as more practical than

waiting for steady–state conditions, and has resulted in a number of methods being developed to estimate other important hydraulic attributes from the *S* relationship. Derivation of these attributes is reviewed by Reynolds and Topp (2008b) and includes hydraulic conductivity, $K(\Psi_m)$, the characteristic mean pore size, λ_m, the sorptive number α^*, and the flux potential Φ.

In the results of this study, the early-time infiltration is often characterised by a pattern where i_t starts slowly and increases with time, the reverse of the behaviour predicted by Equation 6-1. This atypical behaviour raises the possibility that features of the tension infiltrometer system used in this study may have influenced infiltration behaviour and generated artefacts in measured hydraulic attributes, or that some other soil attribute was suppressing the influence of capillarity.

These results indicate that there is an important research question that needs to be addressed: Is there evidence that other mechanisms outside of sorptivity are influencing the early-time infiltration behaviour?

6.2 Methods

The methods used for the experiments in this chapter are described in chapter 3.

6.3 Results

6.3.1 Measurement of infiltration rate

Infiltration experiments were conducted on the four lysimeters using the tension infiltrometer to supply infiltrating water under surface-imposed suctions of 0, 0.5, 1 and 1.5 kPa. Figure 6-1 shows the effect of controlling surface suction on lysimeter infiltration rate (i_t), where i_t for each surface-imposed suction has been calculated for every 10 mm of cumulative infiltration. The respective graphs of cumulative infiltration with time are presented in Appendix 6.

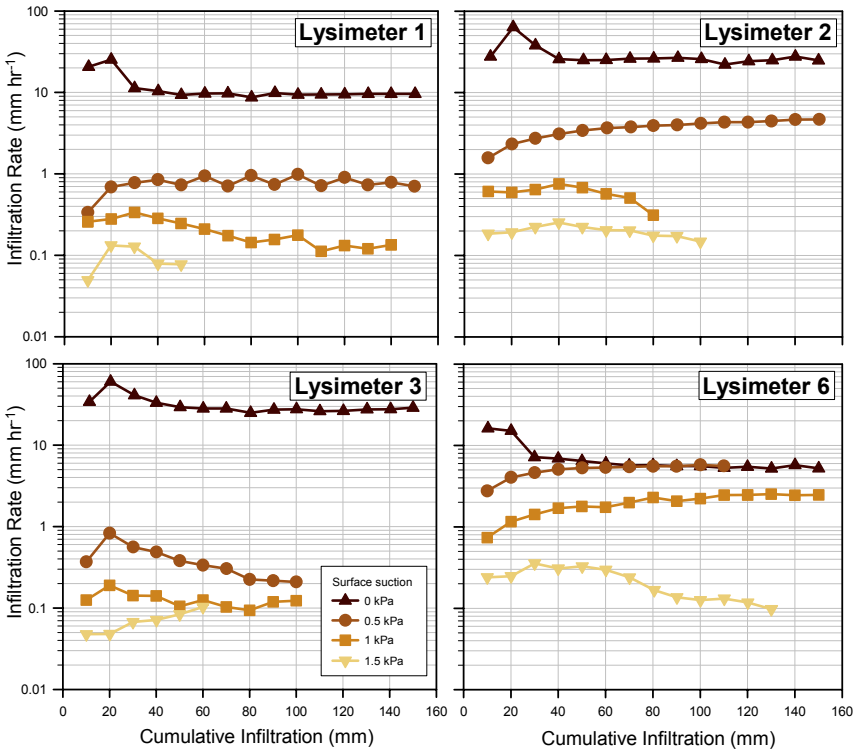

Figure 6-1 Comparison of infiltration rate for four lysimeters, where infiltration occurs under controlled surface suctions of 0, 0.5, 1 and 1.5 kPa.

The infiltration behaviour predicted by Equation 6-1 is not apparent in the results of Figure 6-1. According to the Philip model the infiltration pattern should have a transient phase with higher i_t, followed by a decline to a stable value of the steady-state phase. These results do have a transient phase, but i_t more typically increases (e.g. L3 0, 0.5 and 1 kPa). The only experiment where i_t decreases during the transient phase is L6 0 kPa, and even then not strictly consistent with $t^{1/2}$ behaviour.

The early-time infiltration behaviour is revealed more clearly using infiltration rates calculated over 1 mm cumulative infiltration intervals for the first 20 mm (Figure 6-2). An initially higher i_t is apparent during the first 3 – 4 mm of saturated infiltration for L2, L3 and L6, and also is apparent during the first 1 – 3 mm of unsaturated infiltration into L2 and L6 (e.g. L2 0.5 and 1 kPa). However, these data also show a pattern in which an initial sharp decline in i_t is followed by a steady increase. The remaining experiments of L1 and L3 show a contrasting infiltration pattern, where i_t starts slowly and then steadily increases. In some experiments i_t fluctuates, with no clear overall pattern (e.g. L3 1 and 1.5 kPa). The only experiment consistent with the Philip model is L2 1.5 kPa, where i_t starts at 10 mm hr^{-1}, and then steadily declines to 0.1 – 0.2 mm hr^{-1} by 6 mm of cumulative infiltration.

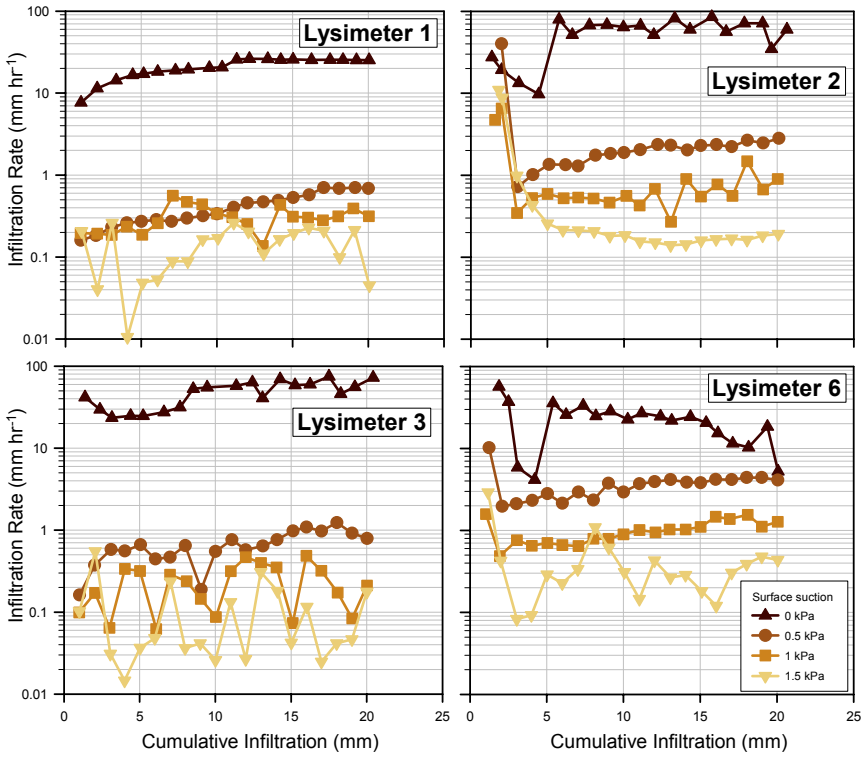

Figure 6-2 Comparison of infiltration rates of four lysimeters during the transient phase of infiltration, where infiltration occurs under controlled surface suctions of 0, 0.5, 1 and 1.5 kPa. The transient phase is assumed to occur within the first 20 mm cumulative infiltration.

6.3.2 Estimation of soil sorptivity

The influence of capillarity on early-time infiltration is usually studied by fitting Equation 6-1 to measured infiltration data, to estimate a value of the soil sorptivity, S (Minasny and

McBratney, 2000). The most common method assumes that at some early time capillarity dominates all other forces, and therefore

$$I = S\sqrt{t} \qquad \text{Equation 6-2}$$

such that a plot of I against $\sqrt{t}$ produces a straight line with zero intercept and slope equal to S (Cook, 2008; Minasny and McBratney, 2000). The results of applying this standard method (Figure 6-3), demonstrate the problem with identifying discrete linear portions of the graph from which S can be derived. It is well recognised that initial infiltration into the contact layer of a tension infiltrometer offsets the actual start time of soil infiltration (t_0), which in turn makes it difficult to determine the later time when gravity starts to significantly influence infiltration, and therefore Equation 6-2 is no longer applicable (Clothier, 2001; Cook, 2008; Minasny and McBratney, 2000).

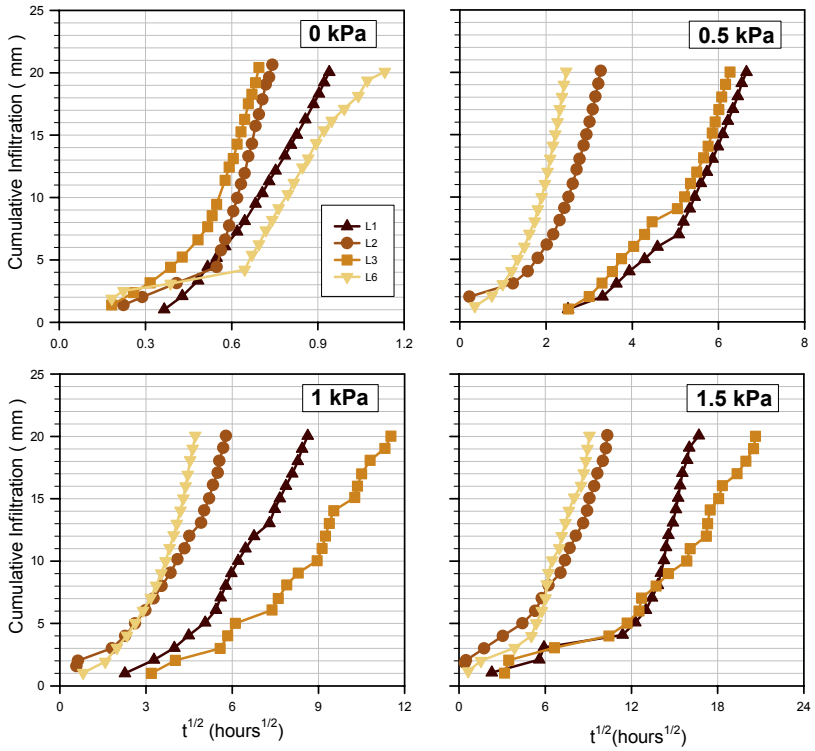

Figure 6-3 Plot of cumulative infiltration versus square-root of time ($t^{1/2}$) for four lysimeters, during early-time infiltration under surface imposed suctions of 0, 0.5, 1, and 1.5 kPa.

Cook (2008) recommends a better method to identify t_0 is to follow Smiles and Knight (1976) and perform a square-root-of-time transformation on cumulative infiltration,

$$\frac{I}{\sqrt{t}} = S + A\sqrt{t} \qquad \text{Equation 6-3}$$

When $I/\sqrt{t}$ is plotted against $\sqrt{t}$ the non-linear first points are attributed to the effects of the contact material, but should be followed by a linear plot, where fitting of a straight line will produce an intercept equal to *S*. If capillarity is the sole mechanism for infiltration then the linear portion of the plot should have a slope of zero (Cook, 2008). The results of applying the Smiles and Knight (1976) method are presented in Figure 6-4, and show it is difficult to unambiguously identify periods when capillarity is the dominant mechanism for infiltration. Under saturated infiltration, fitting of Equation 6-3 to the early-time linear plot may be suitable for L2, L3 and L6, but would produce a negative value of *S* for L1. There are some unsaturated experiments where fitting of Equation 6-3 would produce credible estimates of *S* (e.g. L2 & L6 1.5 kPa), but the majority of experiments show an apparent negative *S* (e.g. 0.5 kPa L1 & L3), or no clear linear behaviour (e.g. L3 1 and 1.5 kPa experiments). The lack of a consistent and clear linearity in the results indicates that direct use of Equation 6-1 is not appropriate to describe infiltration into the soil under the boundary conditions applied (Smiles and Knight, 1976).

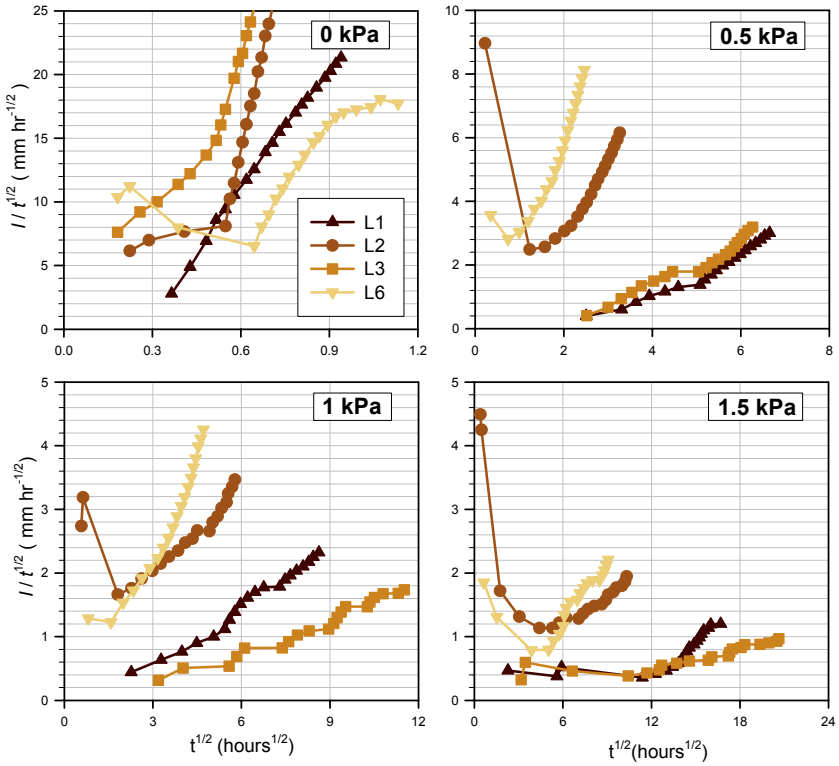

Figure 6-4 Plot of square-root-of-time transformation on cumulative infiltration ($I / t^{1/2}$) versus square-root of time ($t^{1/2}$) for four lysimeters, during early-time infiltration under surface imposed suctions of 0, 0.5, 1, and 1.5 kPa.

By applying the method of Smiles and Knight (1976) it becomes clear that even where rapid early infiltration behaviour was measured, the behaviour may not be solely the result of sorptivity. This is illustrated by the L2 1.5 kPa experiment, where the rapid early-time infiltration (Figure 6-2) results from 2 mm of infiltration that was necessary to wet the contact material (Figure 6-4). This is shown in Figure 6-5 by the measurements of Ψ_m at 2 cm depth. Although 2 mm of cumulative infiltration had occurred within the first 15 minutes, it took at least 50 minutes for Ψ_m to respond. If the infiltrating water had immediately entered the soil there should have been a clear Ψ_m response, because 2 mm of infiltration is 30 – 50% of the estimated antecedent infiltration capacity for the surface layer (Table 6-1).

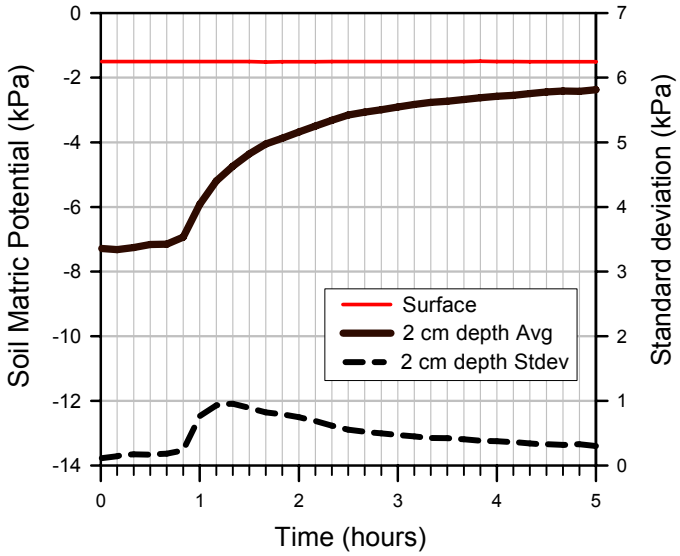

Figure 6-5 Response of tensiometers at 2 cm depth of lysimeter two, after infiltration was initiated under a surface suction of 1.5 kPa.

6.4 Discussion: What other mechanisms are influencing the early-time infiltration behaviour?

If sorptivity is not the dominant force governing early-time infiltration, then some other mechanism is preventing or slowing capillary forces from drawing the infiltrating water into the soil pores. Slow infiltration may be an artefact of the tension infiltrometer system, or otherwise is an intrinsic soil effect. Possible mechanisms arising from the infiltrometer-lysimeter system include a restriction on the flow rate and poor contact with the soil surface, or an air 'back-pressure' effect caused by confinement of displaced soil air. Possible soil mechanisms include hydrophobicity, high antecedent soil wetness, air-entrapment, and surface seal development. The mechanisms are discussed below.

6.4.1 Possible restrictions of the Tension Infiltrometer

The design specifications of the tension infiltrometer are described in Chapter 3, and demonstrate that there should not be a flow rate restriction. Potentially the rate-limiting factor is the hydraulic conductivity of the contact material (K_{cs}), but the measured i_t were <100 mm hr^{-1}, well below the reported K_{cs} of 410 to 264 mm hr^{-1} for the range of infiltration suctions applied in experiments of this study (Bagarello et al., 2001; Reynolds, 2006; Reynolds and Zebchuk, 1996). Generally the contact material will also exhibit a high S, especially when dry, which will accelerate early-time infiltration and result in overestimation of S compared to the true soil S (Minasny and McBratney, 2000).

Despite the known effect that contact material can have on early-time behaviour, Minasny and McBratney (2000) found that the effect of contact material on estimation of S had not been rigorously evaluated. Their research compared the effect of contact material on five methods to estimate S from early-time unsaturated infiltration. The contact material effect was modelled using a numerical study of a loam and clay, as well as field tested on heavy clay. The results of both the numerical and field study found that all methods over-estimated S when contact material was used. In the field experiment, S estimates were always higher when using contact material, even after the effect of the initial contact material wetting was eliminated. The consistently higher S was attributed to better contact with the soil surface. The results of Minasny and McBratney (2000) are the opposite of what is observed in this study, which indicates that contact material is not likely to be the mechanism impeding sorptivity behaviour.

In the experiments of this study a retaining membrane was used between the contact material and the soil surface, to avoid the possibility of contact material blocking surface pores. Hence, under the largest surface suction of 1.5 kPa, any gap >0.2 mm between the membrane and the soil surface would restrict infiltration. The likelihood of poor contact is explored in Figure 6-6, which shows that installation of the contact material onto the retaining membrane resulted in an immediate response in the tensiometers at 2 cm depth. The variability between tensiometers also decreased immediately, indicating a uniform wetting of the surface layer, even when the initial Ψ_m of the beads was -1 to -1.5 kPa, and gaps >0.2 – 0.3 mm would restrict response from areas of the soil. Furthermore, the presence of slow early-time infiltration in the saturated infiltration experiments also

indicated that poor contact is not the governing mechanism, as gaps between the contact material and the soil surface would not restrict infiltration.

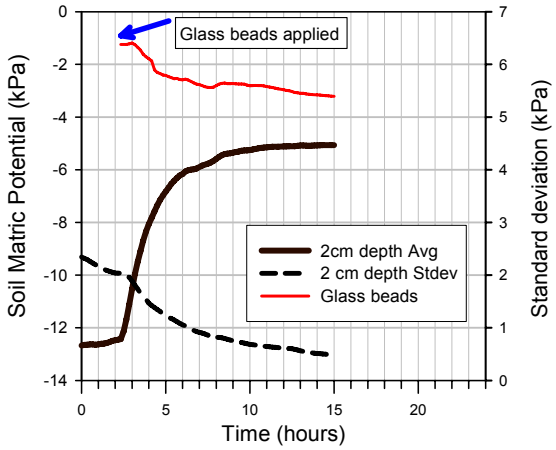

Figure 6-6 Response of tensiometers at 2 cm depth of lysimeter one, when just moist glass beads (~ 2 cm deep) are placed on surface, but the tension infiltrometer is not installed. Any gaps greater than ~0.2 – 0.3 mm between the glass beads and the soil surface would have restricted wetting of the surface soil layer, as well as further restriction by smaller gaps as the Ψ_m of the beads decreased.

6.4.2 Blockage of surface-connected soil pores

The development of a surface seal or crust which acts to block surface pores is well recognised as a mechanism that can impede infiltration. Surface seal development can be caused by a number of factors including deposition of fine particles by surface runoff, high percentage of sodium on the exchange complex, encapsulated air, and weak aggregate strength caused by low clay, organic matter, and iron-aluminium oxides (Hillel, 1998; Marshall et al., 1996). Schwarzel and Punzel (2007) implicated surface sealing as the mechanism behind the lower infiltration rates measured by a tension infiltrometer, when compared to measurements by a hood infiltrometer. They suggested that disturbance during surface preparation and establishment of the contact layer resulted in smearing and clogging of the surface pores.

In this study a surface seal is not considered to be of major importance because the early-time i_t often starts slowly, then increases (Figure 6-2), which is not typical of infiltration through a surface seal (Hillel, 1998). The results of the wet-sieve stability tests also indicate high aggregate stability, reflecting the moderate clay and organic matter contents (refer to Figures 4-6 and 4-7, chapter 4). For aggregates of the surface layer, the wet sieve stability was 82%, which is considered high for the experimental conditions of this study,

where wetting from the tension infiltrometer was much less vigorous than during the wet-sieve stability test. The development of a surface seal is also often associated with mechanical disturbance arising from the kinetic energy of raindrops (Hillel, 1998; Marshall et al., 1996), whereas wetting from the tension infiltrometer has very low kinetic energy, particularly under unsaturated infiltration.

The soils are also unlikely to have high exchangeable sodium levels, and a 0.005M $CaS0_4$ infiltrating solution was used to further promote aggregate stability. Care was taken to not disturb the soil surface when vegetation was removed, and a membrane was placed on the surface to prevent blocking of soil pores by the contact material. Results of section 6.4.5 below indicate that air encapsulation did occur during early-time infiltration, but the results of the slaking test indicate high aggregate stability during rapid saturation (refer to Plate 4-2, chapter 4), and therefore the entrapped air is not thought to have caused any significant aggregate breakdown.

6.4.3 Antecedent soil wetness

The antecedent soil wetness at the beginning of infiltration is a critical determinant of the pattern of early-time infiltration, in particular the degree of influence that the soil's capillarity (sorptivity) exerts on the infiltrating water. Sorptivity tends to decrease with increasing antecedent water content (θ_i), because both the matric potential gradient and the available water storage capacity decreases (Reynolds, 2008). Reynolds (Reynolds, 2008) recommends that the antecedent matric potential (Ψ_i) should be $\leq$ -5 to -10 kPa to ensure sufficient matric potential gradient. Kumke and Mullins (1997) observed the relation between S and Ψ_i was exponential, with a rapid increase in S when Ψ_i is below about -6 kPa, although S still increased from two to seven times as Ψ_i decreased from -2 to -6 kPa. For this study the Ψ_i for each experiment ranged from -5.1 to -9 kPa (Table 6-1), which was the quasi-steady state achieved after 7 – 10 days drainage from the previous experiment. This was interpreted as 'field capacity' during the winter-time drainage season, and thus a relevant Ψ_i for these experiments.

The antecedent infiltration capacity (I_c) is also a key factor for sorptivity driven infiltration. The I_c is defined here as the depth (mm) of infiltrating water required to wet the 0 – 5 cm layer from Ψ_i to the 'target' Ψ_m, set by the suction of the tension infiltrometer. Two estimates of I_c are provided in Table 6-1:

1. *In-situ* water content reflectometers (WCR) located horizontally at 2 cm depth.

2. Water content interpretation from the $\theta_v(\Psi_m)$ relationship of small cores sub-sampled from each lysimeter.

Surface suction	L1			L2			L3		
	Ψ_i	*WCR* I_c	*Core* I_c	Ψ_i	*WCR* I_c	*Core* I_c	Ψ_i	*WCR* I_c	*Core* I_c
kPa	*kPa*	*mm (%)*	*mm (%)*	*kPa*	*mm (%)*	*mm (%)*	*kPa*	*mm (%)*	*mm (%)*
0	-8.44	9 (17)	7 (14)	-5.14	9 (18)	9 (17)	-9.00	11 (22)	7 (15)
0.5	-8.17	6 (12)	5 (9)	-5.30	6 (11)	5 (9)	-8.90	7 (13)	4 (8)
1	-6.25	6 (12)	4 (8)	-7.13	10 (19)	5 (10)	-6.95	9 (19)	4 (7)
1.5	-6.20	7 (14)	4 (7)	-7.28	7 (14)	4 (8)	-8.43	8 (15)	4 (7)

Table 6-1 Antecedent matric potential (Ψ_i) and water storage capacity (I_c) for the 0 – 5 cm depth of each lysimeter, prior to infiltration under different surface suctions. I_c is provided as a depth (mm) of infiltrating water, with the equivalent percentage volume in parentheses. Data are not available for lysimeter 6, because no sensors were installed in the surface layer. Two estimates of I_c are provided, from: A. In-situ water content reflectometers (WCR I_c); B. Water release data from three small cores (10 x 5 cm deep) sampled from each lysimeter (Core I_c). The 95% confidence interval of the pooled variance is approximately ± 2 mm for the WCR, and ± 1 mm for cores.

The WCR indicates a higher I_c than that estimated from the small cores. The difference may partly be explained by the temperature sensitivity of the WCR (refer to section 3.3.2, chapter 3), although in a number of experiments the differences are larger than the WCR error alone. For example, under 1.5 kPa surface suction the temperature sensitivity of the WCR can only explain a difference of 1 – 1.5 mm between the WCR and core estimate of the I_c. The higher estimate of I_c by the WCR may also indicate entrapped air, which is likely to be less in the small cores which were saturated for one week prior to measurement. The differences may also reflect the larger sample volume of the soil cores (1180 cm^3), compared to volumes of 338 cm^3 (Logsdon and Hornbuckle, 2006) and 79.2 cm^3 (Blonquist et al., 2005) estimated for the WCR, on the basis of radii of 1.3 and 0.65 cm around each wave guide.

Table 6-1 indicates that I_c was at least 4 mm prior to unsaturated infiltration, and at least 7 mm prior to saturated infiltration. Therefore, sorptivity behaviour should have been observed for at least these depths of infiltration, assuming that 0 – 5 cm is the soil depth which controls the sorptivity stage, and that the contact material absorbs none of the infiltrating water. As discussed in section 6.4.1 the contact material is likely to have

absorbed some of the infiltrating water, which would in effect increase the amount of cumulative infiltration over which sorptivity behaviour should be dominant.

The magnitude of I_c is particularly important in determining the relative depth of infiltration over which sorptivity can be expected to drive infiltration. In Table 6-1 the 0 – 5 cm depth is used to estimate I_c largely because this depth coincides with the soil depth of both the *in-situ* WCR and small cores. From practical experience Clothier and Smettem (1990) also identify that steady-state infiltration can be expected once the wetting front has penetrated 5 – 10 cm depth. An alternative approach to testing the validity of the estimates of I_c in Table 6-1 is to estimate the sorptivity dominated time scale (t_c), using the equation (White and Sully, 1987)

$$t_c = b(S/K_0 - K_i)^2 \qquad \text{Equation 6-4}$$

where $K_0 - K_i$ is the difference in hydraulic conductivity between the antecedent matric potential and the matric potential set by the tension infiltrometer, with $b = 0.55$ assumed for most soils (White and Sully, 1987). Essentially t_c is the time period when the influence of gravity on infiltration is <~25% (White and Sully, 1987), with a first approximation of I_c calculated by substituting t_c and S into Equation 6-2.

In this study t_c is difficult to estimate because S is often indeterminate, as shown in section 6.3.2. L2 does show some apparent sorptivity driven behaviour under 0 and 1.5 kPa infiltration (Figure 6-2), for which respective values of S are 8 and 1.1 mm $hr^{-1/2}$ can be estimated in Figure 6-4 from the intercept of the portion of the plot with zero slope (Cook, 2008). For these experiments t_c is estimated as 0.004 and 66.6 hours respectively using Equation 6-4, where $K_0 - K_i$ is ~100 and 0.1 mm hr^{-1} (derived from Figure 7-10, Chapter 7). Substituting these estimates of t_c and S into Equation 6-2 provides respective I_c estimates of 0.5 and 9 mm, for the respective L2 0 and 1.5 kPa infiltration experiments.

The I_c estimate for L2 1.5 kPa is consistent with Table 6-1. The I_c estimate for L2 0 kPa is much lower, and at first glance indicates that antecedent wetness is limiting sorptivity under these conditions. However, Table 6-1 shows that the 0 kPa experiment had a greater fillable pore volume (17 % compared to 8 %). This is due to the availability of large macropores for infiltration, which is shown in $K_0 - K_i$ being 1000 times larger. Under 1.5 kPa suction the estimate of S is larger relative to K, which is similar to other studies that have measured both the $S(\Psi_{TI}, \Psi_i)$ and $K(\Psi)$ relationships (AnguloJaramillo et

al., 1997; Clothier and Smettem, 1990; Sauer et al., 1990; Thony et al., 1991). In the 0 kPa experiment the S estimate is small relative to $K(\Psi_m)$, which does not correspond with these other studies. Therefore it is interpreted that under 0 kPa infiltration the estimate of S and the corresponding I_c prediction are too small, and that given the potential fillable pore volume it is not antecedent wetness limiting sorptivity driven infiltration.

6.4.4 Hydrophobicity

Wallis (1991) showed that hydrophobicity is potentially widespread in New Zealand soils, although the antecedent water contents (θ_i) were considerably drier than the θ_i of the experiments in this study. Hydrophobicity is usually associated with dry soils, and generally it is thought that there is a critical moisture content above which hydrophobicity disappears (Dekker et al., 2001). In a survey of 41 common soil and landuse types in the UK it was observed that hydrophobicity was virtually absent when θ_i was > 28% (Doerr et al., 2006). However, Jarvis et al. (2008) notes that this study used the water drop penetration test, which is only sensitive to severe hydrophobicity. Strong sub-critical hydrophobicity has been observed by Clothier et al. (2000) for the Ramihi soil where θ_i was $\approx$ 40%, and by Jarvis et al. (2008) when θ_i was 36%. This is similar to this study where θ_i was 30 – 50%. Clothier et al. (2000) observed that hydrophobicity in the Ramihi silt loam (Allophanic Brown soil) kept the infiltration rate (i_t) low for about 100 minutes, before it increased rapidly to a steady rate ~5 times greater. This infiltration pattern is similar to that observed during a number of the experiments in this study, and indicates hydrophobicity may be a mechanism influencing early-time infiltration behaviour.

The degree of hydrophobicity was assessed following the intrinsic sorptivity method of Tillman et al. (1989), which compares the sorptivity of water (S_w) to ethanol (S_e), where ethanol is used as a reference liquid that is not affected by hydrophobic compounds during infiltration. In a non-hydrophobic soil the ratio S_w/S_e should be 1.95, due primarily to the greater surface tension of water. The degree of hydrophobicity is indicated by the Repellency Index (RI),

$$RI = 1.95(S_e/S_w) \qquad \text{Equation 6-5}$$

where RI values greater than unity indicate hydrophobicity. The RI indicates the magnitude that hydrophobicity has lowered S_w, with the potential S_w in non-hydrophobic conditions estimated as S_w multiplied by RI (Hallett et al., 2001; Wallis et al., 1991).

The main advantage of using the intrinsic sorptivity method is that it allows the effects of hydrophobicity on the infiltration behaviour to be assessed on undisturbed soils at any antecedent water content. In this study the effects of hydrophobicity were assessed retrospectively, in response to the unusual early-time infiltration behaviour that had been consistently observed for the lysimeters. Three small cores (10 x 5 cm depth) were sampled from the surface of lysimeter one, following completion of the lysimeter infiltration experiments. Infiltration of water and ethanol were measured separately for each core under a surface suction of 0.4 kPa, with the cores equilibrated prior to each infiltration experiment at a Ψ_m of -8 kPa, which is the same antecedent Ψ_m measured for the equivalent L1 0.5 kPa infiltration experiment (Table 6-1).

The results of these measurements are presented in Figure 6-7, where two estimates of S_w and S_e have been made for each core, from the early-time linear section of the plot $I(t^{1/2})$, as well as the zero slope section of the plot $It^{-1/2}$ $(t^{1/2})$. From these plots the average S_w is estimated as 1.6 mm hr $^{-1/2}$, compared to an average S_e estimate of 5.1 mm hr $^{-1/2}$. This provides an average RI of 6.8 for the three cores, with a total range in RI of 4.3 to 9.3. These RI values clearly indicate that hydrophobicity is present under these infiltration conditions, and is likely to have been an important mechanism governing the early-time infiltration behaviour of the lysimeters.

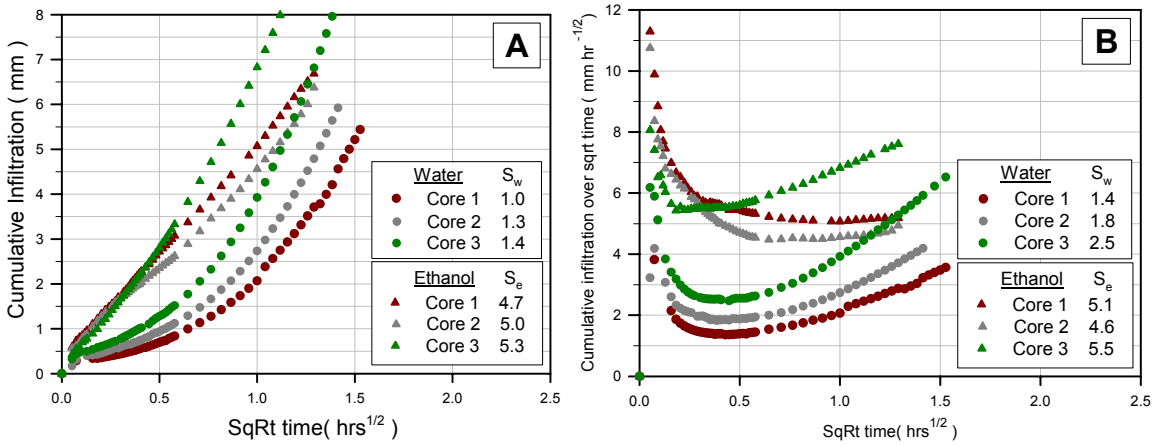

Figure 6-7 Comparison of the early-time infiltration of water and ethanol into three small cores sampled from the 0 – 5 cm depth of lysimeter one, to estimate the sorptivity of water (S_w) compared to the ethanol sorptivity (S_e). Two graphs are presented of the same data: in graph A sorptivity is estimated from the slope of the most linear portion of early-time infiltration; whilst in graph B sorptivity is estimated from the intercept of the portion of the plot with zero slope.

The hydrophobicity results also have important implications for assessing the significance of antecedent soil wetness on early-time infiltration behaviour. When sorptivity is reduced by hydrophobicity the infiltration capacity (I_c) calculated by Equation 6-4 is a large under-estimate. For example, extrapolation of the potential S_w derived from the hydrophobicity experiment to the equivalent L1 0.5 kPa experiment estimates an I_c of ~ 48 mm, where K_0 - K_i is ~1.5 mm hr^{-1}. The actual I_c is likely to be smaller as the hydraulic attributes of the surface layer change with depth. However, these results clearly indicate that if hydrophobicity was consistent for all the lysimeters, then antecedent wetness is unlikely to be responsible for the slow early-time behaviour.

6.4.5 Air Encapsulation

In the study of Faybishenko (1999) infiltration followed a three stage pattern. This was attributed to the effects of air encapsulation that initially slowed infiltration, followed by an increase in i_t as mobile air is removed, before a reduction in i_t to a quasi-steady value. This infiltration pattern is similar to that observed during a number of the experiments in this study (Figure 6-1) suggesting air encapsulation may be a mechanism influencing early-time infiltration behaviour.

Figure 6-8 shows that under saturated infiltration, the slow early-time infiltration of all lysimeters coincided with high air-filled porosity (ε_a), with i_t increasing as ε_a decreased. The relationship is particularly clear for L1 and L3, where ε_a was measured every minute and can be determined for 1 mm cumulative infiltration intervals. For L2 and L6 the ε_a was only recorded as a 10 minute average, although it still indicates a relationship between a slow i_t and a high ε_a. However, it is uncertain the extent to which air encapsulation is a direct influence on infiltration, as opposed to being an indirect effect of hydrophobicity. The rapid wetting after 5 – 10 mm infiltration may represent the breakdown of hydrophobicity. Clothier et al. (2000) also observed that hydrophobicity appeared to break down by about 5 mm of infiltration.

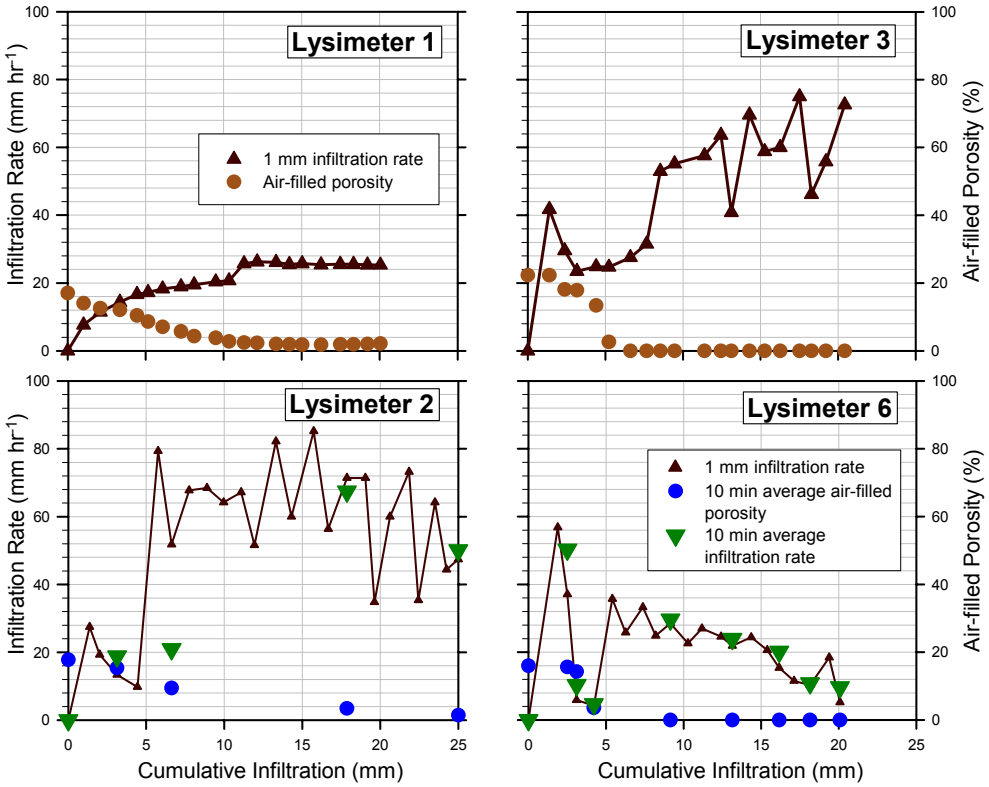

Figure 6-8 Comparison of the pattern of infiltration rate (i_t) and air-filled porosity (ε_a) of the 0 – 5 cm depth, for four lysimeters during saturated infiltration. The ε_a is calculated as the difference between the total porosity and water-filled porosity measured by the *in-situ* WCR.

Air-encapsulation also appears to be an important component of unsaturated infiltration (Figure 6-9). This may be because air-filled pores are an inherent component of unsaturated infiltration, particularly when using a tension infiltrometer to exclude macro-pores from the infiltration process. In this sense the antecedent ε_a can be split into two components during unsaturated infiltration:

1. Pores which remain air-filled because they have a water entry suction lower than that imposed by the tension infiltrometer, herein termed the 'non-fillable' air-filled porosity (ε_{anf}), and;

2. Pores that have a water entry suction greater than that imposed by the infiltrometer, and therefore may fill with infiltrating water. These pores are those that provide the antecedent infiltration capacity (I_c) defined in section 6.4.3. Here I_c is expressed as a percentage of the soil volume from 0 – 5 cm depth that is fillable for infiltration, if the soil wets from Ψ_i to the 'target' Ψ_m, set by the tension infiltrometer.

In Figure 6-9 the ε_{anf} is shown as the 'target' air-filled porosity that the 0 – 5 cm depth should wet to during unsaturated infiltration, as I_c becomes water-filled. The ε_{anf} is considered unfillable to infiltrating water, and if it occupies a sufficiently large volume, may restrict sorptivity-driven infiltration where the non-fillable network acts to isolate parts of the I_c pore network from the infiltrating water.

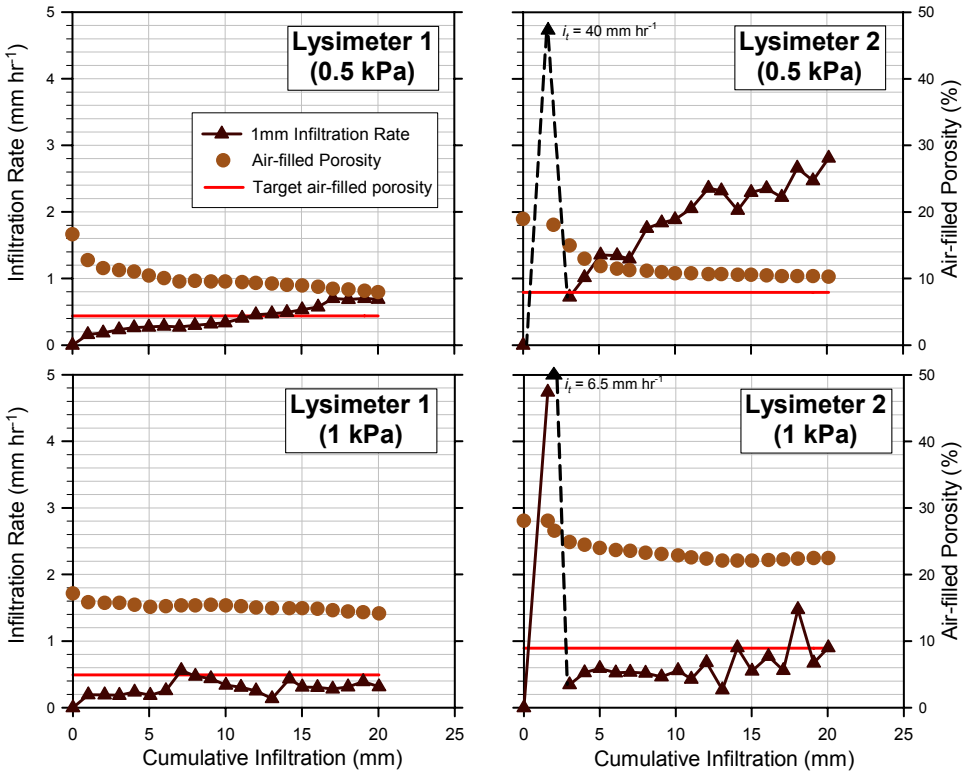

Figure 6-9 Comparison of the pattern of air-filled porosity (ε_a) for the 0-5 cm depth and infiltration rate (i_t) as unsaturated infiltration progresses, under surface suctions of 0.5 and 1 kPa. The 'target' ε_a value is indicated, which is the value that ε_a should decline to (termed the non-fillable air-filled porosity, ε_{anf}).

Table 6-2 shows a comparison of the I_c with the expected ε_{anf} of each experiment, assuming that the 0 – 5 cm depth wets as expected (i.e. Ψ_m would equal that imposed by the tension infiltrometer). The results in Table 6-2 indicate that during unsaturated infiltration the ε_{anf} is likely to be large proportionally to the I_c that could induce sorptivity-driven infiltration. Assuming that both air- and water-filled components are interwoven in the pore network, it seems plausible that ε_{anf} could have a large restrictive influence on early-time infiltration.

Surface suction	L1				L2				L3			
	Ψ_i	ε_{anf}	*WCR* I_c	*Core* I_c	Ψ_i	ε_{anf}	*WCR* I_c	*Core* I_c	Ψ_i	ε_{anf}	*WCR* I_c	*Core* I_c
(kPa)	*(kPa)*	*(%)*	*(%)*	*(%)*	*(kPa)*	*(%)*	*(%)*	*(%)*	*(kPa)*	*(%)*	*(%)*	*(%)*
0	-8.44	0	17	14	-5.14	0	18	17	-9.00	0	22	15
0.5	-8.17	4	12	9	-5.30	8	11	9	-8.90	7	13	8
1	-6.25	5	12	8	-7.13	9	19	10	-6.95	7	19	7
1.5	-6.20	5	14	7	-7.28	10	14	8	-8.43	8	16	7

Table 6-2 Comparison of the non-fillable air-filled porosity (ε_{anf}) and the potential infiltration capacity (I_c) that could contribute to sorptivity-driven infiltration, if the 0 – 5 cm depth wet as expected from the antecedent matric potential (Ψ_i) to that imposed by the tension infiltrometer. Two estimates of I_c are provided, from: A. *In-situ* water content reflectometers (WCR); B. Water release from three small cores (10 x 5 cm deep) sampled from each lysimeter. ε_{anf} is estimated from the small core porosity relationships.

The restricting effect of ε_{anf} will be enhanced if further air-encapsulation occurs as infiltrating water fills the I_c component of the pore network. This appears evident in Figure 6-9, where under 0.5 kPa surface suction ε_a slowly declines towards the 'target' ε_{anf} value, whilst under 1 kPa suction ε_a remains much larger than the 'target' ε_{anf} value. Under 1 kPa suction the ε_a of L1 remains 9% above the 'target' ε_{anf} value, with L2 14% above the ε_{anf} value, which is much larger difference than the 2% potential measurement error arising from the temperature sensitivity of the WCR (refer section 3.3.2, chapter 3).

A clearer picture of air encapsulation during infiltration is shown in Figure 6-10. Under 0.5 kPa surface suction, < 30% of the I_c remains air-filled after the first 5 mm infiltration, decreasing further to < 10% after 20 mm infiltration. However, under 1 kPa surface suction 40 – 60% of the I_c remains air-filled up to the first 20 mm infiltration. This indicates that when infiltration occurs under a surface suction of > 1 kPa, the excluded macropores create a ε_{anf} network that has sufficiently large volume and interconnectedness to isolate large portions of the water-fillable pore network.

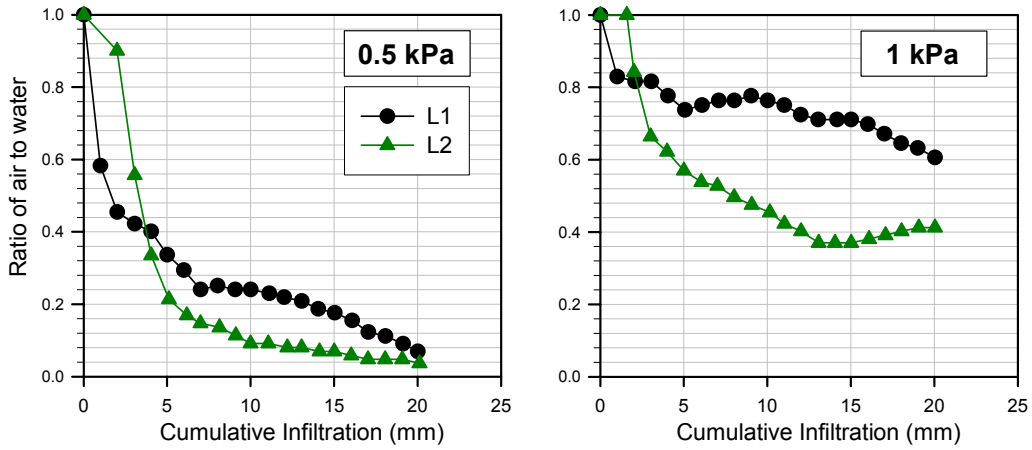

Figure 6-10 The ratio of air to water in the component of soil porosity (I_c) that can contribute to sorptivity-driven infiltration. The ratio is estimated from the proportional change in the *in-situ* measurements of water content by the reflectometers (WCR). The ratio is compared for lysimeters 1 and 2 during unsaturated infiltration, with surface suction controlled at 0.5 and 1 kPa.

Whilst it can be expected that hydrophobicity will be influencing the unsaturated infiltration experiments, the 0 kPa infiltration experiments indicate that its effects should be limited to the first 5 – 10 mm of infiltration. It is possible that the initial hydrophobicity and ε_{anf} network both interact to restrict the potential infiltration pathways, essentially creating preferential flow, which in turn creates air encapsulation. Preferential flow has been previously recognised as a mechanism that may lead to air encapsulation, where the variation in flow velocities of infiltrating pores may lead to parts of the pore network not being able to fill with water, because other water-filled pores have blocked escape routes for the soil air (Fayer and Hillel, 1986). Results from my experiments suggest that a dynamic interaction between hydrophobicity, the ε_{anf} network, and preferential flow leads to air encapsulation being a significant mechanism governing early-time infiltration behaviour.

Potential air entrapment by the infiltrometer-lysimeter system

It is possible that the air entrapment is also present, as an artefact of the tension infiltrometer and lysimeter system. The infiltrometer may block air escaping through the soil surface, and the lysimeter walls may block lateral air displacement. This effect has been observed in lysimeter studies by Wang et al. (1998), when air was not allowed to escape out of the base of a lysimeter. Air entrapment has also been observed in field soils with a high water table or slowly permeable subsoil that restricts the vertical displacement of air (Fayer and Hillel, 1986; Hammecker et al., 2003; Navarro et al., 2008).

In the air-confining situation of Wang et al. (1998) the soil air became compressed ahead of the wetting front until the air-pressure was great enough to allow escape to the surface. Infiltration rate (i_t) was found to follow a 'surging' pattern, inversely related to the rise and fall of the air pressure ahead of the wetting front. In the study of Fayer and Hillel (1986) infiltration at 137 mm hr^{-1} resulted in soil air pressures increasing 0.5 – 1 kPa ahead of the wetting front, whilst Wang et al (1998) measured increases of 1 to 5 kPa.

The experiments of this study do not generally show a 'surging' i_t during early-time infiltration, except during saturated infiltration into L2, L3 and L6 (Figure 6-2). These lysimeters appear to show an early stalling then rise in i_t, that appears to be inversely related to the air-filled porosity (Figure 6-8), which may reflect air confinement. However, the tensiometers at 20 cm depth remained steady during early-time infiltration, with no indication of an air pressure spike prior to the arrival of the wetting front, indicating that the subsoil air permeability was adequate to cope with the displaced air.

During unsaturated infiltration, air compression is less likely to occur, because soil air should be able to be displaced into macropores. Importantly, it was also observed that it was difficult to maintain the applied drainage suction during early-time unsaturated infiltration. The drainage air-pumps needed to be on high, or additional pumps required (L2 and L3), to cope with excess air that was draining through the lysimeters. Once the lysimeters had wet up, the drainage suction could be maintained by a single air-pump on low speed, and was often further restricted by a pipe clamp to reduce the bubble rate in the bubble tower. This further indicates that there was adequate subsoil air permeability.

Adequate subsoil air permeability is also supported by Figure 6-11, which shows replicate saturated infiltration experiments into a large (22 x 22 cm) core sampled from the topsoil layer of L3. The antecedent matric potential and experimental setup (refer section 3.8, chapter 3) were similar to the equivalent lysimeter experiment. Slow early-time infiltration is still evident, which should not occur if the similar lysimeter behaviour was due to subsoil induced air-confinement. Infiltration is consistently stalled for the first 4 – 5 mm, which was also observed in the equivalent lysimeter experiment. This period of slow infiltration is consistent with hydrophobicity effects observed in this study and Clothier et al. (2000).

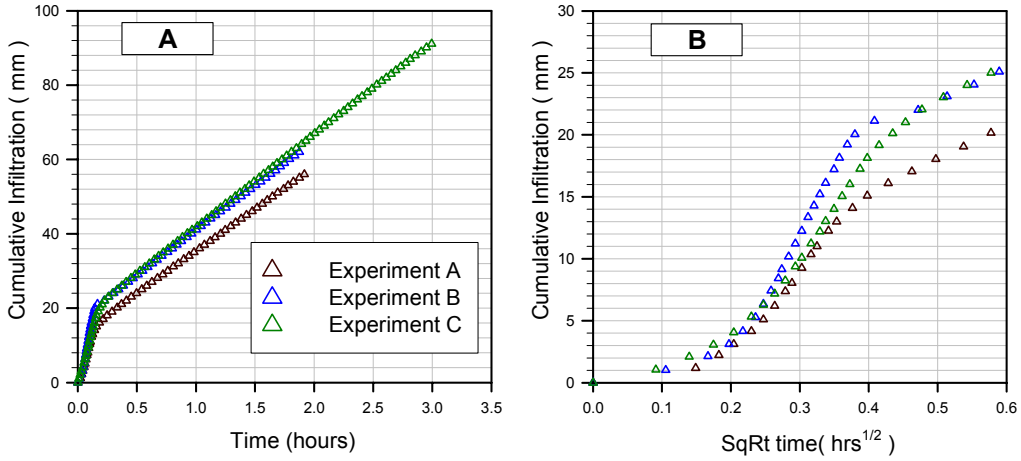

Figure 6-11 Replicated saturated infiltration experiments into a large (22 x 22 cm) core sampled from the topsoil layer of L3. Graph A shows the complete pattern of cumulative infiltration. Graph B focuses on early-time infiltration, plotting cumulative infiltration versus square-root of time ($t^{1/2}$).

The most interesting feature of Figure 6-11 is that once hydrophobicity breaks down, infiltration follows the 'classic' behaviour of the Philip model (Equation 2-1), where a sorptivity phase is consistently evident, followed by the steady-state phase. The sorptivity phase is also evident at the lysimeter scale, but was not initially recognised in section 6.3.2 because of the confounding influence of hydrophobicity. Ignoring the hydrophobicity phase provides sorptivity values during saturated infiltration of 70 – 100 mm hr $^{-1/2}$ for the core experiments, and 70 mm hr $^{-1/2}$ for the equivalent lysimeter experiment.

6.5 Summary

Analysis of early-time infiltration behaviour found an absence of clear sorptivity-driven behaviour, of the type predicted by the commonly used infiltration model of Philip (1957). The lack of sorptivity behaviour was consistent across four lysimeters, and during infiltration under different surface imposed suctions.

Some other mechanism is believed to govern the early-time infiltration behaviour. The tension infiltrometer-lysimeter system is not thought to be the rate-limiting mechanism, and neither is blockage of infiltrating pores by the development of a surface seal. The infiltration experiments were conducted at conditions typical of winter-time, when the antecedent water content is at or above field capacity. The antecedent conditions could limit the infiltration capacity available for sorptivity-driven infiltration, but measurements of soil-water status indicate the infiltration capacity was at least 4 – 10 mm across the

experiments. This is accepted as adequate for expression of sorptivity, particularly if sorptivity dominated infiltration is not just confined to wetting the surface layer (0 – 5 cm depth), as assumed in this study.

The most likely mechanism is weak hydrophobicity, which appears to restrict infiltration for the first 5 – 10 mm of infiltration. During unsaturated infiltration some macropores are non-fillable to infiltrating water, and it is suggested that the non-fillable pores may also act to isolate parts of the pore network that could exhibit sorptivity, and thus restrict early-time infiltration. It is also suggested that the interaction between hydrophobicity and the non-fillable pore network may be an important mechanism causing non-uniform infiltration through preferential flowpaths. Preferential flow may be another important mechanism that acts to encapsulate air in parts of the pore network by effectively blocking the escape root for the displaced air, further restricting the expression of sorptivity.

In this sense the early-time infiltration behaviour of this soil is seen to be governed by the dynamic interaction between sorptivity, hydrophobicity, the network of air-filled pores, preferential flow and air encapsulation. Although this study focuses on the mechanisms governing early-time infiltration at antecedent conditions near field capacity, it is likely that these mechanisms will still have a strong influence under drier antecedent conditions. It can be expected that as the soil dries hydrophobicity will strengthen, restricting the matrix sorptivity, whilst promoting preferential flow through macropores and air encapsulation. This is an area where further research is warranted.

Chapter 7
Characterisation of the *in-situ* hydraulic conductivity of individual soil layers during infiltration over long time periods

7.1 Introduction

Knowledge of the nature of a soil's hydraulic conductivity is critical to understanding soil water movement. The hydraulic conductivity, $K(\Psi_m)$, and soil water retention, $\theta_v(\Psi_m)$, relationships are the two key attributes necessary to describe a soil's hydraulic character (Clothier and Scotter, 2002). Models of soil water movement are commonly based on solving Richards' equation, which requires knowledge of $K(\Psi_m)$ and $\theta_v(\Psi_m)$. It follows that the reliability of these models depends on the quality of the $K(\Psi_m)$ and $\theta_v(\Psi_m)$ measurements.

It is important to select an appropriate method to measure $K(\Psi_m)$, particularly because $K(\Psi_m)$ can be hysteretic in nature. Tension infiltrometers have become the standard method for measuring the wetting curve of $K(\Psi_m)$ at low surface applied suctions (Clothier and Scotter, 2002; Clothier, 2001; Cook, 2008; McKenzie et al., 2002). The wetting curve is an important determinant of soil hydraulic behaviour, controlling how water enters the soil and moves downwards during infiltration events. The advantage of tension infiltrometers is that they allow the user to control the maximum actively conducting pore size at the infiltration surface. This is particularly important as numerous studies have shown that $K(\Psi_m)$ can reduce by orders of magnitude as the actively conducting pore-size reduces, particularly when Ψ_m is in the range 0 to -1.5 kPa (AnguloJaramillo et al., 1997; Clothier and Smettem, 1990; Coquet et al., 2005; Jarvis, 2007; Jarvis and Messing, 1995).

This chapter presents the results of long-time infiltration experiments using tension infiltrometers. The results provide insight into long-time infiltration behaviour, and the *in-situ* $K(\Psi_m)$ relationship, as well as providing insight into two key issues raised in the literature. The first issue is that identification of steady-state is often a subjective decision of the experimenter (Wang et al., 1998b), which will affect the quality of the $K(\Psi_m)$

measurement. The second issue, raised by Smettem and Smith (2002), is that there has been no investigation of the effect of soil layering on hydraulic attributes derived from infiltration studies. The experiments of this study contribute in both respects.

The objectives of this chapter are:

1. To determine the *in-situ* $K(\Psi_m)$ relationship for the individual layers of each lysimeter using steady-state analysis.

2. To determine the effects of different criteria for recognising steady-state on the $K(\Psi_m)$ relationship.

3. To determine the main soil mechanisms that govern the long-time infiltration behaviour, and their degree of influence on determining $K(\Psi_m)$.

7.2 Methods

7.2.1 Experimental setup

The methods used for the experiments in this chapter are described in chapter 3.

7.2.2 Calculation of hydraulic conductivity

The $K(\Psi_m)$ relationship was calculated for the four soil layers of each lysimeter, over four separate infiltration experiments carried out under controlled surface suctions of 0, 0.5, 1 and 1.5 kPa. $K(\Psi_m)$ was calculated over 10 mm cumulative infiltration intervals and the $K(\Psi_m)$ relationship constructed from the hydraulic conductivity plotted against the average Ψ_m of a layer over a given interval. The average Ψ_m was calculated as the average of the spatial and temporal mean of the Ψ_m measurements at the upper (U) and lower (L) boundaries of a layer. The choice of a 10 mm interval to calculate $K(\Psi_m)$ was somewhat arbitrary, but was chosen as the smallest interval for which the maximum measurement error in cumulative infiltration was <10%.

$K(\Psi_m)$ was calculated using the steady-state Darcy-Buckingham flux law (Jury and Horton, 2004),

$$K(\Psi_m) = i_t \Big/ \left[1 + \frac{(\Psi_U - \Psi_L)}{(z_L - z_U)} \right] \qquad \text{Equation 7-1}$$

where i_t (mm hr^{-1}) is the infiltration rate over the 10 mm interval of cumulative infiltration; Ψ_U ,Ψ_L (mm) are the spatial and temporal means of Ψ_m at the upper and lower layer boundaries respectively, over the 10 mm interval; and z_U, z_L (mm) are the soil depths at the upper and lower boundaries. The internal flow rate within a soil layer will vary spatially due to heterogeneity in the pore network. Equation 7-1 assumes that the spatially averaged flow rate of each layer within the column is the same as i_t. This is difficult to independently verify, although drainage rates were also measured. A consistent flow rate within the column is more likely to occur when drainage matches infiltration.

The effect of temperature variation

It is well recognised that hydraulic conductivity is dependent on temperature (Stoffregen et al., 1999). In this study the effect of temperature was partially controlled by conducting experiments within a large shed. However, individual experiments lasted up to 1000 hours, and were done at different times of the year, so temperature variation cannot be neglected. The air and soil temperature variability during each experiment are shown in Appendix 1.

The effect of temperature on $K(\Psi_m)$ was accounted for using the exponential function of Stoffregen et al. (1999),

$$K_{10^oC}(\Psi_m) = K(\Psi_m)\exp(0.04(10 - Tp)) \qquad \text{Equation 7-2}$$

where $K(\Psi_m)$ is corrected to a reference temperature of 10°C, from the mean soil temperature (Tp) over which $K(\Psi_m)$ was calculated.

Estimation of error in hydraulic conductivity

Two error bars are calculated for each value of $K(\Psi_m)$; one expressing the uncertainty in the matric potential, and the other the uncertainty in the hydraulic conductivity. Uncertainty in the matric potential is calculated as the standard error of the mean of the tensiometer measurements from the upper and lower boundaries of a layer, over the duration of a 10 mm cumulative infiltration interval.

Similar to the method of Fluhler et al. (1976), the conductivity uncertainty is calculated from first order, second moment Gaussian error propagation (Taylor, 1982), using the standard error of the matric potential, infiltration rate and tensiometer location over the duration of a 10 mm cumulative infiltration interval.

7.3 Results

7.3.1 Infiltration behaviour over long-time periods

For all lysimeters the infiltration rate (i_t) decreases as the surface suction increases (Figure 7-1), except L6, where long-time i_t for 0 and 0.5 kPa suctions are the same. The decrease in i_t is typically two orders of magnitude between saturated infiltration (0 kPa) and the largest suction of 1.5 kPa. Under saturated infiltration i_t stabilises at between 6 – 25 mm hr^{-1}, compared to 0.1 – 0.3 mm hr^{-1} for 1.5 kPa suction. Under suctions of 0.5 or 1 kPa there is a variation in i_t of over one order of magnitude among lysimeters. Under a suction of 0.5 kPa i_t varies between 0.2 – 5 mm hr^{-1}, whilst at 1 kPa suction the variation is between 0.1 – 2.5 mm hr^{-1}.

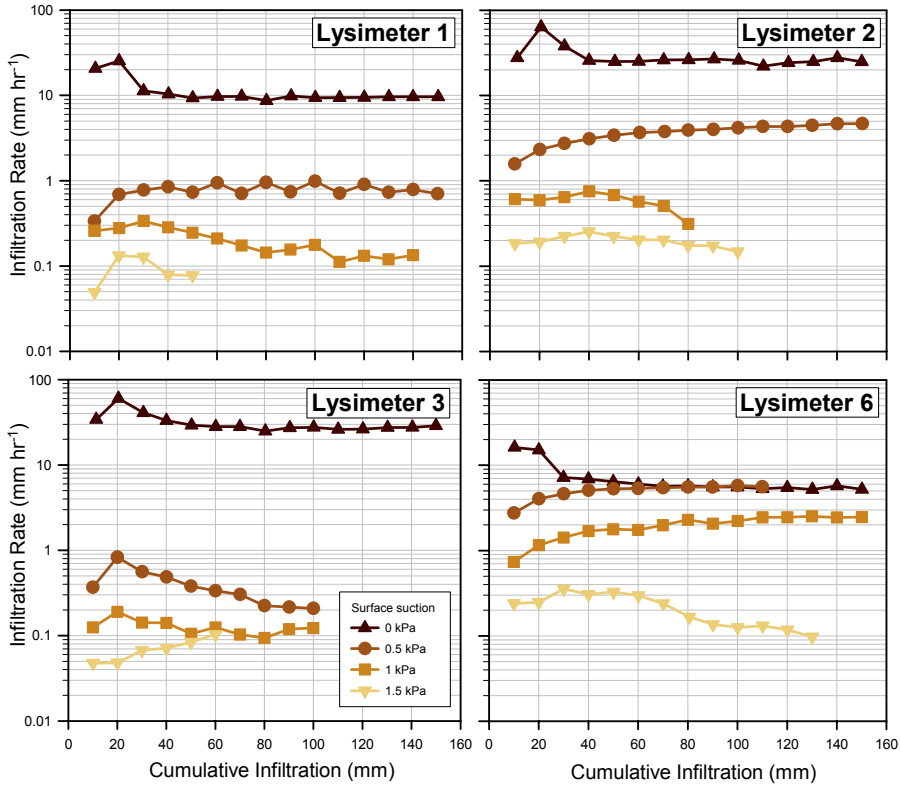

Figure 7-1 Comparison of infiltration rates (i_t) among lysimeters, where infiltration occurs under controlled surface suctions of 0, 0.5, 1 and 1.5 kPa. For each surface-imposed suction, i_t has been calculated for every 10 mm of cumulative infiltration. The respective graphs of cumulative infiltration versus time are in Appendix 6.

The lysimeters all have a similar pattern of infiltration behaviour at 0 kPa suction, where i_t decreases to a stable value after 40 – 60 mm infiltration. During unsaturated infiltration different lysimeters under the same suction exhibit different behaviours, with i_t gradually decreasing or increasing. In some experiments the change in i_t is less than 0.1 mm hr^{-1}

(e.g. L2 and L3 1.5 kPa), whereas in other experiments i_t increases by at least 1 mm hr^{-1} (e.g. L2 0.5 kPa). In most experiments i_t changes gradually, suggesting a soil mechanism, rather than measurement error.

7.3.2 Dynamics of matric potential over long time periods

The temporal pattern of Ψ_m is highly dynamic (Figure 7-2). In all experiments tensiometer arrays show wetting in a sequence corresponding to the wetting front moving down the lysimeter. After the initial wetting phase, the rate of change in Ψ_m reduces so that quasi-steady phases can be recognised, but typically Ψ_m never reaches a clear stable value, but continues to gradually decrease (e.g. L6 1.5 kPa) or increase (e.g. L6 1 kPa).

For each lysimeter the temporal pattern of Ψ_m changes for infiltration under different surface suctions. Likewise, for infiltration under the same suction the temporal change of Ψ_m varies among different lysimeters, as illustrated for infiltration under 0.5 kPa suction. Importantly, the temporal change in Ψ_m tends to mirror the i_t pattern (Figure 7-1), showing that infiltration is primarily being driven by the dynamics of Ψ_m within the soil column. At 0 kPa surface suction i_t increases as Ψ_m increases, and reaches a quasi-steady value once the soil column becomes saturated. During unsaturated infiltration, after the initial wetting of the column, i_t continues to rise slowly if Ψ_m continues to increase (e.g. L6 1 kPa), or else i_t decreases if the soil internally switches to drainage behaviour, and Ψ_m starts to decrease (e.g. L3 0.5 and 1 kPa).

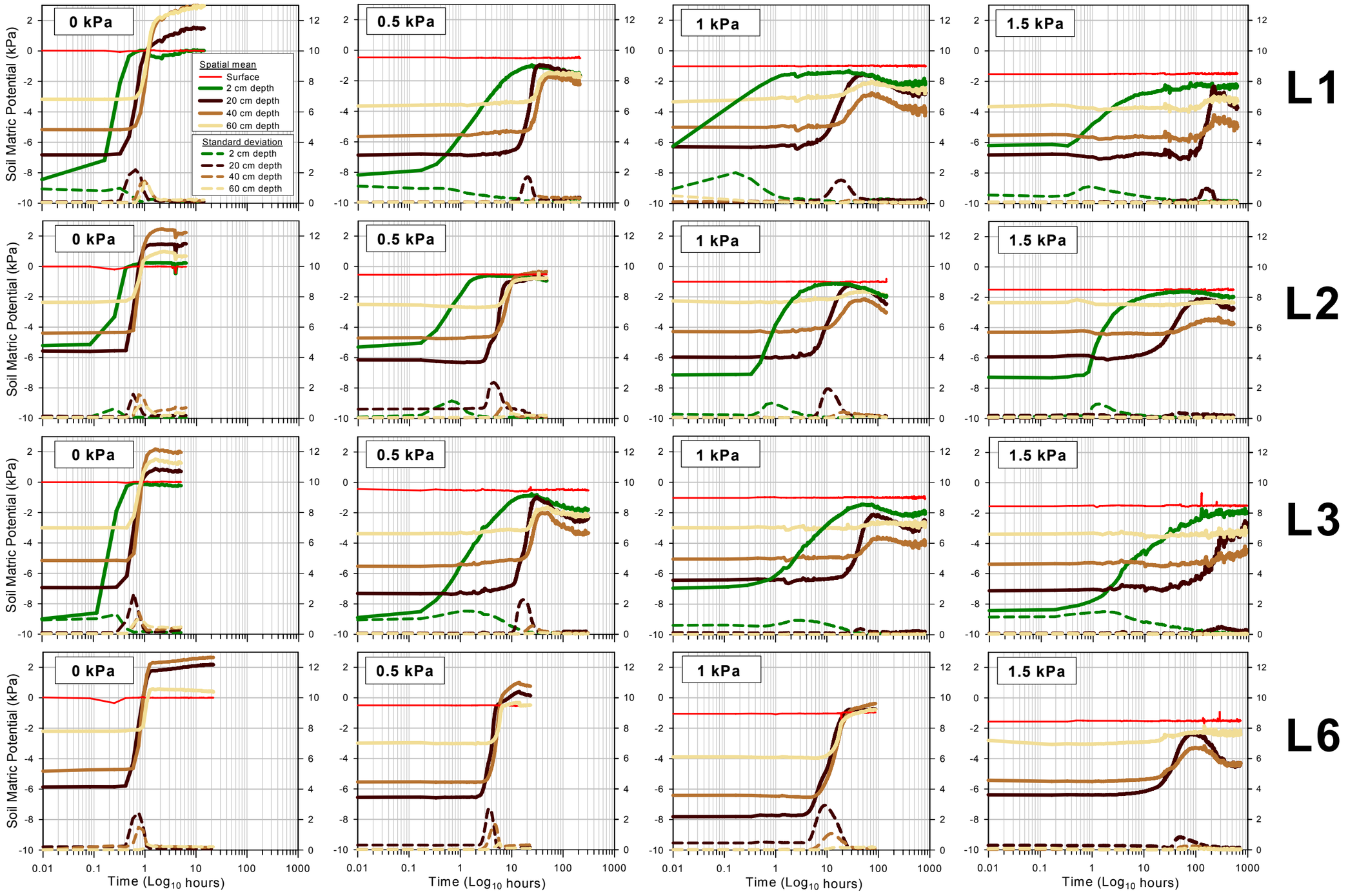

Figure 7-2 Comparison of the dynamics of soil matric potential (Ψ_m) for four lysimeters, during infiltration under controlled surface suctions of 0, 0.5, 1 and 1.5 kPa. For each experiment, the suction at the drainage base of the lysimeter was the same as that applied at the surface. Solid lines represent the spatial average of Ψ_m at the set soil depths, with the scale on the left Y-axis. Dashed lines represent the standard deviation of Ψ_m at the set soil depths, with the scale on the right Y-axis. Note that to enable comparison of all the experiments, time is represented on a logarithmic scale (Log_{10} hours).

At first glance the dynamics of Ψ_m appear to confound the use of steady-state analysis to derive hydraulic conductivities. Under *ideal* conditions in a homogenous soil, steady-state manifests as a constant Ψ_m with depth, and a unit hydraulic gradient (purely related to the gravitational potential). In general this cannot be achieved in a layered soil profile, because it would imply that at steady-state all layers had the same $K(\Psi_m)$ – which contradicts the existence of layers with different attributes. Instead, in a *real* layered soil steady-state will be reflected by a depth varying Ψ_m that generates hydraulic gradients which compensate for the layer-related changes in $K(\Psi_m)$ so that a constant flux rate is maintained, and infiltration equals drainage. However, the internal adjustments of Ψ_m are highly dynamical whereby layers can oscillate between wetting and draining behaviour over long time periods (Figure 7-2). In recognition of this behaviour I defined the 'best practicable' conditions by which quasi-steady state could be recognised, and for which $K(\Psi_m)$ could be calculated. The criteria were: 1. the average Ψ_m in the layer is as close to constant as possible; 2. the hydraulic gradient was as stable as possible; and 3. there was only small variation in Ψ_m and low uncertainty in the hydraulic gradient.

According to these criteria quasi-steady state phases occur in most experiments. In these phases the rate of change is slow enough that discrete intervals can be identified where the temporal variation in Ψ_m is relatively small. Further, a consistent feature of quasi-steady state is that the whole layer wets up or drains in relative unison. This occurs where any change in Ψ_m at the top of the layer is matched by approximately the same change in Ψ_m at the base of the layer. The result is a relatively stable hydraulic gradient. This is illustrated in Figure 7-3, where the hydraulic gradients of the individual layers of L1 are plotted for each infiltration experiment. The hydraulic gradients for all the lysimeters, during each experiment, are shown in Appendix 7.

Figure 7-3 shows that a quasi-steady hydraulic gradient occurs in each soil layer after 10 – 40 mm infiltration. During the quasi-steady state the hydraulic gradient may continue to change slowly (e.g. layer S at 0.5 kPa suction). Any drift of the hydraulic gradient during quasi-steady state phases of itself does not contravene assumptions inherent in the calculation of $K(\Psi_m)$ (Equation 7-1), since the integrated effects of variation in the hydraulic gradient would be reflected in the average infiltration rate. What is important is any variation of Ψ_m associated with the drift in hydraulic gradient. Drift in hydraulic gradient is most noticeable in unsaturated experiments. However, during quasi-steady state in these experiments Ψ_m is generally < -1 kPa, where $K(\Psi_m)$ shows low sensitivity to changes in Ψ_m, and Ψ_m varies little over 10 mm cumulative infiltration intervals. The other feature of Figure 7-3 is that during the

quasi-steady state the uncertainties are generally small, at <10%, except for layer S where the uncertainty can be up to 35%, reflecting the high uncertainty in defining the depth of thin soil layers.

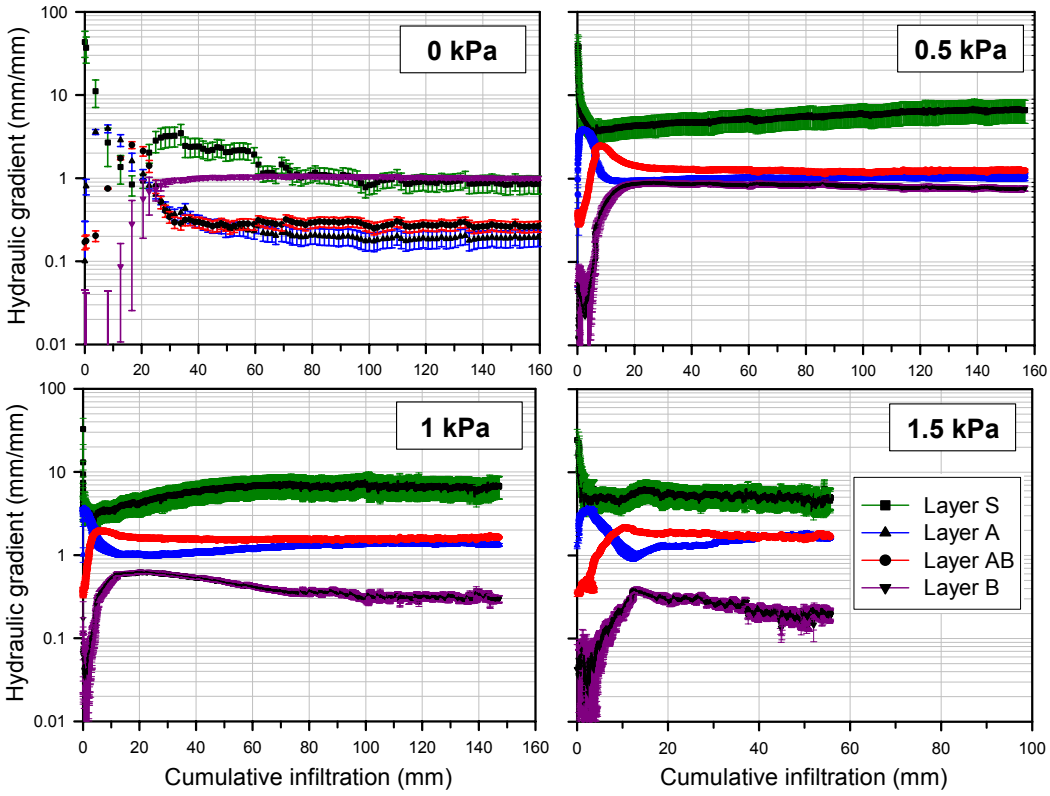

Figure 7-3 The hydraulic gradient of individual soil layers of Lysimeter 1, for infiltration under controlled surface suctions of 0, 0.5, 1 and 1.5 kPa. Individual layers are shown by the colour of the error bars. The gradient is calculated as the average of every 10 minute infiltration interval. Error bars represent the absolute error calculated from the standard error of the matric potential, and uncertainty of the soil depth.

7.3.3 Interpretation of hydraulic conductivity for individual layers

It is clear from these results that the i_t pattern for each lysimeter is closely coupled to the dynamics of Ψ_m. Of particular importance is that after medium to long-time infiltration a quasi-steady state phase can be identified in the hydraulic gradient of individual soil layers making it is possible to use steady-state analysis to calculate $K(\Psi_m)$ for discrete intervals of cumulative infiltration.

Figure 7-4 sets the context for interpretation of $K(\Psi_m)$, where the complete dataset, regardless of steady-state conditions, has been used to calculate $K(\Psi_m)$ for the individual layers of each lysimeter, for every 10 mm interval of cumulative infiltration. A clear $K(\Psi_m)$ relationship is apparent for each layer, where K decreases as Ψ_m decreases, but there is large scatter in the data presumably caused by inclusion of non-steady state infiltration. In the following

subsections I test the effectiveness of three commonly used methods to identify steady-state and filter the $K(\Psi_m)$ data in order to define a more accurate K versus Ψ_m curve.

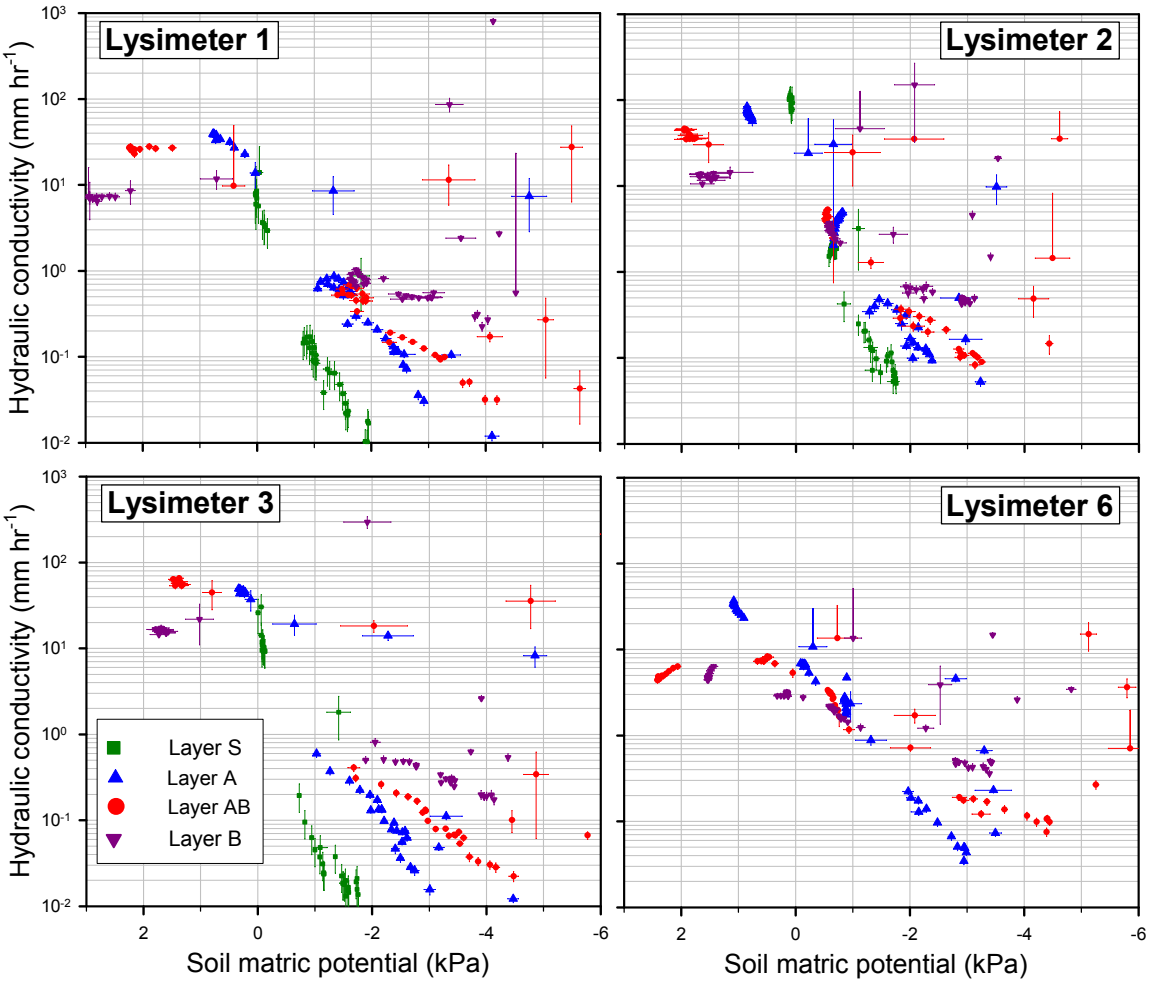

Figure 7-4 The $K(\Psi_m)$ relationship for the individual layers of four lysimeters, determined from the complete dataset, including both transient and steady-state infiltration. $K(\Psi_m)$ was calculated every 10mm interval of cumulative infiltration, from four separate infiltration experiments with infiltration under controlled surface suctions of 0, 0.5, 1 and 1.5 kPa.

Data Filter 1: Steady-state cumulative infiltration

The standard approach to identify steady state infiltration uses the cumulative infiltration curve, commencing from the point at which its slope remains constant (Jacques et al., 2002; McKenzie et al., 2002). As a guide McKenzie et al. (2002) recommend the slope should be constant for a minimum of five consecutive measurements.

In this study, linear regression was progressively fitted backward from the final infiltration observation, until the rate of decrease in the correlation coefficient (R^2) started to change markedly. In all cases this identified a linear segment of the cumulative infiltration curve with an R^2 of > 0.99, which was interpreted as quasi-steady state infiltration (Figure 7-5).

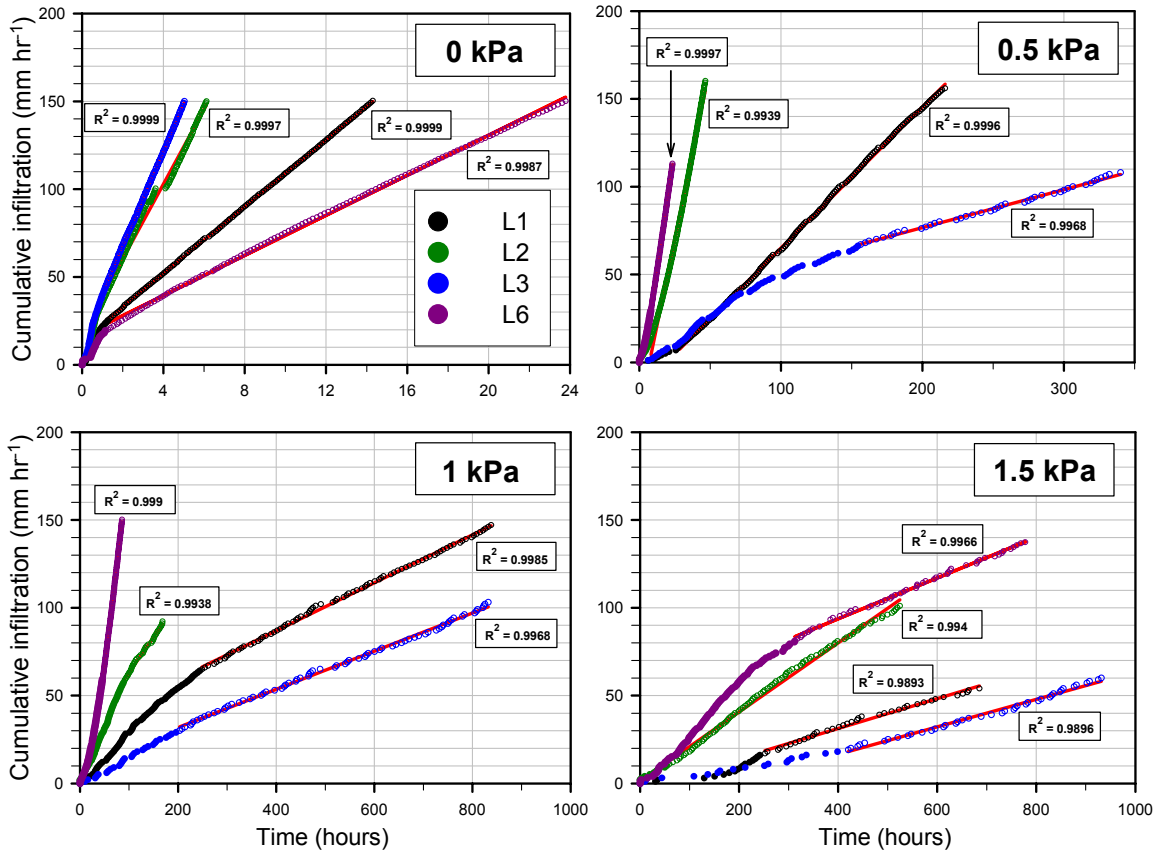

Figure 7-5 Cumulative infiltration versus time during infiltration experiments on four lysimeters, with infiltration under controlled surface suctions of 0, 0.5, 1 and 1.5 kPa. The red line shows the linear segment of each curve, which is interpreted as the quasi-steady state phase of infiltration.

When the data are filtered to include only the quasi-steady state infiltration phase, as identified from the linear portion of the cumulative infiltration curve, a large part of the scatter in the $K(\Psi_m)$ relationship is removed (Figure 7-6). This approach removes $K(\Psi_m)$ values arising from the transient infiltration phase, but some excess filtering of good data is apparent, and outliers remain. For L3 and L6 there is a loss of $K(\Psi_m)$ values between Ψ_m of -1 and -3 kPa, where there appeared to be good data forming a smooth curve in the original dataset of Figure 7-4. For L1 there is a cluster of $K(\Psi_m)$ values between Ψ_m of -1 and -2 kPa, indicating some of the data scatter remains.

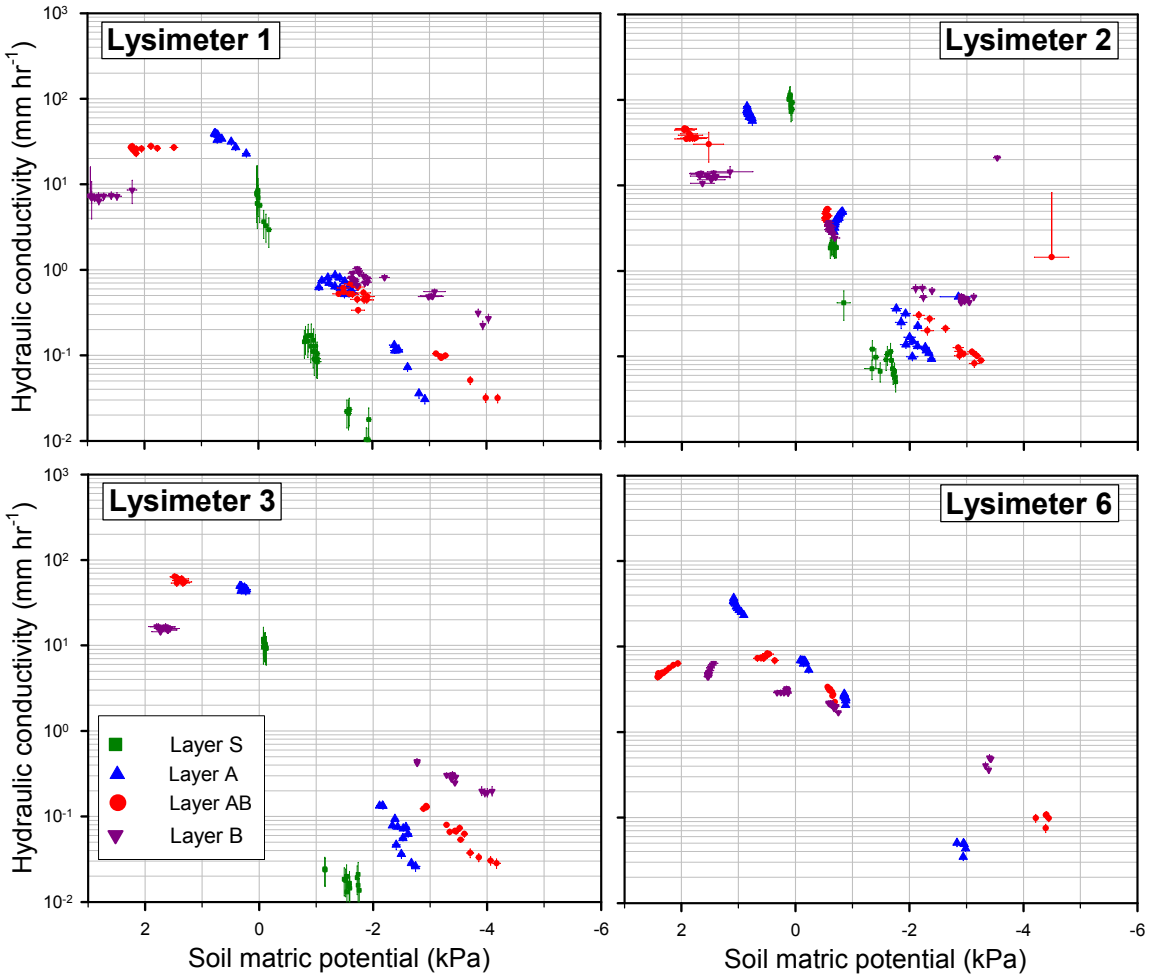

Figure 7-6 The $K(\Psi_m)$ relationship for the individual layers of four lysimeters, after filtering the data to include only the quasi-steady state infiltration phase, as identified from the linear portion of the cumulative infiltration curves in Figure 7-5.

Closer examination of Figure 7-5 indicates that this criterion may be over- or under-estimating the onset of quasi-steady state. Given the relatively similar antecedent Ψ_m of each infiltration experiment, the $\theta_v(\Psi_m)$ relationships (Figure 4-10) show that the onset of quasi-steady state would be expected to require the greatest amount of cumulative infiltration (I) under saturation. The amount of I required would be expected to decrease as the surface suction was increased, due to the reduction in the pore volume available for infiltration. However, this is not apparent in Figure 7-5 where, for example, onset of quasi-steady state infiltration for L1 is estimated at 26, 9, 65, and 17 mm cumulative infiltration under respective surface suctions of 0, 0.5, 1, and 1.5 kPa. This highlights that it may be unreliable to determine the onset of the steady state phase based purely on infiltration data, where a subjective decision is required on whether the gradual change in i_t is significant. Rather than a global fit regression to the cumulative infiltration curve, a piecewise regression may be more reliable, confined to the cumulative infiltration interval over which $K(\Psi_m)$ is calculated (i.e. 10 mm infiltration).

Data Filter 2: Drainage matches infiltration

Because this study used large soil columns, an alternative criterion for defining steady state is when drainage matches infiltration. If the flux at both ends of the column is equal, the internal fluxes and hydraulic gradients may also be approximately time invariant. This criterion is a standard method used for laboratory measurements of hydraulic conductivity (Cook, 2008; Dirksen, 1999). According to this criterion a quasi-steady state is apparent in all experiments, with infiltration closely matching drainage by 20 – 50 mm of infiltration (Figure 7-7). As a first approximation, quasi-steady state was identified when the relative difference between infiltration and drainage rates was <15%.

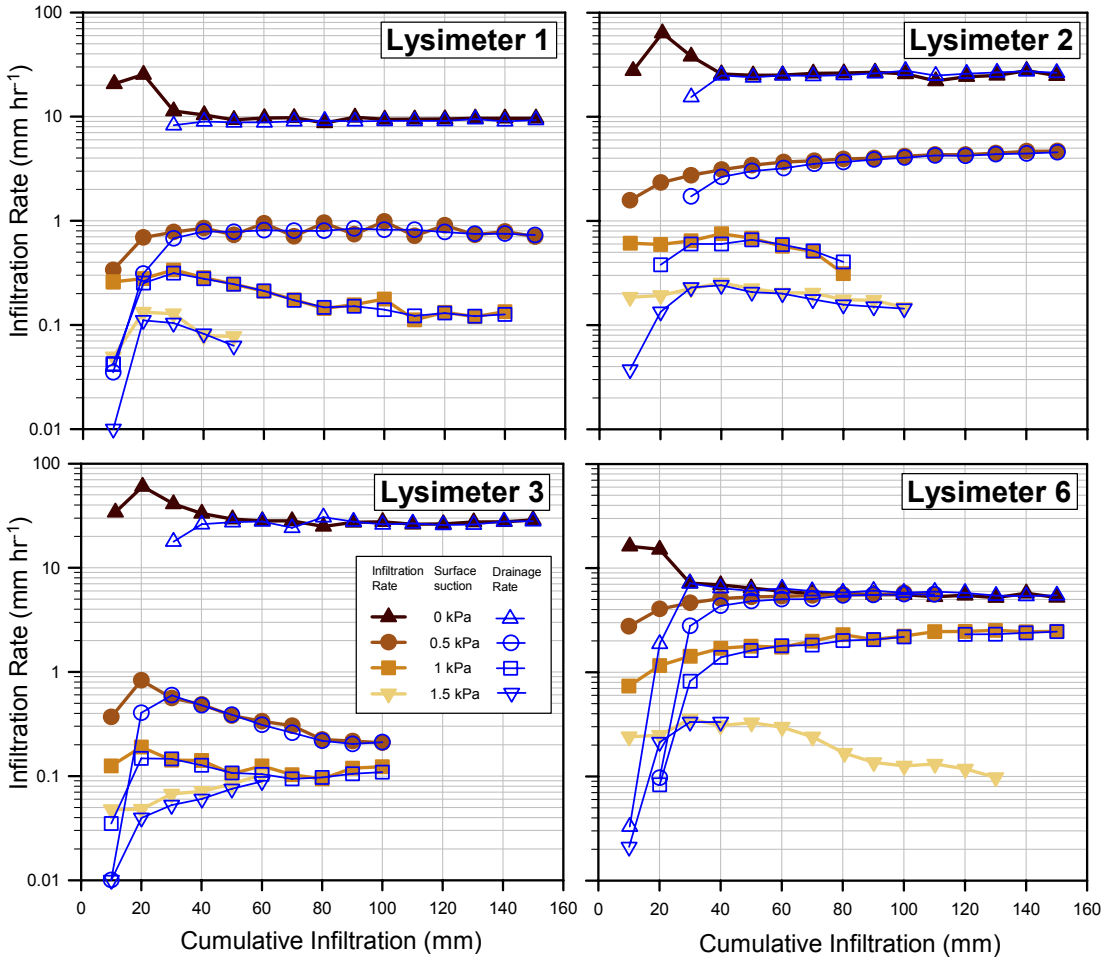

Figure 7-7 Comparison of infiltration and drainage rates for the four lysimeters, calculated for every 10 mm of cumulative infiltration, when infiltration is under controlled surface suctions of 0, 0.5, 1 and 1.5 kPa.

The revised $K(\Psi_m)$ curves using this criterion to filter the full dataset are shown in Figure 7-8. Scattered data in the $K(\Psi_m)$ curves that remained after the previous filtering criterion are largely resolved, indicating that the scatter arose from the initial soil column wetting. Compared to the previous criterion there also appears to be less filtering of good data. However, some outliers remain, e.g. the cluster of $K(\Psi_m)$ values for L1 between Ψ_m of -1 and -

2 kPa. Scatter is also evident under saturated infiltration (i.e. positive Ψ_m), as shown by L2 where $K(\Psi_m)$ varies between 60 and 100 mm hr^{-1} for both layers S and A. This indicates that other mechanisms may be having a significant influence on the reliability of interpreting $K(\Psi_m)$ using quasi-steady state analysis, beyond the obvious influence of the initial column wetting.

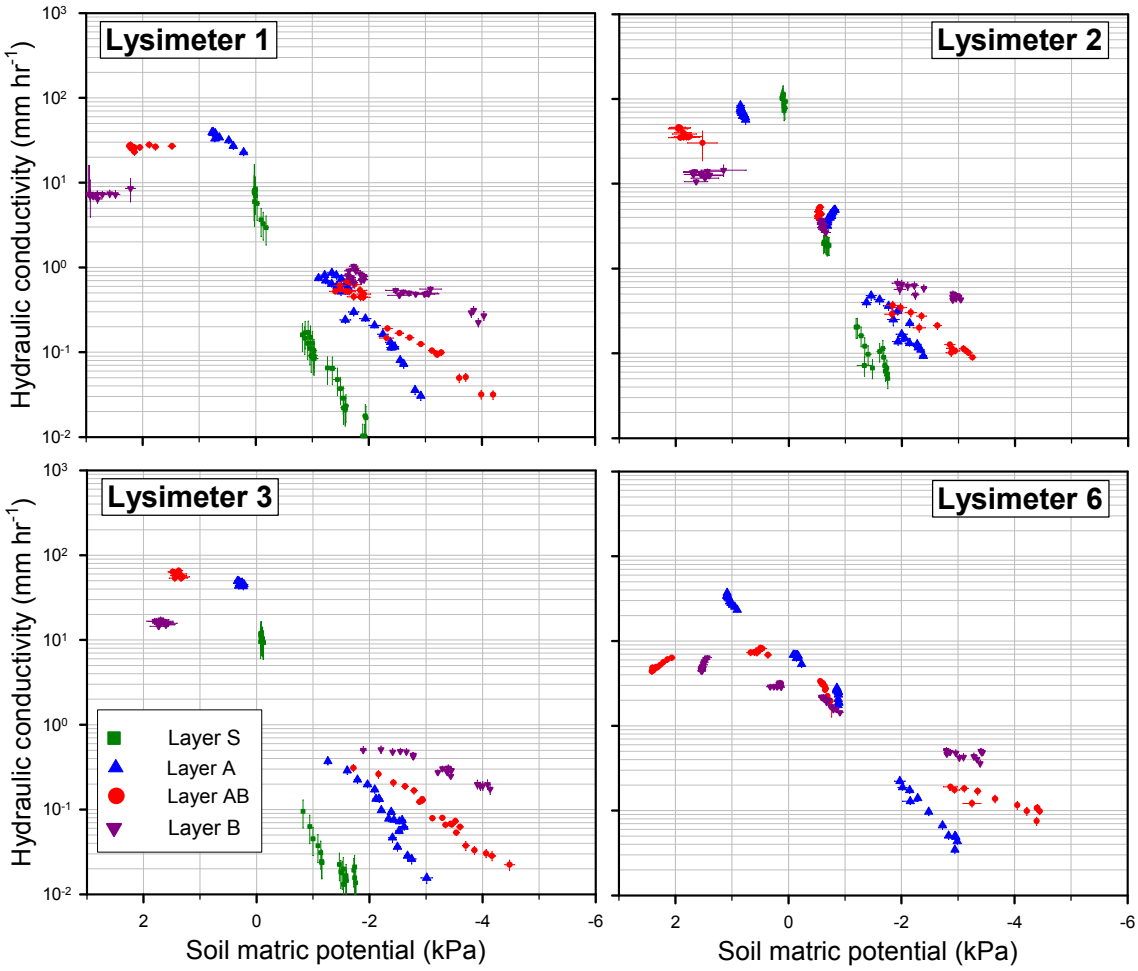

Figure 7-8 The $K(\Psi_m)$ relationship for the individual layers of four lysimeters, when the data are filtered to include only the quasi-steady state infiltration phase, as identified from when drainage closely matches infiltration in Figure 7-7.

Data filter 3: Stable hydraulic gradient

Arguably the most robust way of defining steady state is to identify periods when the hydraulic gradient and water flux are constant (Dirksen, 1999). This criterion was imposed by further filtering the $K(\Psi_m)$ data that remained after filtering by criterion 2 according to a quasi-steady state hydraulic gradient condition. The revised $K(\Psi_m)$ relationship (Figure 7-9) shows improvement on the previous methods, but the previously unresolved variability still remains (e.g. the cluster of $K(\Psi_m)$ values for L1 between Ψ_m of -1 and -2 kPa).

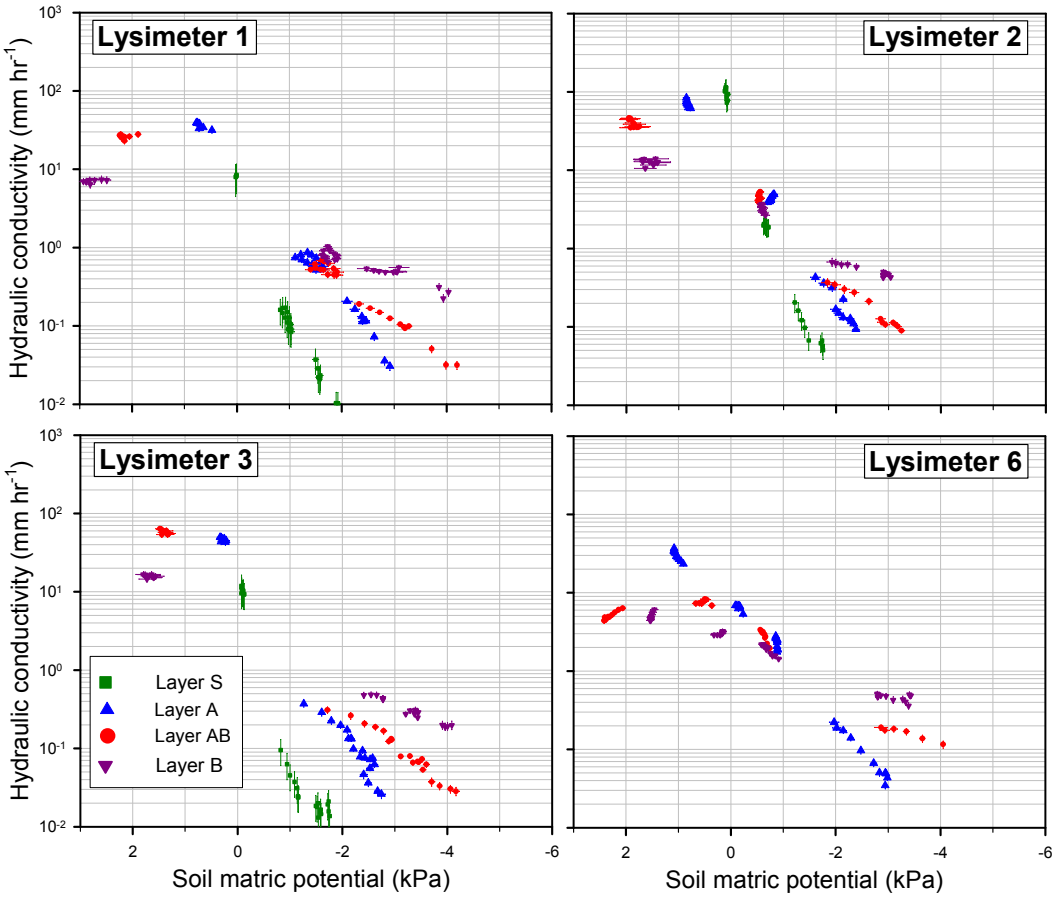

Figure 7-9 The $K(\Psi_m)$ relationship for the individual layers of four lysimeters, when the data are filtered to include only the quasi-steady state infiltration phase, defined to occur when both drainage closely matches infiltration (Figure 7-7) and the layer hydraulic gradient is stable (Appendix 7).

This remaining scatter may be due to how quasi-steady state conditions are identified. The results in Appendix 7 show that a quasi-steady hydraulic gradient can be easily identified for individual layers during most experiments. The exception is layer S where the hydraulic gradient often increases slowly during unsaturated infiltration. For this layer quasi-steady state was tentatively estimated to occur when the rate of change in the hydraulic gradient was < 0.5 mm mm^{-1} per 10 mm interval of cumulative infiltration (e.g. Layer S of L1 0.5 kPa after 40 mm infiltration).

Retrospective study of Figure 7-7 shows that the unresolved scatter in the $K(\Psi_m)$ curves in Figures 7-8 and 7-9 is largely an artefact of the subjective identification of a constant water flux. For example, cyclic fluctuations in the infiltration rate of L1 0.5 kPa results in the cluster of $K(\Psi_m)$ values in layers A, AB, and B between Ψ_m of -1 and -2 kPa. Under saturated conditions both L2 and L6 show non-steady $K(\Psi_m)$ values, which in L2 was caused by disturbance in the flow network after refilling the infiltrometer water tank at 90 – 100 mm infiltration, and in L6 steady-state was interpreted to occur too early at 30 mm rather than 80

mm cumulative infiltration. Removing $K(\Psi_m)$ values calculated for these phases produces 'clean' curves of the $K(\Psi_m)$ relationship (Figure 7-10).

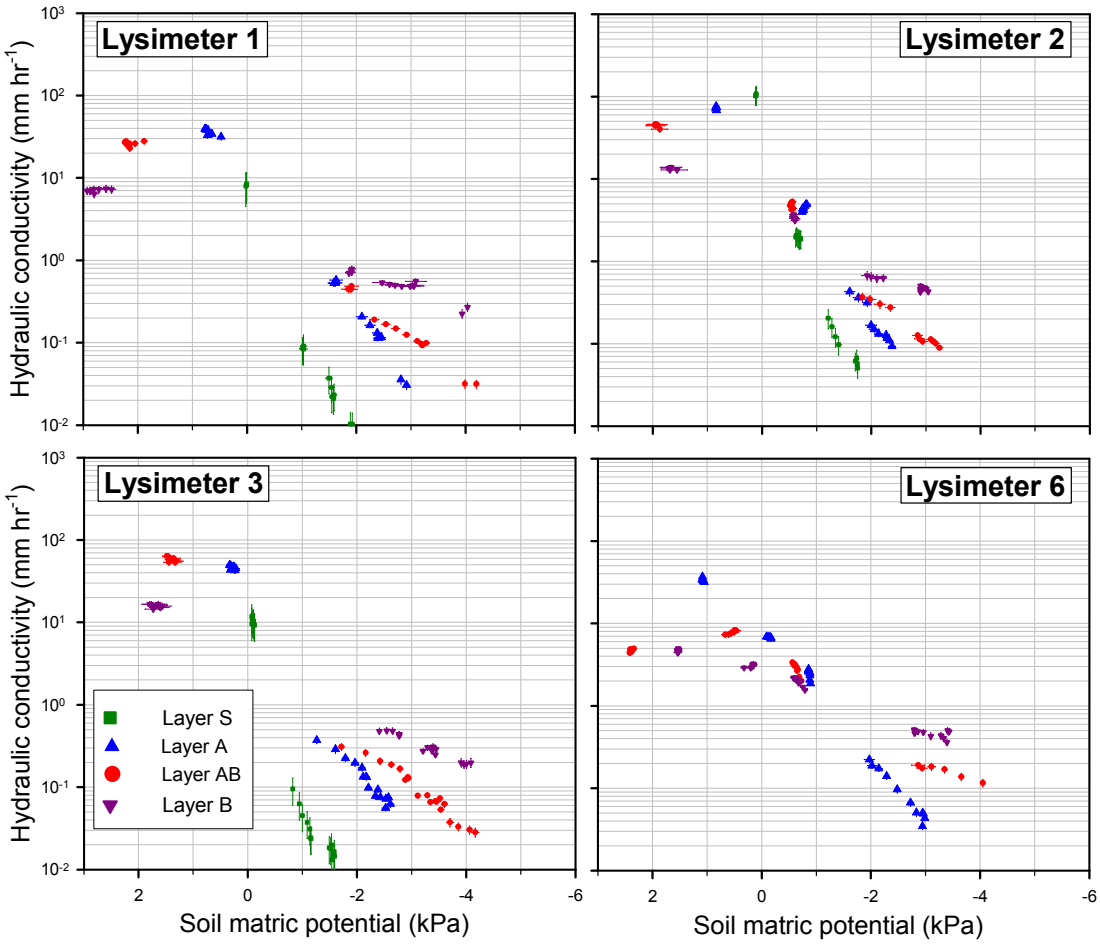

Figure 7-10 The $K(\Psi_m)$ relationship for the individual layers of four lysimeters, where Figure 7-9 is further refined by re-interpretation of quasi-steady state water flux in Figure 7-7.

7.3.4 Comparison of $K(\Psi_m)$ between soil layers

Figure 7-10 shows that $K(\Psi_m)$ is distinctly different for the individual soil layers, and that these differences are consistent between the four lysimeters. Under positive pressures of saturated flow the subsoil (layer B) had the slowest $K(\Psi_m)$, and was the restricting layer. Most interestingly this pattern reversed during unsaturated flow, where at Ψ_m of less than -0.5 to -1 kPa the subsoil has a markedly faster conductivity, with the topsoil (Layers S and A) becoming the restricting layer. At a Ψ_m of -3 kPa the $K(\Psi_m)$ of layer B was approximately one order of magnitude greater than for layer A.

All soil layers demonstrate a sharp decline in $K(\Psi_m)$ as Ψ_m decreases. The sharpest decline is for layer S, where $K(\Psi)$ decreases by approximately three orders of magnitude between saturation and Ψ_m of -1.5 kPa. The rate of decrease in $K(\Psi_m)$ with Ψ_m reduces down the soil

profile, and is only approximately one order of magnitude for layer B, between saturation and Ψ_m of -1.5 kPa.

The pattern of $K(\Psi_m)$ generally follows an exponential decline as Ψ_m decreases. For only a few layers the simple exponential function of Gardner (1958) would describe $K(\Psi_m)$ well, such as layer A of L1. For most of the layers, a two-line exponential model may be more appropriate (Keng and Lin, 1982; Messing and Jarvis, 1993),

$$K(\Psi_m) = K^* \exp\left[\alpha_1\left(\Psi_m - \Psi_m^*\right)\right] \quad \Psi_m > \Psi_m^* \qquad \text{Equation 7-3}$$

$$K(\Psi_m) = K^* \exp\left[\alpha_2\left(\Psi_m - \Psi_m^*\right)\right] \quad \Psi_m \leq \Psi_m^*$$

where α_1 and α_2 are the exponential slopes, Ψ_m^* the 'break-point' Ψ_m where the two exponential lines converge, and K^* is the conductivity at Ψ_m^* given by

$$K^* = K_{sat} \exp(\alpha_1 \Psi_m^*) \qquad \text{Equation 7-4}$$

where K_{Sat} is the conductivity under saturated conditions.

The good fit of this model (Figure 7-11) highlights that this soil may be considered a dual-permeability soil, where Ψ_m^* between the two permeability regions is in the range of -0.5 to -1.5 kPa. This finding correlates with the concept of distinctly different macro- and mesopore regions. Numerous studies have shown a sharp increase in conductivity, and preferential flow behaviour, when the soil wets to Ψ_m > -1 kPa (Jarvis, 2007). In previous applications of the two line exponential model, Messing and Jarvis (1993) estimated Ψ_m^* to lie between -0.4 to -0.6 kPa for a structured clay soil, whilst for six soils of contrasting texture Ψ_m^* was estimated at -0.25 to -0.6 kPa (Jarvis and Messing, 1995).

Comparison of the slopes in $K(\Psi_m)$ between the macro- and mesopore regions illustrates that the contrast is greatest in layer B, and more subtle in layers S and A. The key feature of the topsoil (i.e. layers S and A) is that the slope of both regions is steep, particularly the mesopore region where its slope (α_2) is fives times greater than for layer B. This is attributed to the much higher abundance of macropores in the topsoil, which during unsaturated flow form a well connected air-filled pore network that acts to impede water flow through the mesopore network, as discussed in Chapter 6. The sharp change in slope between the two regions of layer B highlights that the mesopore region has a much better interconnectivity during unsaturated flow, compared to the topsoil layers. This is because the macropore region of layer B is not as spatially extensive compared to the topsoil, as shown in the dye study of

Chapter 5, due to the smaller abundance of biological activity, as well as the larger size of aggregates.

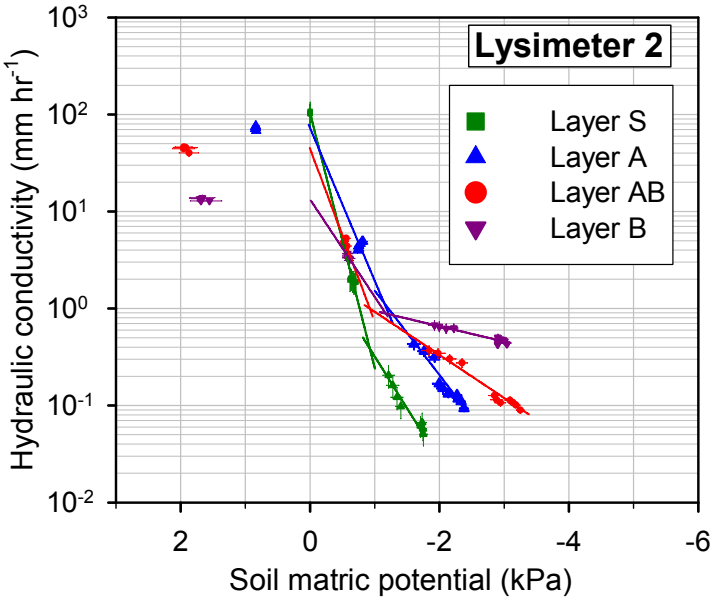

	α_1(mm^{-1})	α_2(mm^{-1})
Layer S	0.06	0.02
Layer A	0.04	0.02
Layer AB	0.04	0.01
Layer B	0.02	0.004

Figure 7-11 The $K(\Psi_m)$ relationship for the individual layers of lysimeter 2. The lines show the fit of a two-line exponential model to describe $K(\Psi_m)$. The slope (α_1 and α_2) of each line is also shown.

7.4 Discussion: Mechanisms governing long-time infiltration and the interpretation of hydraulic conductivity

It is argued here that preferential flow and soil layer interactions are the two main mechanisms which dominate the spatial and temporal patterns of soil matric potential and infiltration behaviour, and therefore have a corresponding influence on the measurement of *in-situ* hydraulic conductivity. The reasons for the importance of these mechanisms are discussed in the following sections.

7.4.1 The influence of preferential flowpaths

As discussed in Chapter 5, a key feature of the initial wetting phase is the strong influence of preferential flowpaths at infiltration suctions of 1 kPa or less, as shown in Figure 7-2 by the spike in the standard deviation of Ψ_m at each depth as the wetting front passes. Comparison of the historical rainfall pattern (Figure 4-3, Chapter 4) and the derived $K(\Psi_m)$ curves (Figure 7-11) further supports that preferential infiltration is likely to be the norm, rather than the exception in this soil. Antecedent conditions notwithstanding, the intensity of individual rainfall events are typically > 1 mm hr^{-1}, which in Figure 7-11 exceeds the conductivity of the mesopore region, and therefore is likely to activate macropores. As shown in Chapter 6 the

presence of hydrophobicity will also reduce mesopore sorptivity, and enhance macropore flow.

Chapter 6 identifies that preferential wetting results from a dynamic interaction between sorptivity, hydrophobicity, the network of air-filled pores, and air-entrapment in otherwise water-filled pores. The effects of sorptivity and hydrophobicity should reduce as infiltration progresses, whereas the effects of the soil air phase may persist throughout long-time infiltration. Non-uniform wetting, as demonstrated in Figure 5-1, creates a spatially and temporally variable hydraulic gradient which violates the assumptions of Darcian flow and makes calculation of $K(\Psi_m)$ using steady-state analysis invalid and inappropriate, as shown by the large scatter in Figure 7-4.

Preferential flowpaths also act to create strong inter-layer connectivity. A common assumption of infiltration measurements is that there will be sufficient time for steady-state infiltration to develop before interference from wetting of lower layers, which may have distinctly different $K(\Psi_m)$ relationships (McKenzie et al., 2002). This assumption relies on a uniform piston-like wetting front moving downwards sequentially through one layer and then the next (Smettem and Smith, 2002). Providing the upper layer has sufficient thickness, it is assumed there will be some point when the wetting front sorptivity has a minor effect on the infiltration rate, compared to the hydraulic conductivity of the transmission zone behind the front.

Using the peaks in the standard deviation of Ψ_m in Figure 7-2 to identify the duration of preferential flow shows that this assumption is often violated because phases of preferential flow in adjacent soil layers overlap (Figure 7-12). It is clear that during saturated infiltration the wetting front reaches lower layers within 5 – 15 mm of infiltration, and between 2 – 10 mm during unsaturated infiltration. The results of Chapter 6 demonstrate that infiltration during these periods is dominated by transient mechanisms. The strong inter-layer connectivity is interpreted as meaning that determining $K(\Psi_m)$ values for individual layers is not likely to be reliable until the whole column has wet up. This was demonstrated in Figure 7-8 where stable $K(\Psi_m)$ data became apparent once drainage matched infiltration. Figure 7-12 indicates that preferential wetting of the whole column takes 22 – 50 mm of saturated infiltration, and ~10 – 30 mm during unsaturated infiltration, after which the horizontal variation in Ψ_m in any given layer becomes minimal.

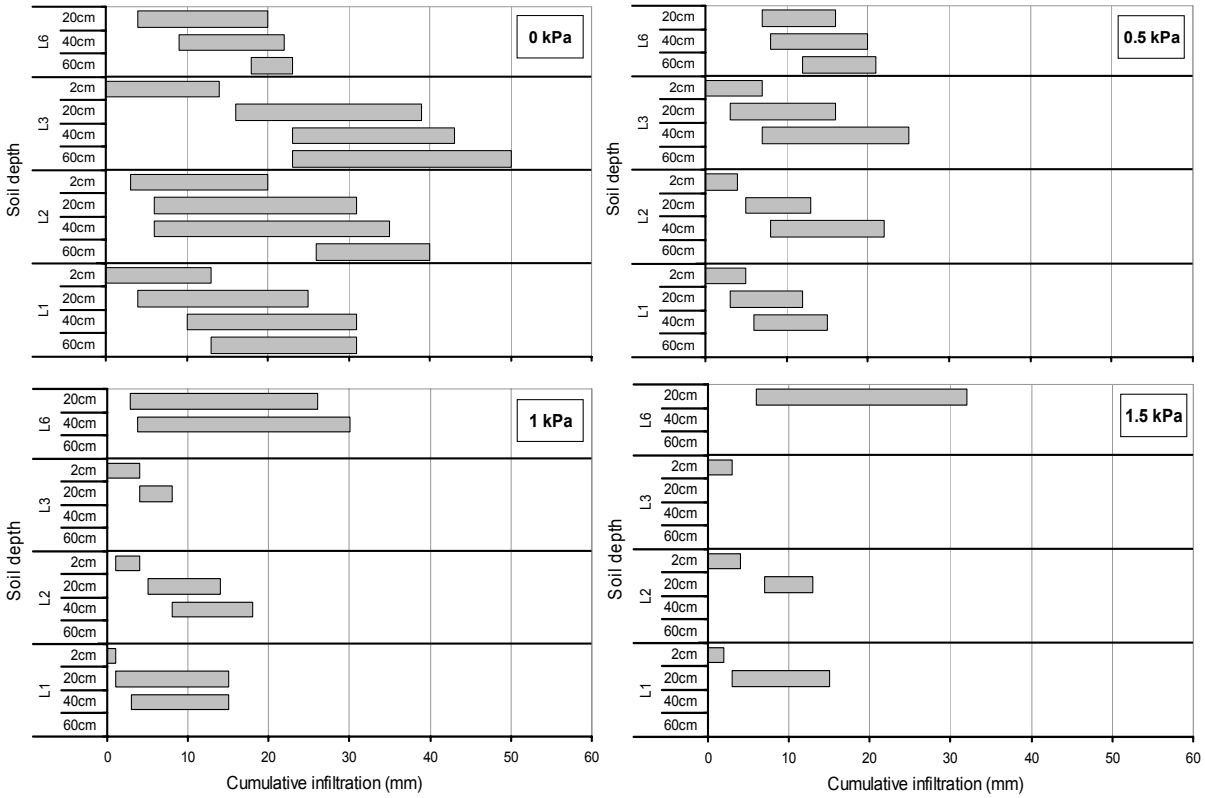

Figure 7-12 Comparison of the duration of non-uniform wetting at different depths within each lysimeter, where infiltration occurs under controlled surface suctions of 0, 0.5, 1 and 1.5 kPa. Grey bars represent the period over which there is a spike in the spatial standard deviation of matric potential, as shown in Figure 7-2.

7.4.2 The influence of interactions between soil layers

Figure 7-2 shows that once the soil column has wet up, the variability in Ψ_m becomes minimal, indicating a spatial uniformity of Ψ_m at all depths within the column. The spatial uniformity in Ψ_m persists over long time periods, and even when the soil internally switches from wetting to drainage behaviour (e.g. at 30 – 50hrs infiltration for L2 1 kPa), the change occurs uniformly at each depth. After the initial passage of the wetting front Ψ_m appears to follow a pattern of either slower wetting (e.g. L6 0.5 and 1 kPa), or slow draining (e.g. 1 kPa suction into L1, L2 and L3). The slow decrease in Ψ_m was the most common behaviour during unsaturated infiltration, occurring in 75% of the experiments where infiltration occurred under a surface suction of either 1 or 1.5 kPa. This indicates that even with constant boundary conditions the soil switched from wetting to draining.

This behaviour is attributed to interaction between the soil layers with contrasting $K(\Psi_m)$ relationships. During the infiltration experiments two contrasting modes of layer interaction were observed. The first mode occurs when the conductivity of layer A exceeds that of the

lower layers, causing the soil to wet up at the layer interface. The Ψ_m in both layers increases, causing i_t to increase as larger pores become activated. This is illustrated in L6 for infiltration under 1 kPa suction (Figure 5-1). The conductivity of layer A slightly exceeds that of the AB layer (refer Figure 7-10), causing a slow increase of Ψ_m and gradually increasing i_t. During infiltration under 0.5 kPa suction the $K(\Psi_m)$ contrast is much greater, with a rapid rise in i_t as the layer interaction sees Ψ_m increase to saturation. This explains why after ~70 mm of cumulative infiltration (i.e. at 'steady state') the 0.5 kPa i_t was equal to the 0 kPa i_t.

A contrasting mode of layer interaction occurred when the soil internally switched from wetting to draining, and was the most common behaviour during unsaturated infiltration. This occurred when unsaturated flow in an upper layer interacted with a lower layer with a pore network that had a greater conductivity at the prevailing Ψ_m. The greater conductivity in the underlying layer dried the upper layer which further decreased the flux rate. The overall effect was to cause a subsequent switch from wetting to draining in both layers. This is illustrated in L6 for infiltration under 1.5 kPa suction. Initially the soil wets as expected, but once Ψ_m at 40 cm depth increases to ~ -3 kPa the conductivity of layer A is exceeded (refer Figure 7-10), and the lower layers start to drain layer A. This continues until the product of the hydraulic conductivity and gradient of each layer (i.e. Darcy velocity) is in balance throughout the column, and the tensiometer measurements of Ψ_m at each layer boundary settle at quasi-steady values (Figure 7-2). These measurements indicate the average Ψ_m across each layer is -2.75 kPa in layer A, -4 kPa in the AB, and -3 kPa in layer B.

The effect of layer interaction on achieving the surface applied suction

Recognition of the role of layer-interaction is important because there is an implicit assumption that a tension infiltrometer will control the maximum actively conducting pore size. These experiments demonstrate that only under saturated infiltration do the soil columns attain the degree of saturation applied at the soil surface, with the positive Ψ_m values indicating that the column had reached saturation. The initial assumption in these experiments was that after the initial transient wetting phase, the whole column would equilibrate at or near the 'target' surface-imposed suction. However, the experiments show that this assumption is rarely achieved during unsaturated infiltration (0.5, 1, 1.5 kPa experiments), with Ψ_m in 11 of the 12 experiments not meeting the applied surface value. Even at 2 cm depth Ψ_m was typically different from the surface imposed suction, with differences of 0.5 to 1 kPa observed. When Ψ_m at 2 cm depth did get close to the target value (e.g. L2 1 and 1.5 kPa), later feedback from wetting of the column at greater depths (e.g. 20 cm depth) resulted in a decrease in Ψ_m at 2 cm depth, as the soil internally switched to drainage behaviour. The

only experiment that appears to behave as expected was L2 0.5 kPa, where Ψ_m at all depths in the column equilibrated at close to the 'target' value of -0.5 kPa.

In one of the few experiments on a field soil that has measured the dynamics of Ψ_m under a tension infiltrometer, Wang et al. (1998b) also observed that Ψ_m did not match the applied surface suction. During steady state infiltration under both 0.5 and 1 kPa suction the two tensiometers at 2.5 cm depth responded promptly, but stabilised at Ψ_m of -1.5 to -1.7 kPa. Greater differences were observed under a larger disk (20 cm diameter), where under 0.5 kPa suction the Ψ_m at 2.5 and 5 cm depths was -5.6 and -8.1 kPa, respectively, at steady-state.

Similar behaviour was observed by Silva et al. (2000) who measured Ψ_m at 3 depths (15, 30 and 60 cm) in a lysimeter during leaching experiments. Two experiments were conducted, where a tension infiltrometer maintained a respective 0 and 0.5 kPa surface suction, over 2 and 10 week time periods. At all depths Ψ_m was consistently 1 to 4 kPa more negative than the applied surface suction. This was attributed to self-adjustment in a vertically layered and heterogenous soil profile, where Ψ_m keeps adjusting through the profile until local layer conductivity and hydraulic gradient are matched to maintain a constant horizontally averaged Darcy velocity throughout the profile.

This recognition of the differences between the suction applied by the tension infiltrometer and the steady-state Ψ_m in the underlying soil is a critical caveat for the measurement of $K(\Psi_m)$ by surface infiltration methods. This is because at steady-state flow the hydraulic gradient is commonly considered to be at unity, and therefore $K(\Psi_m)$ is simply equated to the steady-state infiltration rate. If the gradient is less than unity, for example when Ψ_m is greater than the surface value, $K(\Psi_m)$ will be larger than the flux. Conversely, if the gradient exceeds unity $K(\Psi_m)$ will be smaller than the flux (usually when Ψ_m is drier than the surface suction). Of further importance is that the Ψ_m at which K is measured will be different from the surface suction and hence the derived $K(\Psi_m)$ relationship will be inaccurate. This discrepancy may be a source of some of the previously reported high variability in measurements of unsaturated $K(\Psi_m)$.

In the experiments of this study the discrepancy between the infiltration suction and Ψ_m was most variable at 0.5 kPa suction. In only one experiment did Ψ_m approximate the imposed value, with Ψ_m either wetter or drier in the other experiments, resulting in a highly variable i_t of 0.2 – 6 mm hr^{-1} among the lysimeters. This is of particular importance for infiltration measurement in New Zealand, where the standard measurement of unsaturated $K(\Psi_m)$ is at a

suction of 0.4 kPa (Joe, 1986; Joe and Watt, 1984; Watt and Vincent, 1991; Watt et al., 1992; Webb et al., 2000). Whereas those studies used detached small cores (9.8 cm diameter x 6.5 cm deep) which should eliminate the effect of layer interaction, *in-situ* field measurements would be vulnerable to this effect.

The dynamic nature of infiltration at 0.5 kPa suction also poses problems for modelling the $K(\Psi_m)$ function. Figure 7-10 shows that for only two of the four lysimeters were measurements of $K(\Psi_m)$ able to be derived for Ψ_m between 0 and -1 kPa.. This is particularly important for this soil due to the dual permeability nature of the pore network, where activation of macropores responsible for preferential flow occurs when Ψ_m is between -0.5 to -1.5 kPa (Figure 7-11). Therefore a key component of this soil's hydraulic characterisation will be accurate modelling of $K(\Psi_m)$ in the Ψ_m range of 0 to -1.5 kPa.

Because it was difficult to obtain accurate datapoints for the macropore region using steady-state analysis, the application of a transient analysis method may be warranted. However, reliable transient analysis will need to be robust to soil mechanisms such as hydrophobicity, preferential flow, and inter-layer feedback. Further, a continuous model of the $K(\Psi_m)$ relationship that accounts for macropore flow may be more appropriate, such as that of Ross and Smettem (2000), rather than the typical approach of dual permeability models which characterise separate $K(\Psi_m)$ functions for each pore region (Simunek et al., 2003). This approach is further complicated because it is often found that dual-permeability behaviour can be best described using different types of $K(\Psi_m)$ models for each region (Simunek et al., 2003). Although a simple dual permeability model worked well to conceptualise the $K(\Psi_m)$ relationship for L2, it is reliant on a spread of datapoints in both pore domains to accurately identify both the slope of the $K(\Psi_m)$ function for each pore region and the 'breakpoint' Ψ_m which separates the two regions.

Layer interaction and hysteresis

Another important implication of layer interaction is that it can generate hysteretic behaviour during infiltration. This is important because it is assumed that tension infiltrometers are used to observe the unidirectional *wetting* behaviour of a soil. Figure 7-2 shows that this applies during early to medium infiltration times, but does not necessarily hold true at long infiltration times. At long infiltration times the interaction between soil layers may see measurements continue under wetting conditions, or switch to draining behaviour or show composite wetting and draining, in that one layer is wetting while another is drying. The implication is that the $K(\Psi_m)$ relationship will include non-unique values of K for certain

values of Ψ_m, depending on whether a layer exhibited both wetting and drying during infiltration. This hysteresis would arise mainly from the larger pores filled during the wetting phase not emptying as the soil layer switches to a draining phase, resulting in higher measured conductivities.

Figure 7-13 shows the $K(\Psi_m)$ relationship for lysimeter 3, when the data points are discriminated according to whether the calculated value of $K(\Psi_m)$ applied to a wetting or draining soil layer. Appendix 8 shows the separation of $K(\Psi_m)$ data points for all the lysimeters. Figure 7-13 shows that hysteresis does not have a major influence on the observed $K(\Psi_m)$ relationship, despite the mixture of both wetting and draining measurements.

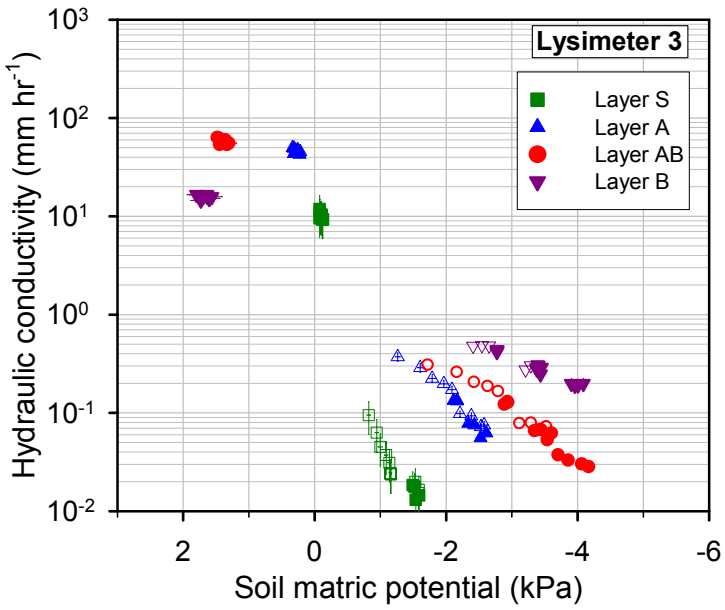

Figure 7-13 Re-interpretation of the $K(\Psi_m)$ relationship for L3, using the filtered dataset where drainage matched infiltration and there was a stable hydraulic gradient (Figure 7-10). The data points are separated if measured when the soil column was internally wetting (solid symbols) or draining (hollow symbols).

However, the results of Figure 7-13 may be an artefact of layer interaction, where during unsaturated infiltration the greater conductivity of layer B, compared to the upper layers, prevented the column from ever wetting sufficiently to activate the macropore domain. Figure 7-14 shows that strong hysteresis behaviour is possible if the soil wets to activate the macropores, before Ψ_m drains down to the mesopore region.

This example (Figure 7-14) shows two infiltration experiments for lysimeter 3 under the same 1 kPa surface suction. Experiment A produced the data used in this chapter. Experiment B was a previous experiment where a temporary failure of the suction pump caused a temporary loss of the applied surface suction, resulting in an 'infiltration flush' that saw Ψ_m rise

sufficiently to activate the macropore domain. When suction was restored, the column appeared to internally drain back down to similar 'pre-flush' Ψ_m levels. Excluding the flush period, both experiment A and B achieved similar levels of Ψ_m under the same surface suction, and the cumulative infiltration pattern was also similar during the pre-flush period. The infiltration flush caused an expected jump in the cumulative infiltration and Ψ_m of experiment B. After the flush Ψ_m decreased to levels very similar to the long-time Ψ_m of experiment A, but the infiltration and drainage rates of experiment B remained high. This discrepancy is attributed to hysteresis, whereby part of the macropore region did not empty during the post-flush drain down, resulting in markedly higher infiltration rates at a similar Ψ_m. Further use of the experiment B data would result in quite different $K(\Psi_m)$ values, compared to the $K(\Psi_m)$ values presented in this chapter.

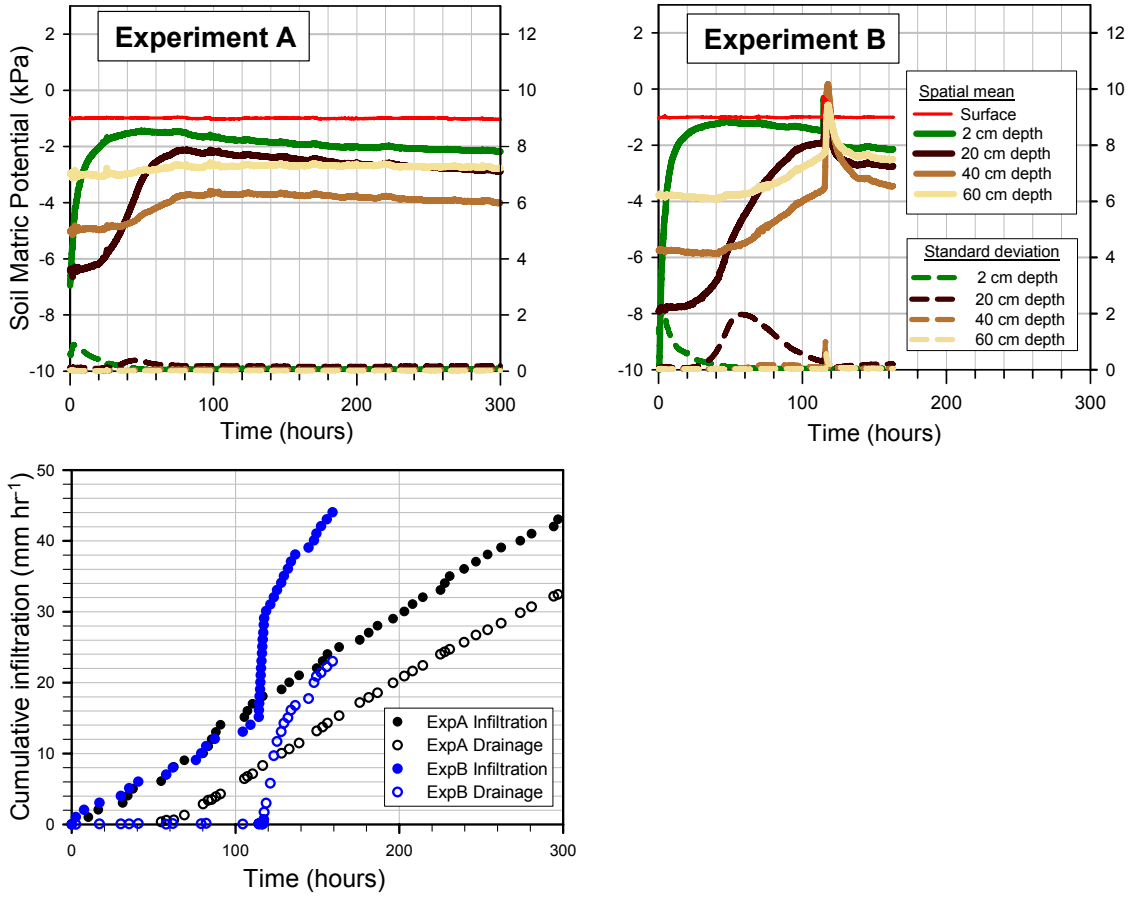

Figure 7-14 Comparison of cumulative infiltration and Ψ_m for two infiltration experiments of L3, under the same 1 kPa surface suction. Experiment A provided the data used in this chapter. Experiment B shows the results of a temporary loss of surface suction, causing an infiltration 'flush' that activated macropores.

The whole column $K(\Psi_m)$ relationship

An obvious question that arises from the strong layer interaction is whether there is a single soil layer that controls the whole column behaviour. The simplest approach to answer this question is to ignore the layered character of the lysimeters and assume a steady-state unit

hydraulic gradient is reached when infiltration and drainage are equal. This treats the whole column as an equivalent homogenous single layer where $K(\Psi_m)$ is described as the profile effective conductivity [$K_e(\Psi_m)$] (Lal and Shukla, 2004). The whole column $K_e(\Psi_m)$ can then be constructed by plotting the steady-state infiltration rate value versus the imposed surface suction (Figure 7-15).

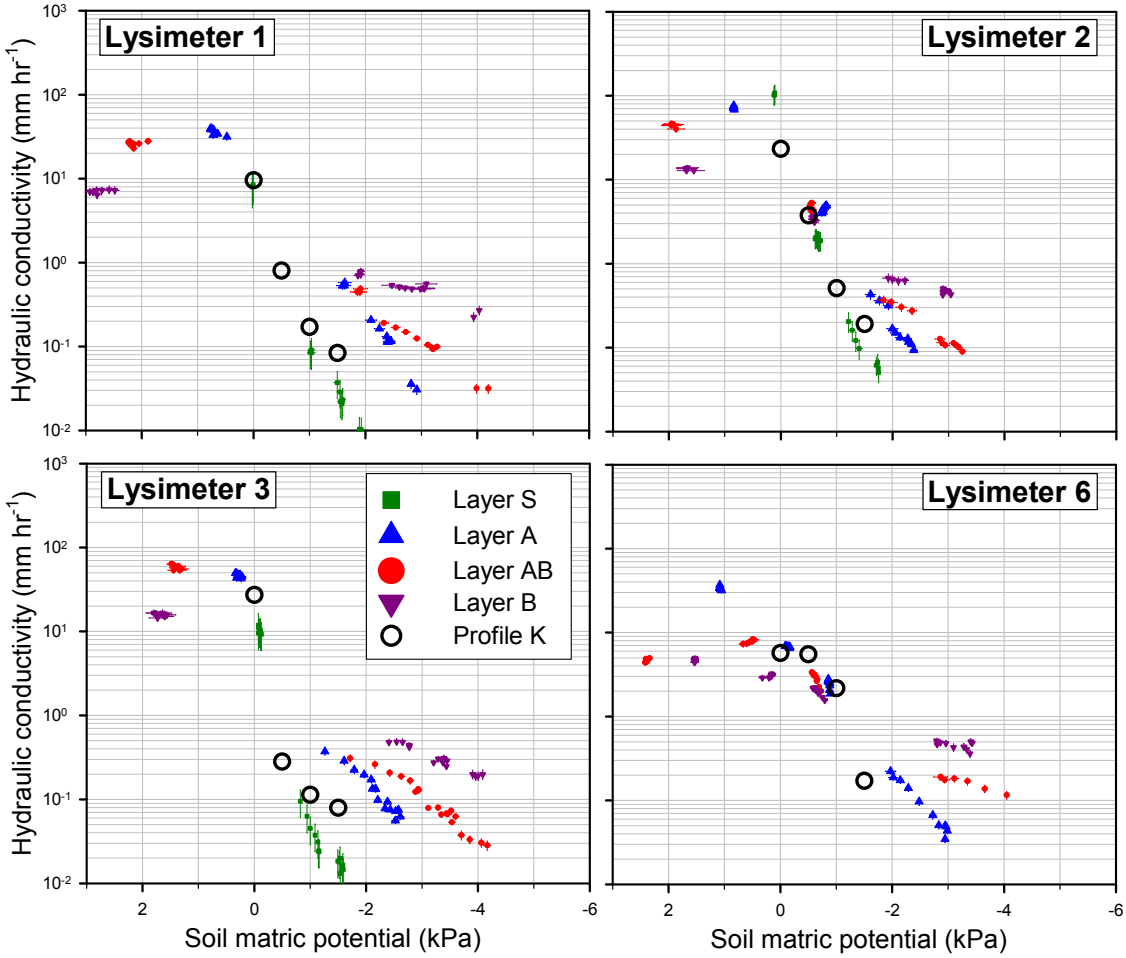

Figure 7-15 Comparison of the profile effective conductivity, $K_e(\Psi_m)$, with the $K(\Psi_m)$ of individual soil layers for each lysimeter. The four $K_e(\Psi_m)$ data points are from each infiltration experiment, under respective surface suctions of 0, 0.5, 1 and 1.5 kPa.

The similarities between $K_e(\Psi_m)$ and the $K(\Psi_m)$ relationship of layer S are striking, except for L6 where layer S was not measured. It is logical that the surface layer is the key layer controlling the infiltration behaviour. The complex Ψ_m dynamics within the soil column during infiltration are a response to the constant suction boundary conditions applied to layer S by the tension infiltrometer. The most important feature of Figure 7-15 is that it again highlights the importance of hydraulic characterisation for layer S. This reinforces the findings of Chapters 5 and 6, where it is clear that characterisation of layer S is critical to understanding both early-time infiltration and preferential flow behaviour. This is contrary to

the classic approach of NZ soil survey where layer S is rarely recognised, even in the surveys which focussed on detailed hydraulic characterisation (Joe and Watt, 1984; Watt and Vincent, 1991; Watt et al., 1992; Webb et al., 2000).

7.5 Summary

The results of this chapter clearly show that infiltration and drainage rates are intimately linked to temporal Ψ_m dynamics which, themselves, are determined by preferential flow and layer interaction. Because of these mechanisms true steady-state was never attained during the unsaturated infiltration experiments, although a quasi-steady phase did occur. Identification of quasi-steady state is to an extent a subjective decision of the experimenter, that can affect the quality of the derived $K(\Psi_m)$ values. It was shown to be difficult to determine steady-state reliably from just the cumulative infiltration curve. Quasi-steady state was more robustly identified as when infiltration matched drainage, and Ψ_m measurements showed each layer had a stable hydraulic gradient.

The *in-situ* $K(\Psi_m)$ relationship of individual soil layers can be reliably determined from lysimeter-scale infiltration experiments. For the Gorge soil the $K(\Psi_m)$ is distinctly different for the individual soil layers, and these differences are consistent between the four lysimeters. All four soil layers demonstrate a sharp decline in $K(\Psi_m)$ as Ψ_m decreases. A consistent feature is that all layers have a distinct change in the slope of the $K(\Psi_m)$ relationship, in the Ψ_m range of -0.5 to -1.5 kPa. This highlights that in the range of soil wetness measured, the soil may be considered a dual-permeability soil, such that the $K(\Psi_m)$ relationships are adequately represented by a two-line exponential dual permeability model. The whole column infiltration behaviour was strongly linked to the $K(\Psi_m)$ relationship of the surface layer, and therefore hydraulic characterisation of this layer should be a critical component of soil survey.

The experiments show that *in-situ* profile measurements of Ψ_m are essential for determining hydraulic conductivity from infiltration experiments. Matric potential within the soil column was almost universally never what was set at the surface boundary, and large errors could result if one makes the implicit assumption that a tension infiltrometer will control the maximum actively conducting pore size. In these experiments the difference between the surface suction and the soil Ψ_m was most variable under 0.5 kPa suction, resulting in a highly variable i_t of 0.2 – 6 mm hr^{-1}. This would feed through as erroneous $K(\Psi_m)$ data if Ψ_m had not been directly measured. Errors would have been generated via the hydraulic gradient, as well as the Ψ_m at which the conductivity was being calculated. I postulate that this may be a source of some of the high variability in other reported measurements of unsaturated $K(\Psi_m)$.

Chapter 8
Conclusions and recommendations

8.1 Introduction

The main objectives of this study were to:

1. Compare different methods of characterising preferential flow behaviour.
2. Determine the mechanisms that govern early-time infiltration behaviour, and their potential effect on deriving hydraulic attributes from early-time data.
3. Determine the key mechanisms governing long-time infiltration behaviour, and to test if the *in-situ* hydraulic conductivity of individual soil layers within a soil monolith can be reliably determined;

Secondary objectives included: to review the practical demand in New Zealand for measurement of soil infiltration attributes; review what mechanisms could influence the reliability of these measurements; and to design and construct a tension infiltrometer – lysimeter system that minimises measurement errors.

These objectives were achieved by:

- Collecting four large lysimeters, 50 cm diameter by 70 cm deep. The lysimeters contained undisturbed soil monoliths of the Gorge silt loam, a structured soil with distinct and spatially consistent soil layers.
- Conducting four separate infiltration experiments on each lysimeter, using a custom-built 49 cm diameter tension infiltrometer to supply infiltrating water under controlled surface suctions of 0, 0.5, 1, and 1.5 kPa. Each lysimeter was intensively instrumented with 30 tensiometers, located in arrays at the layer boundaries.
- Conducting dye experiments at the time of lysimeter sampling to characterise visually the pattern of preferential flow under ponded infiltration. Following the lysimeter infiltration experiments the monoliths were dissected and small sub-cores were collected to measure the soil water characteristics and bulk densities. Samples were also collected in order to measure the soil depth distributions of organic carbon and particle size.

8.2 Main conclusions

In relation to the thesis objectives the main conclusions are:

Review of practical demand and mechanisms that can affect measurement reliability

- The history of measuring soil water movement attributes has been sporadic in New Zealand, with most research focussed on a few soil types (chapter 1). However, at present, the practical demand for infiltration studies should be large from authorities and industry dealing with irrigation and disposal of dairy farm effluent, as well as municipal / domestic waste and stormwater disposal. I argue that a wider range of soil types needs to be characterised, and measurements should encompass near-saturated infiltration behaviour, particularly the phenomenon of preferential flow (chapter 2).

- Tension infiltrometers are an appropriate tool to meet much of the practical demand. However, previous research shows a number of mechanisms could introduce measurement uncertainty, and confound inter-study comparison (chapter 2). Uncertainty can arise from the experimental setup, particularly through the use of contact material, as well as using a small sample volume that does not contain a representative sample of the soil pore network. Infiltrometer measurements can also be strongly affected by temporal variation in factors such as hydrophobicity, air encapsulation, hysteresis, biological activity, pore network instability, and temperature fluctuations. Preferential flow and soil layering are also identified as effects with little research on their impact on tension infiltrometer measurements.

- This study has successfully designed and constructed a tension infiltrometer-lysimeter system that has proven to be both reliable and accurate for studying the infiltration behaviour of a structured and layered soil column (chapter 3).

Preferential flow

- Analysis of dye patterns, temporal variability in Ψ_m during infiltration experiments, and solute breakthrough curves all show that preferential flow is an important infiltration mechanism in the Gorge soil (chapter 5). Overall, the three methods give a similar understanding of preferential flow behaviour, and in combination greatly enhance the interpretation of underlying mechanisms.

- Dye image analysis and solute breakthrough curves show that preferential flow occurs during both early and long-time saturated infiltration. Preferential flow is also a feature

of unsaturated infiltration, although at the highest surface suction of 1.5 kPa the occurrence of preferential flow is minimal. The variability in Ψ_m measurements (chapter 5) and the derived $K(\Psi_m)$ curves (chapter 7) indicate preferential flowpaths are activated when Ψ_m increases to between -1.5 to -0.5 kPa.

- During saturated infiltration at least 97% of drainage was through the 'mobile' pore volume of the lysimeter (θ_m), estimated as the water-filled pores between saturation and Ψ_m of -5 kPa. This equates to a θ_m estimate of 5.4 – 8.7 % among the lysimeters. Good predictions were obtained from the mobile-immobile model when these θ_m estimates were used as a fixed parameter to inversely model the solute breakthrough curves. The dye image analysis and model predictions indicate that lateral infiltration from the θ_m into the soil matrix is an important mechanism in this soil, transferring solute from the mobile pore network into the immobile pore network. This mechanism explains why 40 – 50 % of the tracer was not recovered after 1.5 pore volumes of lysimeter drainage.

Early-time infiltration

- Early-time infiltration behaviour was not solely governed by soil sorptivity, as typically assumed in many previous studies (chapter 6). This manifested as early-time infiltration not showing square-root of time behaviour. The lack of classical sorptivity behaviour was consistent across four lysimeters, and during infiltration under different surface imposed suctions. I conclude that this behaviour was not an artefact of the tension infiltrometer-lysimeter system, or the antecedent water content, or blockage of infiltrating pores by the development of a surface seal.

- The most likely mechanism restricting sorptivity is weak hydrophobicity, which appears to restrict infiltration for the first 5 – 10 mm of infiltration. Overall, the Gorge soil's early-time infiltration behaviour is governed by the dynamic interaction between sorptivity, hydrophobicity, the network of air-filled pores, preferential flow and air encapsulation. I suggest that hydrophobicity and the soil-air phase behaviour may be important mechanisms which enhance non-uniform infiltration through preferential flowpaths.

Long-time infiltration and derivation of in-situ hydraulic conductivities

- Long-time infiltration behaviour was intimately linked to the dynamics of Ψ_m. The results show that 'true' steady-state infiltration is not likely to occur in layered soils. A

quasi-steady state was identified once the whole column had fully wet and soil layer interactions had settled to where Ψ_m changes occurred in unison through each layer.

- Preferential flow and layer interactions are the two mechanisms that dominate the temporal Ψ_m pattern during long-time infiltration. Preferential wetting creates a temporally variable hydraulic gradient with a large vertical and horizontal variability in Ψ_m. Preferential flowpaths also create strong inter-layer connectivity, so that the wetting front reaches lower layers within 5 – 15 mm of saturated infiltration, and between 2 – 10 mm during unsaturated infiltration. Wetting of the whole column by preferential flow persisted for 10 – 50 mm of infiltration, after which the horizontal variation in Ψ_m became minimal.

- After the initial preferential wetting the infiltration behaviour was determined by the interaction between soil layers with contrasting $K(\Psi_m)$ relationships. During the infiltration experiments two contrasting modes of layer interaction were observed. The first mode occurred when the conductivity of the upper layers exceeds that of the lower layers, resulting in Ψ_m increasing in both layers. The contrasting mode was the most common behaviour during unsaturated infiltration and occurred when the conductivity of the lower layers exceeded that of the upper layers. The soil internally switched from wetting to draining, Ψ_m decreased (after having initially increased), and i_t slowed as water movement was confined to smaller pores.

- The *in-situ* hydraulic conductivity, $K(\Psi_m)$, of individual soil layers can be reliably determined from lysimeter-scale infiltration experiments (chapter 7). This relied on identifying quasi-steady state infiltration, which in turn is based on the subjective decision of the researcher. Quasi-steady state is difficult to determine from just the cumulative infiltration curve. Instead it was more robustly identified as when infiltration matched drainage, and Ψ_m measurements showed each layer had a stable hydraulic gradient.

- My results show that for the Gorge soil $K(\Psi_m)$ is different for each soil layer, and that differences are consistent among the four lysimeters. Under positive pressures of saturated flow the subsoil (layer B) had the lowest conductivity, and was the restricting layer. Most interestingly this pattern reversed during unsaturated flow when, at Ψ_m of less than -0.5 to -1 kPa, the subsoil was markedly more conductive, so that the topsoil layers (S and A) became the restricting layers.

- All four soil layers demonstrate a sharp decline in $K(\Psi_m)$ as Ψ_m decreases. The sharpest decline is for layer S, where $K(\Psi_m)$ decreases by about three orders of magnitude between saturation and Ψ_m of -1.5 kPa, compared to a decline of only about one order of magnitude for layer B. A consistent feature is that all layers have a sharp change in the slope of the $K(\Psi_m)$ relationship, in the Ψ_m range of -0.5 to -1.5 kPa. This shows the soil behaves as a dual-permeability soil, and $K(\Psi_m)$ can be adequately represented by a two-line exponential dual permeability model.

- The 0 – 5 cm depth (layer S) should be defined as a separate soil layer. The infiltration experiments in this study demonstrate the hydrological importance of the surface layer. Even though this layer was not at first apparent in my morphological description, and seldom recognised in standard soil survey descriptions, the surface layer had a controlling influence over infiltration, and the subsequent behaviour of the lower soil layers.

8.3 Implications for infiltration measurement methods

- I recommend that tensiometers are used during tension infiltrometer experiments. In this study Ψ_m rarely matched the surface suction applied by the infiltrometer, even at 2 cm depth. The infiltration behaviours observed in this study would not have been understood without *in-situ* measurements of Ψ_m. This could lead to calculation of erroneous $K(\Psi_m)$ values when using a tension infiltrometer to characterise $K(\Psi_m)$ for an *in-situ* soil layer in the field, and it was assumed that Ψ_m matched the infiltrometer suction.

- Alternatively, if measurements of $\theta_v(\Psi_m)$ are available then the soil Ψ_m could be calculated from the *in-situ* θ_v. However, accurate measurement of $\theta_v(\Psi_m)$ can be difficult. Using small cores, I detected little or no decline in porosity at Ψ_m of -0.5 to -2 kPa by measuring $\theta_v(\Psi_m)$, yet the infiltration experiments showed large changes in infiltration rate, preferential flow, and $K(\Psi_m)$ over the same Ψ_m range.

- I have also shown that accurate *in-situ* θ_v measurements are difficult to achieve, because of the temperature sensitivity of water content reflectometers, with the manufacturer supplied temperature calibration proving to be inadequate. Site specific calibration is required to have accuracy sufficient for use in infiltration studies at or near saturation.

- This project showed that it was difficult to derive hydraulic attributes from early-time infiltration behaviour. Although it is possible to derive $K(\Psi_m)$ from quasi-steady phases during long-time infiltration, the duration of experiments needed to do so, particularly for unsaturated infiltration were prohibitively long (often >100 hrs) for practical application. It may be more practical to use a method that derives hydraulic attributes from transient infiltration, but such a method would have to be robust to the dynamic interaction between mechanisms such as preferential flow, interlayer feedback, and hydrophobicity. Field measurements of transient infiltration are often limited to less than one hour at individual suctions; however, such short timeframes would make it difficult to detect the effects of mechanisms such as hydrophobicity, which in this study persisted for a number of hours. Alternatively, a quasi-steady phase may be reached sooner if infiltrating water was supplied at a constant flux (i.e. via an irrigation sprinkler), which would dampen the effect of interactions between soil layers.

- Measurements of soil hydraulic attributes should include the measurement uncertainty arising from instrument error, as well as be based on experiments where uncertainty from temporal variation in the soil pore network is mitigated. A useful step would be to develop a protocol for measurement of soil infiltration attributes in New Zealand. Such a protocol would greatly improve the comparability of results between studies, and between different soils.

8.4 Practical implications

- The climate region of the Gorge soil is characterised by rainfall events with low intensity and quantity, with less than 10 mm rain on ~78% of rain days and 10 – 30 mm occurring on 18% of rain days. Individual rain events are typically less than 5 mm depth, with an intensity below 10 mm hr^{-1}. The results of this study show that such rain events are most likely to generate unsaturated infiltration. This questions the practical usefulness of just using saturated experiments to characterise a soil's infiltration and solute transport behaviour, when unsaturated conditions occur far more frequently.

- This research highlights the practical importance of understanding the soil's pore network for optimising irrigation. Application of dairy shed effluent (DSE) is the most likely form of irrigation. This research shows that preferential flow is an inherent feature of infiltration in this soil. To minimise preferential flow irrigation rates should be < 1 mm hr^{-1} to minimise activation of the macropore network, based on the derived

$K(\Psi_m)$ curves (chapter 7). Alternatively, it may be possible to use higher rates, but apply only a small amount (e.g. < 10 mm). An application rate > 1 mm hr^{-1} would generate preferential flow, but the small amount should minimise the depth to which the DSE penetrates down preferential flowpaths, before being absorbed by lateral infiltration. The dye study in Chapter 5 illustrates that the topsoil has a good capacity for lateral infiltration, but is markedly lower in the subsoil.

- Low rate or small depth irrigation may still be necessary under drier antecedent conditions than those used in this study, which focussed on infiltration behaviour at field capacity. This is because of the presence of hydrophobicity, which is likely to strengthen as the antecedent conditions become drier. Even though the infiltration capacity would have increased, this could be offset by hydrophobicity restricting the matrix sorptivity, creating matrix ponding and thus generation of preferential flow via macropores. Further research is warranted to observe if this occurs in the field.

8.5 Research needs

- The literature review (chapter 2) shows that texture is often used to predict soil hydraulic attributes. My infiltration experiments have shown that there is substantial variation in the infiltration and conductivity attributes both among the lysimeters, and among the individual soil layers, despite the Gorge soil's remarkable uniformity in soil texture. This highlights that better pedotransfer functions need to be developed to predict hydraulic attributes of NZ soils. The results of this study indicate that soil organic carbon and bulk density may be useful.

- Further work is required to improve soil-water sensor accuracy, particularly for their application in infiltration experiments. I have shown that near or at saturation only a small change in θ_v or Ψ_m can result in substantial changes to the infiltration behaviour.

- There is a need to widen the breadth of infiltration attributes that are considered necessary to represent a soil's hydraulic character. For example, more research is needed on independent measurements of solute transport attributes, particularly definition of θ_m in dual porosity / permeability soils.

- There is a need to quantify the degree of temporal variability in soil infiltration attributes. A comprehensive study would measure temporal variation in sorptivity, conductivity, hydrophobicity, and preferential flow (i.e. θ_m) that arises from different

antecedent conditions (e.g. moisture status, temperature, management conditions). This would aid in quantifying the degree of uncertainty for infiltration attributes, which are usually based on measurements from a single point in time. Such knowledge would also test the common assumption that each soil layer has a unique $K(\Psi_m)$ function. The experience of this study leads me to question this assumption, and wonder if a cluster of $K(\Psi_m)$ functions exists, with the cluster 'spread' expressing the degree of temporal variation.

References

Alaoui, A., and B. Goetz. 2008. Dye tracer and infiltration experiments to investigate macropore flow. Geoderma 144:279-286.

Alletto, L., Y. Coquet, P. Vachier, and C. Labat. 2006. Hydraulic conductivity, immobile water content, and exchange coefficient in three soil profiles. Soil Science Society of America Journal 70:1272-1280.

Anderson, J.L., and J. Bouma. 1973. Relationships between saturated hydraulic conductivity and morphometric data of an argillic horizon. Soil Science Society of America Proceedings 37:408-413.

Angulo-Jaramillo, R., J.P. Vandervaere, S. Roulier, J.L. Thony, J.P. Gaudet, and M. Vauclin. 2000. Field measurement of soil surface hydraulic properties by disc and ring infiltrometers - A review and recent developments. Soil & Tillage Research 55:1-29.

AnguloJaramillo, R., F. Moreno, B.E. Clothier, J.L. Thony, G. Vachaud, E. FernandezBoy, and J.A. Cayuela. 1997. Seasonal variation of hydraulic properties of soils measured using a tension disk infiltrometer. Soil Science Society of America Journal 61:27-32.

Ankeny, M.D. 1992. Methods and theory for unconfined infiltration measurements, p. 123-141, *In* G. C. Topp, et al., eds. Advances in measurement of soil physical properties: Bringing theory into practice. Proceedings of a symposium San Antonio, Texas 1990, Vol. SSSA Special Publication Number 30. Madison USA: Soil Science of America Inc.

Ankeny, M.D., T.C. Kaspar, and R. Horton. 1988. Design for an automated tension infiltrometer. Soil Science Society of America Journal 52:893-896.

Ankeny, M.D., M. Ahmed, T.C. Kaspar, and R. Horton. 1991. Simple field method for determining unsaturated hydraulic conductivity. Soil Science Society of America Journal 55:467-470.

AS/NZS. 2000. Australia/New Zealand Standard 1547: 2000. On-site domestic-wastewater management. Jointly published by Standards Australia and Standards New Zealand.

Bagarello, V., M. Iovino, and G. Tusa. 2000. Factors affecting measurement of the near-saturated soil hydraulic conductivity. Soil Science Society of America Journal 64:1203-1210.

Bagarello, V., M. Iovino, and G. Tusa. 2001. Effect of contact material on tension infiltrometer measurements. Transactions of the ASAE 44:911-916.

Bagarello, V., M. Castellini, and M. Iovino. 2005. Influence of the pressure head sequence on the soil hydraulic conductivity determined with tension infiltrometer. Applied Engineering in Agriculture 21:383-391.

Bagarello, V., M. Iovino, E. Palazzolo, M. Panno, and W.D. Reynolds. 2006. Field and laboratory approaches for determining sodicity effects on saturated soil hydraulic conductivity. Geoderma 130:1-13.

Barton, L., L.A. Schipper, G.F. Barkle, M. McLeod, T.W. Speir, M.D. Taylor, A.C. McGill, A.P. van Schaik, N.B. Fitzgerald, and S.P. Pandey. 2005. Land application of domestic effluent onto four soil types: plant uptake and nutrient leaching. Journal of Environmental Quality 34:635-643.

Bear, J. 1972. Dynamics of fluids in porous media. Elsevier, New York.

Bergstrom, L., N. Jarvis, M. Larsson, F. Djodjic, and A. Shirmohammadi. 2001. Factors affecting the significance of macropore flow for leaching of agrochemicals, *In* D. Bosch and K. King, (eds.) Preferential flow water: movement and chemical transport in the environment. Pp 25-28. ASAE, Honolulu, Hawaii, USA.

Beven, K., and P. Germann. 1982. Macropores and water-flow in soils. Water Resources Research 18:1311-1325.

Blakemore, L.C., P.L. Searle, and B.K. Daly. 1987. Methods for chemical analysis of soils. New Zealand Soil Bureau Scientific Report 80. NZ Soil Bureau Lower Hutt, N.Z.

Blonquist, J.M., Jr., S.B. Jones, and D.A. Robinson. 2005. Standardizing characterization of electromagnetic water content sensors: Part 2. Evaluation of seven sensing systems. Vadose Zone Journal 4:1059-1069.

Bodner, G., W. Loiskandl, G. Buchan, and H.P. Kaul. 2008. Natural and management-induced dynamics of hydraulic conductivity along a cover-cropped field slope. Geoderma 146:317-325.

Booltink, H.W.G., and J. Bouma. 1991. Physical and morphological characterization of bypass flow in a well-structured clay soil. Soil Science Society of America Journal 55:1249-1254.

Bouma, J. 1981. Soil morphology and preferential flow along macropores Agricultural Water Management 3:235-250.

Bradley, C., M. Mosugu, and J. Gerrard. 2007. Seasonal dynamics of soil-water pressure in a cracking clay soil. Catena 69:253-263.

Braga, A., M. Horst, and R.G. Traver. 2007. Temperature effects on the infiltration rate through an infiltration basin BMP. Journal of Irrigation and Drainage Engineering-ASCE 133:593-601.

Butters, G.L., and G.E. Cardon. 1998. Temperature effects on air-pocket tensiometers. Soil Science 163:677-685.

Cameron, K.C., H.J. Di, and R.G. McLaren. 1997. Is soil an appropriate dumping ground for our wastes? Australian Journal of Soil Research 35:995-1035.

Cameron, K.C., N.P. Smith, C.D.A. McLay, P.M. Fraser, R.J. McPherson, D.F. Harrison, and P. Harbottle. 1992. Lysimeters without edge flow: an improved design and sampling procedure. Soil Science Society of America Journal 56:1625-1628.

Campbell Scientific. 2006. CS616 and CS625 Water Content Reflectometers: Instruction manual. [Online]. Available by Campbell Scientific, Inc., Utah, USA http://www.campbellsci.com/documents/manuals/cs616.pdf (verified March 2009).

Canterbury Regional Council. 2002. Proposed Canterbury natural resources regional plan [Online]. Available by Environment Canterbury http://www.ecan.govt.nz/Plans+and+Reports/NRRPNEW/ (verified 2009).

Canterbury Regional Council. 2009. The calm before the storm. Application guidebook for stormwater discharges. [Online]. Available by Environment Canterbury http://www.ecan.govt.nz/Resource+Consents/CalmBeforeStorm.htm (verified 2009).

Carey, P.L., J.J. Drewry, R.W. Muirhead, and R.M. Monaghan. 2004. Potential for nutrient and faecal bacteria losses from a dairy pasture under border-dyke irrigation: a case study. Proceedings of the New Zealand Grassland Association 66:141-149.

Casey, F.X.M., and N.E. Derby. 2002. Improved design for an automated tension infiltrometer. Soil Science Society of America Journal 66:64-67.

Casey, F.X.M., R. Horton, S.D. Logsdon, and D.B. Jaynes. 1997. Immobile water content and mass exchange coefficient of a field soil. Soil Science Society of America Journal 61:1030-1036.

Casey, F.X.M., R. Horton, S.D. Logsdon, and D.B. Jaynes. 1998. Measurement of field soil hydraulic and solute transport parameters. Soil Science Society of America Journal 62:1172-1178.

Casey, F.X.M., D.B. Jaynes, R. Horton, and S.D. Logsdon. 1999. Comparing field methods that estimate mobile-immobile model parameters. Soil Science Society of America Journal 63:800-806.

Castiglione, P., P.J. Shouse, B. Mohanty, and M.T. van Genuchten. 2005b. Analysis of temperature effects on tension infiltrometry of low permeability materials. Vadose Zone Journal 4:481-487.

Castiglione, P., P.J. Shouse, B. Mohanty, D. Hudson, and M.T. van Genuchten. 2005. Improved tension infiltrometer for measuring low fluid flow rates in unsaturated fractured rock. Vadose Zone Journal 4:885-890.

Christchurch City Council. 2003. Waterways, wetlands and drainage guide = Ko te anga whakaora mo nga arawai repo. Christchurch City Council, Christchurch, N.Z.

Christchurch City Council. 2008. Draft south-west Christchurch area plan. Christchurch City Council, Christchurch, N.Z.

Chu, X.F., and M.A. Marino. 2005. Determination of ponding condition and infiltration into layered soils under unsteady rainfall. Journal of Hydrology 313:195-207.

Clayden, B., and T.H. Webb. 1994. Criteria for defining the soilform - the fourth category of the New Zealand soil classification. Landcare Research Science Series, No.3. Manaaki Whenua - Landcare Research, Lincoln, New Zealand.

Claydon, J.J. 1989. Determination of particle-size distribution in fine-grained soils - pipette method. DSIR Division of Land and Soil Sciences Technical Record LH5.

Close, K.R., G. Frasier, G.H. Dunn, and J.C. Loftis. 1998. Tension infiltrometer contact interface evaluation by use of a potassium iodide tracer. Transactions of the ASAE 41:995-1004.

Close, M., R. Dann, A. Ball, R. Pirie, M. Savill, and Z. Smith. 2008. Microbial groundwater quality and its health implications for a border-strip irrigated dairy farm catchment, South Island, New Zealand. Journal of Water and Health 6:83-98.

Close, M.E., L. Pang, G.N. Magesan, R. Lee, and S.R. Green. 2003. Field study of pesticide leaching in an allophanic soil in New Zealand. 2: Comparison of simulations from four leaching models. Australian Journal of Soil Research 41:825-846.

Clothier, B., and D.R. Scotter. 2002. Unsaturated water transmission parameters obtained from infiltration data, *In* J. H. Dane, et al., eds. Methods of soil analysis. Part 4 - physical methods. Soil Science Society of America, Madison, Wisconsin.

Clothier, B., I. Vogeler, S. Green, and D. Scotter. 1998. Transport in unsaturated soil: aggregates, macropores, and exchange, p. 273-293, *In* H. M. Selim and L. Ma, eds. Physical nonequilibrium in soils: modelling and application. Ann Arbor Press, Inc., Chelsea, Michigan, USA.

Clothier, B.E. 2001. Infiltration, p. 239-281, *In* K. A. Smith and C. E. Mullins, eds. Soil and environmental analysis: physical methods, Two ed. Marcel Dekker, New York.

Clothier, B.E., and I. White. 1981. Measurement of sorptivity and soil water diffusivity in the field. Soil Science Society of America Journal 45:241-245.

Clothier, B.E., and K.R.J. Smettem. 1990. Combining laboratory and field measurements to define the hydraulic properties of soil. Soil Science Society of America Journal 54:299-304.

Clothier, B.E., I. White, and G.J. Hamilton. 1981. Constant-rate rainfall infiltration: field experiments. Soil Science Society of America Journal 45:245-249.

Clothier, B.E., I. Vogeler, and G.N. Magesan. 2000. The breakdown of water repellency and solute transport through a hydrophobic soil. Journal of Hydrology 231-232:255-264.

Clothier, B.E., S.R. Green, and M. Deurer. 2008. Preferential flow and transport in soil: progress and prognosis. European Journal of Soil Science 59:2-13.

Clothier, B.E., L. Heng, G.N. Magesan, and I. Vogeler. 1995. The measured mobile-water content of an unsaturated soil as a function of hydraulic regime. Australian Journal of Soil Research 33:397-414.

Clothier, B.E., G.N. Magesan, L. Heng, and I. Vogeler. 1996. In situ measurement of the solute adsorption isotherm using a disc permeameter. Water Resources Research 32:771-778.

Clothier, B.E., S.R. Green, I. Vogeler, M.M. Greven, R. Agnew, C.W. van den Dijssel, S. S. Neal, B.H. Robinson, and P. Davidson. 2006. CCA transport in soil from treated-timber posts: pattern dynamics from the local to regional scale. Hydrology and Earth System Sciences Discussions 3, pp. 2037–2061. [Online] http://hal-sde.archives-ouvertes.fr/hal-00298745/ (verified February 2009).

Clough, T.J., H.J. Di, K.C. Cameron, R.R. Sherlock, A.K. Metherell, H. Clark, and G. Rys. 2007. Accounting for the utilization of a N2O mitigation tool in the IPCC inventory methodology for agricultural soils. Nutrient Cycling in Agroecosystems 78:1-14.

Collins, R., M. McLeod, M. Hedley, A. Donnison, M. Close, J. Hanly, D. Horne, C. Ross, R. Davies-Colley, C. Bagshaw, and L. Matthews. 2007. Best management practices to mitigate faecal contamination by livestock of New Zealand waters. New Zealand Journal of Agricultural Research 50:267-278.

Constantz, J. 1982. Temperature-dependence of unsaturated hydraulic conductivity of 2 soils. Soil Science Society of America Journal 46:466-470.

Constantz, J., and F. Murphy. 1991. The temperature-dependence of ponded infiltration under isothermal conditions. Journal of Hydrology 122:119-128.

Constantz, J., W.N. Herkelrath, and F. Murphy. 1988. Air encapsulation during infiltration. Soil Science Society of America Journal 52:10-16.

Cook, F.J. 2008. Unsaturated hydraulic properties: laboratory tension infiltrometer, p. 1075 - 1087, *In* M. R. Carter and E. G. Gregorich, eds. Soil Sampling and Methods of Analysis, Two ed. Canadian Society of Soil Science & CRC Press Boca Raton, FL.

Cook, F.J., and A. Broeren. 1994. 6 Methods for determining sorptivity and hydraulic conductivity with disc permeameters. Soil Science 157:2-11.

Cook, F.J., F.M. Kelliher, and S.D. McMahon. 1994b. Changes in infiltration and drainage during wastewater irrigation of a highly permeable soil. Journal of Environmental Quality 23:476-482.

Coquet, Y., P. Vachier, and C. Labat. 2005. Vertical variation of near-saturated hydraulic conductivity in three soil profiles. Geoderma 126:181-191.

Cresswell, H.P. 2002. The soil water characteristic., p. 62-84, *In* N. McKenzie, et al., eds. Soil physical measurement and interpretation for land evaluation. CSIRO, Collingwood, Australia.

DairyNZ. 2006. Dairy industry strategy for sustainable environmental management. Report of the Dairy Environment Review Group, March 2006 [Online]. Available by DairyNZ http://www.dairynz.co.nz/file/fileid/4174 (verified February 2009).

Davis, S.H., R.A. Vertessy, and R.P. Silberstein. 1999. The sensitivity of a catchment model to soil hydraulic properties obtained by using different measurement techniques. Hydrological Processes 13:677-688.

Dekker, L.W., K. Oostindie, and C.J. Ritsema. 2005. Exponential increase of publications related to soil water repellency. Australian Journal of Soil Research 43:403-441.

Dekker, L.W., S.H. Doerr, K. Oostindie, A.K. Ziogas, and C.J. Ritsema. 2001. Water Repellency and Critical Soil Water Content in a Dune Sand. Soil Sci Soc Am J 65:1667-1674.

Di, H.J., and K.C. Cameron. 2002a. Nitrate leaching and pasture production from different nitrogen sources on a shallow stoney soil under flood-irrigated dairy pasture. Australian Journal of Soil Research 40:317-334.

Di, H.J., and K.C. Cameron. 2002b. Nitrate leaching in temperate agroecosystems: sources, factors and mitigating strategies. Nutrient Cycling in Agroecosystems 64:237-256.

Di, H.J., K.C. Cameron, S. Moore, and N.P. Smith. 1998. Nitrate leaching from dairy shed effluent and ammonium fertiliser applied to a free-draining pasture soil under spray or flood irrigation. New Zealand Journal of Agricultural Research 41:263-270.

Di, H.J., K.C. Cameron, V.J. Bidwell, M.J. Morgan, and C. Hanson. 2005. A pilot regional scale model of land use impacts on groundwater quality. Management of Environmental Quality 16:220-234.

Dikinya, O., C. Hinz, and G. Aylmore. 2008. Decrease in hydraulic conductivity and particle release associated with self-filtration in saturated soil columns. Geoderma 146:192-200.

Dirksen, C. 1999. Soil physics measurements. Catena, Reiskirchen, Germany.

Dirksen, C. 2001. Unsaturated conductivity, p. 183-280, *In* K. A. Smith and C. E. Mullins, eds. Soil and environmental analysis: physical methods, Two ed. Marcel Dekker, New York.

Doerr, S.H., R.A. Shakesby, L.W. Dekker, and C.J. Ritsema. 2006. Occurrence, prediction and hydrological effects of water repellency amongst major soil and land-use types in a humid temperate climate. European Journal of Soil Science 57:741-754.

Drewry, J.J., and R.J. Paton. 2000b. Effects of cattle treading and natural amelioration on soil physical properties and pasture under dairy farming in Southland, New Zealand. New Zealand Journal of Agricultural Research 43:377-386.

Drewry, J.J., R.P. Littlejohn, and R.J. Paton. 2000. A survey of soil physical properties on sheep and dairy farms in southern New Zealand. New Zealand Journal of Agricultural Research 43:251-258.

Durner, W., U. Jansen, and S.C. Iden. 2008. Effective hydraulic properties of layered soils at the lysimeter scale determined by inverse modelling. European Journal of Soil Science 59:114-124.

ECAN. 2009. Canterbury plains soil map [Online]. Available by Environment Canterbury. http://www.ecan.govt.nz/ECanMapping/viewer.htm.

Elliot, S., G. McBride, U. Shankar, A. Semandi-Davies, J. Quinn, D. Wheeler, L. Wedderburn, B. Small, A. Hewitt, R. Gibb, R. Parfitt, B. Clothier, S. Green, S. Harris, and G. Rys. 2008. CLUES Spatial DSS: from farm-scale leaching models to regional decision support [Online] http://www.iemss2008/index.php?n=Main.Proceedings (verified February 2009).

Emerson, C.H., and R.G. Traver. 2008. Multiyear and seasonal variation of infiltration from storm-water best management practices. Journal of Irrigation and Drainage Engineering-Asce 134:598-605.

Ersahin, S., R.I. Papendick, J.L. Smith, C.K. Keller, and V.S. Manoranjan. 2002. Macropore transport of bromide as influenced by soil structure differences. Geoderma 108:207-223.

Everts, C.J., and R.S. Kanwar. 1993. Interpreting tension-infiltrometer data for quantifying soil macropores - some practical considerations. Transactions of the ASAE 36:423-428.

Faybishenko, B. 1999. Comparison of laboratory and field methods for determining the quasi-saturated hydraulic conductivity of soils, p. 279 - 292, *In* M. T. Van Genuchten, et al., eds. Characterization and measurement of the hydraulic properties of unsaturated porous media : proceedings of the International Workshop on Characterization and Measurement of the Hydraulic Properties of Unsaturated Porous Media, Riverside, California, October 22-24, 1997, Vol. 1. University of California, Riverside, California.

Fayer, M.J., and D. Hillel. 1986. Air encapsulation: I. Measurement in a field soil. Soil Science Society of America Journal 50:568-572.

Flemmer, C.L., and R.C. Flemmer. 2008. Water effluent from New Zealand dairy farms from 1997 to 2000. New Zealand Journal of Agricultural Research 51:181-189.

Fluhler, H., M.S. Ardakani, and L.H. Stolzy. 1976. Error propagation in determining hydraulic conductivities from successive water content and pressure head profiles. Soil Science Society of America Journal 40:830-836.

Flury, M., and H. Fluhler. 1994. Brilliant blue FCF as a dye tracer for solute transport studies - a toxicological overview. Journal of Environmental Quality 23:1108-1112.

Flury, M., and N.N. Wai. 2003. Dyes as tracers for vadose zone hydrology. Reviews of Geophysics 41(1): 1-37.

Flury, M., H. Fluhler, W.A. Jury, and J. Leuenberger. 1994. Susceptibility of soils to preferential flow of water - a field-study. Water Resources Research 30:1945-1954.

Forrer, I., A. Papritz, R. Kasteel, H. Fluhler, and D. Luca. 2000. Quantifying dye tracers in soil profiles by image processing. European Journal of Soil Science 51:313-322.

Fuentes, J.P., and M. Flury. 2005. Hydraulic conductivity of a silt loam soil as affected by sample length. Transactions of the ASAE 48:191-196.

Gardner, W.R. 1958. Some steady-state solutions of the unsaturated moisture flow equation with application to evaporation from a water table. Soil Science 85:228-232.

Gillingham, A.G., and B.S. Thorrold. 2000. A review of New Zealand research measuring phosphorus in runoff from pasture. Journal of Environmental Quality 29:88.

Gradwell, M.W. 1974. Measured and predicted hydraulic conductivities for some New Zealand subsoils at water contents near field capacity. New Zealand Journal of Science 17:463-473.

Gradwell, M.W. 1979. Subsoil hydraulic conductivities of major New Zealand soil groups at water contents near field capacity. New Zealand Journal of Agricultural Research 22:603-614.

Gradwell, M.W., and W.C. Rijkse. 1988. An evaluation of the physical properties of some Gisborne Plains soils for irrigation purposes. New Zealand Journal of Experimental Agriculture 16:287-294.

Green, S.R. 2007. Modelling the environmental effects of wastewater disposal at the Masterton land-based sewage effluent disposal scheme. Report to Beca Carter

Hollings & Ferner. HortResearch Client Report No. 21183. HortResearch Palmerston North.

Greenwood, P.B. 1999. Irrigation of farm dairy effluent in Southland. SoilWork Ltd Report SW-MR-0196. Report for Southland Regional Council, Invercargill, New Zealand.

Greenwood, P.B., and R.M. McNamara. 1992. An analysis of the physical condition of two intensively grazed Southland soils. Proceedings of the New Zealand Grassland Association 54:71-75.

Griffioen, J.W., D.A. Barry, and J.Y. Parlange. 1998. Interpretation of two-region model parameters. Water Resources Research 34:373-384.

Griffiths, E., T.H. Webb, J.P.C. Watt, and P.L. Singleton. 1999. Development of soil morphological descriptors to improve field estimation of hydraulic conductivity. Australian Journal of Soil Research 37:971-982.

Grismer, M.E., M.N. Orang, V. Clausnitzer, and K. Kinney. 1994. Effects of air compression and counterflow on infiltration into soils. Journal of Irrigation and Drainage Engineering 120:775-795.

Hallett, P.D., T. Baumgartl, and I.M. Young. 2001. Subcritical water repellency of aggregates from a range of soil management practices. Soil Science Society of America Journal 65:184-190.

Hammecker, C., A.C.D. Antonino, and J.L. Maeght P. Boivin. 2003. Experimental and numerical study of water flow in soil under irrigation in northern Senegal: evidence of air entrapment. European Journal of Soil Science 54:491-503.

Hawke, R.M., and S.A. Summers. 2006. Effects of land application of farm dairy effluent on soil properties: a literature review. New Zealand Journal of Agricultural Research 49:307-320.

Haws, N.W., B.W. Liu, C.W. Boast, P.S.C. Rao, E.J. Kladivko, and D.P. Franzmeier. 2004. Spatial variability and measurement scale of infiltration rate on an agricultural landscape. Soil Science Society of America Journal 68:1818-1826.

Hendrickx, J.M.H., and M. Flury. 2001. Uniform and preferential flow mechanisms in the vadose zone, p. 149-187. In: Conceptual Models of Flow and Transport in the Fractured Vadose Zone. National Research Council, National Academy Press, Washington, DC.

Hewitt, A.E. 1998. New Zealand soil classification. Landcare Research Science Series, No.1. Landcare Research, Lincoln, New Zealand.

Hill, D.E., and J.Y. Parlange. 1972. Wetting front instability in layered soils. Soil Science Society of America Proceedings 36:697-702.

Hillel, D. 1998. Environmental soil physics Academic Press, San Diego, CA.

Hopmans, J.W., J. Simunek, N. Romano, and W. Durner. 2002. Inverse methods, p. 963-1004, *In* J. H. Dane, et al., eds. Methods of soil analysis. Part 4 - physical methods. Soil Science Society of America, Madison, Wisconsin.

Houlbrooke, D.J., D.J. Horne, M.J. Hedley, J.A. Hanly, and V.O. Snow. 2004. A review of literature on the land treatment of farm-dairy effluent in New Zealand and its impact on water quality. New Zealand Journal of Agricultural Research 47:499-511.

Houlbrooke, D.J., D.J. Horne, M.J. Hedley, V.O. Snow, and J.A. Hanly. 2008. Land application of farm dairy effluent to a mole and pipe drained soil: implications for nutrient enrichment of winter-spring drainage. Australian Journal of Soil Research 46:45-52.

Irrigation New Zealand. 2007. Irrigation code of practice and design standards [Online]. Available by Irrigation New Zealand Inc, Christchurch, NZ http://www.irrigationnz.co.nz/ (verified February, 2009).

Irrigation New Zealand. 2009. Irrigated agriculture in New Zealand (web page) [Online]. Available by Irrigation New Zealand Inc, Christchurch, NZ http://www.irrigationnz.co.nz/ (verified February, 2009).

Iversen, B.V., P. Moldrup, P. Schjonning, and P. Loll. 2001. Air and water permeability in differently textured soils at two measurement scales. Soil Science 166:643-659.

Iwata, S., T. Tabuchi, and B.P. Warkentin. 1995. Soil-water interactions : mechanisms and applications. 2nd ed, rev. and expand ed. M. Dekker, New York.

Jacques, D., B.P. Mohanty, and J. Feyen. 2002. Comparison of alternative methods for deriving hydraulic properties and scaling factors from single-disc tension infiltrometer measurements. Water Resources Research 38.

Jarvis, N., A. Etana, and F. Stagnitti. 2008. Water repellency, near-saturated infiltration and preferential solute transport in a macroporous clay soil. Geoderma 143:223-230.

Jarvis, N., M. Larsbo, S. Roulier, A. Lindahl, and L. Persson. 2007b. The role of soil properties in regulating non-equilibrium macropore flow and solute transport in agricultural topsoils. European Journal of Soil Science 58:282-292.

Jarvis, N.J. 2007. A review of non-equilibrium water flow and solute transport in soil macropores: principles, controlling factors and consequences for water quality. European Journal of Soil Science 58:523-546.

Jarvis, N.J., and I. Messing. 1995. Near-saturated hydraulic conductivity in soils of contrasting texture measured by tension infiltrometers. Soil Science Society of America Journal 59:27-34.

Jaynes, D.B., S.D. Logsdon, and R. Horton. 1995. Field method for measuring mobile immobile water-content and solute transfer rate coefficient. Soil Science Society of America Journal 59:352-356.

Jiang, G., M.J. Noonan, G.D. Buchan, and N. Smith. 2005. Transport and deposition of Bacillus subtilis through an intact soil column. Australian Journal of Soil Research 43:695-703.

Jiang, S., G.D. Buchan, M.J. Noonan, N. Smith, L. Pang, and M. Close. 2008. Bacterial leaching from dairy shed effluent applied to a fine sandy loam under irrigated pasture. Australian Journal of Soil Research 46:552-564.

Joe, E.N. 1986. Soil water characterisation of 6 soils in the Waikato District, New Zealand. N.Z. Soil Bureau SWAMP Data sheets 1984:[1-6].

Joe, E.N., and J.P.C. Watt. 1984. Soil water characterisation of 11 soils in central and coastal Otago, New Zealand. N.Z. Soil Bureau SWAMP Data sheets 1983:[1-11].

Johnson, D.O., F.J. Arriaga, and B. Lowery. 2005. Automation of a falling head permeameter for rapid determination of hydraulic conductivity of multiple samples. Soil Science Society of America Journal 69:828.

Jury, W.A., and R. Horton. 2004. Soil physics. 6th ed. Wiley, Hoboken, N.J.

Kear, B.S., R.B. Miller, and H.S. Gibbs. 1967. Soils of the downs and plains, Canterbury and North Otago, New Zealand DSIR, Wellington.

Keng, J.C.W., and C.S. Lin. 1982. A two-line approximation of hydraulic conductivity of structured soils. Canadian Agricultural Engineering 24:77-80.

Kim, J., C. Chon, and J. Lee. 2004. Effect of structure and texture on infiltration flow pattern during flood irrigation. Environmental Geology 46:962-969.

Kumke, T., and C.E. Mullins. 1997. Field measurement of time to ponding. Soil Use and Management 13:24-28.

Lal, R., and M. Shukla. 2004. Principles of soil physics Marcel Dekker, New York.

Landcare Research. 2008. New Zealand National Soils Database [Online]. Available by Landcare Research http://soils.landcareresearch.co.nz/contents/SoilData_NSD_About.aspx?currentPage=SoilData_NSD&menuItem=SoilData.

Langner, H.W., H.M. Gaber, J.M. Wraith, B. Huwe, and W.P. Inskeep. 1999. Preferential flow through intact soil cores: Effects of matric head. Soil Science Society of America Journal 63:1591-1598.

Latifi, H., S.N. Prasad, and O.J. Helweg. 1994. Air Entrapment and Water Infiltration in Two-Layered Soil Column. Journal of Irrigation and Drainage Engineering 120:871-891.

Lauren, J.G., R.J. Wagenet, J. Bouma, and J.H.M. Wosten. 1988. Variability of saturated hydraulic conductivity in a Glossaquic Hapludalf with macropores. Soil Science 145:20-28.

Leonard, M., and B. Gilpin. 2006. Potential impacts of on-site sewage disposal. ESR Client report CSC 0603, prepared for Gisborne District Council. [Online] http://www.envirolink.govt.nz/reports/documents/92-Gsdc1-SepticTankContaminationOfGroundwater.pdf (verified February 2009).

Lilburne, L.R., and T.H. Webb. 2002. Effect of soil variability, within and between soil taxonomic units, on simulated nitrate leaching under arable farming, New Zealand. Australian Journal of Soil Research 40:1187-1199.

Lilburne, L.R., T.H. Webb, and G.S. Francis. 2003. Relative effect of climate, soil, and management on risk of nitrate leaching under wheat production in Canterbury, New Zealand. Australian Journal of Soil Research 41:699-709.

Lin, C.Y., D. Greenwald, and A. Banin. 2003. Temperature dependence of infiltration rate during large scale water recharge into soils. Soil Science Society of America Journal 67:487-493.

Lin, H.S., and K.J. McInnes. 1995. Water flow in clay soil beneath a tension infiltrometer. Soil Science 159:375-382.

Lin, H.S., K.J. McInnes, L.P. Wilding, and C.T. Hallmark. 1998. Macroporosity and initial moisture effects on infiltration rates in Vertisols and vertic intergrades. Soil Science 163:2-8.

Logsdon, S.D., and D.B. Jaynes. 1993. Methodology for determining hydraulic conductivity with tension infiltrometers. Soil Science Society of America Journal 57:1426-1431.

Logsdon, S.D., and B.K. Hornbuckle. 2006. Soil moisture probes for a dispersive soil, pp. 14 TDR 2006, Purdue University, West Lafayette, USA, Sept. 2006, paper ID 13, https://engineering.purdue.edu/TDR/Papers.

Logsdon, S.D., E.L. McCoy, R.R. Allmaras, and D.R. Linden. 1993b. Macropore characterization by indirect methods. Soil Science 155:316-324.

Magesan, G.N., I. Vogeler, D.R. Scotter, B.E. Clothier, and R.W. Tillman. 1995. Solute movement through two unsaturated soils. Australian Journal of Soil Research 33:585-596.

Mallants, D., B.P. Mohanty, A. Vervoort, and J. Feyen. 1997. Spatial analysis of saturated hydraulic conductivity in a soil with macropores. Soil Technology 10:115-131.

Marshall, T.J., J.W. Holmes, and C.W. Rose. 1996. Soil physics. 3rd ed. Cambridge University Press, Cambridge [England] ; New York.

McDowell, R.W., and D. Rowley. 2008. The fate of phosphorus under contrasting border-check irrigation regimes. Australian Journal of Soil Research 46:309-314.

McDowell, R.W., R.M. Monaghan, and D. Wheeler. 2005. Modelling phosphorus losses from pastoral farming systems in New Zealand. New Zealand Journal of Agricultural Research 48:131-141.

McKenzie, N., K. Coughlan, and H. Cresswell. 2002. Soil physical measurement and interpretation for land evaluation. CSIRO, Collingwood, Australia.

McKenzie, N.J. 2004. Australian soils and landscapes : an illustrated compendium CSIRO Publishing, Collingwood, Vic.

McKenzie, N.J. 2008. Guidelines for surveying soil and land resources. 2nd ed. CSIRO Publishing, Collingwood, Vic.

McKenzie, N.J., and H.P. Cresswell. 2002b. Selecting a method for hydraulic conductivity, p. 90-107, *In* N. McKenzie, et al., eds. Soil physical measurement and interpretation for land evaluation. CSIRO, Collingwood, Australia.

McKenzie, N.J., and H.P. Cresswell. 2002c. Field sampling, p. 11-34, *In* N. McKenzie, et al., eds. Soil physical measurement and interpretation for land evaluation. CSIRO, Collingwood, Australia.

McKenzie, N.J., H.P. Cresswell, and T.W. Green. 2002d. Field measurement of unsaturated hydraulic conductivity using tension infiltrometers, p. 119-130, *In* N. McKenzie, et al., eds. Soil physical measurement and interpretation for land evaluation. CSIRO, Collingwood, Australia.

McKenzie, N.J., T.W. Green, and D. Jacquier. 2002e. Laboratory measurement of hydraulic conductivity p. 150-162, *In* N. McKenzie, et al., eds. Soil physical measurement and interpretation for land evaluation. CSIRO, Collingwood, Australia.

McKenzie, N.J., H.P. Cresswell, P.J. Ryan, and M. Grundy. 2000. Contemporary land resource survey requires improvements in direct soil measurement. Communications in Soil Science and Plant Analysis 31:1553-1569.

McKenzie, N.J., H.P. Cresswell, H. Rath, and D. Jacquier. 2001. Measurement of unsaturated hydraulic conductivity using tension and drip infiltrometers. Australian Journal of Soil Research 39:823-836.

McLaren, R.G., L.M. Clucas, M.D. Taylor, and T. Hendry. 2004. Leaching of macronutrients and metals from undisturbed soils treated with metal-spiked sewage sludge. 2. Leaching of metals. Australian Journal of Soil Research 42:459-471.

McLaren, R.G., R. Simcock, D. Thornburrow, and J. Clayden. 2005. Can swale performance be increased by manipulating soil condition? [Online]. Available by Landcare Research http://www.landcareresearch.co.nz/research/built/liudd/swales_more.asp (verified February 2009).

McLeod, M., J. Aislabie, J. Ryburn, and A. McGill. 2004. Microbial and chemical tracer movement through granular, ultic, and recent soils. New Zealand Journal of Agricultural Research 47:557-563.

McLeod, M., J. Aislabie, J. Ryburn, and A. McGill. 2008. Regionalizing potential for microbial bypass flow through New Zealand soils. Journal of Environmental Quality 37:1959-1967.

McLeod, M., J. Aislabie, J. Ryburn, A. McGill, and M. Taylor. 2003. Microbial and chemical tracer movement through two Southland soils, New Zealand. Australian Journal of Soil Research 41:1163-1169.

McLeod, M., J. Aislabie, J. Smith, R. Fraser, A. Roberts, and M. Taylor. 2001. Viral and chemical tracer movement through contrasting soils. Journal of Environmental Quality 30:2134-2140.

McQueen, D.J. 1993. Glossary of soil physical terms. Manaaki Whenua - Landcare Research, Lincoln, New Zealand.

Menneer, J.C., C.D.A. McLay, and R. Lee. 2001. Effects of sodium-contaminated wastewater on soil permeability of two New Zealand soils. Australian Journal of Soil Research 39:877-891.

Messing, I., and N.J. Jarvis. 1993. Temporal variation in the hydraulic conductivity of a tilled clay soil as measured by tension infiltrometers. Journal of Soil Science 44:11-24.

Milne, J.D.G., B. Clayden, P.L. Singleton, and A.D. Wilson. 1995. Soil description handbook. Rev. ed. Manaaki Whenua Press, Landcare Research., Lincoln, N.Z.

Minasny, B., and A.B. McBratney. 2000. Estimation of sorptivity from disc-permeameter measurements. Geoderma 95:305-324.

Ministry for the Environment. 2007. Environment New Zealand 2007 [Online]. Available by Ministry for the Environment, Wellington, N.Z. http://www.mfe.govt.nz/publications/ser/enz07-dec07/index.html (verified February 2009).

Ministry for the Environment. 2008. Proposed national environmental standard for on-site wastewater systems: discussion document [Online]. Available by Ministry for the Environment, Wellington, N.Z. http://www.mfe.govt.nz/laws/standards/wastewater-systems-standards.html (verified February 2009).

Ministry for the Environment. 2007. Environment New Zealand 2007 [Online]. Available by Ministry for the Environment, Wellington, N.Z. http://www.mfe.govt.nz/publications/ser/enz07-dec07/index.html (verified February 2009).

Miyazaki, T. 2006. Water flow in soils. 2nd ed. Taylor & Francis, Boca Raton.

Mohrath, D., L. Bruckler, P. Bertuzzi, J.C. Gaudu, and M. Bourlet. 1997. Error analysis of an evaporation method for determining hydrodynamic properties in unsaturated soil. Soil Science Society of America Journal 61:725-735.

Monaghan, R.M. 2008. The environmental impacts of non-irrigated pasture-based dairy farming., p. 209 - 231, *In* R. W. McDowell, ed. Environmental impacts of pasture-based farming. CABI, Wallingford.

Monaghan, R.M., C.A.M. de Klein, and R.W. Muirhead. 2008b. Prioritisation of farm scale remediation efforts for reducing losses of nutrients and faecal indicator organisms to waterways: A case study of New Zealand dairy farming. Journal of Environmental Management 87:609-622.

Monaghan, R.M., M.J. Hedley, H.J. Di, R.W. McDowell, K.C. Cameron, and S.F. Ledgard. 2007. Nutrient management in New Zealand pastures - recent developments and future issues. New Zealand Journal of Agricultural Research 50:181-201.

Monaghan, R.M., R.J. Wilcock, L.C. Smith, B. Tikkisetty, B.S. Thorrold, and D. Costall. 2007b. Linkages between land management activities and water quality in an intensively farmed catchment in southern New Zealand. Agriculture, Ecosystems & Environment 118:211-222.

Monaghan, R.M., P.L. Carey, R.J. Wilcock, J.J. Drewry, D.J. Houlbrooke, J.M. Quinn, and B.S. Thorrold. 2009. Linkages between land management activities and stream water quality in a border dyke-irrigated pastoral catchment. Agriculture, Ecosystems & Environment 129:201-211.

Moret, D., and J.L. Arrue. 2007. Characterizing soil water-conducting macro- and mesoporosity as influenced by tillage using tension of infiltrometry. Soil Science Society of America Journal 71:500-506.

Nash, D., and K. Barlow. 2008. Impacts of irrigated dairying on the environment p. 232 - 248, *In* R. W. McDowell, ed. Environmental impacts of pasture-based farming. CABI, Wallingford.

Navarro, V., A. Yustres, M. Candel, and B. García. 2008. Soil air compression in clays during flood irrigation. European Journal of Soil Science 59:799-806.

Nimmo, J.R., and K.S. Perkins. 2002. Aggregate stability and size distribution, p. 317-328, *In* J. H. Dane, et al., eds. Methods of soil analysis. Part 4 - physical methods. Soil Science Society of America, Madison, Wisconsin.

NIWA. 2009. CLIFLO - National climate database [Online]. Available by National Institute of Water & Atmospheric Research. http://cliflo.niwa.co.nz/.

Nobles, M.M., L.P. Wilding, and K.J. McInnes. 2004. Pathways of dye tracer movement through structured soils on a macroscopic scale. Soil Science 169:229-242.

NZWERF. 2004. On-site stormwater management guideline. New Zealand Water Environment Research Foundation, Wellington, New Zealand.

OECD. 2007. OECD environmental performance review of New Zealand. Organisation for Economic Co-operation and Development, Paris.

OECD. 2008. OECD environmental outlook to 2030. Organisation for Economic Co-operation and Development, Paris.

Öhrström, P., M. Persson, J. Albergel, P. Zante, S. Nasri, R. Berndtsson, and J. Olsson. 2002. Field-scale variation of preferential flow as indicated from dye coverage. Journal of Hydrology 257:164-173.

Pang, L., M.E. Close, J.P.C. Watt, and K.W. Vincent. 2000. Simulation of picloram, atrazine, and simazine leaching through two New Zealand soils and into groundwater using HYDRUS-2D. Journal of Contaminant Hydrology 44:19-46.

Pang, L., C. Nokes, J. Simunek, H. Kikkert, and R. Hector. 2006. Modeling the impact of clustered septic tank systems on groundwater quality. Vadose Zone Journal 5:599-609.

Pang, L., M. McLeod, J. Aislabie, J. Simunek, M. Close, and R. Hector. 2008. Modeling Transport of Microbes in Ten Undisturbed Soils under Effluent Irrigation. Vadose Zone J 7:97-111.

Parfitt, R.L., W.T. Baisden, and A.H. Elliot. 2008. Phosphorus inputs and outputs for New Zealand in 2001 at national and regional scales. Journal of the Royal Society of New Zealand 38:37-50.

Parker, J.C., and K.A. Albrecht. 1987. Sample volume effects on solute transport predictions. Water Resources Research 23:2293-2301.

Perroux, K.M., and I. White. 1988. Designs for disc permeameters. Soil Science Society of America Journal 52:1205-1215.

Philip, J.R. 1957. The theory of infiltration. 4. Sorptivity and algebraic infiltration equations. Soil Science 84:257-264.

Phillip, J.R. 1969. The theory of infiltration. Advances in Hydrosciences 5:215-296.

Power, I., S.F. Ledgard, and R.M. Monaghan. 2002. Nutrient budgets for three mixed farming catchments in New Zealand. MAF Technical Paper No: 2002/17. Ministry of Agriculture and Forestry, Wellington, NZ.

Prieksat, M.A., M.D. Ankeny, and T.C. Kaspar. 1992. Design for an automated, self-regulating, single-ring infiltrometer. Soil Science Society of America Journal 56:1409-1411.

Ragusa, S.R., D.S.d. Zoysa, and P. Rengasamy. 1994. The effect of microorganisms, salinity and turbidity on hydraulic conductivity of irrigation channel soil. Irrigation Science 15:159-166.

Reynolds, W.D. 2006. Tension infiltrometer measurements: implications of pressure head offset due to contact sand. Vadose Zone Journal 5:1287-1292.

Reynolds, W.D. 2008. Unsaturated hydraulic properties: field tension infiltrometer, p. 1107 - 1128, *In* M. R. Carter and E. G. Gregorich, eds. Soil Sampling and Methods of Analysis, Two ed. Canadian Society of Soil Science & CRC Press Boca Raton, FL.

Reynolds, W.D., and D.E. Elrick. 1991. Determination of hydraulic conductivity using a tension infiltrometer. Soil Science Society of America Journal 55:633-639.

Reynolds, W.D., and W.D. Zebchuk. 1996. Use of contact material in tension infiltrometer measurements. Soil Technology 9:141-159.

Reynolds, W.D., and W.D. Zebchuk. 1996b. Hydraulic conductivity in a clay soil: two measurement techniques and spatial characterization. Soil Science Society of America Journal 60:1679-1685.

Reynolds, W.D., and G.C. Topp. 2008b. Soil water analyses: principles and parameters, p. 913 - 938, *In* M. R. Carter and E. G. Gregorich, eds. Soil Sampling and Methods of Analysis, Two ed. Canadian Society of Soil Science & CRC Press Boca Raton, FL.

Reynolds, W.D., E.G. Gregorich, and W.E. Curnoe. 1995. Characterisation of water transmission properties in tilled and untilled soils using tension infiltrometers. Soil and Tillage Research 33:117-131.

Rickard, D.S., and G.G. Cossens. 1966. Irrigation investigations in Otago, New Zealand. I. Description and physical properties of irrigated soils of the Ida valley. New Zealand Journal of Agricultural Research 9:197-217.

Rickard, D.S., and G.G. Cossens. 1968. Irrigation investigations in Qtago, New Zealand. IV. Physical properties of soils of the Arrow Basin and Upper Clutha Valley. New Zealand Journal of Agricultural Research 11:701-732.

Ritchie, H., P.R. Heatley, and Dairying and the Environment Committee (N.Z.). 2006a. Managing farm dairy effluent. 3rd rev. and updated ed. Dairying and the Environment Committee, [Palmerston North, N.Z.].

Ritchie, H., P.R. Heatley, and Dairying and the Environment Committee (N.Z.). 2006b. Farm management issues. Rev. and updated ed. Dairying and the Environment Committee, [Palmerston North, N.Z.].

Rosen, M.R., R.R. Reeves, S. Green, B. Clothier, and N. Ironside. 2004. Prediction of groundwater nitrate contamination after closure of an unlined sheep feedlot. Vadose Zone Journal 3:990-1006.

Ross, P.J., and K.R.J. Smettem. 2000. A simple treatment of physical nonequilibrium water flow in soils. Soil Science Society of America Journal 64:1926-1930.

Saggar, S., D.L. Giltrap, C. Li, and K.R. Tate. 2007. Modelling nitrous oxide emissions from grazed grasslands in New Zealand. Agriculture, Ecosystems & Environment 119:205-216.

Sarmah, A.K., K. ller, and R. Ahmad. 2004. Fate and behaviour of pesticides in the agroecosystem - a review with a New Zealand perspective. Australian Journal of Soil Research 42:125-154.

Sarmah, A.K., M.E. Close, L. Pang, R. Lee, and S.R. Green. 2005. Field study of pesticide leaching in a Himatangi sand (Manawatu) and a Kiripaka bouldery clay loam (Northland). 2. Simulation using LEACHM, HYDRUS-1D, GLEAMS, and SPASMO models. Australian Journal of Soil Research 43:471-489.

Sarmah, A.K., M.E. Close, R. Dann, L. Pang, and S.R. Green. 2006. Parameter estimation through inverse modelling and comparison of four leaching models using experimental data from two contrasting pesticide field trials in New Zealand. Australian Journal of Soil Research 44:581-597.

Sauer, T.J., B.E. Clothier, and T.C. Daniel. 1990. Surface measurements of the hydraulic properties of a tilled and untilled soil. Soil and Tillage Research 15:359-369.

Schwarzel, K., and J. Punzel. 2007. Hood infiltrometer - A new type of tension infiltrometer. Soil Science Society of America Journal 71:1438-1447.

Schwarzel, K., J. Simunek, H. Stoffregen, G. Wessolek, and M.T. van Genuchten. 2006. Estimation of the unsaturated hydraulic conductivity of peat soils: laboratory versus field data. Vadose Zone Journal 5:628-640.

Seki, K., T. Miyazaki, and M. Nakano. 1998. Effects of microorganisms on hydraulic conductivity decrease in infiltration. European Journal of Soil Science 49:231-236.

Selwyn District Council. 2008. The Lincoln integrated catchment management plan.

Selwyn District Council. 2009. Selwyn District Council subdivision design guide. Revised draft January 2009. .

Seyfried, M.S., and P.S.C. Rao. 1987. Solute transport in undisturbed columns of an aggregated tropical soil: preferential flow effects. Soil Science Society of America Journal 51:1434-1444.

Silva, R.G., K.C. Cameron, H.J. Di, and T. Hendry. 1999. A lysimeter study of the impact of cow urine, dairy shed effluent, and nitrogen fertiliser on nitrate leaching. Australian Journal of Soil Research 37:357-369.

Silva, R.G., K.C. Cameron, H.J. Di, N.P. Smith, and G.D. Buchan. 2000. Effect of macropore flow on the transport of surface-applied cow urine through a soil profile. Australian Journal of Soil Research 38:13-23.

Simcock, R., M. Taylor, J. Dando, and S. Trowsdale. 2006. Designing and testing substrates for raingardens that infiltrate, store and treat stormwater. Proceedings of NZ Society of Soil Science annual conference, Rotorua, November 2006. [Online] http://www.landcareresearch.co.nz/research/built/liudd/morepublications.asp?research_ID=12#publication (verified February 2009).

Simcock, R., J. Zanders, D. Worthy, J. Dando, D. Thornburrow, R.G. McLaren, M. Mcleod, K. Daysh, A. Taylor, and J. Claydon. 2005. Use the right soil to get the stormwater treatment you want. [Online]. Available by Landcare Research. http://www.landcareresearch.co.nz/research/built/liudd/swales.asp.

Simunek, J., and M.T. van Genuchten. 2008. Modeling Nonequilibrium Flow and Transport Processes Using HYDRUS. Vadose Zone J 7:782-797.

Simunek, J., N.J. Jarvis, M.T. van Genuchten, and A. Gardenas. 2003. Review and comparison of models for describing non-equilibrium and preferential flow and transport in the vadose zone. Journal of Hydrology 272:14-35.

Simunek, J., M.T. van Genuchten, M. Sejna, N. Toride, and F.J. Leij. 1999. The STANMOD computer software for evaluating solute transport in porous media using analytical solutions of the convection-disperson equation. Version 2.0. IGWMTC-TPS-70. Int. Ground Water Modelling Ctr., Colorado School of Mines.

Singleton, P.L., M. Boyes, and B. Addison. 2000. Effect of treading by dairy cattle on topsoil physical conditions for six contrasting soil types in Waikato and Northland, New Zealand, with implications for monitoring. New Zealand Journal of Agricultural Research 43:559-567.

Skaggs, T.H., G.V. Wilson, P.J. Shouse, and F.J. Leij. 2002a. Solute transport: experimental methods, p. 1381-1402, *In* J. H. Dane and G. C. Topp, eds. Methods of soil analysis: physical methods, Vol. 5(part 4). Soil Science Society of America, Madison, Wisconsin, USA.

Skaggs, T.H., D.B. Jaynes, R.G. Kachanoski, P.J. Shouse, and A.L. Ward. 2002b. Solute transport: data analysis and parameter estimation, p. 1403-1434, *In* J. H. Dane and G. C. Topp, eds. Methods of soil analysis: physical methods, Vol. 5(part 4). Soil Science Society of America, Madison, Wisconsin, USA.

Smettem, K.R.J., and R.E. Smith. 2002. Field measurement of infiltration parameters, p. 135 - 156, *In* R. E. Smith, ed. Infiltration theory for hydrological applications. Water Resources Monograph 15. American Geophysical Union, Washington, DC.

Smettem, K.R.J., C. Kirkby, and D.J. Chittleborough. 1994. Hydrologic response of undisturbed soil cores to simulated rainfall. Australian Journal of Soil Research 32:1175-1187.

Smettem, K.R.J., D.J. Chittleborough, B.G. Richards, and F.W. Leaney. 1991. The influence of macropores on runoff generation from a hillslope soil with a contrasting textural class. Journal of Hydrology 122:235-251.

Smiles, D.E. 2002. Water and solute transfer in porous media, p. 107-119, *In* P. A. C. Raats, et al., eds. Environmental mechanics : water, mass and energy transfer in the

biosphere. Geophysical monograph 129. American Geophysical Union, Washington, D.C.

Smiles, D.E., and J.H. Knight. 1976. A note on the use of the Philip infiltration equation. Australian Journal of Soil Research 14:103-108.

Smith, R.E. 1990. Analysis of Infiltration through a 2-Layer Soil-Profile. Soil Science Society of America Journal 54:1219-1227.

Sparling, G.P., L. Barton, L. Duncan, A. McGill, T.W. Speir, L.A. Schipper, G. Arnold, and A. Van Schaik. 2006. Nutrient leaching and changes in soil characteristics of four contrasting soils irrigated with secondary-treated municipal wastewater for four years. Australian Journal of Soil Research 44:107-116.

Statistics New Zealand. 2007. 2007 agricultural production census [Online]. Available by Staistics New Zealand, Wellington, NZ. http://www.stats.govt.nz/tables/2007-ag-prod/default.htm (verified February 2009).

Stenger, R., G. Barkle, and C. Burgess. 2005. Laboratory calibrations of water content reflectometers and their in-situ verification. Australian Journal of Soil Research 43:607-615.

Stoffregen, H., G. Wessolek, and M. Renger. 1999. Effect of temperature on hydraulic conductivity, p. 497-506, *In* M. T. Van Genuchten, et al., eds. Characterization and measurement of the hydraulic properties of unsaturated porous media : proceedings of the International Workshop on Characterization and Measurement of the Hydraulic Properties of Unsaturated Porous Media, Riverside, California, October 22-24, 1997. University of California, Riverside, Calif.

Tamari, S., L. Bruckler, J. Halbertsma, and J. Chadoeuf. 1993. A simple method for determining soil hydraulic properties in the laboratory. Soil Science Society of America Journal 57:642-651.

Taylor, J.R. 1982. An introduction to error analysis. University Science Books.

Taylor, M., M. Mulholland, and D. Thornburrow. 2008. Infiltration of water into soil under forestry and agriculture in the upper Waikato catchment. New Zealand Soil News 56:1 6-10.

The Heinz Centre. 2008. The state of the nation's ecosystems 2008 : measuring the lands, waters, and living resources of the United States. The H. John Heinz III Center for Science, Economics and the Environment. Center for Resource Economics, Washington, D.C.

Thomas, S.M., S.F. Ledgard, and G.S. Francis. 2005. Improving estimates of nitrate leaching for quantifying New Zealand's indirect nitrous oxide emissions. Nutrient Cycling in Agroecosystems 73:213-226.

Thompson, C.S. 2002. HIRDS: High intensity rainfall design system. 2.0 ed. National Institute of Water and Atmospheric Research, Wellington, NZ.

Thony, J.L., G. Vachaud, B.E. Clothier, and R. Angulo Jaramillo. 1991. Field measurement of the hydraulic properties of soil. Soil Technology 4:111-123.

Tillman, R.W., D.R. Scotter, M.G. Wallis, and B.E. Clothier. 1989. Water repellency and its measurement by using intrinsic sorptivity. Australian Journal of Soil Research 27:637-644.

Tillman, R.W., D.R. Scotter, B.E. Clothier, and R.E. White. 1991. Solute movement during intermittent water flow in a field soil and some implications for irrigation and fertilizer application. Agricultural Water Management 20:119-133.

Toor, G.S., L.M. Condron, H.J. Di, K.C. Cameron, and J.T. Sims. 2004. Assessment of phosphorus leaching losses from a free draining grassland soil. Nutrient Cycling in Agroecosystems 69:167-184.

Toor, G.S., L.M. Condron, B.J. Cade-Menun, H.J. Di, and K.C. Cameron. 2005. Preferential phosphorus leaching from an irrigated grassland soil. European Journal of Soil Science 56:155-167.

Topoclimate. 2009. Southland soil map [Online]. Available by Environment Southland. http://map.es.govt.nz/departments/landsustainability/soil/Default.aspx.

Trowsdale, S., and R. Simcock. 2008. Raingarden soils and efficiency. Proceedings of the NZWWA Conference, Rotorua, May, 2008. [Online] http://www.landcareresearch.co.nz/research/built/liudd/Rain_gardens.asp (verified February 2009).

van Es, H.M. 2002. Soil variability, p. 1-14, *In* J. H. Dane, et al., eds. Methods of soil analysis. Part 4 - physical methods. Soil Science Society of America, Madison, Wisconsin.

van Genuchten, M.T., and P.J. Wierenga. 1976. Mass Transfer Studies in Sorbing Porous Media I. Analytical Solutions. Soil Sci Soc Am J 40:473-480.

Vandervaere, J.P., M. Vauclin, and D.E. Elrick. 2000. Transient flow from tension infiltrometers: I. The two-parameter equation. Soil Science Society of America Journal 64:1263-1272.

Vogeler, I. 2009. Effect of long-term wastewater application on physical soil properties. WATER AIR AND SOIL POLLUTION 196:385-392.

Vogeler, I., D.R. Scotter, B.E. Clothier, and R.W. Tillman. 1998. Anion transport through intact soil columns during intermittent unsaturated flow. Soil & Tillage Research 45:147-160.

Walker, C., H.S. Lin, and D.D. Fritton. 2006. Is the tension beneath a tension infiltrometer what we think it is? Vadose Zone Journal 5:860-866.

Walker, S.E., J.K. Mitchell, M.C. Hirschi, and K.E. Johnson. 2000. Sensitivity analysis of the root zone water quality model. Transactions of the ASAE 43:841-846.

Wallis, M.G., D.R. Scotter, and D.J. Horne. 1991. An evaluation of the intrinsic sorptivity water repellency index on a range of New Zealand soils. Australian Journal of Soil Research 29:353-362.

Wang, D., S.R. Yates, and F.F. Ernst. 1998b. Determining soil hydraulic properties using tension infiltrometers, time domain reflectometry, and tensiometers. Soil Science Society of America Journal 62:318-325.

Wang, Z., J. Feyen, D.R. Nielsen, and M.T. Van Genuchten. 1997. Two-phase infiltration equations accounting for air entrapment effects. Water Resources Research 33:2759-2767.

Wang, Z., J. Feyen, M.T. van Genuchten, and D.R. Nielsen. 1998. Air entrapment effects on infiltration rate and flow instability. Water Resources Research 34:213-222.

Warrick, A.W., and D.R. Nielsen. 1980. Spatial variability of soil physical properties in the field, p. 319-344, *In* D. Hillel, ed. Applications of soil physics. Academic Press, New York.

Warrick, A.W., P.J. Wierenga, M.H. Young, and S.A. Musil. 1998. Diurnal fluctuations of tensiometric readings due to surface temperature changes. Water Resources Research 34:2863-2869.

Watt, J.P.C., and K.W. Vincent. 1991. Physical properties of six soils of the Blenheim area. Derived data and hydraulic character statements. DSIR Land Resources Technical Record 42. DSIR, Lower Hutt, NZ.

Watt, J.P.C., E. Griffiths, and F.J. Cook. 1982. Towards an hydraulic characterisation of NZ soils: Soil Bureau's soil water assessment and measurement programme, 'SWAMP'. *In* DSIR, (ed.) Proceedings of Soil and Plant Water Symposium, Flock House, Bulls, New Zealand, 27-30 September 1982. Department of Scientific and Industrial Research (DSIR), Plant Physiology Division, Palmerston North, New Zealand.

Watt, J.P.C., S.J. Burgham, and DSIR Land Resources (N.Z.). 1992. Physical properties of eight soils of the Lincoln area, Canterbury : derived data and hydraulic character statements DSIR Land Resources, Dept. of Scientific and Industrial Research, Lower Hutt, N.Z.

Webb, T.H. 2003. Identification of functional horizons to predict physical properties for soils from alluvium in Canterbury, New Zealand. Australian Journal of Soil Research 41:1005-1019.

Webb, T.H., A.D. Wilson, and Manaaki Whenua-Landcare Research New Zealand Ltd. 1995. A manual of land characteristics for evaluation of rural land. Manaaki Whenua Press, Lincoln, N.Z.

Webb, T.H., J.J. Claydon, and S.R. Harris. 2000. Quantifying variability of soil physical properties within soil series to address modern land-use issues on the Canterbury Plains, New Zealand. Australian Journal of Soil Research 38:1115-1129.

Webb, T.H., L.R. Lilburne, and G.S. Francis. 2001. Validation of the GLEAMS simulation model for estimating net nitrogen mineralisation and nitrate leaching under cropping in Canterbury, New Zealand. Australian Journal of Soil Research 39:1015-1025.

Weiler, M., and F. Naef. 2003. An experimental tracer study of the role of macropores in infiltration in grassland soils. Hydrological Processes 17:477-493.

Weiler, M., and H. Fluhler. 2004. Inferring flow types from dye patterns in macroporous soils. Geoderma 120:137-153.

Western, A.W., and M.S. Seyfried. 2005. A calibration and temperature correction procedure for the water-content reflectometer. Hydrological Processes 19:3785-3793.

White, I., and M.J. Sully. 1987. Macroscopic and microscopic capillary length and time scales from field infiltration. Water Resources Research 23:1514-1522.

White, I., and K.M. Perroux. 1989. Estimation of unsaturated hydraulic conductivity from field sorptivity measurements. Soil Science Society of America Journal 53:324-329.

White, I., M.J. Sully, and K.M. Perroux. 1992. Measurement of surface-soil hydraulic properties: disk permeameters, tension infiltrometers, and other techniques, p. 69-102, *In* G. C. Topp, et al., eds. Advances in measurement of soil physical properties: Bringing theory into practice. Proceedings of a symposium San Antonio, Texas 1990, Vol. SSSA Special Publication Number 30. Madison USA: Soil Science of America Inc.

Whitehouse, L.J., H. Wang, and M.D.E. Tomer. 2000. New Zealand guidelines for utilisation of sewage effluent on land. New Zealand Land Treatment Collective and Forest Research, Rotorua, N.Z.

Wilcock, R.J., R.M. Monaghan, J.M. Quinn, A.M. Campbell, B.S. Thorrold, M.J. Duncan, A.W. McGowan, and K. Betteridge. 2006. Land-use impacts and water quality targets in the intensive dairying catchment of the Toenepi Stream, New Zealand. New Zealand Journal of Marine and Freshwater Research 40:123-140.

Woehling, T., R. Stenger, F. Wang, G. Barkle, and N. Schutze. 2008. Water flow in the vadose zone and groundwater. WISPAS 100:4 - 6.

Yang, H., H. Rahardjo, and E.C. Leong. 2006. Behavior of unsaturated layered soil columns during infiltration. Journal of Hydrologic Engineering 11:329-337.

Yarwood, R.R., M.L. Rockhold, M.R. Niemet, J.S. Selker, and P.J. Bottomley. 2006. Impact of microbial growth on water flow and solute transport in unsaturated porous media. Water Resources Research 42.

Young, M.H., and J.B. Sisson. 2002. Tensiometry, p. 575 - 608, *In* J. H. Dane, et al., eds. Methods of soil analysis. Part 4 - physical methods. Soil Science Society of America, Madison, Wisconsin.

Zavattaro, L., and C. Grignani. 2001. Deriving hydrological parameters for modeling water flow under field conditions. Soil Science Society of America Journal 65:655-667.

Zhan, T.L.T., C.W.W. Ng, and D.G. Fredlund. 2007. Field study of rainfall infiltration into a grassed unsaturated expansive soil slope. Canadian Geotechnical Journal 44:392-408.

Appendices

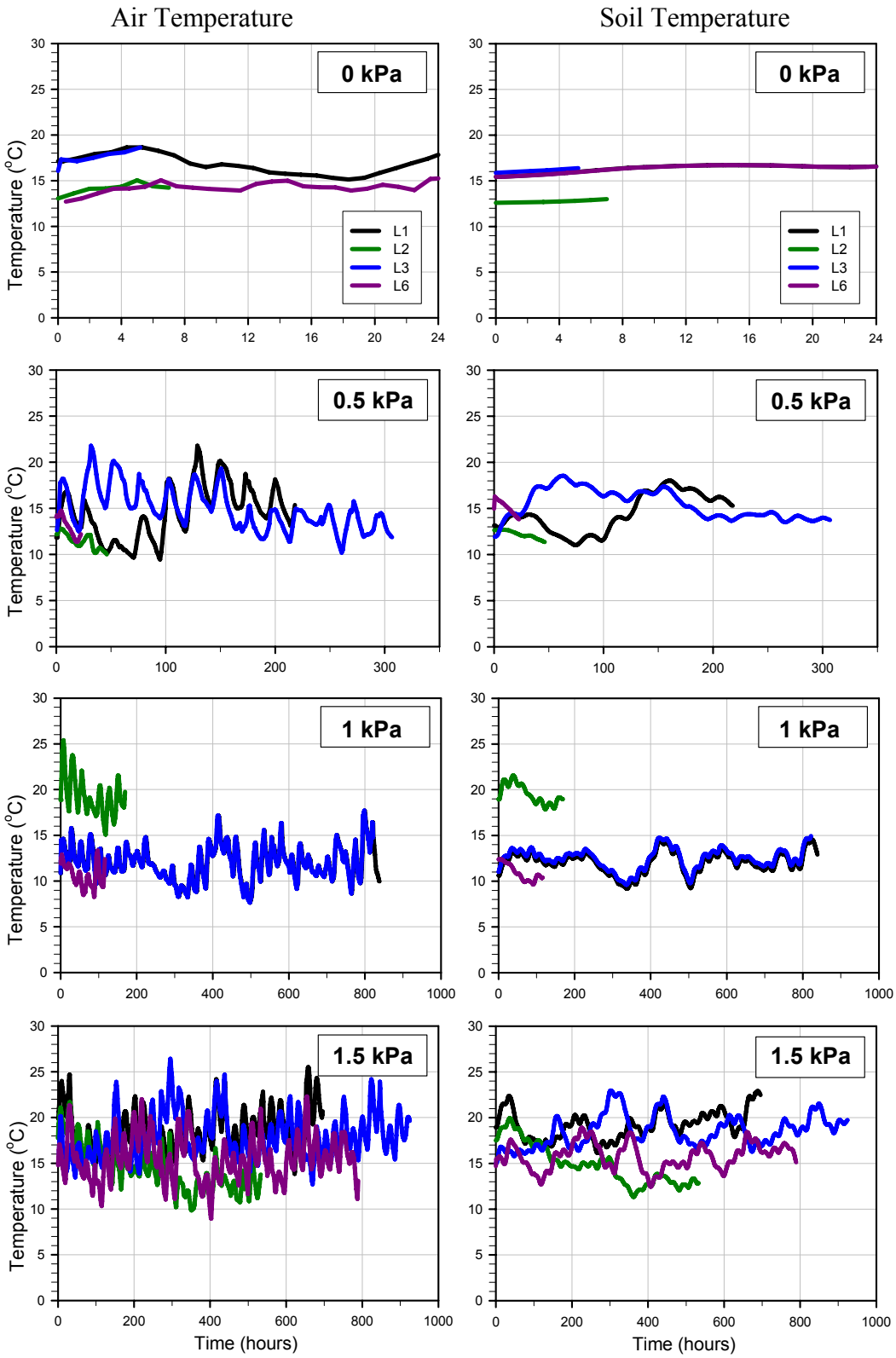

Appendix 1 Variations in air and soil temperature over time during the infiltration experiments on four lysimeters, with infiltration under controlled surface suctions of 0, 0.5, 1, and 1.5 kPa. Temperature variations reflect the changing outdoor weather conditions, partially buffered by the lysimeters being located within a large shed.

Appendix 2 Profile descriptions from 3 sites.
Profile 1

Depth (cm)	Horizon	Description
0 – 24	Ap	Dark greyish brown (2.5Y 4/2) silt loam; weak soil and ped strength; semi-deformable failure; very high penetration resistance and particle packing; strongly developed, abundant, very fine to fine polyhedral peds; abundant roots between and within peds; distinct occluded boundary; moisture content 10 cm depth, 30%; 20 cm 28%
24 – 40	AB	Dark greyish brown (2.5Y 4/2) and light yellowish brown (2.5Y 6/4) silt loam; weak to slightly firm soil strength; slightly firm ped strength; brittle failure; very high penetration resistance and extremely high particle packing; strongly developed, abundant, fine polyhedral and many medium to coarse prismatic peds; many reducing to common roots with depth, between and within peds; indistinct occluded boundary; moisture content 30 cm depth, 27%; 40 cm 31%
40 – 100	Bw	Light yellowish brown (2.5Y 6/4) silt loam; slightly firm soil strength; slightly firm ped strength; brittle failure; extremely high penetration resistance and particle packing; weakly developed coarse to extremely coarse prismatic structure, breaking to moderately developed fine to coarse polyhedral and prismatic peds; common reducing to few roots with depth, between peds; indistinct wavy boundary; moisture content 50 cm depth, 27%; 60 cm 26%; 70 cm 26%; 80 cm 28%; 90 cm 28%
100+	2C	On gravels

Notes:

1. 16.4 kg soil block sampled for laboratory analysis of aggregate size distribution, between 5 – 25 cm depth.

2. 20.70 kg soil block sampled for laboratory analysis of aggregate size distribution, between 30 – 50 cm depth.

Profile 2

Depth (cm)	Horizon	Description
0 – 25	Ap	Dark greyish brown (10YR 4/1) silt loam; weak soil and slightly firm ped strength; semi-deformable failure; moderate to high penetration resistance; high particle packing; strongly developed, abundant, very fine to fine polyhedral peds; abundant roots between and within peds; distinct occluded boundary; moisture content 10 cm depth, 30%; 20 cm 28%
25 – 45	AB	Dark greyish brown (2.5Y 4/2) and light yellowish brown (2.5Y 6/4) silt loam; weak soil strength; slightly firm ped strength; brittle failure; high penetration resistance; very high particle packing; strongly developed, abundant, fine polyhedral and many medium to coarse prismatic peds; abundant reducing to many roots with depth, between and within peds; indistinct occluded boundary; moisture content 30 cm depth, 29%; 40 cm 31%
45 – 82	Bw1	Light yellowish brown (2.5Y 6/4) silt loam; slightly firm soil strength; slightly firm ped strength; brittle failure; extremely high penetration resistance and particle packing; very weakly developed very coarse to extremely coarse prismatic structure, breaking to moderately developed fine to coarse polyhedral and prismatic peds; few roots in macropores; distinct irregular boundary; moisture content 50 cm depth, 27%; 60 cm 29%; 70 cm 26%
82 – 110	Bw2	Light yellowish brown (2.5Y 6/4) silt loam; slightly firm soil strength; slightly firm ped strength; brittle failure; very high penetration resistance; extremely high particle packing; massive apedal; few roots in macropores; indistinct wavy boundary; moisture content 80 cm depth, 30%; 90 cm 28%
110+	2C	On gravels

Notes:

1. 15.5 kg soil block sampled for laboratory analysis of aggregate size distribution, between 10 – 25 cm depth.

2. 22.60 kg soil block sampled for laboratory analysis of aggregate size distribution, between 30 – 50 cm depth.

3. 20.50 kg soil block sampled for laboratory analysis of aggregate size distribution, between 60 – 80 cm depth.

Profile 3

Depth (cm)	Horizon	Description
0 – 27	Ap	Dark greyish brown (2.5Y 4/2) silt loam; weak soil and ped strength; semi-deformable failure; high penetration resistance; very high particle packing; strongly developed, abundant, very fine to fine polyhedral peds; abundant roots between and within peds; indistinct occluded boundary; moisture content 10 cm depth, 30%; 20 cm 28%
27 – 45	AB	Dark greyish brown (2.5Y 4/2) and light yellowish brown (2.5Y 6/4) silt loam; slightly firm soil and ped strength; brittle failure; extremely high penetration resistance and particle packing; strongly developed, abundant, fine polyhedral and many medium to coarse prismatic peds; many reducing to common roots with depth, between and within peds; indistinct occluded boundary; moisture content 30 cm depth, 31%; 40 cm 35%
45 – 87	Bw1	Light yellowish brown (2.5Y 6/4) silt loam; slightly firm soil and ped strength; brittle failure; extremely high penetration resistance and particle packing; weakly developed very coarse to extremely coarse prismatic structure, breaking to moderately developed fine to coarse polyhedral and prismatic peds; few roots in macropores; distinct irregular boundary; moisture content 50 cm depth, 34%; 60 cm 34%; 70 cm 32%
87 – 110	Bw2	Light yellowish brown (2.5Y 6/4) silt loam; slightly firm soil and ped strength; brittle failure; very high penetration resistance; extremely high particle packing; massive apedal; no roots in macropores; indistinct wavy boundary; moisture content 80 cm depth, 31%; 90 cm 32%
110+	2C	On gravels

Notes:

1. 15.4 kg soil block sampled for laboratory analysis of aggregate size distribution, between 10 – 25 cm depth.

2. 21.90 kg soil block sampled for laboratory analysis of aggregate size distribution, between 30 – 50 cm depth.

3. 20 kg soil block sampled for laboratory analysis of aggregate size distribution, between 60 – 80 cm depth.

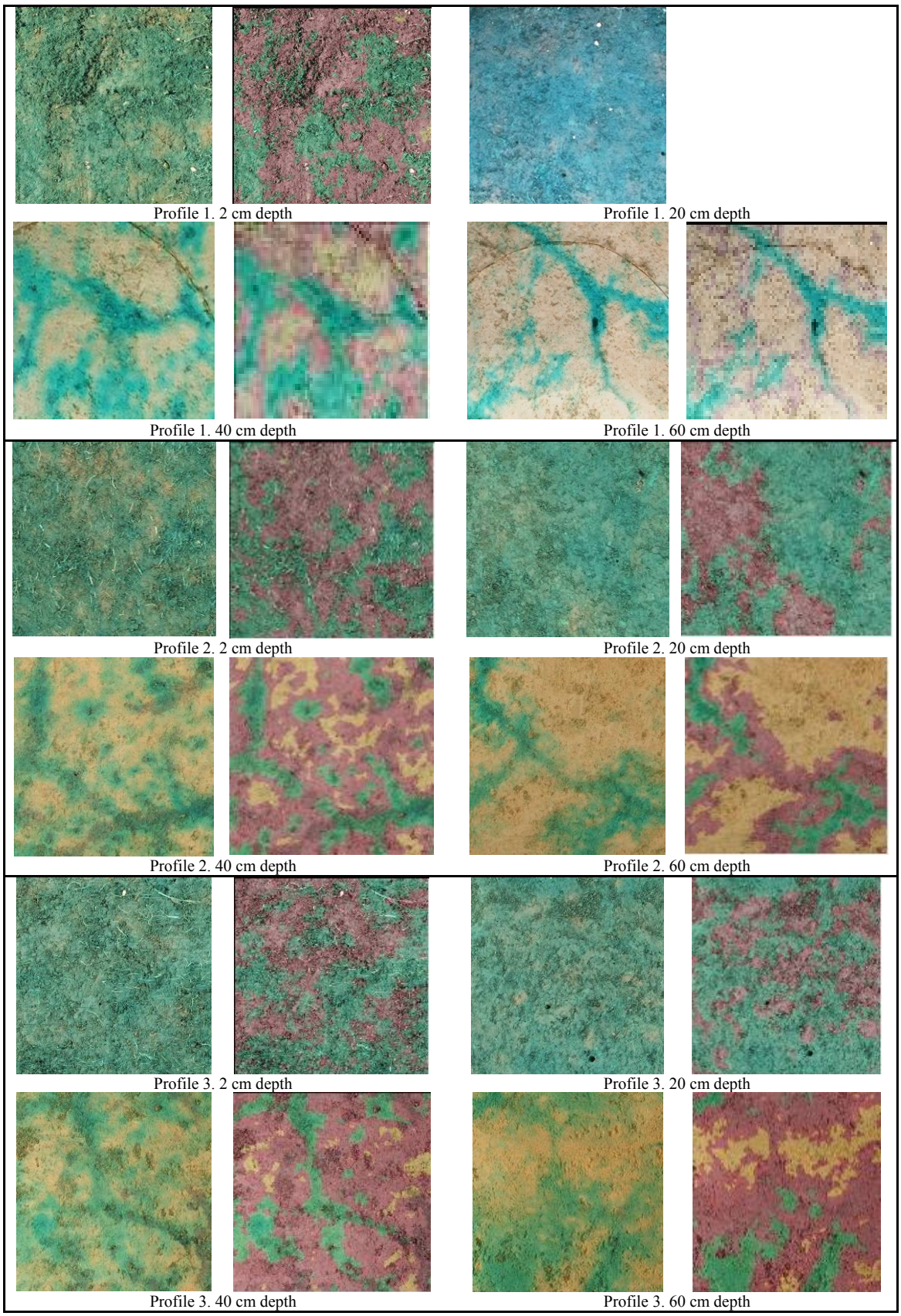

Appendix 3 Results of using image analysis to identify differences in dense vs pale dye coverage at soil depths of 2, 20, 40, and 60 cm. The analysed areas are the same horizontal sections in Plate 5-2**. Image analysis was not performed on the 20 cm depth of Profile 1 because the photo is over-exposed.**

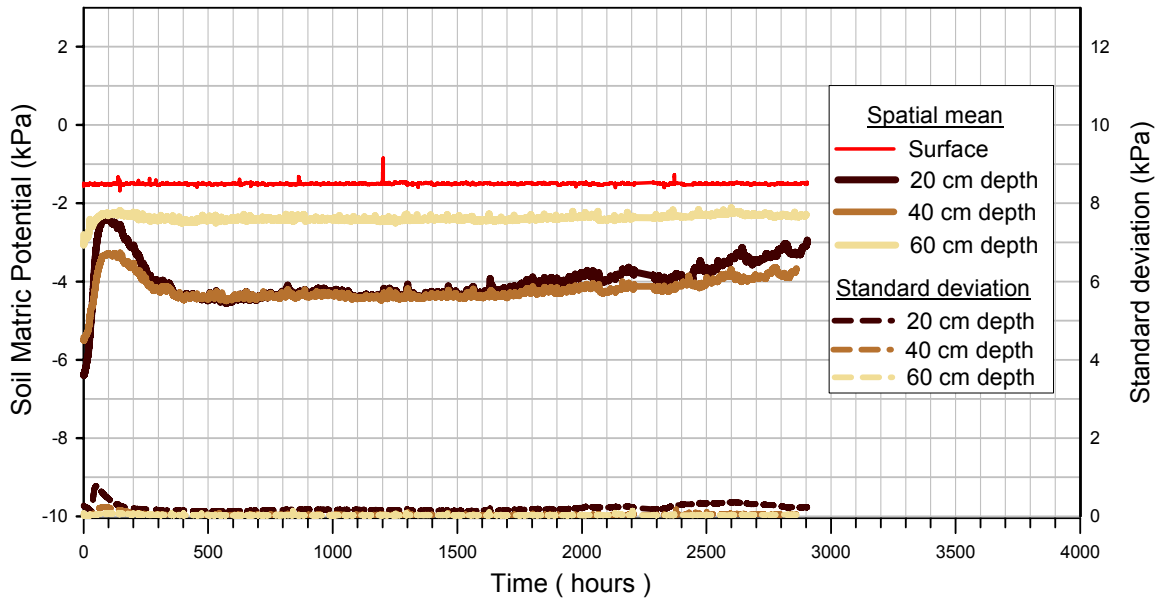

Appendix 4 Dynamics of matric potential, as well as infiltration and drainage rates, during the unsaturated leaching of a chloride tracer through lysimeter 6, where infiltration occurred under a surface suction of 1.5 kPa.

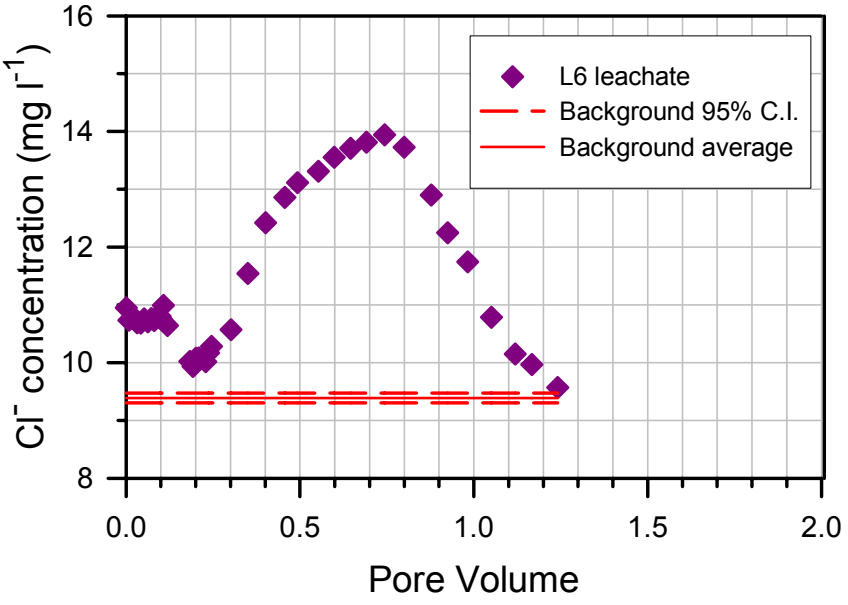

Appendix 5 The breakthrough curve of chloride tracer from unsaturated leaching through lysimeter 6, compared to the background chloride concentration. The estimate of background chloride is based on 62 samples from tap water and lysimeter leachate where no chloride tracer was applied.

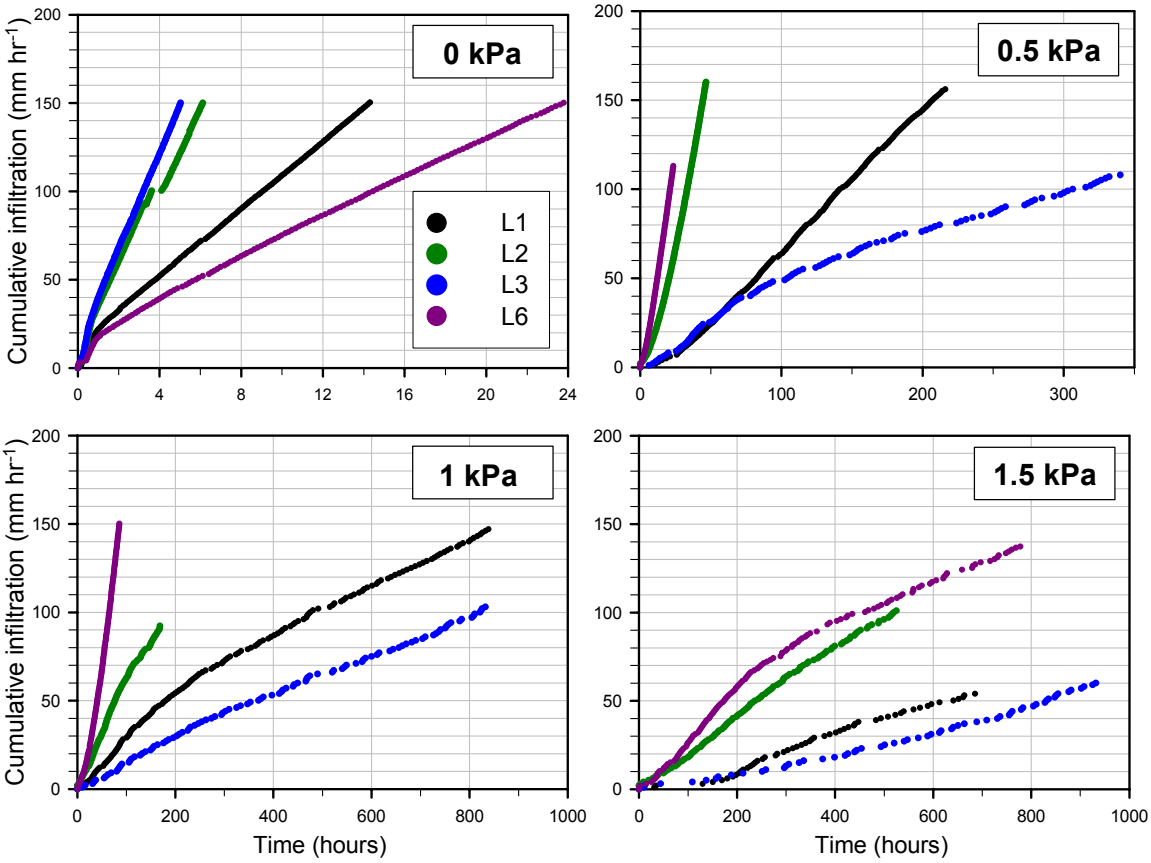

Appendix 6 Comparison of cumulative infiltration over time for four lysimeters, where infiltration occurs under controlled surface suctions of 0, 0.5, 1, and 1.5 kPa. Cumulative infiltration was recorded in 1 mm intervals.

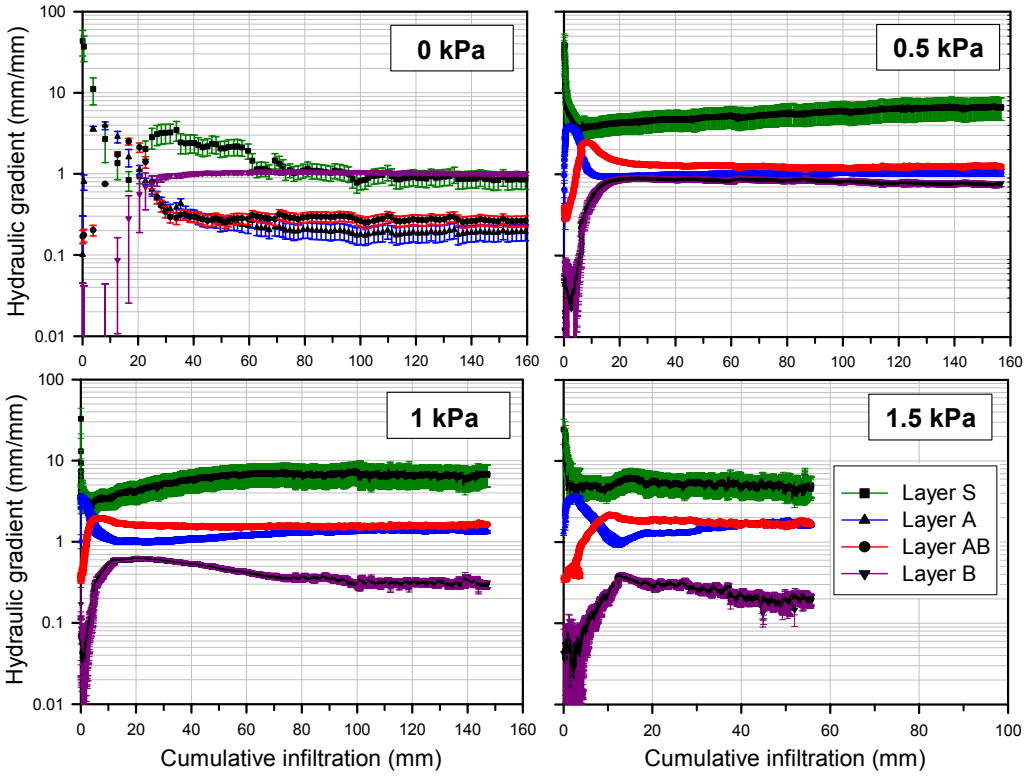

Appendix 7(a) Comparison of the pattern in the hydraulic gradient for the individual layers of lysimeter 1 during infiltration under controlled surface suctions of 0, 0.5, 1, and 1.5 kPa. Coloured lines represent error bars.

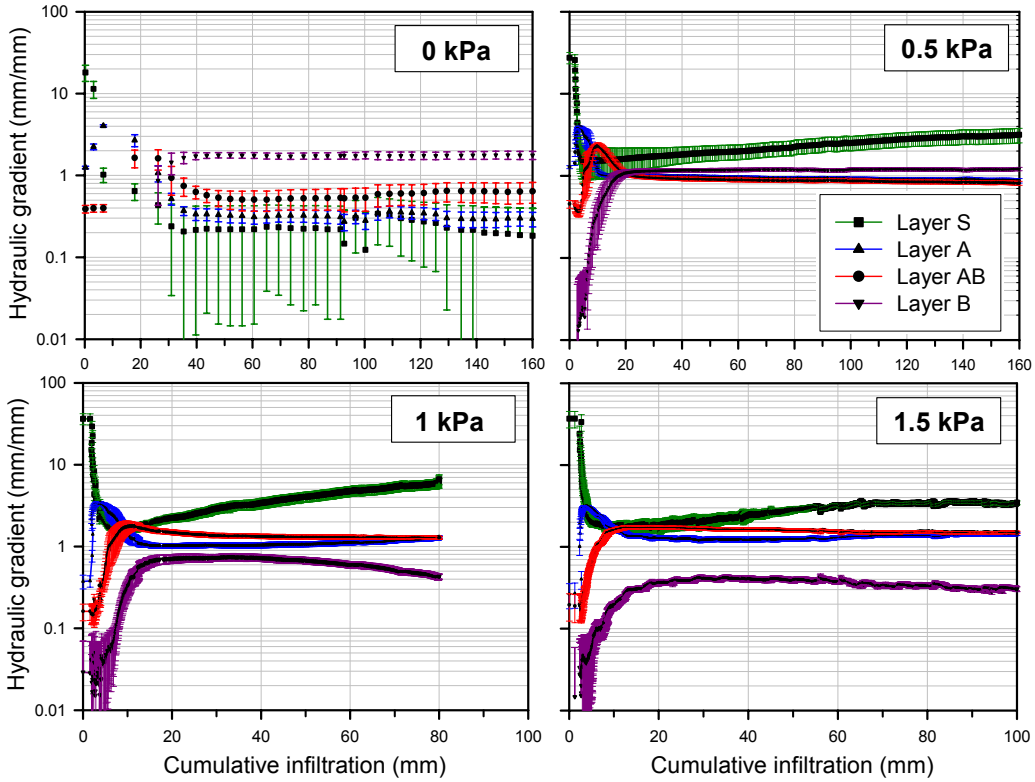

Appendix 7(b) Comparison of the pattern in the hydraulic gradient for the individual layers of lysimeter 2 during infiltration under controlled surface suctions of 0, 0.5, 1, and 1.5 kPa. Coloured lines represent error bars.

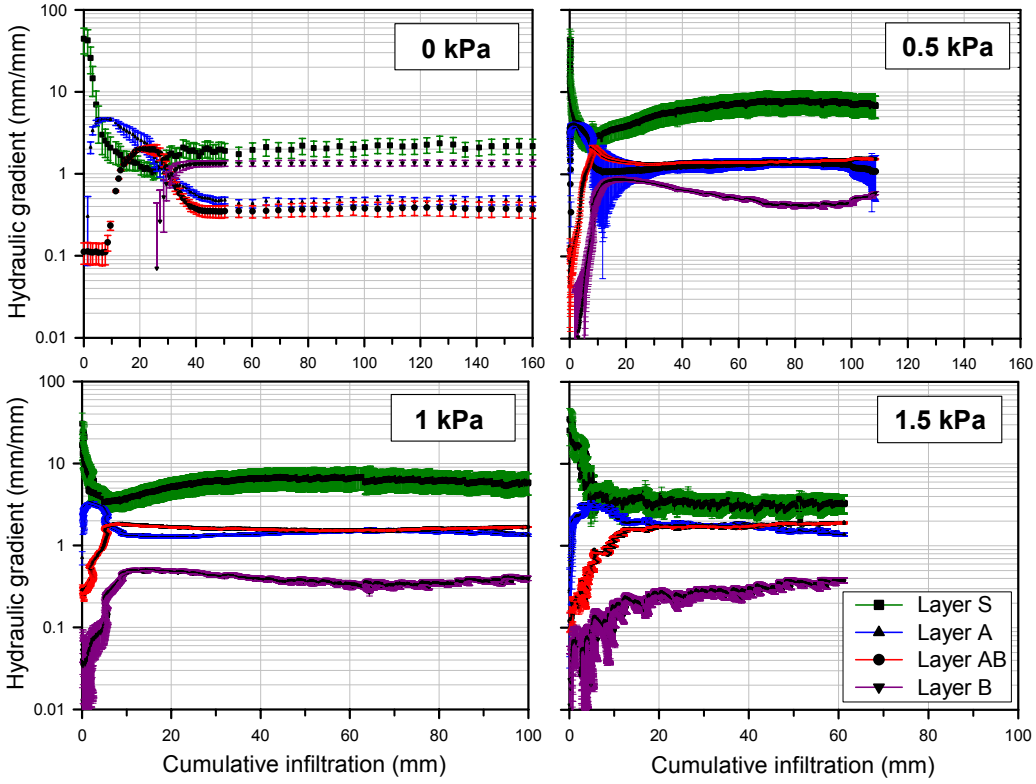

Appendix 7(c) Comparison of the pattern in the hydraulic gradient for the individual layers of lysimeter 3 during infiltration under controlled surface suctions of 0, 0.5, 1, and 1.5 kPa. Coloured lines represent error bars.

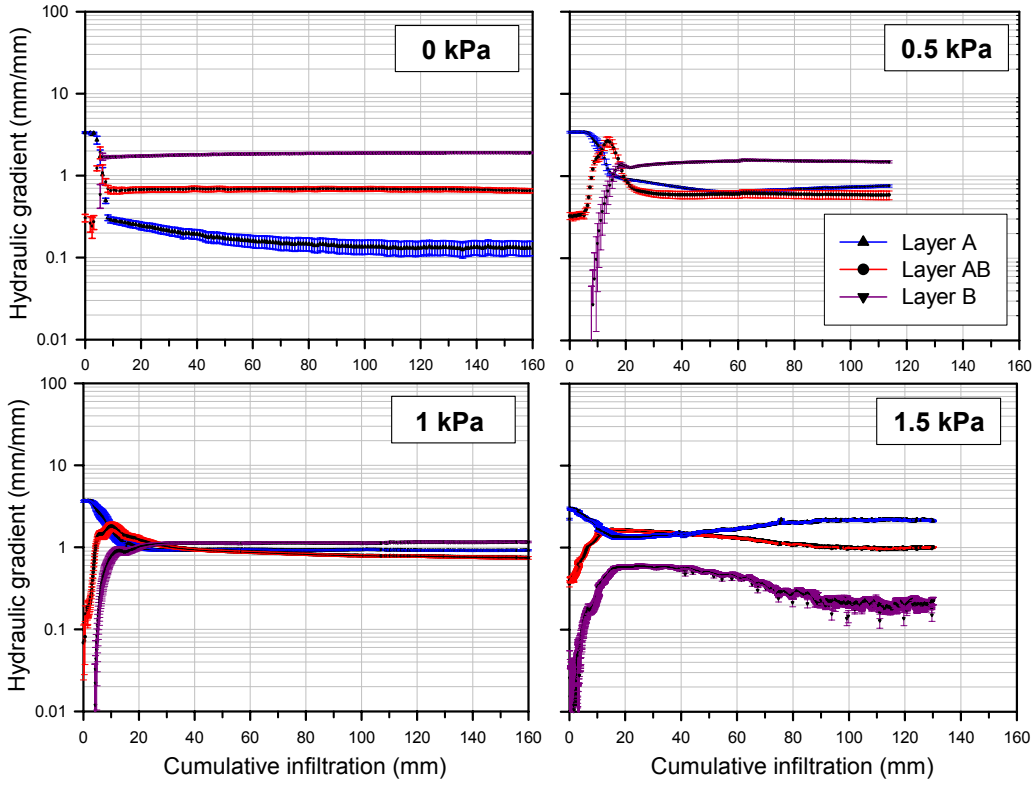

Appendix 7(d) Comparison of the pattern in the hydraulic gradient for the individual layers of lysimeter 6 during infiltration under controlled surface suctions of 0, 0.5, 1, and 1.5 kPa. Coloured lines represent error bars.

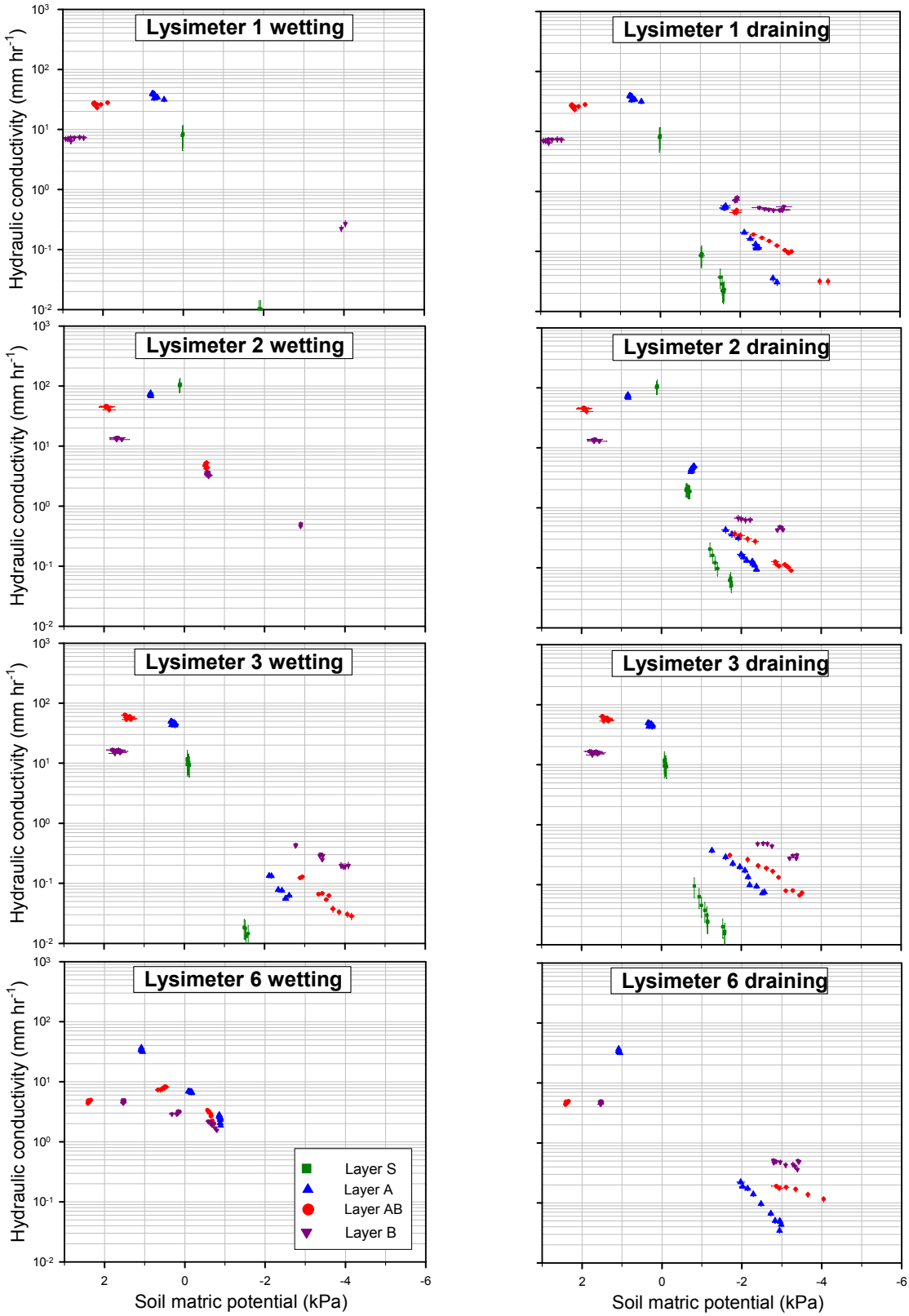

Appendix 8 The $K(\Psi_m)$ relationship for the individual layers of four lysimeters, when separated into wetting and draining curves. The separation was based on the behaviour of Ψ_m at the upper and lower boundaries of each layer during different experiments, when a tension infiltrometer was used to impose surface suctions of 0, 0.5, 1, and 1.5 kPa. If Ψ_m was increasing, $K(\Psi_m)$ was interpreted as being measured on the wetting curve, or correspondingly on the draining curve if Ψ_m was decreasing.